ADVISORY COMMITTEE

EDITORIAL BOARD

[1] The Faculty of Civil Engineering, Wrocław University of Technology
Wybrzeże Wyspiańskiego 27, 50-370 Wrocław, Poland
Tel. +48 71 320 41 35, Fax. +48 71 320 41 05, E-mail: jan.kmita@pwr.wroc.pl

[2] The Faculty of Mechanical Engineering, Wrocław University of Technology
ul. Łukasiewicza 5, 50-371 Wrocław, Poland
Tel. +48 71 320 21 73, Fax. +48 71 320 34 22, E-mail: matalplast@pwr.wroc.pl

POLISH ACADEMY OF SCIENCES – WROCŁAW BRANCH
WROCŁAW UNIVERSITY OF TECHNOLOGY

ARCHIVES OF CIVIL AND MECHANICAL ENGINEERING

Quarterly
Vol. VIII, No. 2

WROCŁAW 2008

EDITOR IN CHIEF

ZBIGNIEW GRONOSTAJSKI

EDITORIAL LAYOUT AND PROOF-READING

WIOLETTA GÓRALCZYK

TYPESETTING

SEBASTIAN ŁAWRUSEWICZ

SECRETARY

WIOLETTA GÓRALCZYK

Publisher: Committee of Civil and Mechanical Engineering
of Polish Academy of Sciences – Wrocław Branch,
Faculty of Civil Engineering and Faculty of Mechanical Engineering
of Wrocław University of Technology

OFICYNA WYDAWNICZA POLITECHNIKI WROCŁAWSKIEJ
Wybrzeże Wyspiańskiego 27, 50-370 Wrocław
http://www.oficyna.pwr.wroc.pl
e-mail: oficwyd@pwr.wroc.pl

ISSN 1644-9665

Drukarnia Oficyny Wydawniczej Politechniki Wrocławskiej. Zam. nr 308/2008.

Contents

Spis treści

ARCHIVES OF CIVIL AND MECHANICAL ENGINEERING

Vol. VIII 2008 No. 2

Theoretical analysis of rolling-extrusion process of axi-symmetrical parts

J. BARTNICKI, Z. PATER, A. GONTARZ
Lublin University of Technology, ul. Nadbystrzycka 36, 20-618 Lublin, Poland

Rolling-extrusion process is potentially one of the new manufacturing technologies of stepped, hollowed parts. In this process material is formed by means of three rotational tools. The charge is provided by means of a pusher pushing the billet in a working space between the profiled rolls. Numerical research of this process in a few tools variants with the use of hollowed billets were made in order to determine the influence of tool shape geometry in this new forming method. In numerical simulations the MSC SuperForm2005 software was used. This software based on the finite element method and it allowed for analyzing of the influence of different geometrical and technological parameters on the course of the rolling-extrusion process. On the basis of calculations it was stated that the process stability depends on different shapes of profiled rolls and its rotary velocities correlated with pusher displacement. One of the phenomenon which disturbed the proper course of the hollowed parts manufacturing process was excessive ovalization of cross-sections of the formed workpiece. This disturbance was eliminated by the application of correctly combined tools velocities and reduction ratios. In this work the authors focused on determining the practical range of tools geometrical and kinematical parameters guaranteeing the proper course of the rolling-extrusion process of hollowed parts.

Keywords: *rolling-extrusion, FEM*

1. Introduction

The application of hollowed parts in the place of full shafts and axles allows for reduction of the construction weight. Modern forming technologies, more widely used at present, give hollowed parts new, not available so far, application possibilities, mainly in automotive and machine industries. This results directly in decreasing of exploitation costs by means of lowering energy and fuel consumption.

Mainly applied technologies of hollowed shafts manufacturing include: swaging, rotary forging, cold extrusion and hydrostatic pressing [1] The newer solutions concern e.g. application of flow forming technology – within the scope of thin – walled parts and spin extrusion of possible wider scope of application [2]. Solutions dealing with forming of hollowed parts in cross-wedge rolling (CWR) and wedge-rolls rolling (WRR) technologies, were confirmed in laboratory and industrial tests [3].

In cross rolling technologies the tool width limits the part forming possibilities within the scope of its length. Application of rolling-extrusion technology allows for any setting of forming cycle concerning rolls and pusher movement. Hence, depending on the size of charge feeder, it is possible to form parts of larger length-diameter ratio, which is present e.g. in axle-shafts, transmission and gear boxes components. In

favor of making numerical analyses of the new rolling-extrusion process was also the possibility of retaining unquestionable advantages of cross rolling methods that is obtaining axi-symmetrical macrostructure with the metal fibers continuity.

2. Scope of research

A case of forming of a single step (necking) of hollowed shaft was considered in the research, and, for making comparison, full product of analogous external diameters was also analyzed. The results presented in literature and the results of own experiences dealing with cross-wedge rolling with application of rolling mill equipped with two and three working tools were taken into consideration during determining the scope of research [4–6].

While analyzing the influence of rotary tools geometrical parameters on the rolling-extrusion process, a case of forming of central step of workpiece within the scope of geometrical parameters shown in Figure 1 was considered. In further simulations the following parameters were changed: the forming angle α, width of calibration zone L, profiled rolls rotary velocity and velocity of pusher movement pushing the material into the working space between rolls.

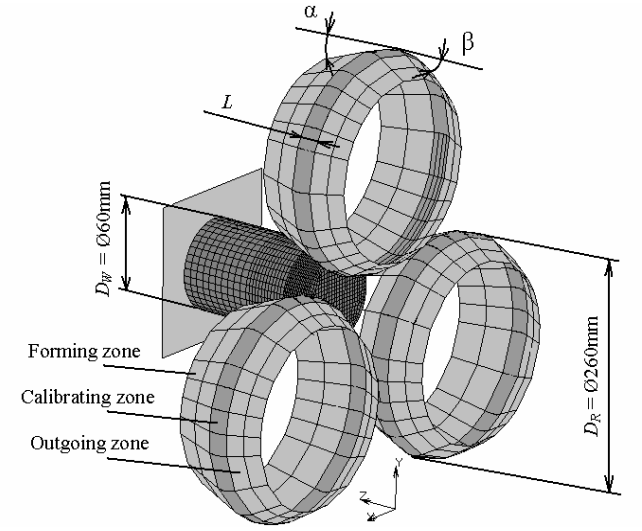

Fig. 1. The worked out for the calculations needs model of rolling – extrusion process with most important parameters

The commercial FEM software MSC.SuperForm 2005 was used for simulations of rolling-extrusion of hollowed and full parts. This software gives the possibility of modelling of forming processes in 3D state of strain with taking into consideration thermal phenomena appearing during forming. It was assumed that the charge was

heated up to 1150 ºC and that tools temperature was constant during forming and was 50 ºC for profiled rolls and pusher. It was also assumed that the coefficient of heat transfer between tools and material was 5000 W/m^{2}K and between material and environment its value was 200 W/m^{2}K.

The process geometrical model (Figure 1), worked out for the calculations needs, consists of three rotating tools – profiled rolls (moving in the same direction with the velocity ω = 2 or 3 rad/s (each), pusher pushing the charge with changeable velocity (within the scope of 5–20 mm/s) and charge modeled by means of hexahedral elements. As a charge were applied tubes and bars of external diameter D_w = Ø60 mm made from steel C45. All material model data for this steel were taken from the library of MSC.SuperForm 2005 software. Internal diameter of analyzed hollowed charges was Ø40 mm at the length 160 mm. Charges external diameter D_w = 60 mm was reduced to D_r = Ø40 mm achieving reduction ratio δ = 1.5 ($\delta = D_w / D_r$). The research were done within the scope of forming angle α = (20–45)°.

3. Results of numerical research

The conducted numerical research allowed for analyzing of the progression of part shape during the rolling-extrusion process. According to Figure 2, at the beginning of the process the workpiece underwent forming within the scope of side edge and surface adherent at increasing area to the rolls forming surface. This stage of the process, because of the appearing shape of workpiece, was called “chamfering”. As the large deformations of finite elements mesh describing the workpiece appeared during this stage of the process, it was necessary to rebuilt the mesh quite often. In the software the option of remeshing initiation at exceeding the given by user strains values was applied. Because this stage of the process did not add much to the research, causing difficulties at the same time, it was decided to design charges with initially formed chamfer. The angle of the chamfer was the same as the forming angle of a chosen set of profiled rolls. Hence, it was possible to retain contact on the whole surface at the stage when rolls touched the workpiece. Considering high time consumption of simulations, this solution shortened time of making these calculations.

In the next stage of rolling-extrusion process, the material was upset (it depended on the value of forming angle α and correlating working velocities of tools) and began to flow axially through the working space between profiled rolls. Cylindrical calibrating surfaces of the rolls, rotating at the same velocity, form the part final shape with single step. The proper forming process ended when the pusher stopped moving.

At the beginning of research on profiled rolls geometry it was assumed that: the value of forming angle is α = 30°, the forming zone of the tool changes into outgoing fluently, with considering relatively large radius. However, in the results of further research it was stated that at the rolls constant rotary velocity ω = 2 rad/s and constant pusher velocity v_p = 10 mm/s, the lack of separated calibrating zone causes disturbances of the formed part profile (especially it concerns hollowed parts). Introducing

in tools separate calibrating zone of length L = 10 mm resulted in a considerable increase of the dimension stability of formed parts. The comparison of the parts front views obtained in process without calibrating zone and with the length of this zone L = 10 mm is shown in Figure 3.

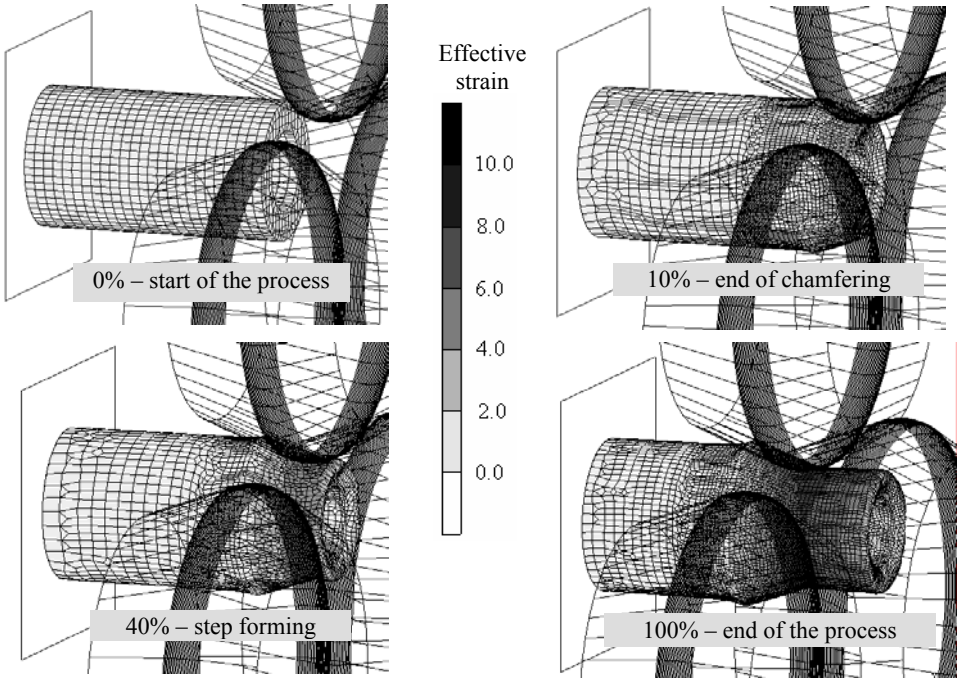

Fig. 2. The hollowed workpiece progression of shape and effective strain distributions during rolling-extrusion process at: $\alpha = \beta = 30°$, v_p = 15 mm/s

The further research allowed for noticing that together with the increase of the pusher movement velocity to v_p = 20 mm/s it is necessary, because of the appearance of the part shape disturbances, to prolong the tools calibrating zone – the assumed value was L_1 = 16 mm.

In the case of applying tools with forming angle $\alpha = 40°$ and $\alpha = 45°$ similar observations were made. Rolls of such changed shape did not guarantee dimensions stability of the part leading to the remeshing mistakes aborting the calculations procedure. Additional, appearing in these cases, problem was the workpiece intensive upsetting at the chamfering stage of process. Moreover, this resulted in a considerable increase of loads and moments values.

Single tests of forming with the application of profiled rolls with forming angle α = 20–25° showed that in the case of hollowed parts, large problems with numerical stability of process simulation caused by the intensive material flow to the axis of the formed workpiece appeared. In the real conditions it would probably lead to the ap-

pearance of excessive ovalization of the part or its uncontrolled squeezing by loss of stability. Because of this limitation, the best was to apply tools with the angle α = 30–35°, guaranteeing a certain state of equilibrium between axial and radial material flow during the process. However, this relates only to forming cases of single step of hollowed shaft within the scope of external diameter reduction from Ø60 mm to Ø40 mm (δ = 1.5). In the case of lower diameters reduction ratios looking for analogy to the cross-wedge rolling processes, the proper seems to be the application of tools with larger value of forming angle.

As it can be seen the danger of appearance of excessive ovalization and workpiece upsetting is caused by the lack or shortening of calibrating zone of the profiled rolls together with the increase of the pusher velocity.

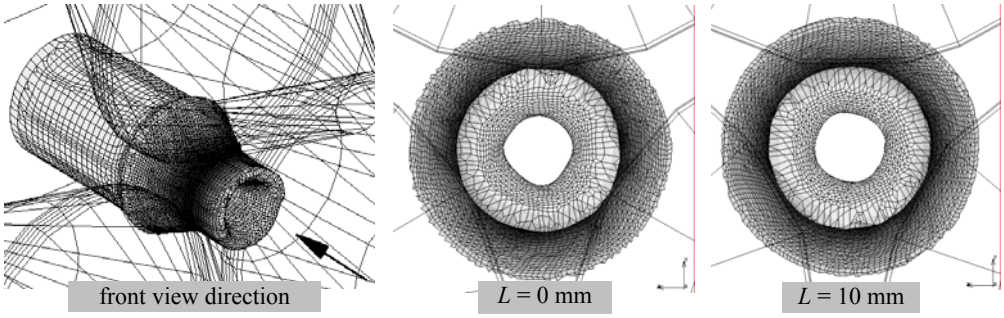

Fig. 3. The comparison of the parts front views obtained with different calibrating zone length during rolling-extrusion process at: $\alpha = \beta = 30°$, $\omega = 2$ rad/s, without calibrating zone and with this zone length $L = 10$ mm

Hence, it was possible to analyze the change of profiled rolls shape in such a way that the intensive upsetting before the rolls was limited. The rolling-extrusion process, shown in Figure 4, with controlled upsetting of the workpiece, extends the scope of application of this forming method. Formed in controlled way (through increasing the pusher velocity to v_p = 20 mm/s and imposed geometrically limitation of material radial flow) local thickening of part can be, depending on needs, used for further machining e.g. cylindrical or conical teeth.

Simulations made with the increased rolls rotary velocity (3 rad/s) showed slight limitation of workpieces upsetting tendency in the material – tool forming zone areas. This was, however, connected with relatively high values of strains, and in the case of simulation of processes for hollowed parts, with the risk of uneven distributions of wall thickness.

4. Conclusions

The possibility of applying the rolling-extrusion method for manufacturing of stepped shafts and axles is confirmed by the simulation research within the scope of

modelling of forming process of both full and hollowed parts by means of this technology.

The influence of relation of tools geometrical parameters and their working velocities on the process stability were analyzed in the numerical research. The presence of limitations of the process in the form of the excessive ovalization of the cross section of formed parts and their considerable upsetting before the profiled rolls forming zones were noticed. Considering hollowed charges, the additional limitation which appeared was the risk of presence of uneven distributions of walls thickness in the longitudinal sections of formed parts.

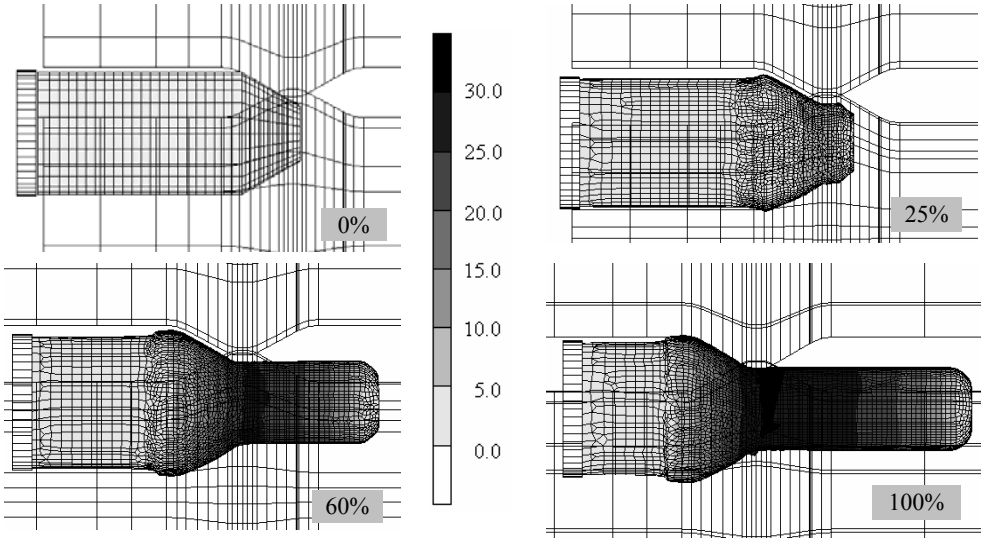

Fig. 4. Progression of shape and distributions of effective strain of full workpiece during rolling-extrusion process with modified design of rolls ($\alpha = \beta = 30°$, $v_p = 20$ mm/s)

It was observed that increase of rolls rotary velocity limits the excessive upsetting of workpiece and the ovalization problems in parts formed by means of that method.

A large problem in doing research of such a complex processes of metal forming is caused by numerical difficulties and time consuming calculations. The tools rotary velocity increase is connected with the presence of numerical lack of stability and hence, further detailed research of shape and tools velocities on stability disturbances (especially the distributions of walls thickness) need modification of the process numerical model.

What is more, basing on the results of numerical simulations the prototype test stand for experimental research verifying the presented numerical model of the process is finally assembled. In the developing experimental research conception it is possible to realize the process with possibility of changing the rolls spacing during form-

ing. This solution is the final conception of applying the rolling-extrusion process for forming of stepped hollowed and full axi-symmetrical parts.

Acknowledgements

The authors would like to acknowledge financial support from The State Committee for Scientific Research, Poland, grant No. N508 025 31/1447.

References

[1] Glass R., Hahn F., Kolbe M., Meyer L.W.: *Processes of partial bulk metal-forming – aspects of technology and FEM simulation*, J. Mat. Proc. Tech, Vol. 80–81, 1998, pp. 174–178.
[2] Neugebauer R., Glass R., Kolbe M., Hoffmann M.: *Optimisation of processing routes for cross rolling and spin extrusion*, Journal of Materials Processing Technology 125–126, 2002, pp. 856–862.
[3] Bartnicki J., Pater Z.: *Cross wedge rolling of hollowed parts*, Lublin University of Technology, Lublin, 2005, pp. 1–160 (in Polish).
[4] Danno A., Tanaka T.: *Hot forming of stepped steel shafts by wedge rolling with three rolls*, Journal of Mechanical Working Technology, No. 9, 1984, pp. 21–35.
[5] Bartnicki J., Pater Z.: *The aspects of stability in cross – wedge rolling processes of hollowed shafts*, Journal of Material Processing Technology 155–156C, 2004, pp. 1867–1873.
[6] Pater Z., Bartnicki J., Gontarz A., Weroński W.: *Numerical Modeling of Cross – Wedge Rolling of Hollowed Shafts*, Proceedings of the 8 International Conference on Numerical Method in Industrial Forming Processes – Numiform, 2004, Ohio, pp. 672–678.

Analiza teoretyczna procesu przepychania obrotowego wyrobów osiowosymetrycznych

W pracy przedstawiono koncepcję kształtowania stopniowanych wyrobów pełnych i drążonych, za pomocą przepychania obrotowego. W procesie tym materiał jest kształtowany za pośrednictwem trzech obracających się narzędzi rolkowych. Wsad wprowadzany jest do przestrzeni roboczej pomiędzy rolkami za pomocą popychacza wykonującego równocześnie ruch postępowy i obrotowy. W przedstawionych w pracy badaniach numerycznych określono wpływ kształtu narzędzi oraz podstawowych parametrów kinematycznych procesu na jego przebieg. W obliczeniach stosowano komercyjny pakiet oprogramowania MSC.SuperForm 2005 oparty na metodzie elementów skończonych. Na podstawie przeprowadzonych badań numerycznych stwierdzono, że stabilność procesu przepychania obrotowego jest uzależniona od doboru właściwego kształtu i prędkości obrotowej rolek profilowych oraz ustalenia prędkości liniowej popychacza.

ARCHIVES OF CIVIL AND MECHANICAL ENGINEERING

Vol. VIII 2008 No. 2

Analysis of strain and stress in the lower forging limit of Ti-6Al-2Mo-2Cr titanium alloy

S. BEDNAREK, A. ŁUKASZEK-SOŁEK, J. SIŃCZAK
AGH – University of Science and Technology, al. Mickiewicza 30, 30-059 Kraków, Poland

Hot-forging process of dual-phase titanium alloy was analysed. The aim of the work concerned selected technological problems of impression-die forging. Calculation included two variants of forging with variable temperature of billet. Estimation was made based on maps of distribution of temperature, effective strain and mean stress in a part and in the tools. A verification of the results with physical modelling was also carried out. Computer simulation was made with a use of commercial program QForm2D/3D.

Keywords: *Ti-6Al-2Mo-2Cr, hot forging, numerical modelling*

1. Introduction

One of the most common methods of serial production of titanium alloy components is hot-forging process. Depending on a grade of the alloy, forging temperature to which the material is preheated ranges from 850 °C to 1200 °C. This temperature is above upper limit of $\alpha+\beta$ range. What is more, this temperature brings about workability, which enables forging parts of any shape and size [1]. Plastic behaviour of titanium and some of its alloys is often compared to that of steel H18N9S [2–3].

For forging titanium alloys the same forging equipment and heating systems can be used as are traditionally used for steel components. Also dies are usually manufactured of the same materials as for steel forgings, however they should be more massive and, as a rule, their working surfaces have better finishing [2].

Microstructure and properties of forgings made of titanium alloys are strongly dependent on temperature, degree and rate of deformation. High friction between tools and deformed metal makes it harder to deform the metal, which may be a cause of coarse-grained structure in those areas, and that is why attention should be paid to uniform deposition of lubricant layer. Deformation of titanium alloys is accompanied by strong heat effect and metal temperature increase, which may lead to local preheating in areas of large deformation. A solution of this may be decreasing forging workpiece temperature, but it can lead to increase in deformation resistance and thereby to increase in loading of the tool and shortening tool life [1]. Taking the abovementioned into consideration, in the present work a forging process of titanium alloy is analysed. Analysis is based on physical and numerical modelling of the impression-die forging process of axi-symmetrical part.

2. Modelling of the forging process

Numerical calculation of hot-forging process was performed for a dual-phase titanium alloy and the tool made of 55NiCrMoV6 tool steel [3]. Physical properties of the deformed material were assumed on a basis of data determined for titanium alloy Ti-6Al-2Mo-2Cr (Figure 1), with assumption of viscoplastic model of a deformed body [4], whereas for the tool – ideal elastic model was used. The first case of analysis involved uniform heating to temperature 950 °C, and the other to 1000 °C. In both cases tool temperature 300 °C and ram velocity 10 mm/s was assumed. Friction factor between tool and the deformed metal was 0.3. The problem was analysed in axi-symmetrical state of strain.

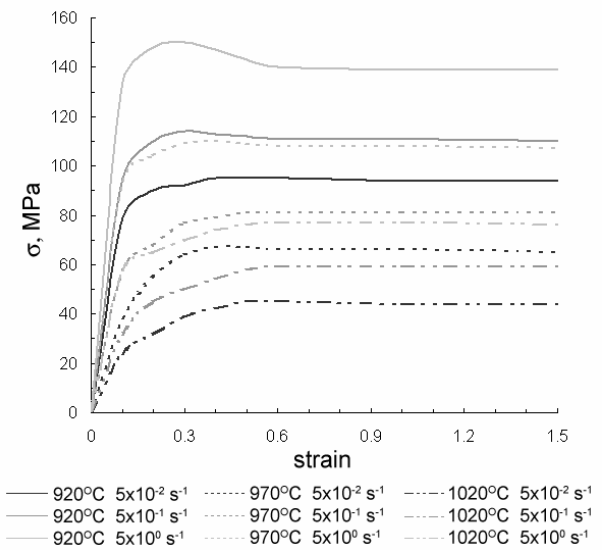

Fig. 1. Flow curves of Ti-6Al-2Mo-2Cr titanium alloy

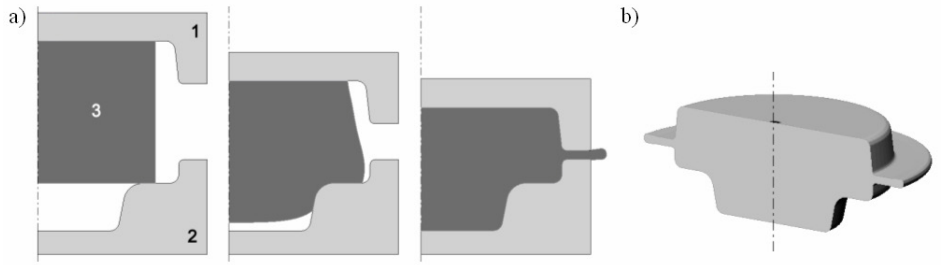

Fig. 2. Consecutive stages during a stroke (a) and finished part (b):
1 – upper die, 2 – lower die, 3 – workpiece

In Figure 2 intermediate stages of a stroke during forging of the analysed part (Figure 2a) and the finished part (Figure 2b). As a forging billet cylindrical rod of diameter ∅50 mm and height 30 mm was used. The billet dimensions were determined based on the impression geometry so as to provide complex metal flow pattern during a whole forging cycle with extrusion-alike state of stress prevailing.

3. Results of physical and numerical modelling

In the Figure 3 effective strain distribution maps in the lengthwise cross-section for the end stage for the forging operation are presented. For the investigated variants of forging, as expected, the maximum values are located in the peripheral region of the lower die cavity (direct extrusion pattern) and in area of the flash (lateral extrusion pattern). Initial billet temperature (950 °C or 1000 °C) seems not to affect absolute value of effective strain. For both cases similar values of effective strain were reported (Figure 3). Nevertheless, temperature has an effect on its distribution in a volume. For higher temperature (1000 °C) less gradient was observed (Figure 3a). The least deformed areas are the core zone and at the contact surface with an upper tool. These areas are more extended for the lower forging temperature (Figure 3b).

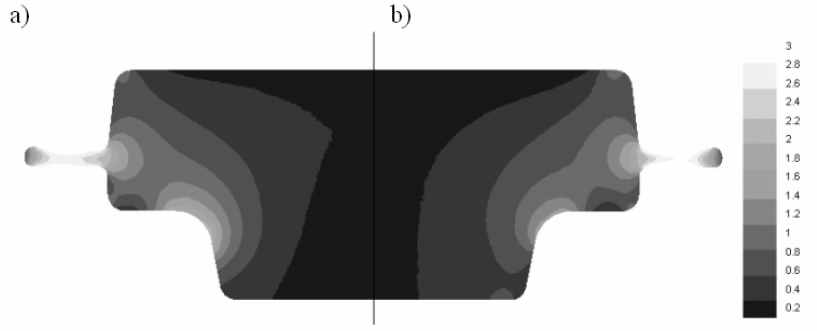

Fig. 3. Effective strain distribution for forging temperature 950 °C (a) and 1000 °C (b)

The effective strain distribution obtained from numerical modelling comes along with that obtained in physical modelling. The comparison was done on the strength distortion of rectangular grid engraved in lengthwise cross-section (Figure 4). Figures 4a and 4b show the shape of the grid in the last stage of deformation for two analysed temperature cases, 950 °C and 1000 °C, whereas, in Figure 4c shows grid of physical model of lead deformed at room temperature. It should be noted that in case of modelling on lead forging is carried out in isothermal-forging conditions and there is no additional influence neither of tool nor workpiece on the strain distribution in the bulk of the part.

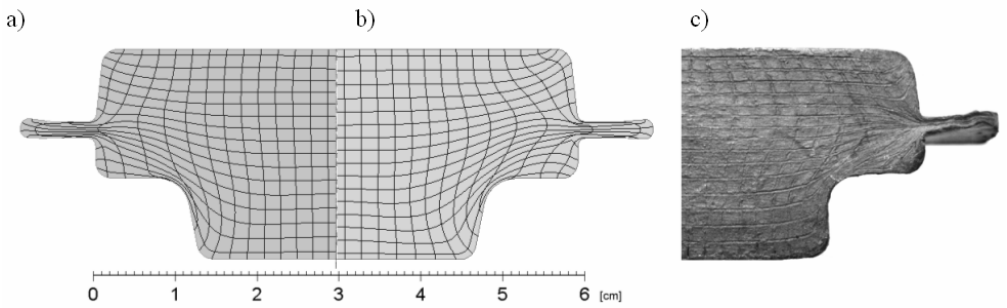

Fig. 4. Rectangular grid of deformation in forging temperature 950 °C (a), 1000 °C (b) and physical modelling on lead (c)

During forging of titanium alloy two processes which influence the temperature interact (Figure 5). One of them is die cooling of the workpiece in the contact surface die-billet, particularly in the beginning of the forging process, which results from the temperature differences 650–700 °C (depending on the billet initial temperature). The other process is the temperature increase in the aftermath of plastic deformation and local increase in effective strain rate. In both cases of initial temperature, in a region of the flash, temperature rises of 30 °C in relation to the starting point. The difference between the maximum and the minimum temperature in a forged part is 350 °C.

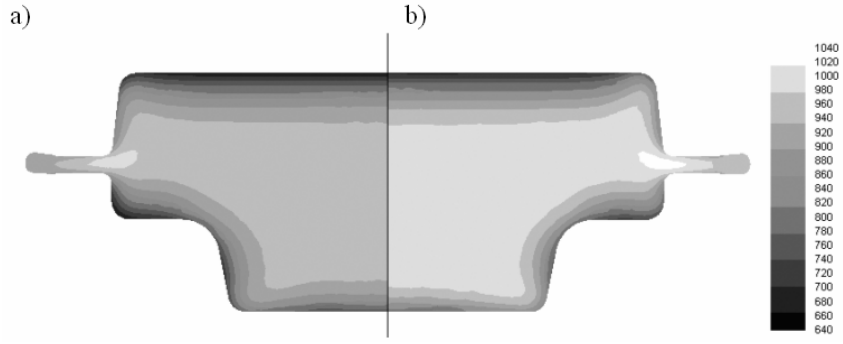

Fig. 5. Temperature profile (°C) in a part forged in 950 °C (a) and 1000 °C (b)

In Figure 6 mean stress distribution is presented. The maximum level of mean stress is in the core zone of the part. For forging temperature 950 °C they gain a maximum level, reaching 780 MPa (Figure 6a) which is 15% higher as compared to those for billet heated to 1000 °C (Figure 6b). Large values of compression stress are a determinant factor as for low tool life, even for such a relatively simple geometry. From the mean stress distribution maps it can be said that independently on the forging temperature, loading of the upper tools in the axial zone is bigger in relation to the

loading of the bottom tool in the same zone. Simultaneously, the bottom die is subjected to maximum loading in the outer region of the central hub cavity for temperature 950 °C. For this reason the process should be carried out in the temperature of 100 °C or higher, close to the upper forging limit of the alloy.

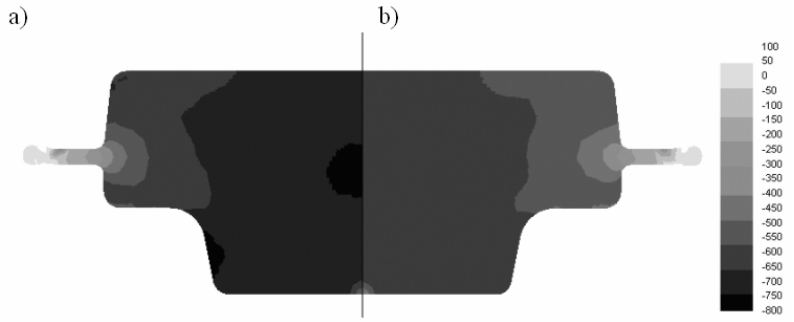

Fig. 6. Mean stress distribution (MPa) in a part forged from billet heated to 950 °C (a) and 1000 °C (b)

Results of the numerical estimation of load of the press and deformation work plot in the process of forging of the analysed dual-phase titanium alloy are presented in Figure 7. Numerical simulation indicates lower forging load, quite similar to mean stress values, about 15% in the whole cycle of forging a billet heated up to the higher temperature, which results from the characteristics of Ti-6Al-2Mo-2Cr titanium alloy (stress – strain in function of temperature and strain rate – Figure 1) [5].

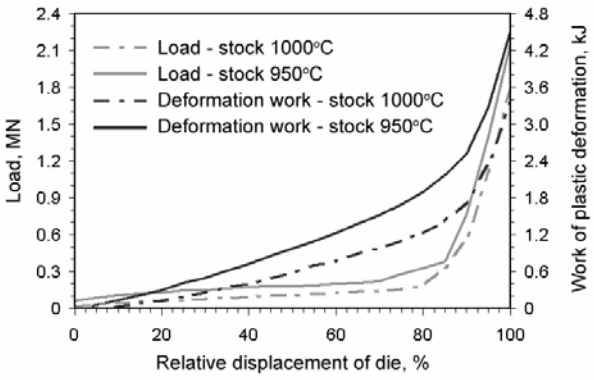

Fig. 7. Effect of temperature on the load and deformation work in forging of dual-phase titanium alloy

The changes of load and deformation work for forging in temperature 950 °C and 1000 °C, shown if Figure 7, have similar character, but different end values, 4.5 kJ and 3.6 kJ, respectively. For forging carried out in temperature 1000 °C it means 20% lower plastic deformation work needed to complete the process.

During the whole process, two characteristic stages can be distinguished, in both of them linear increase of plastic deformation work is observed. The first one comprises about 80 % of the total deformation (point B, Figure 8). In the characteristic points the total work of the plastic deformation necessary to obtain a given part can be calculated from formula (1):

$$L_{pl} = k_l \cdot \varepsilon_l \tag{1}$$

where:

k_l – coefficient describing the analysed forging stage, kJ,

ε_l – relative displacement of a tool throughout the analysed stage.

The coefficient k_l determined an increase in the plastic deformation work in a unit of deformation. As a rule, for the process of impression-die forging a constant value for a characteristic stage of the process is assumed. As mentioned, for the analysed part two stages can be distinguished. The first stage is characterised by uniform distribution of deformation in the whole volume, the second – rapid growth of deformation in the areas of forward and side extrusion. For analysed forging of Ti-6Al-2Mo-2Cr titanium alloy deformed in 950 °C (Figure 8) in the first stage the coefficient k_l is 10 times smaller than in the second stage (k_{AB} = 22.5 J, k_{BC} = 215 J).

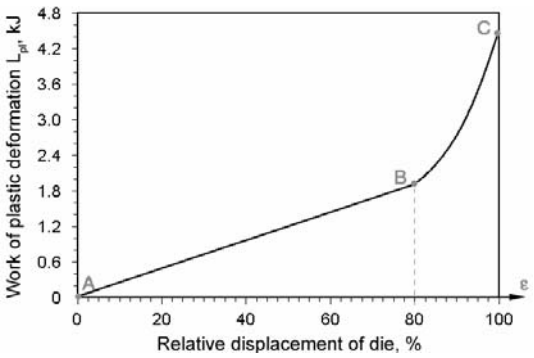

Fig. 8. Work of plastic deformation for forging temperature 950 °C

In addition to that coefficient, for estimation of the loading of tools and the quality of the produced parts temperature gradient can be used (Figure 5). In the end stage of forging the temperature gradient in a deformed metal was Δt_m = 310 °C for temperature of billet t_k = 950 °C and Δt_m = 360 °C for initial temperature of billet t_k = 1000 °C.

4. Loading of tools

In Figure 9 effective stress distribution in tools for variable forging billet initial temperature is presented. The geometry of the part and the metal flow pattern exerts higher force upon the upper tool.

Effective stress in the upper tool during forging billet of 950 °C reach 1480 MPa, and for the billet preheated to temperature higher by 50 °C the maximum stress value is 1365 MPa. The higher temperature of the billet reduces the mechanical loading (Figure 9b). From effective stress distribution it can be noticed that the highest unit pressure is located in the vicinity of the inner radius (highest hazard of rupture formation) and in the area from which the metal is pushed out to the flash (hazard of fracture). The level of stress in the bottom tool is on average 200 MPa lower in corresponding areas. Taking the loading (1280 MPa) and displacement of the deformed material (abrasive wear) it can be predicted that the outer fillet region of the bottom die is a most likely for damage to occur.

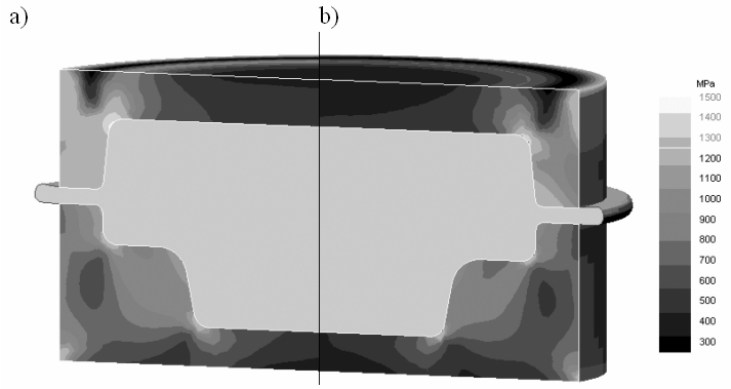

Fig. 9. Effective stress distribution (MPa) in tools for forging billet of temperature 950 °C (a) and 1000 °C (b)

5. Summary and conclusions

The simulations of impression-die forging process of dual-phase titanium alloy Ti-6Al-2Mo-2Cr in temperature 950 °C and 1000 °C allowed estimation of effect of initial temperature of billet on strain distribution, temperature profile and plots of load and work of plastic deformation work in consecutive stages of the forging process, as well as, estimation of the mean stress distribution and local loading of the tool.

Numerical modelling in the range of strain distribution and the course of load was verified on the strength of physical modelling. On the basis of the last stage of the process reasonable conformity of results of numerical and physical modelling was concluded. It was also noticed that the metal flow pattern of the analysed geometry boils down to two principal stages significantly differing in the load. Almost tenfold increase in the loading of the tool in relation to relative deformation is an indicator of the effect of process conditions on likely die wear.

Results of simulation, especially effective stress distribution in the lower die proves that the analysed temperature range affects not only workability of the alloy in a forg-

ing process and localisation of effective strain and stresses in transition areas between characteristic cross-sections of the impression but also on the loading of the tools and eventually on tool life.

Acknowledgement

Financial assistance of MEiN is acknowledged; agreement nr 3 T08B 010 30.

References

[1] Bylica A., Sieniawski J.: *Tytan i jego stopy*, PWN, Warszawa, 1985.
[2] Kaczyński J.: *Tytan*, WNT, Warszawa, 1961.
[3] PN-EN 10095:2002.
[4] Sińczak J.: Zeszyty Naukowe AGH, Zeszyt 144, Kraków 1992.
[5] Sińczak J., Bednarek S.: *Fizyczne i numeryczne modelowanie procesu kucia dwufazowych stopów tytanu w warunkach izotermicznych*, Przegląd Mechaniczny, 2007, No. 7–8, pp. 21–25.

Analiza naprężeń i odkształceń w dolnym zakresie temperatur kucia stopu tytanu Ti-6Al-2Mo-2Cr

Analizie poddano proces kucia na gorąco odkuwki z dwufazowego stopu tytanu. Zasadniczym celem pracy było zwrócenie uwagi na wybrane problemy technologiczne występujące podczas kucia. Obliczenia wykonano dla dwóch wariantów kształtowania, różniących się temperaturą wsadu. Oceny procesu dokonano na podstawie map rozkładu temperatury, intensywności odkształcenia i naprężeń średnich w odkuwce oraz narzędziach. Rozkład odkształceń analizowano również w oparciu o modelowanie fizyczne. Symulację wykonano komercyjnym programem QForm2D/3D.

ARCHIVES OF CIVIL AND MECHANICAL ENGINEERING

Vol. VIII 2008 No. 2

Review of different material separation criteria in numerical modeling of the self-piercing riveting process – SPR

ROBERT CACKO
Warsaw University of Technology,
Institute of Materials Processing, Narbutta 85, 02-524 Warszawa, Poland

Numerical modeling of the SPR process can be very efficient way for optimization of the strength of a joint obtained by this method. During numerical simulation one of the important problems is to define precisely the moment of upper layer separation leading to rivet penetration of lower layer(s). In the paper, a review of selected material separation criteria available in commercial MSC software applied for the SPR process simulation is presented.

Keywords: *self-piercing riveting, fem modeling, material separation*

1. Introduction

The body in white is the largest single component in a vehicle. For an average vehicle it accounts for about 25–30% of the total weight. Therefore the automotive industry is working on weight-reductions on the body in white. One way of lightweight constructions is based on aluminum structures. But for cost reasons and because of the easier recycling many car manufacturers prefer the use of high strength steels. Thinner high strength steels with reasonable expense can substitute conventional mild steel. By use of steels with an increased yield strength the strength of spot-welded structures increases under static load. Under fatigue load conditions the benefit from the higher material's strength is not transformed into higher joint's strength. Since spot-welding is the major joining technique today the use of high strength steels in the automotive industry is therefore rather small up to now.

Riveting is one of the oldest joining techniques known by man. Since the very beginning of the metalworking in the Bronze Age, solid rivets have been used for joining metals. Because of the increasing knowledge in welding techniques and the availability of weldable steels as well as other metals for structures, riveting was more and more displaced by less expensive welding techniques, mainly due to easiness to automation. Today there is an increasing demand on joining techniques for coil coated sheets, high strength steels, aluminum alloys, composites, and other modern materials for lightweight constructions. Most of these materials are only difficult or not gratifyingly to weld. Since riveting and blind riveting seem to be an alternative to welding, a lot of research effort is directed for improvement of these methods.

As a development based on conventional riveting, self-piercing riveting of metals is used since the middle of the seventies, because of economical and technological ad-

vantages. Sheet metal assembly using self-piercing rivets is shown to be ideal for joining dissimilar metals, aluminum panels and panels which are pre-coated. This kind of joints are leak proof, they have high fatigue strength and can be made with a high degree of reliability. With placement equipment that ranges from hand held manual tools to fully automated systems, self-piercing technology can provide complete assembly solutions that meet the highly variable needs of manufacturing industry.

A schematic of the stack-up of the SPR process and a joint formed with a self-piercing rivet is shown in Figure 1 and 2. The process characteristics can be described as a continuous cold forming operation in which the rivet during setting both pierces the material and forms a permanent mechanical interlock as a combination of positive and non-positive locking within two or more layers of material. Usually the operation takes place in a special press tool between a punch and a die and therefore access to both sides of the joint is required. Two completely different types of self-piercing riveting are in use - the riveting with solid and with semi-tubular rivets. The self-piercing riveting with solid rivet has a share of approximately 10% on the European market while the semi-tubular rivets have a share of approximately 90% of the market. In the US this ratio is different. The riveting process using the solid rivet is used when an even surface on both sides is required. The semi tubular rivet is used in higher stressed structures, like automotive components, and household appliance. The assembly process is complete within 0.5–3 seconds depending on the equipment solution selected. Self-pierce rivets can be manufactured in a range of metals to enable optimum joint strengths to be achieved in a variety of sheet materials.

Today the penetration of the die side material is avoided by the choice of dies and rivets in order to increase the joint's fatigue strength and corrosion resistance. The rivets' hardness, diameter, and length have a distinct influence on the joint's quality. Rivet, die and process parameters should be chosen in close contact to the suppliers of the riveting systems, because they have got experience with different applications.

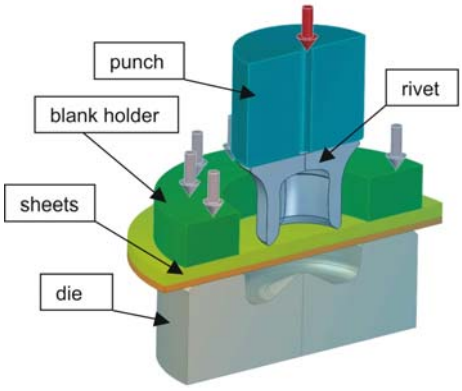

Fig. 1. Geometrical model of the SPR stack-up

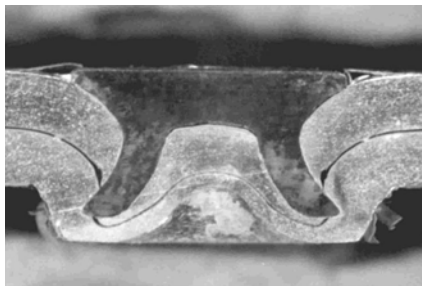

Fig. 2. Cross-section of the SPR joint

More details about SPR technique – advantages, disadvantages, properties comparison between e.g. spot welding and clinching – can be found in e.g. [1–4].

2. SPR joint verification

The industry expresses need for an optimization of the SPR in two aspects: technological (symmetry of the joint assurance, production rate increase, etc.) and joint quality improvement (strength of a joint increase/optimization, the bottom part of the joint shape and dimension control, decreasing the time of the process planning and die design for new materials and new designed stack-ups, etc). At the beginning of the SPR industrial application, so-called geometrical analysis were carried out based mainly on the industrial experiments. Nowadays, this approach is supported by stress/strain analysis, which potentially can answer more general questions.

Currently, there are three ways of the SPR joint verification: the setting force observation, visual joint assessment, and static and/or cycling loading strength tests (shear and peel test) [3–4].

One of the most important parameters during SPR joint assessment is a setting force as a function of punch displacement. It can be a useful indicator of process performance and joint quality. Evaluation of it became a benchmark showing various process stages, Figure 3, when a characteristic curve of a joint formation is compared for every rivet set. Monitoring of the force-displacement curve provides a process control while major deviations give signal of a possible need for correction. This relation is usually a first verification of the SPR process numerical model since both important groups of parameters – material and geometry – are taken into account. More detailed analysis of the SPR force-displacement course can be found in [8–9].

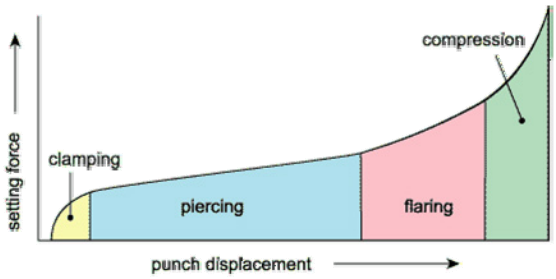

Fig. 3. SPR process stages on the force – displacement curve [3]

Frequently visual evaluation of the SPR joint is worthwhile, because appearance can give a good validation of joint quality. On the top layer, a good joint will have the rivet head in firm contact with the material, there should be no cracks in the head of the rivet or in the surrounding material and on the die side, it should be a symmetrical button of the correct diameter and shape (determined by the die). Ideally, the tail of the rivet should not cut through the bottom sheet or be noticeable. For some applica-

tions it can be not crucial, but for components subjected to fatigue loading or corrosive environments it is important. More detailed inspection can include examining a cross-sectioned joint. This will allow assessment of the joint's interior features.

Static and fatigue strength tests are carried out in precisely defined schedule (sample, type of loading, etc.) to finally answer the question concerning real joint performance during loading. Two types of figures are usually generated for analysis: force versus displacement curve for static, and force amplitude versus number of cycles for fatigue strength tests. Some more detailed information concerning experimental and numerical procedure one can find e.g. in [3], [6], [8–9].

3. Some aspects of the upper layer separation FEM modeling

To have SPR joint completely verified, both forming and loading of a joint must be analyzed. In both aspects, finite element method became a very useful tool. When joint forming is modeled, there are two aspects make this kind of simulation not an easy task: locally concentrated strains and material separation in the upper layer. Significant development concerning effectiveness and reliability of remeshing techniques allow to model large strains quite precisely. In several applications the finite element method is used to predict failure. This is mainly done by comparison between the calculated solution and failure criteria, or by using classical fracture mechanics. In case of the SPR, either simple, geometrical approach or the damage models appropriate for ductile metals must be used.

3.1. Geometrical and stress/strain failure criteria

For the purpose of numerical analysis of the SPR joining, at first geometrical failure criteria have been used. Generally, there are two different procedures available in the commercial software based on the FEM: with elements separation and elements removal. Both types are mostly equivalent, however the latter is not sensitive to the way in which material flows, what sometimes became a limitation. On the other side, it needs slightly more effort because of an extra simulation run for finding elements to be removed. Both are quite easy to use and there is no need to gather any material properties besides standard stress – strain curve needed for material plasticity properties description. The only one parameter is needed: thickness of a sheet at which material separation appears. Disadvantage rely on the fact that these procedures need a few trials to fulfill the experimental verification when the main criteria for comparison between numerical and experimental results is setting force. As a consequence it needs experimental results to be compared with. Following that, it is difficult to use this approach for analysis of completely new SPR design, as a preliminary numerical analysis, for example. In detail these two methods are described in [4].

Depending on the type of numerical software that is used, there are a few damage criteria available, which can be used for the SPR process modeling. The Lemaitre

model was chosen for the comparison in this paper. This model is a phenomenological approach to ductile damage in ferrous materials that are subject to large plastic deformations as they occur in the manufacturing processes. It is based on the concept of effective stress. It calculates three damage values that have different meanings: D_c – critical damage value at fracture, ε_D – threshold strain for damage initiation, ε_R – value of strain at fracture [11–12]. Macroscopic damage is characterized by plastic deformation that leads to pore growth, and then pore coalescence and final rupture of the material. The damage growth begins approximately after an equivalent plastic strain threshold is reached. Comparing to geometrical criteria, at first sight the disadvantage is related with necessity of obtaining particular materials parameters from experiments.

4. Analysis of differences in applied failure criteria

For the purpose of the analysis aiming at comparison between two material separation approaches, an example of one of the experimental and numerical stack-up (rivet – sheets – die) has been chosen. Numerical modeling of joining and loading are accompanied with experimental tests, Figure 4.

Fig. 4. An example of experimentally obtained SPR joint: left – after forming, right – after shear test

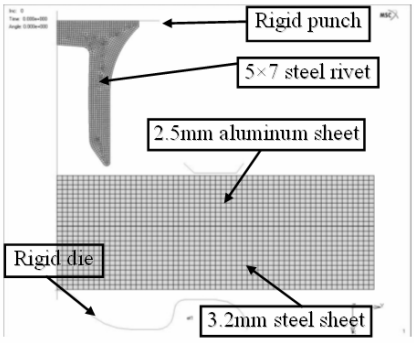

Fig. 5. FEM model of a selected stack-up

Numerical model for joint formation, Figure 5, contains of deformable rivet, two deformable – lower and upper – sheets, and rigid tools: die, punch and blank holder. Every deforming body was meshed with 2D, axisymmetric, 4-node elements. Both rivet and sheets materials are modeled as elastic-plastic with isotropic hardening.

Rivet is made of 10B35 (0.35% C) carbon steel delivered as forged (hardness level around 320 HV). The rivet material behavior has been described by the stress-strain curve $\sigma = 1600\varepsilon^{0.12}$ which states for steel 1020 (AISI/SAE/ASTM), with initial stress yield σ_y = 1000 MPa determined by micro hardness tests. Type of the selected rivet, 5×7, states for 5 mm diameter (tube part) and 7 mm height. The upper sheet is made of aluminum alloy 5052-H32 of 2.5 mm thickness while the lower one is made of steel 18-41581 and 3.2 mm thickness, giving 5.7 mm in total thickness. Parameters for Lemaitre damage model have been obtained as follows: $D_c = 0.42$, $\varepsilon_D = 0.16$, $\varepsilon_R = 0.56$. For the geometrical material damage model, there were three different values of thickness t_f assumed for an upper sheet at which material separates: 0.3, 0.2 and 0.1 mm. To take into account contact conditions the adhesive model of friction in which the friction stress is based upon the coefficient of friction and the normal stress at the surface (Coulomb friction model) was selected in the numerical model. The friction coefficient of $\mu = 0.15$ was preliminary assumed as a basic parameter. The modeling process is 2D axisymmetric, static and isothermal. The experiments were carried out on the originally design testing machine [4].

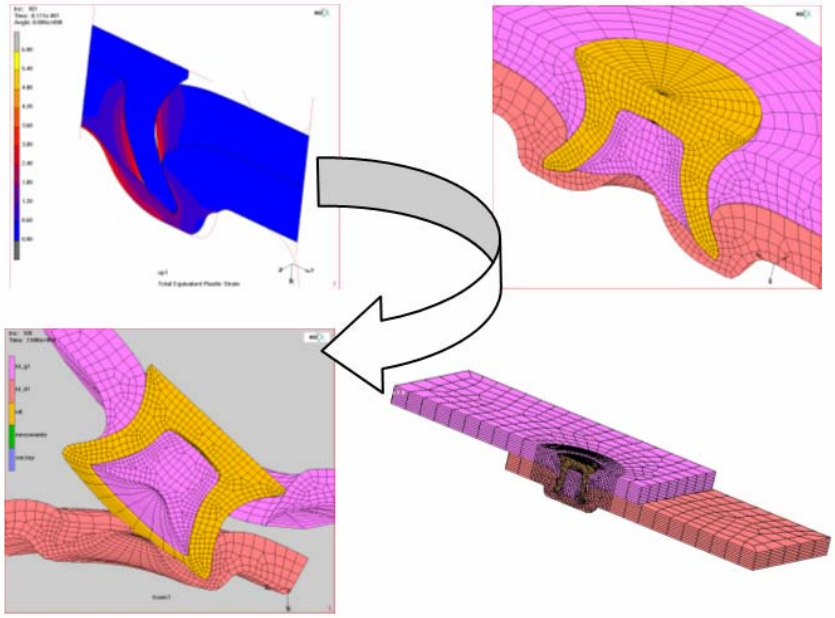

Fig. 6. 3D model for FEM simulation of loading and stage of failure

Numerical model for static strength analysis is described in detail including thee procedure of stress/strain field transfer from 2D simulation over 3D model used in MSC.Marc in [8]. In Figure 6 a brief view of simulation procedure is presented. It proceeds in two stages. First, special, axisymmetric model to 3D expand" procedure

for expanding axisymmetric mesh to 3D is applied. Rotation angles and number of repetitions must be defined, where the latter means the number of elements created in circumferential direction. In this example, the 2D section was uniformly expanded over 180° in 12 sections. Then, the, axisymmetric to 3D" route within, Initial conditions" module is used. This process converts stress/strain field results on 2D elements, to the new ones on the new 3D mesh. Once the 3D joint is developed, the rest of a sample, assumed to have zero stress/strain level, has to be made around created core. 8-node hexahedron elements are used in this case. The distance from the axis of symmetry that has to be taken into account during SPR simulation was prescribed in [8].

In the Figure 7 results of numerical simulations for both material separation modes are superimposed on experimental results. First conclusion is that the force-displacement curve when Lemaitre damage model is used is in the best accordance to real process.

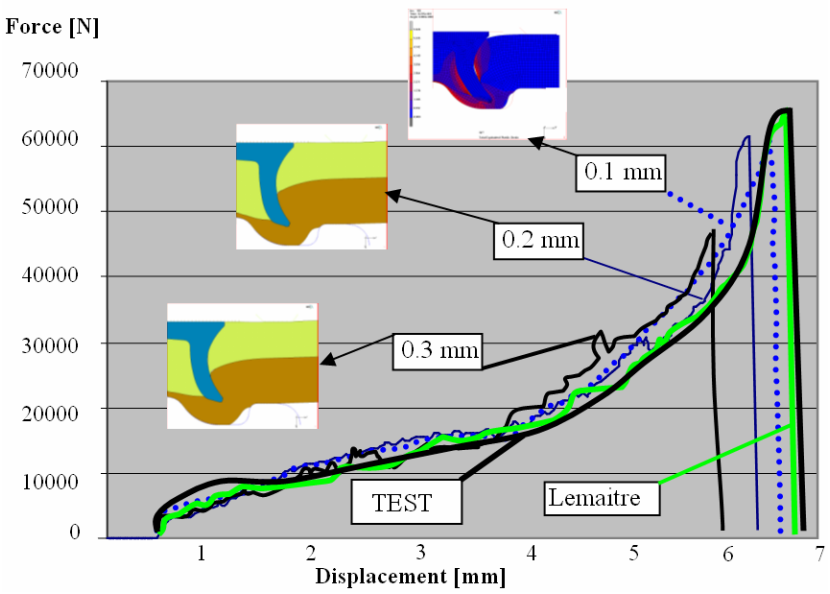

Fig. 7. Force-displacement curve taken from experiments and numerical simulation with various material separation failures

A small influence of the t_f parameter on the force – displacement curve and final shape of a joint is noticeable. When 0.2 and 0.1 mm for separation threshold is applied, the force-displacement is almost the same, though the differences occur at the end of the process. In analyzed case, the force adjustment becomes worse after moment of upper layer separation. Although a tolerance range can be introduced to the benchmark curve representing the zone of acceptable process changes, established by experiments and supporting quality checks, deviations outside the tolerance range

used to indicate faults, or variations in the process or materials, which may lead to unacceptable joint quality. So the question is, if the differences observed during simulation influence the strength of a joint. Influence of the applied procedure on the joint strength is verified by the standard shear loading procedure [3–4].

Both numerical and experimental tests have been carried out and comparison between the results is presented in Figure 8. Qualitatively the shapes of all obtained curves are quite similar. General remark should be, that the finite element model containing Lemaitre damage criteria the best way reflects results from laboratory experiments. Both finite element models with 0.3 and 0.1 mm thickness limit to separation – works worse. Elongation, or distance to fracture, Δl, is about 1 mm smaller for them comparing to experiments. Also the maximum force from a certain point of loading is over 1 kN lower than it was measured during tests.

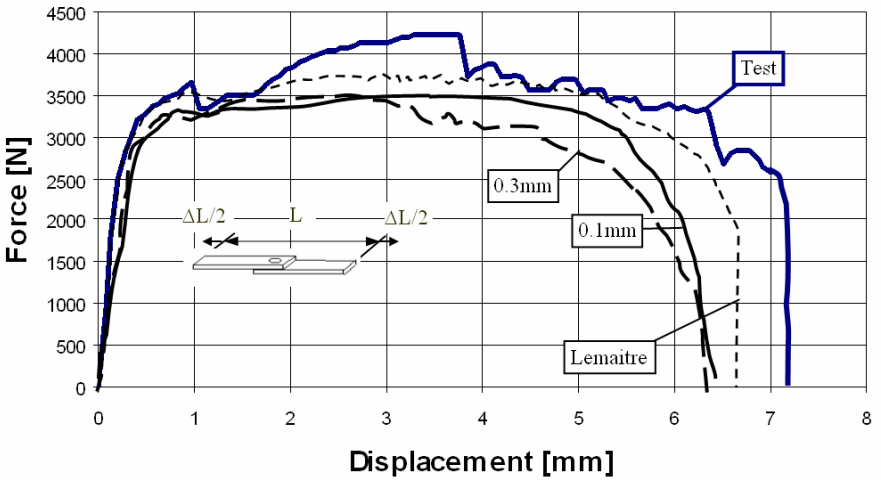

Fig. 8. Comparison of loading force taken from FEM analysis and experiments

5. Summary

An example of the SPR stack-up consisted of two different layers of aluminum and steel sheets and chosen die geometry is presented. Two different approaches for material separation in the process modeling are compared due to their utility for joint properties assessment. Both forming a joint and its strength has been taken into consideration.

Simple geometrical separation approach can be characterized following way:

- it is quite easy to use and no special data (material properties) are needed,
- it offers an answer only for expected cracks/fracture (e.g. penetration of the die side/lower layer by rivet will not be taken into account/noticed),

- a few trials are needed for adjustment of setting force versus punch displacement curve between numerical results and experiments (following that, this approach is difficult to apply for unknown results from experiments),
- after adjustment – thickness limit to fracture – this approach results in a very good accordance concerning either joint shape and numerical prediction of static strength,
- sometimes it needs relatively long lasting procedure for adaptation of remeshing and elements separation parameters (depending also on which of the two of the geometrical procedures are to be used).

With stress/strain damage criteria:

- having a good material data one can faster fit numerical and experimental setting force flow than in case of geometrical failure models,
- it is possible to take into account unexpected fractures leading to corrupt joint,
- a good strength prediction can be obtained,
- since they are based on the material properties they can be used for unknown (not experimentally tested) joints,
- one has to remember that they are reliable material data (damage properties) sensitive.

References

[1] Hahn O., Schulte A.: *Performance and Reliability of Self-Piercing Riveted Joints in Steel and Aluminum Alloys*, Mechanical Fastening Seminar, Troy, Michigan, January 1998, pp. 1–13.

[2] Bokhari N., LaPensee M.: *Self-Piercing Riveting in Automotive Applications*, Mechanical Fastening Seminar, Troy, Michigan, January 1998, pp. 17–22.

[3] TWI World Centre for Materials Joining Technology – Self-Piercing Riveting database, available at www.twi.co.uk.

[4] Cacko R., Czyżewski P., Kocańda A.: *Initial optimization of self-piercing riveting process by means of FEM*, Konf. Metal Forming 2004, ed. Kusiak J, Majta J., Pietrzyk M., Hartley P., Pillinger I., Kraków, 2004, pp. 307–311.

[5] Porcaro R., Hanssen A.G., Langseth M., Aalberg A.: *Self-piercing riveting process: An experimental and numerical investigation*, Journal of Materials Processing Technology, 171, 2006, pp. 10–20.

[6] Abea Y., Kato T., Mori K.: *Joinability of aluminium alloy and mild steel sheets by self piercing rivet*, Journal of Materials Processing Technology, 177, 2006, pp. 417–421.

[7] Porcaro R., Hanssen A.G., Langseth M., Aalberg A.: *The behaviour of a self-piercing riveted connection under quasi-static loading conditions*, International Journal of Solids and Structures 43, 2006, pp. 5110–5131.

[8] Cacko R., Czyżewski P.: *Numeryczne modelowanie kształtowania i obciążania połączeń nitowanych bezotworowo* (in Polish), Przegląd Mechaniczny, 2005, No. 7–8, pp. 50–53.

[9] Cacko R., Czyżewski P.: *Verification of numerical modeling of the SPR joint by experimental stack-up*, Proc. of the Computer Methods in Materials Science, Vol. 7, 2007, No. 1, pp. 124–130.
[10] MSC.Marc Volume D, pp. 6–13.
[11] MSC.SuperForm User's Guide, C-58.

Przegląd różnych metod uwzględniania rozdzielenia materiału w komputerowym modelowaniu procesu nitowania bezotworowego SPR

Modelowanie numeryczne procesu nitowania bezotworowego SPR staje się efektywnym narzędziem w optymalizowaniu wytrzymałości uzyskiwanych tą drogą połączeń. Jednym z najważniejszych czynników wpływających na jakość komputerowego modelu jest dokładne określenie momentu rozdzielenia górnej warstwy umożliwiające wciśnięcie nitu w dolną warstwę i uzyskanie silnego połączenia. W artykule przedstawiono porównanie wybranych metod uwzględniania rozdzielenia materiału dostępnych w komercyjnym oprogramowaniu MSC opartym na metodzie elementów skończonych.

ARCHIVES OF CIVIL AND MECHANICAL ENGINEERING

Vol. VIII 2008 No. 2

Cold rolled profiles for vehicle construction

P. GROCHE, M. HENKELMANN, P. GÖTZ, S. BERNER
Technische Universität Darmstadt, Institute for Production Engineering and Forming Machines,
Petersenstrasse 30, 64287 Darmstadt, Germany

So far car bodies are usually built as self-supporting structures. Recent studies show advantages using cold rolled sections in manufacturing car bodies, e. g. to reduce weight. The success of these components will for one thing be depending on technical feasibilities and for another thing on the profitability of the manufacturing processes. Promising approaches are presented, which can help to increase the amount of cold rolled sections in vehicle construction.

Keywords: *roll forming, profile forming, automotive*

1. Introduction

The integral monocoque construction has been established in the design of the car body. Here cold rolled profiles are of minor application. Nowadays other concepts for the BIW design are in discussion. Especially the space frame concept realized in steel seems to be attractive to minimize weight in a cost neutral way [1].

High strength steels (HSS) and ultra high strength steels (UHSS) become more and more attractive because of the demand to minimize weight. By changing the material into HSS or UHSS sheet thicknesses can be reduced.

The cold roll forming enables the continuous production of standard profiles in large numbers in a cost efficient way. About 8% of the annual word steel production is processed by roll forming nowadays. The main applications of roll formed products are:

- vehicle construction,
- railway cars,
- ship construction,
- transport and handling equipment,
- electric rack, control cabinets and storage rack,
- building industry.

Summarizing, profiles can be a cost effective background for assembly of complex structures. Furthermore, roll formed profiles offer the possibility of integrating performance into the design e.g. the support of sealing in window frames.

2. Flexibility in Geometry

Profiles manufactured by conventional roll forming according to DIN 8586 are limited in geometry by the need of constant cross sections lengthwise. The strong in-

terest of industry in more flexibility in geometry was the starting point for the development of the flexible roll forming technology [2]. The aim was the development of a forming technology based on the roll forming technology that offers the possibility of manufacturing profile families, not only by different lengths but as well with changing cross sections. Integrating NC controlled tooling stands in the manufacturing line a high number of geometrical variants on profiles are possible without changing tools. Examples for profile families manufactured by flexible roll forming are shown in Figure 1.

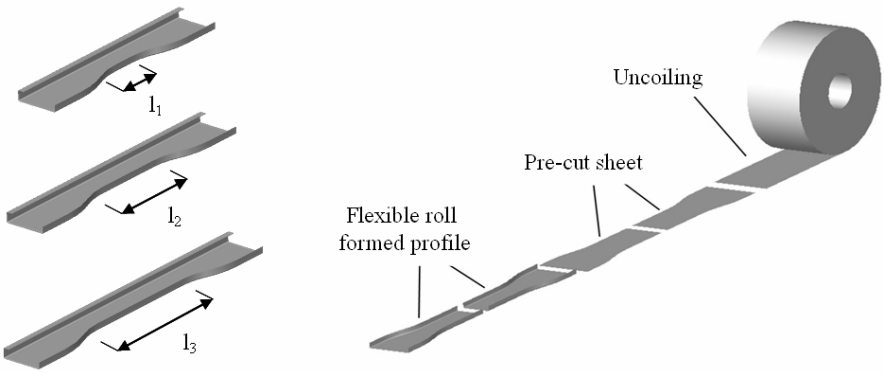

Fig. 1. Examples of flexible roll formed profile families (left),
process chain for the flexible roll forming (right)

The layout of a forming stand for the flexible roll forming is shown in Figure 2. The forming stand consists of a translatory and rotatory driven tool. The drives provide the movement of the forming rolls whose position is directly linked with the quality of the manufactured profile. To avoid additional shear strains and offset in the formed flanges, the forming rolls position has to be tangential on the flange (Figure 2).

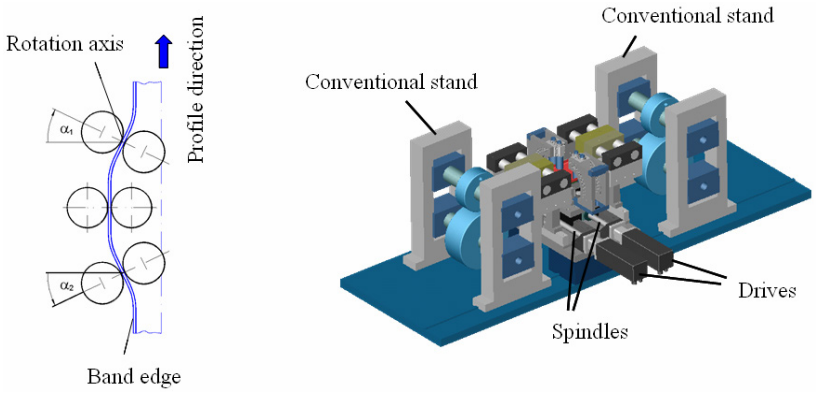

Fig. 2. Position of the forming rolls (left), layout of forming stand for the flexible roll forming (right)

The manufacturing of profiles with variable cross sections and constant flange heights needs for input pre-cut sheets. After uncoiling and straightening the band edges have to be cut in the manner illustrated in Figure 1. The pre-cut can be performed on the one hand by die cutting or on the other hand by more flexible processes like laser cutting or rolling knife. After the pre-cut unit the sheet enters the flexible roll forming devices. Here the conventional stands provide the feed of the strip. These can be used for forming constant sections as well. Besides the feed provided by the conventional forming stands, the forming rolls of the flexible stands can be driven if no constant sections are included in the profile. Changing profile geometries with different cross sections can be performed by change of the input file for the machine control.

Due to the geometrical conditions at the flexible roll forming a typical strain distribution along the profile flanges at the formed profile happens (Figure 3). Along the transition zone characteristic tensile and compression zones occur. Here are the critical areas for the process layout.

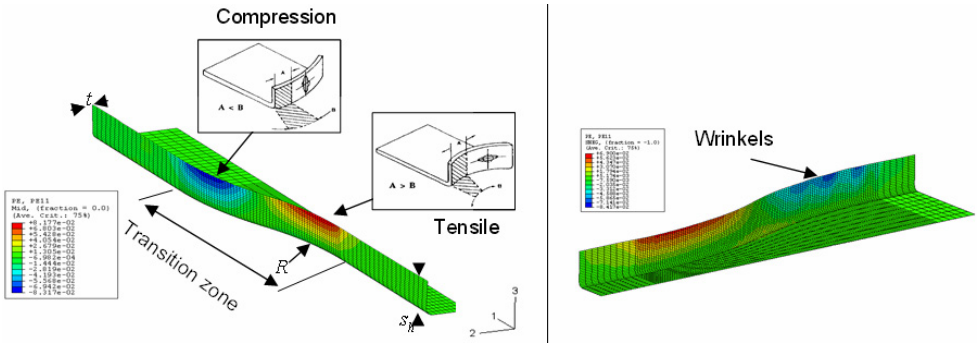

Fig. 3. Strain distribution (left) and wrinkles (right) at a flexible roll formed profile

The strain distribution in the compression zone is critical for the profile quality. At a certain parameter the combination of sheet thickness t, flange height h, contour radius R or material parameters, wrinkles can occur along the compression zone. Current investigations are dealing with the behaviour of the flexible roll formed profiles in the compression zone with the target to develop layout models for the quick design of profiles with variable cross sections. Results of these investigations are e.g. shown in [3].

3. Increasing the dimensional accuracy

The remarkable increase of the utilization of roll-formed structures of high and ultra-high-strength steel in modern car bodies strongly raised the meaning of dimensional accuracy for profiles. Fulfilling the requested dimensional accuracy and tolerances by manufacturing of these steels represent enormous difficulties. Furthermore, the dimension's deviation and the quality characteristics of the starting material are

also influencing factors. These are at the time even more distinctive in high-strength steels than in mild steel. It becomes noticeable especially with regard to the profile's dimensional accuracy.

In today's roll forming enterprises it is usual to control the dimensional tolerances as soon as the profile leaves the last forming stand randomly. This kind of quality control has the disadvantage that manufacturing errors of single rolls, e.g. errors in the bending sequence and the machine and tool alignment, are only detected very late [4]. The following corrective modifications are complex, expensive and very time-consuming. The requirements of modern vehicle structures can be fulfilled very restrictedly.

Continuous quality control and an active defined manipulation during the forming process promise a minimization of the reject rates and an achievement of close tolerances to reach the required dimensional accuracy. Thus, roll forming of high and ultra-high-strength steel can become a more reliable, productive and attractive process.

To attain this aim a vision of a roll forming line was developed, Figure 4. It consists of the conventional roll forming line, the measuring section with optical sensors used in order to measure the cross-section in real time and the controlled calibration stand. These components are linked together into a closed loop control system.

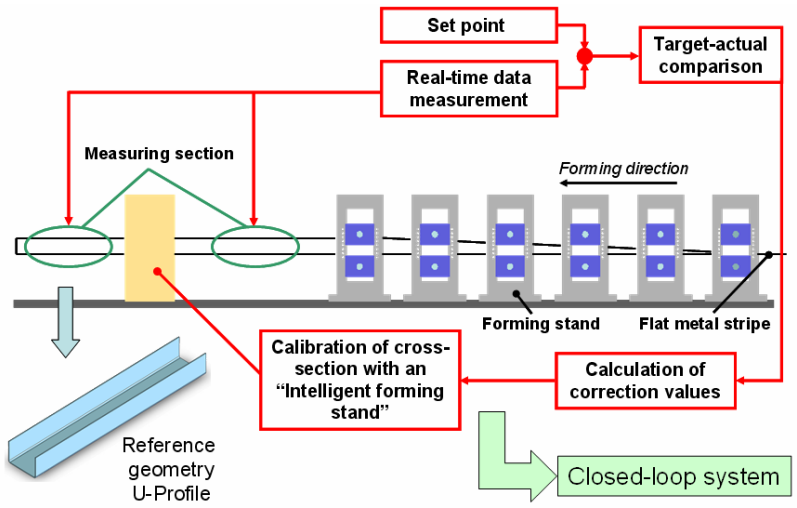

Fig. 4. Vision of a reliable roll-forming process

The roll forming line consists of the individual stands, which can be arbitrarily sequentially ordered in the roll forming process depending on the cross-section geometry. At the beginning of the process, a U-profile is roll-formed by feeding a flat strip of metal through the forming stands. After the profile has left the last forming stand, it has the possibility to spring back in the measuring section. Spring-back leads to a deviation of the target geometry. In the measuring section, optical sensors, based on the

laser split-beam method [5] are used for a real-time measurement of the cross-section (Figure 5). The sensors are positioned at the side below the profile, facing both the profile bottom and the profile side. Thereby the included angle can be determined, independently of a possible profile twist.

The measured values are processed in real-time during the forming process. The loop controller determines afterwards the necessary correction values steering the calibration stand to over-bend the roll-formed profile. With this closed-loop control close tolerances for the profile's bending angle can be achieved. With the calibration stand the deviations between the target and the measured angle α shall be reduced. The tool concept provides two side-rolls, a bottom roll and two inner rolls. The bottom roll is led and pivoted in the "Bottom roll device" (Figure 6). It has the task of supporting the profile's bottom and taking up the expected forces at the over-bending process. The kinematical principle of the angular infeed for the over-bending position of the "Rotating unit" in the "Side roll device" (Figure 6), should be led on a circular path around the sheet metal's bending centre, in order to guarantee an infinitely variable tool supported over-bending process. The angular infeed is carried out with the "Infeed device" (Figure 6). This unity consists of a propelled linear table and a steering rod, which works as an inverted crank mechanism together. The support of the inside bending radii is done with small thin rolls whose axes are fastened and pivoted by dowels and ball bearings in a closed frame ("Inner roll device").

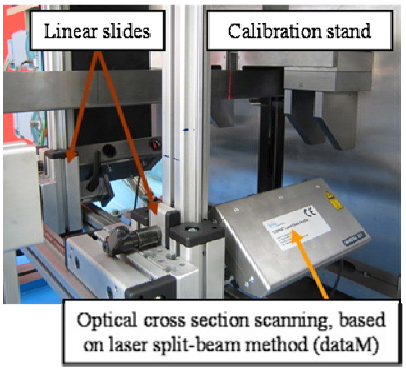

Fig. 5. Optical sensors for cross-section measurement

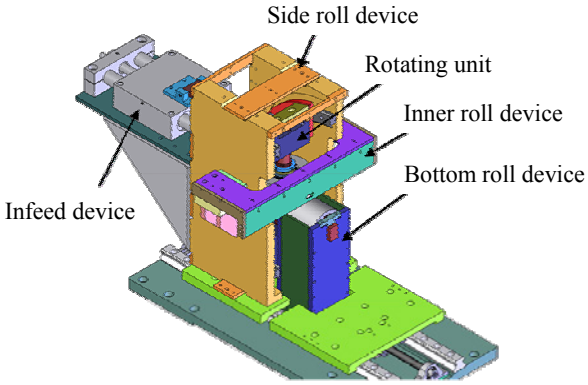

Fig. 6. Concept of the calibration stand

This concept offers the possibility of minimising the consequences of spring-back effects.

4. Cost-effectiveness of integrated manufacturing

Automotive structure parts in most cases are manufactured as pressed parts. At first are describing this process chain, where a closed profile with two flanges is used as

a sample part: The raw material comes from the receiving store to a cutting line in order to cut the blanks needed for the following forming process. Both stacks of blanks will be stored in an intermediate storage. The lower part of the profile will be transferred to the press batchwise in order to get the desired shape before being stacked again in an intermediate storage. After that the upper and the lower part have to be transported to the mounting device, where the parts are assembled and welded together.

In contrast to that an integrated roll forming line can be imagined to manufacture this profile continuously. Only one coil has to be fetched from the receiving store to feed the roll forming line. In that line the two flanges will be formed by linear flow splitting. Afterwards the profile will be formed by conventional stands and cut as you can see in Figure 7 [6].

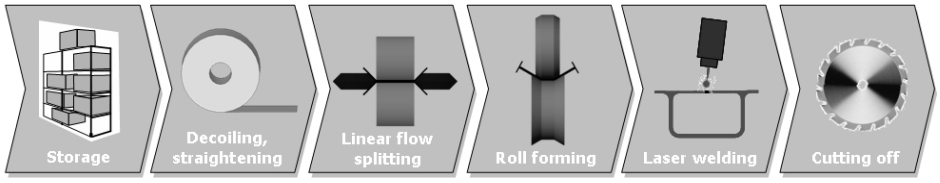

Fig. 7. Continuous manufacturing integrating flow splitting and roll forming

Comparing these two process chains described above the different number of operations is obvious. The conventional batch production of pressed parts demands a significant number of intermediate storages as well as the related transportation, among others caused by different cycle times. Continuous process flows can lead to a significant reduction of lead time, capital lockup and handling/transportation processes. This approach to reduce waste is one of the cores of the Toyota Production System [7, 8]. On the other hand continuous process flows are often very complex leading to high investments as well as a higher risk of a breakdown of the production line.

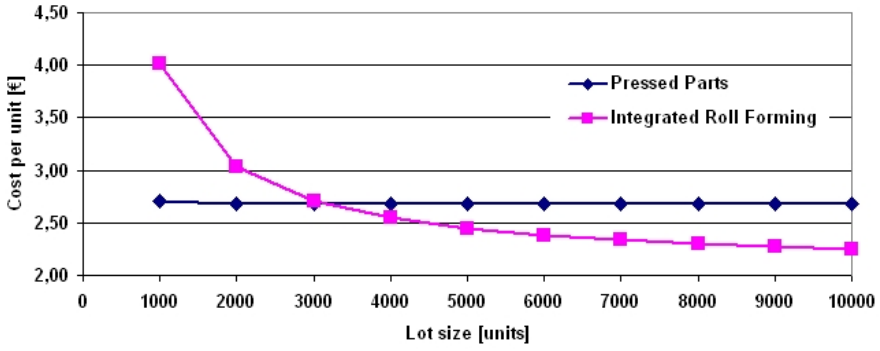

Fig. 8. Comparison of the manufacturing chains

For the sample part mentioned above comparisons of the overall cost-effectiveness based on activity-based costing of the described process chains have been conducted at the PtU (Figure 8). As long as the vision of the integrated process chain does only exist at a laboratory and not in industry, exact figures are not available. To cope with this, problem variations of the assumptions as well as a sensitivity analysis have been carried out. In the following some of the assumptions and the obtained results are listed:

- For longer parts (> 1 m) the output of the integrated line will be higher than the conventional process chain resulting in lower invest for the integrated line.
- Initially, downtimes of the integrated line have been assumed as double of the conventional process chain, set-up times even as six times higher. Both assumptions are very conservative and probably can be improved significantly when used in industrial scale.
- For larger lot sizes (approx. > 3000) the integrated process chain tends to be more cost-effective – even under the very conservative assumptions.
- By reducing downtimes and/or set-up times also the production of smaller lot sizes (approx. < 3000) will become cost effective.
- Labour costs can be considered as more influencing the costs of intermediate storages than capital lockup or expenses for storage space.
- The integrated line is more independent from low labour cost countries as material costs and manufacturing resources represent the highest portions of costs (90% vs. 81%).

Summing up, it can be stated that integrated manufacturing of roll forming profiles in the future will be a lean manufacturing system which can prove its competitiveness in high labour cost countries like Europe.

Acknowledgement

The author thanks the DFG for funding the Collaborative Research Center 666 “Integral sheet metal design with higher order bifurcations – Development, Production, Evaluation” (CRC 666). The investigations presented in chapter 4 were carried out within the research subproject B4 of CRC 666. Furthermore the author thanks the DFG for funding the project GR1818/22-1 – “Auslegungsalgorithmen für „flexible“ Walzprofilierprozesse”.

References

[1] Autorenkollektiv: *New Steel Body*, Thyssen-Krupp, 2003.

[2] Groche, P., Zettler, A.: *Flexibles Profilieren für Leicht“BAU“anwendungen*, In: thema FORSCHUNG 1/2006, Verlag für Marketing und Kommunikation, Monsheim, pp. 26–29.

[3] Groche, P., Zettler, A.: *Analytic one-step-model for the design of flexible roll-formed parts* (Reviewed). In: Production Engineering, Annals of the WGP, Vol. XIII/2, Hannover, 10/2006, ISBN 3-9807670-9-4, pp. 149–152.

[4] Jacob, A., Flaxa, V., Freier, K.: *Karosserieleichtbau und die umfassende Verwendung höherfester Stähle*, In Neugebauer, R. (Hrsg.): „Leichtbau durch Umformtechnik", Tagungsband der 7, Sächsischen Fachtagung Umformtechnik, 2000, pp. 119–143.
[5] data M Engineering GmbH: COPRA ® ProfileCheck, http://www.roll-design.com/de/COPRA-Profilchecker.htm, Juli, 2007.
[6] Groche, P., Walter, M., Ringler, J., Munirathnam, M.: *Flexible Prozessketten für Mehrkammerprofile aus Blech*, In: wt Werkstattstechnik online, Düsseldorf: Springer-VDI-Verlag, 10/2006, pp. 733–739.
[7] Ohno, T.: *Das Toyota-Produktionssystem*, Campus-Verlag, Frankfurt/Main, 1993.
[8] Liker, J.K.: *Der Toyota-Weg: 14 Managementprinzipien des weltweit erfolgreichsten Automobilkonzerns*, FinanzBuch-Verlag, München, 2006.

Walcowane na zimno elementy konstrukcyjne pojazdu

Karoserie samochodowe są zwykle budowane jako konstrukcje samonośne. Ostatnie badania wykazały duże korzyści wynikające z zastosowania walcowania na zimno kształtowników w produkcji karoserii samochodów, m. in. w celu zmniejszenia wagi. Sukces tych komponentów z jednej strony będzie zależał od technologicznej wykonalności a z drugiej strony od opłacalności procesu. W artykule zaprezentowano obiecujące podejścia, które mogą pomóc zwiększyć znaczenie zastosowanie walcowania na zimno kształtowników w konstrukcjach samochodowych.

ARCHIVES OF CIVIL AND MECHANICAL ENGINEERING

Vol. VIII 2008 No. 2

The main aspects of precision forging

Z. GRONOSTAJSKI, M. HAWRYLUK
Wrocław University of Technology, Wybrzeże Wyspiańskiego 25, 50-370 Wrocław, Poland

The article concerns the directions of development the forging and problems with precision forging like tool and preform temperature, slug geometry, press settings, process speed, lubrication and cooling, and tool shape and quality. It was introduced the present state of knowledge as well as crucial problems of the technology. Suggestions solving these problems as well as researches carried out in Metal Forming Processes Department of Wroclaw University of Technology were presented.

Keywords: *closed die, precision forging, tool life*

1. Introduction

The main advantage of precision forging over conventional die forging is its lower (by as much as 60%) material consumption. This is owing to the lack of flash and to the fact that the end product has minimum machining allowances. The forgings generally have very good service properties. Because of its advantages, precision forging is the most popular technology for producing car parts from relatively expensive materials. Connecting rods, skew and straight bevel gears, worm gears, tripods, turbines, alternators, constant-velocity joints and so on (Figure 1) are manufactured in this way [1–6].

Fig. 1. Products manufactured by precision forging

Besides its obvious advantages, precision forging has some drawbacks of which the most serious one is the too short life of the forming tools, mainly dies, punches (Figure 2). The tools used in precision forging wear out long before the end of their expect life.

The life-span of the tools depends on the forging conditions, workmanship of staff, tools material, the shape of the preform and that of the slug, etc. The low durability of the tools lowers the quality of the forgings, in spite of their still control. The most common forging defect due to low tool durability are, i.e. shorts, laps, burrs, bends, cracks, delamination, micro- and macro-fractures and so on. This, in turn, affects the functionality of the final product made from the forging. Because of the large number and variety of factors (and their interactions) having an influence on precision forging the process is very difficult to analyze. Therefore a whole range of computer tools, such as CAD/CAM/CAE, mostly based on FEM and physical modelling, are used for the design, analysis and optimization of the forging process [2, 7–11].

Fig. 2. Most common defects of tools

2. Precision forging

In conventional precision forging the material is formed at ambient temperature or in semi-hot conditions. In the case of very complicated parts, a properly prepared charge is hot formed in isothermal conditions. Sometimes the super plasticity of the formed material is exploited. Initially, enclosed dies were used for forming [5, 12]. Thanks to the material savings and the lower costs of manufacturing products with enhanced properties at competitive prices, precision forging was increasingly applied to alloys of light materials such as aluminium, magnesium and titanium [10, 12].

The expression precision forging does not mean distinct forging process but rather approach to forging. The aim of this approach is to produce a net shape, or at least a near-net shape parts. Precision forging is sometimes described as close-tolerance forging to emphasize the aim of achieving required the dimensional and surface finish tolerances only after forging [13].

Precision forging at ambient temperature, i.e. cold forging, is preceded by making a slug in a few hot forging operations. In conventional hot forging in half dies a substantial amount of the material is lost for the flash and allowances. For this reason closed-die forging (often employing complex formation, i.e. forward and backward

extrusion) was adopted to make preforms for precision forging. Extrusion forging has this advantage that the stress is mostly triaxial compression whereby large deformations can be obtained without losing material cohesion. In addition, no die drafts are used in precision forming. The whole manufacturing process is generally divided into stages. As an example, the process of manufacturing a low-carbon steel product is shown in Figure 3.

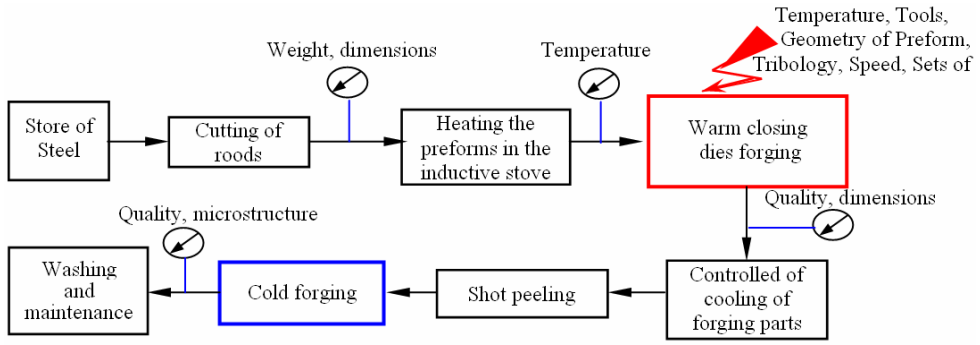

Fig. 3. Flowchart of precision forging process

Metal bundles are delivered from a storeroom to a machine which cuts the rods into pieces with specified dimensions and weight. Then the pieces are heated up to a temperature of about 900 °C in an induction furnace. A constant process temperature must be maintained in order to ensure high quality of the forgings. Preforms heated up to a proper temperature are fed into a press where they are formed in 2–5 operations. The dies are preheated to a temperature close to the operating temperature to reduce the risk of die cracking as a result of thermal shock (Figure 4a).

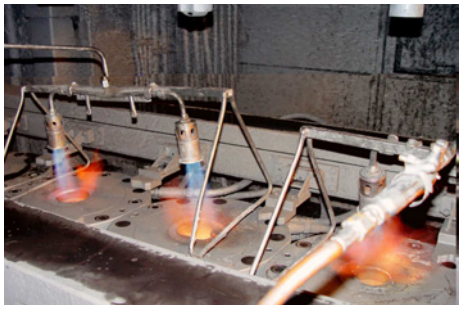

Fig. 4a. Dies are preheated

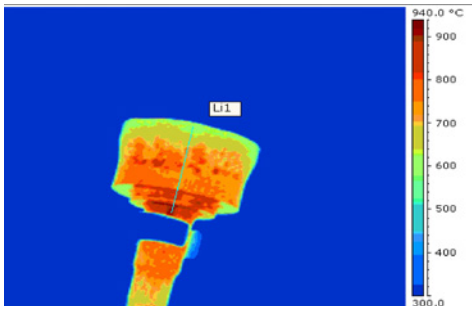

Fig. 4b. Measurement and control of forged object temperature

The forging process lasts only a few seconds. The stability of the process and control conducted according to plan ensure high quality of the forgings. When they leave

the press the forgings are subjected to controlled cooling (Figure 4b). Then they go to a shot peening machine where they are cleaned from graphite. The clean forgings go to cold working where they are oiled and cold formed. In this way the precise shape of the finished forged product is obtained. After cold forming the forgings are washed and greased.

3. Choice of process parameters

As shown above, each of the stages in the forging process is critical. Any shortcomings even at one of them may result in bad quality of the forged products, press jamming and production stoppages. Therefore the process specifications must be adhered to during production, which requires proper shopfloor customs and technical culture. For example, if the hot forging die is improperly lubricated and preheated and there is improper cooling during production, the die heats up excessively, which quickly results in its plastic deformation or thermal fatigue. In the available literature much attention is devoted to the design and optimization of the whole forging process or its key stages [2, 12–16]. Proper design of the particular process stages is the precondition for the optimization of forging parameters [3, 18]. Through the optimum choice of process parameters one may significantly increase the life of the tools and improve the quality of the forgings and consequently, increase the productivity of the whole process. The main factors having an effect on the process of forging are: tool and preform temperature, slug geometry, press settings, process speed, lubrication and cooling, and tool shape and quality.

3.1. Tool and preform temperature

Proper temperature is critical for the reliable operation of the tools. It can affect the die's narrow tolerance zones and the small spaces between the moving parts and the fixed parts of the tools. As a result of thermal expansion the clearance may decrease and the tool components may lock up. Also the thermal expansion of the die affects the quality of the forgings. Numerical simulations of the forging of CV joints showed large temperature differences in the die in the contact area, whereas already at a depth of about 5 mm from the die's inner surface the temperatures are much lower (Figure 5a). So large temperature gradients may adversely affect the state of stress inside the tools. This means that the temperature of the tools needs to be monitored, for example, by a thermovision camera (Figure 5b).

An equally important parameter is the temperature of the slug since it has an effect on the forged object's microstructure and its material flow curve (its formability) and through thermal expansion it causes a change in the slug volume. The temperature distribution in slugs (Figure 6) for different preform diameters was examined in [8]. The initial temperature of the preforms was 920 °C. Then the specimens were cooled for 2 s at a temperature of 50 °C in the press chamber as they were waiting to be

forged. In spite of such a short cooling time the temperature difference in the outer layers amounted to about 50 °C. This can have a significant effect on the forging process.

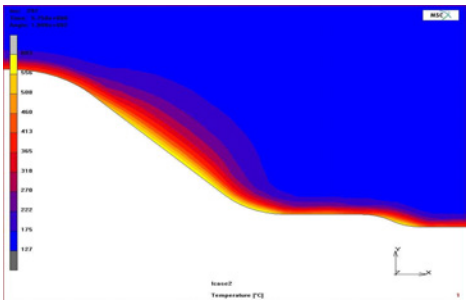

Fig. 5a. Die thermal field distribution determined by FEM [8]

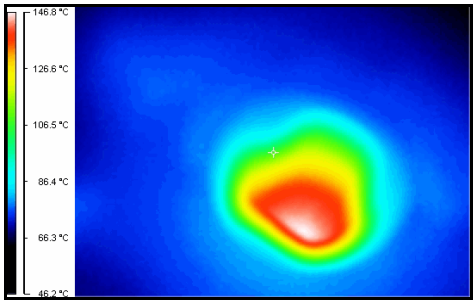

Fig. 5b. Thermovision camera photograph of die

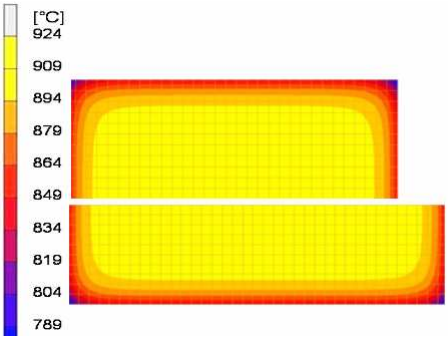

Fig. 6. Temperature field distribution in slugs after 2 s long cooling at temperature of about 50 °C in press chamber [8]

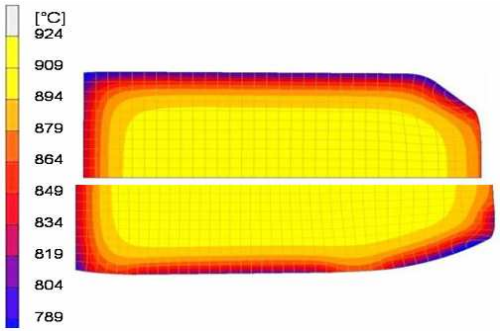

Fig. 7. Temperature field distribution in slugs after 1st forging operation (about 4.5 s) [8]

3.2. Slug geometry

In precision forging there is no flash gap and the charge material volume must be the same as that of the finished part. The allowable differences in mass can amount to 0.5–1%, the angle deviation in the cutting zone to 0.5–2° and the roundness deviation to 2 and 6%. This can be achieved by using special cutting. It is necessary to maintain so narrow tolerances for the preform in order to ensure high quality of the forged product. A too large slug volume may result in damage to the die or the press. During multioperation forging in closed dies proper distribution of slug material volume and slug preparation through upsetting are critical for the proper filling of the die cavity. There exists a notion of an ideal metal body of revolution with appropriately distrib-

uted material masses. Therefore the design of preforms and slugs in forging processes is an important activity aimed at improving product quality and reducing production costs [1, 3, 11]. The preform's shape and mechanical properties will affect the friction conditions at the die/slug interface while its geometry will have an effect on the die and the slug.

In [8] it was shown that the preform's initial dimensions have an effect on temperature distribution. It was found that a larger drop in temperature occurs in a slenderer slug since the surface of contact with the tools is then larger (Figure 7).

3.3. Process speed

Precision Forging processes are usually conducted at high speeds. Currently, tendencies of increasing the speed are dictated by economic reasons. The faster the forging process, the higher the productivity. As many as 30 forgings per minute can be produced in multioperation hot forging in closed dies in crank presses. [7]. The time in which a single forming operation is performed in industrial precision forging is about 0.2 to 1 second. Hence, as mentioned in pt. 3.1, it is so critical to ensure a constant preform temperature (Figures 6–7). Currently attempts are made to maximally utilize the capacity of the forming machines and to reduce the number of forging operations. If the number of strokes during forging is too large, the whole time increases and so do the costs [1]. But the higher the speed of a single operation, the higher the deformation resistance and the greater the required forming forces.

3.4. Press settings

The settings of the forming machines are an important factor affecting the forging process. The main settings include:

Press workspace. The precision forging process and tools require that the tool workspace between the anvil and the press slide should be sufficiently large for the whole system of tools, including the auxiliary components. Moreover, the cooling and lubricating equipment should be integrated with the press.

Constant forging energy. Constant press energy is critical for reproducibility in precision forging in every stroke. Especially, when speed is increased during redesign a new forging process. Excessive energy causes an increase in the pressure inside the die, which may result in the elastic deformation of some tools (such as punches and counterpunches) and ultimately lead to an elastic rebound of the tool. Elastic deformations of tool components should be avoided since they can cause changes in geometry during forging.

Precision guidance of tool components. Precision guidance of the punch is required when the die is closed by the upper punch during forging. The gap between the punch and the die is usually smaller than 0.1 mm in order to avoid a material flash. Moreover, accurate positioning of tool components is necessary to obtain proper forged product geometry.

Accurate positioning of slug inside die. In order to ensure proper die cavity filling the slug must be accurately positioned inside the die, especially when the slug is automatically delivered to the successive forging stations. Using physical modelling to analyze the flow of material it was found in [9] that too slender specimens, incorrectly positioned in the die impression, would undergo buckling. Despite the buckling, the forged object had the correct shape, but the uneven flow of material may affect the durability of the end product (Figure 8).

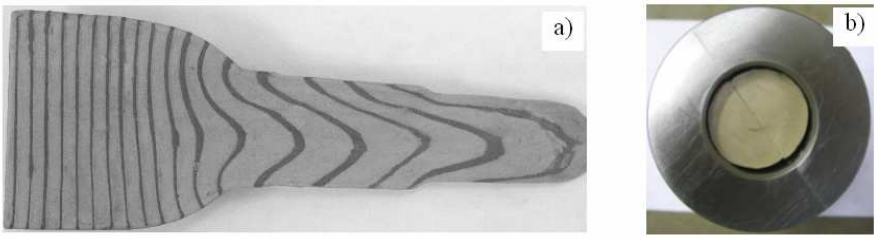

Fig. 8. Uneven flow of material caused by specimen buckling:
a) cross section and b) view from punch

Reliable die closure. Die closure is essential for the proper operation of the set of tools at the machine settings. For many precision forged products the split line lies in the vicinity of the work surfaces and so they may be deformed at improper closure. The die should be closed by accessory elements or simultaneously with the motion of the punches.

3.5. Lubrication and cooling

To a large extent the correctness of forming process depends on the lubricant used. The latter is used to both lubricate and cool. The lubricant should be characterized by a high flash point (so that it does not lose its tribological properties at high temperatures), low heat conduction (to prevent the object being forged from cooling down and the tool from overheating), proper viscosity at the operating temperature and a low coefficient of friction. Moreover, an optimum lubricant should not contain any components having an adverse effect on the process [19]. Graphite, teflon, glass and other substances as well as intermediate metallic layers characterized by low flow stress are usually used in hot forging.

In order to ensure healthier working conditions in the forging industry and minimize its environmental impact as well as to increase the life of the tools, the European Community has recently funded an industry research project called Brite-Euram aimed at developing environmentally friendly systems of tool lubrication (based on lubricants with optimum lubricating properties) for the warm forging of steel and to promote a wide use of forging with a smaller pollutant burden, better working conditions and higher productivity [19]. It was found that in most hot forging processes no proper

tribological conditions were ensured. This is mainly due to the high contact pressures and metal surface gains typical for hot forging, especially forward and backward extrusion forging. In all the cases it is necessary to provide additional lubrication in the form of lubricating film on slugs. Thanks to the project a comprehensive tool lubrication system has been developed. As regards the environmental impact and tool life, the best results have been achieved through the use of tool lubrication systems consisting of a graphite-based slug lubricating film and graphite-free oil greases for dies.

3.6. Tools

The choice of a tool material is a very difficult task for designers and process engineers. The life of a tool and its suitability for production depend on many factors which often have opposing consequences. So far there are no clear-cut criteria for selecting tool materials and to a large extent one must rely on the experience of the manufactures and tool users. Statistical data provided by different tool manufacturers indicate the most common causes of tool failures to be: tool fatigue cracking in cold working and excessive abrasive wear, material plastic flow and thermal fatigue in hot working [20]. The worst situation is in warm working since each of the phenomena can be equally critical. In such conditions the tools must withstand high pressures (as in cold working) and at the same time must be made of heat resistant materials (as in hot working). According to Lange et al. [21], the life of a tool at high forging temperatures depends on wear in over 70% of cases. Therefore tool materials, their heat treatment and machining and tool design and fabrication accuracy must meet very high requirements. Tool materials should be characterized by hardness in a range of 50–55 HRC (considerably higher than that of the forged product), good hardenability, high tensile strength, high impact strength and low abrasibility.

Currently, warm- and hot-work tool steels: WCL, WWV, WNLV, which are characterized by very good mechanical properties (high tensile strength, high hardness, high abrasion resistance, high yield point – 2200 MPa) are quite popular tool materials. Also other alternative tool materials are considered. Moreover, special treatment, such as nitriding, surface coating and laser silicon carbide surface alloying, etc., can significantly reduce the abrasive wear and increase the hardiness of the tool materials, particularly of their surface layer [24].

4. Heat treatment

Heat treatment has a decisive effect on tool life. Figure 9 shows a heat treatment diagram for a hot-work tool steel.

For instance, cracks which appear on the surface of a ground tool made of tool steel can be caused by improper tempering or by overheating during austenitizing. Such heat treatment faults can limit the possibilities of grinding the tool, even if proper precautions are taken.

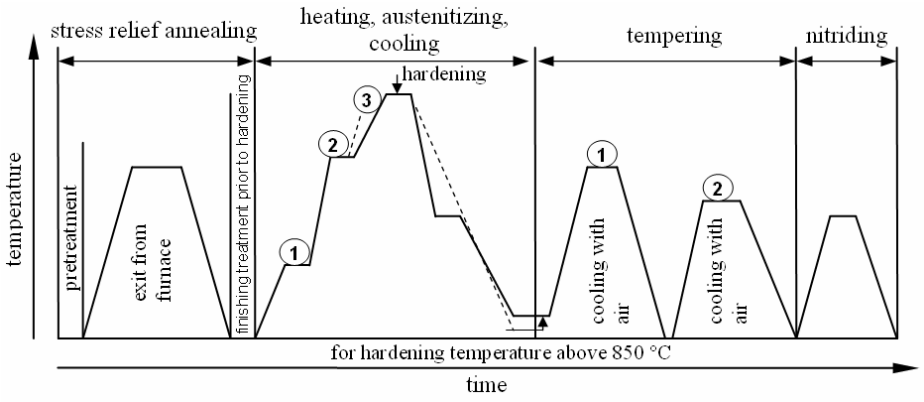

Fig. 9. Exemplary tool material heat treatment diagram

Stress relief annealing. Tool steels are usually delivered annealed; further treatment is done by the user or in toolrooms. The treatment causes stresses to arise, which during heating up to the hardening temperature are released and cause, among others, changes in the dimensions. Therefore tools which must meet high requirements for retaining their dimensions should be annealed after mechanical pretreatment (before the final treatment).

Hardening. It is impossible for steels subjected to hardening to ideally fully retain their dimensions. A change in the structure (from the annealed-state structure to the structure after hardening) means an increase in the volume, which as a result of tempering that follows is again reduced but not restored to the annealed-state volume. Because of buckling it is recommended to use the gentlest possible cooling medium and to perform intermediate cooling at 900 °C for steels whose hardening temperature is above 900 °C. Since there is a risk of strain cracking one should avoid cooling the tools to room temperature. The latter are usually cooled down to about 150 °C. Then at a temperature of about 100–150 °C equalization takes place aimed at eliminating the differences in temperature and structure between the surface and the core. Quenching in a hot bath and in vacuum (as a hot bath simulation) for hot-work tool steels has proved to be effective.

Austenitizing (keeping at hardening temperature). The hardening temperatures specified by the manufacturers should be adhered strictly to. If the hardening temperature is too low, the increase in hardness is insufficient. If it is too high, it results in brittleness, increased grain size, a risk of cracks and so on. Also soaking times are important. An approximate soaking time for hot-work tool steel is 0.5 min per 1 mm of thickness.

Tempering. Immediately after hardening, steel is tempered several times. The aim is to remove any stresses which arose during hardening and to reduce the often too high postcooling hardness in favour of shock resistance. Depending on the desired hardness, a tempering temperature should be chosen in accordance with the proper

tempering diagram. It is reported in [7] that triple tempering gives the best results in the case tool steel W303.

Machining. In order to increase tool life, die cavities and punch work surfaces should be made appropriately smooth. During forging the heated up material rubs against tool work surfaces and abrades them. The degree of abrasion can be reduced through the use of a proper material, but this will not replace finishing consisting in grinding and planishing of the work surfaces. One should note that during such working the tool surface is often overheated and weakened as a result. In some cases, the tempering temperature of the tool steel may be exceeded by overheating. Machining may cause microcracks to appear in the tool. The microcracks will grow during work and result in a premature fracture.

Thermochemical treatment. Sometimes as a result of prolonged operation of the tools at a high temperature the tool material suffers thermomechanical fatigue and its properties sharply deteriorate, whereby its elastic limit is exceeded or the metal spontaneously heats up. Then nitriding is applied to increase the life of the tools by increasing their surface hardness and abrasive wear resistance. The treatment can be applied several times.

5. Optimum die profile

One of the main parameters having an influence on the forging process is the shape of the adopted die. The magnitude of deformation obtainable in a single operation is limited not by material decohesion (cracks) but by material strength (too large hoop stresses). For this reason, instead of producing a forging in one operation, multioperation industrial precision forging is used. Still this does not sufficiently reduce the great forming forces and thereby the wear of the tools.

Die shape optimization receives much attention in the literature [2, 4, 11–15, 22]. It turns out that one of the ways of reducing excessive pressures on the die or the punch is the choice of an optimum die profile (outline). Three types of die profile: streamline, curvilinear and conical are generally used in industrial applications. In forward extrusion the streamline profile ensures the smallest excessive deformation, the smallest extrusion forces and the least deformation inhomogeneity in the cross section. But the problem is with determining the correct profile and fabricating it (the profile is usually to long time). For this reason the profile is often replaced by any curvilinear outline, which often leads to even worse results than when conical profile dies are used. A conical profile, with an angle minimizing excessive deformations, may result in good extrusion parameters and good product quality and it can be very easily made.

Today research on die profile optimization aimed at improving product quality and productivity combines classical mathematical optimization methods with FEM. The die profile optimization problem can be solved by applying one of the mathematical programming methods [18]. Usually Bézier curves and other specially adapted optimization methods are employed to mathematically describe die profiles. Ales and Boris

[12] investigated tool design optimization for stationary extrusion by imposing two-criterion optimization. Wife et al. [16] proposed a special incremental computing method combined with FEM in order to obtain the distribution of pressure on the die walls (for the adopted die profile) during the hot extrusion of a bar. Thanks to studies of optimum die profiles by Lee et al. [18] a more uniform structure of hot forged products can be obtained. In [4] the die profile was optimized by sequential quadratic programming (SQP) which is now successfully applied to solve nonlinear optimization problems.

The present authors et al. in [8] assessed the flow of material in arch and conical dies for forging CV joint tulips.

CV joints are irreplaceable components of front-wheel drive cars. They transmit torque from the gearbox to the front wheels. Their production has been steadily increasing in recent years. A CV joint consists of a spider, a race and a casing. The most difficult to manufacture is the casing, the more so that because of its irregular shape machining is made very difficult. Currently hot and cold multioperation forging in closed dies with a complex formation scheme (forward and backward extrusion) is used in long-run production. The authors employed both physical modelling, using soft modelling materials (synthetic filia wax and Plasticine), and numerical modelling by means of the MSC software package to study material flows. A macroscopic analysis revealed differences in the flow of material in the particular tools. In the case of arch tools the material flow in the specimen's cross section is more uniform than when for conical tools (Figure 10). This is confirmed by the fact that the mesh line curves for the object forged in the arch die are less elongated than the ones for the object forged in the conical die ($L_a < L_b$).

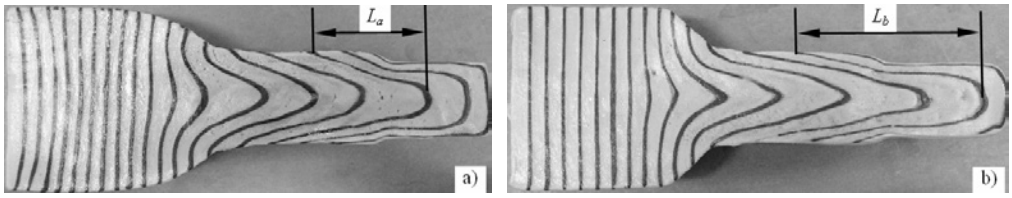

Fig. 10. Comparison of model material flow in: a) arched tools and b) conical tools [8]

The investigations showed that the material flow in the arched dies was more uniform than in the conical dies, whereby the distribution of strains was more uniform too (Figure 11). In addition, the punch forces were smaller for the arched dies.

Figure 12 shows a vector distribution of unit pressures for the tools, obtained by means of the SuperForm2005 software. The unit pressures at the first reduction stage were similar for the two kinds of dies, but at the next stages they were much higher for the conical die.

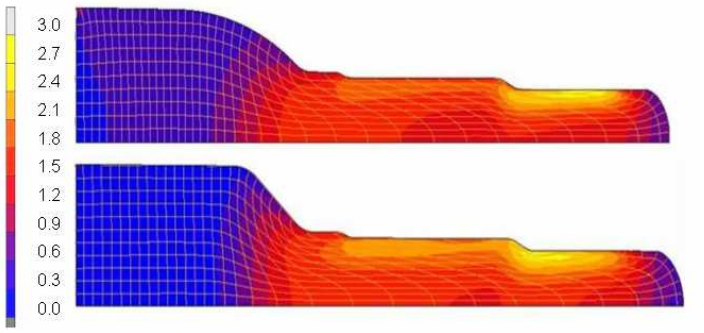

Fig. 11. Distribution of plastic strains in: a) arched tools and b) conical tools [8]

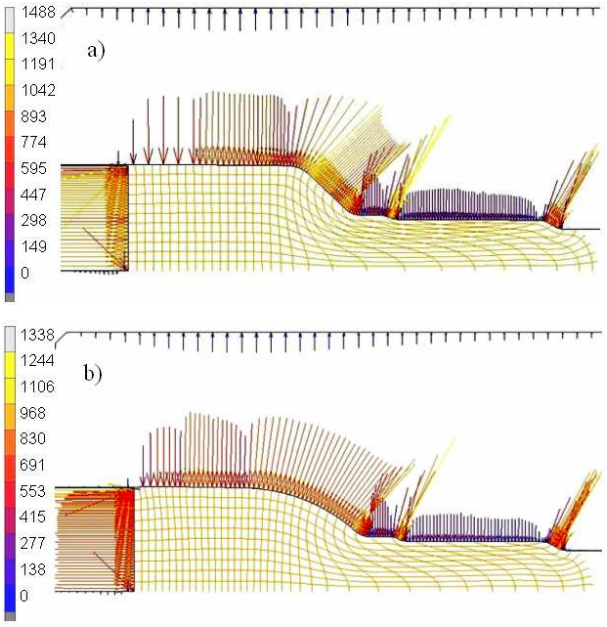

Fig. 12. Vector distribution of unit pressures in: a) conical, b) arched tools [8]

6. Die design

Currently, in order to increase the crack resistance of precision forging tools, pre-stressed dies (i.e. reinforced with a single concentric ring or a larger number of such rings with thermo-compression or forced-in joints in-between) are used. It turns out that by changing the state of stress one can significantly reduce tool cracking [7]. The application of an appropriately high pre-stress (compressive hoop stress) during assembly should compensate for the very high tensile hoop stresses which occur during forging.

The present authors et al. analyzed (using numerical modelling and actual negative allowance measurements) the effect of negative allowance in pre-stressed dies (used in the production of the CV joint casing) on their strain [7].

Numerical modelling was done using the MSC Marc2005 and Super Form 2005 software. It was carried out in two stages: 1) forcing of a compensation ring together with a die onto an elastic sleeve and 2) actual forging based on the first-stage conditions. Figure 12 shows the analyzed set of tools. The function of the compensating ring is to pre-stress the die via the slit elastic sleeve.

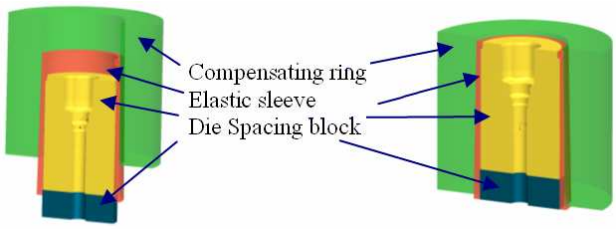

Fig. 12. Schematic of die prestressed by single ring [0]

The nominal negative allowance was w_{nom} = 0.4 mm. But it was found that the actual negative allowance depended on the tools' dimensions determined by their tolerances and wear.

From the field of execution tolerances for the particular tool system components it followed that the negative allowance could range from w_{min} = 0.225 mm to w_{max} = 0.45 mm. Hence one could assume that the expected average negative allowance would be w_{av} = 0.34 mm, i.e. much less than the nominal negative allowance.

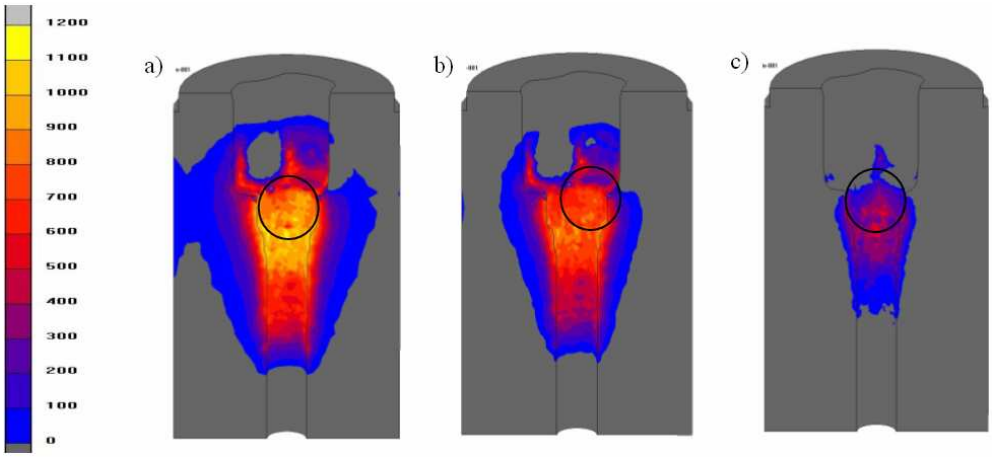

Fig. 13. Distributions of hoop stress in die during forging at negative allowance:
a) w = 0.25, b) w = 0.4, c) w = 0.7 mm [7]

The aim of the research was to determine how the change in negative allowance (resulting from the tolerance fields) can affect the strain of the dies during forging. A negative allowance of 0.25 mm (close to the minimum negative allowance), the nominal negative allowance of 0.4 mm and an increased negative allowance of 0.7 mm were analyzed. Figure 13 shows hoop tensile stress distributions for the different negative allowance values. The maximum hoop stresses occur at the second reduction stage (the circle marks this place).

The hoop tensile stresses at a negative allowance of 0.25 mm are very high, amounting to 1000 MPa. This means that at such low negative allowances the dies may quickly fail.

Then reduced stresses were analyzed. Figure 14 shows reduced stress (von Misses stress) distributions for the assumed negative allowances.

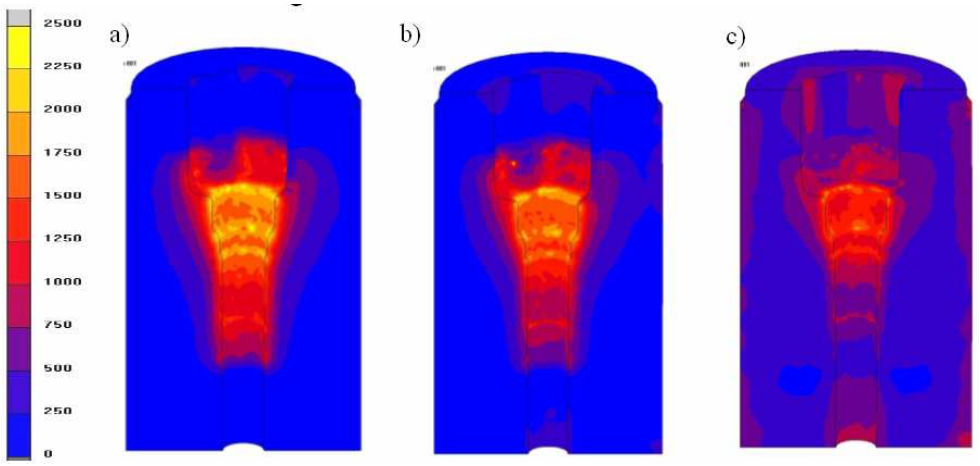

Fig. 14. Distributions of von Mises stress in die during forging at negative allowance: a) $w = 0.25$, b) $w = 0.4$, c) $w = 0.7$ mm [7]

Figure 15 shows the dependence between reduced stress in the most heavily loaded places (the first stage of cross section reduction) and negative allowance. Even though all the flow stress values are below the yield point of the die material, the smallest negative allowance of 0.25 mm may be too small since in the places where the die is most heavily loaded the temperature significantly rises. As a result, the yield point in those areas may go down to below 2000 MPa. In real experiments, plastic flow of die material would be observed at the first stage of reduction. The analysis showed that a negative allowance below 0.4 mm did not ensure sufficient pre-stressing of the dies. This was confirmed by observations of the real process. It was found that the wear of the compensating ring and that of the elastic sleeve and a wide range of execution tolerances of the tools may result in an allowance much smaller than 0.4 mm.

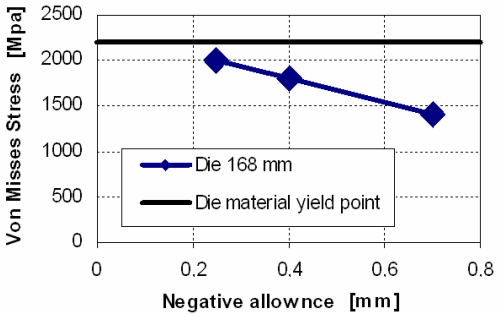

Fig. 15. Reduced stress versus negative allowance at forging stage [7]

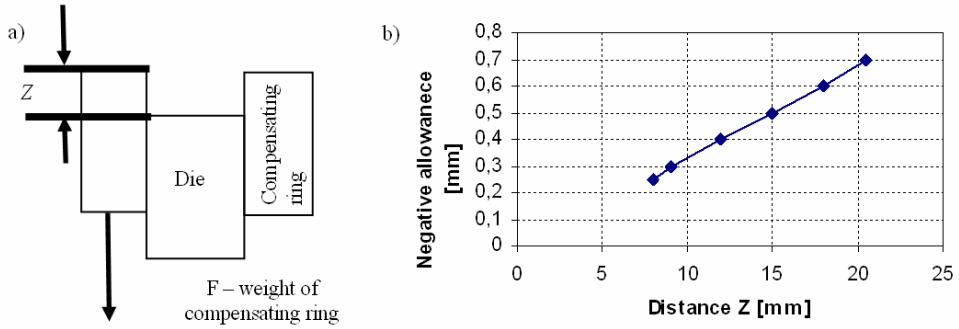

Fig. 16. a) Method of measuring distance "*Z*" and
b) Relation between distance "*Z*" and negative allowance [7]

Therefore it is necessary to control negative allowance when the die is forced into the compensating ring. For this purpose a simple indirect method of determining negative allowance, i.e. on the basis of the distance between the upper surface of the die and the upper surface of the compensating ring forced into the die by the force of gravity (Figure 16a), is proposed. It has been found that if this distance is larger than 15 mm, the negative allowance is larger than 0.4 mm. Figure 16b shows the relation between distance "*Z*" and negative allowance, which allows one to determine the negative allowance value in a simple way during the assembly of the tools.

7. Conclusion

The growing market demand, particularly from the automotive industry, has led to very intensive development of precision forging. Its advantage over other technologies is that it offers considerable material savings owing to the fact that there is no flash and that the end product is almost finished whereby finishing is not needed or reduced to minimum. Currently, precision forging is used mainly as multi-operation industrial

forging to manufacture CV joint tulips, gear wheels, connecting rods and so on. However, it is not a perfect technology yet, as indicated here. Its main drawback is the too quick wear of the forming tools. The life of the tools depends mainly on: the conditions in which forging takes place, the design and workmanship of the tools, their heat treatment proper for the selected tool material, the shape of the pre-form and slug, etc.

The large number and variety of factors having a bearing on the process of precision forging as well as their interactions make analysis of this process difficult. Therefore several CAD/CAM/CAE tools, mostly based on FEM and physical modelling, are used to analyze and optimize the forging process.

The continuous development of the precision forging technology should result in solutions to the problems presented here as well as in higher product quality and productivity.

Acknowledge

The licences of programmes in article were used the MSC. The MARC as well as ProEngineer of Wrocław Centre for Networking and Supercomputing.

References

[1] Bariani P.F., Bruschi S., Dal Negro T.: *Integrating physical and numerical simulation techniques to design the hot forging process of stainless steel turbine blades*, International Journal of Machine Tools & Manufacture, 44, 2004, pp. 945–951.
[2] Doege E., Bohnsack R.: *Closed die technologies for hot forging*, Journal of Materials Processing Technology, 98, 2000, pp. 165–170.
[3] Lin S. Y., Lin F. C: *Influences of the geometrical conditions of die and workpiece on the barreling formation during forging–extrusion process*, Journal of Materials Processing Technology, 140, 2003, pp. 54–58.
[4] Lin Zou, Juchen Xia, Xinyun Wang, Guoan Hu: *Optimization of die profile for improving die life in the hot extrusion process*, Journal of Materials Processing Technology, 142, 2003, pp. 659–664.
[5] Osakada K., Wang X., Hanami S.: *Precision forging process with axially driven container*, Journal of Materials Processing Technology, 71, 1997, pp. 105–112.
[6] Strona internetowa http://www.gkndriveline.com.
[7] Gronostajski Z., Hawryluk M., Niechajowicz A., Polak S., Walczak S., Wodniak A.: *Określenie zmian konstrukcyjnych i montażowych matryc stosowanych do kucia przegubów homokinetycznych w celu podniesienia trwałości narzędzi*, KomPlasTech 2008, pp. 35–44.
[8] Gronostajski Z., Hawryluk M., Jaśkiewicz K., Niechajowicz A., Polak S., Walczak S., Wodniak A.: *Application of physical and mathematical modelling to analysis of different forging processes of constant velocity joint body*, Computer Methods In Materiale Scence, 7, No. 2, 2007, pp. 231–236.

[9] Hawryluk M.: *Modelowanie fizyczne procesu kucia obudowy korpusu przegubu homokinetycznego przy zastosowaniu matryc łukowych oraz stożkowych*, FiMM 2005, pp. 133–138.
[10] Siegert K., Kammerer M., Keppler-Ott Th., Ringhand D.: *Recent developments on high precision forging of aluminum and steel*, Journal of Materials Processing Technology, 71, 1997, pp. 91–99.
[11] Vazquez V., Altan T.: *Die design for flashless forging of complex parts*, Journal of Materials Processing Technology, 98, 2000, pp. 81–89.
[12] Yoshimura Hyoji, Tanaka Katsuhisa: *Precision forging of aluminum and steel*, Journal of Materials Processing Technology, 98, 2000, pp. 196–204.
[13] ASM Metals Handbook Volume 14, *Forming and Forging*, pp. 337–338.
[14] Ales M., Boris S.: *Tool design optimization in extrusion process*, Comput. Struct., 68, 1998, pp. 283–293.
[15] Vazquez V., Altan T.: *New concepts in die design — physical and computer modeling applications*, J. of Mat. Proc. Techn., 98, 2000, pp. 212–223.
[16] Wifi A.S., Shatla M.N., Abdel-Hamid A.: *An optimum-curved die profile for hot forward rod extrusion process*, J. Mater. Process. Technol., 73, 1998, pp. 97–107.
[17] Bariani P.F., Dal Negro T., Fioretti M.: *Joint use of physical and numerical simulation techniques in predicting process parameters evolution and microstructure in forging Nimonic 80A turbine blades*, Proceedings of the 2nd Esaform, Guimares, Portugal, 1999.
[18] Lee S.K., Ko D.C., Kim B.M..: *Optimal die profile design for uniform microstructure in hot extrusion product*, Int. J. Mach. Tool Manuf., 40, 2000, pp. 1457–1478.
[19] Sheljaskow S.: *Tool lubrication systems in warm forging*, Journal of Materials Processing Technology, 113, 2001, pp. 16–21.
[20] Kocańda A.: *Określenie trwałości narzędzia w obróbce plastycznej metali, rozdział w monografii pt. Informatyka w Technologii Metali*, red. A. Piela, F. Grosman, J. Kusiek, M. Pietrzyk, Wydawnictwo Politechniki Śląskiej, Gliwice, 2003, pp. 213–256.
[21] Cser L., Geiger M., Lange K.: *Tool life and tool quality in bulk metal forming*, Proc. Inst. Mech. Eng., 207, 1993, pp. 223–239.
[22] Byon S.M., Hwang S.M.: *Die shape optimal design in cold and hot extrusion*, Journal of Materials Processing Technology, 138, 2003, pp. 316–324.
[23] Bin Y.: *The Optimal Design and Computer Program*, Haerbing University of Technology Publishing Company, 1991 (in Chinese).
[24] Bonek M.: *Struktura i własności warstw wierzchnich uzyskanych w wyniku obróbki laserowej stali narzędziowej stopowej do pracy na gorąco*, Biblioteka Główna Politechniki Śląskiej, Gliwice, 2003.

Najważniejsze zagadnienia dotyczące kucia precyzyjnego

Artykuł dotyczy kierunków rozwoju kuźnictwa i problemów związanych z kuciem na gorąco gotowych lub prawie gotowych wyrobów. W pracy przedstawiono obecny stan wiedzy oraz zwrócono uwagę na problemy kluczowe. Zaprezentowano rozwiązywania tych problemów oraz badania prowadzone z tego obszaru w Zakładzie Inżynierii Procesów Kształtowania Plastycznego Politechnik Wrocławskiej.

ARCHIVES OF CIVIL AND MECHANICAL ENGINEERING

Vol. VIII 2008 No. 2

Quasi-static and dynamic deformation of double-hat thin-walled elements of vehicle controlled body crushing zones joined by clinching

Z. GRONOSTAJSKI, S. POLAK
Wrocław University of Technology, Wybrzeże Wyspiańskiego 25, 50-370 Wrocław, Poland

A controlled body crushing zones are of considerable interest to automotive industry. The most popular technique of joining deformable zone components is spot welding. This paper presents a new technique of joining these elements using a metal forming process called clinching. Two methods of clinching: round press joining (RPJ) and square press joining (SPJ) are considered. Quasi – static and dynamic crushing tests of thin-walled specimens joined by clinching were carried out. The results show that clinch joining could be applied in controlled body crushing zones.

Keywords: *controlled body crushing zones, thin-walled section, clinching*

1. Introduction

Continuous increase in car user's requirements for better passive safety causes the search for lighter and more efficient energy absorbing components. Various kinds of the thin – walled sections are most popular parts of a controlled body crushing zones. There are numerous researches, both experimental and theoretical, into the ability to absorb kinetic energy by the profiles [1, 2]. The elements have different cross-sections like circular, square, polygonal, top-hat and double-hat. The last two are mainly researched due to their possibility of application in construction of body car. A review of literature shows that a lot of study the energy absorption capacity of thin-walled sections with variations in the yield strength, sheet thickness, flange width and method of joining were performed [3].

The most important crashworthy parameter is the total energy that a given profile can absorb. It depends on many geometric and material parameters resulting in folding modes. Crushing force is changed during deformation of thin–walled sections according to folding modes therefore the maximum energy absorption is obtained in a given sample if progressive collapse mode is sustained in a profile throughout the whole deformation process (Figure 1). On the other hand the regular folding process is often disturbed by global bending caused by incorrectly designed profiles and geometric and material imperfection (Figure 2).

For progressive folding it is possible to correlate the size and numbers of the folds formed during deformation with oscillating course of crush force (Figure 3). The first major work in this field was published by Alexander [1] who on the basis of experi-

ments on metal pipes developed a model which made it possible to determine the average pipe deformation force and the size of the folds.

Fig. 1. Progressive folding of double hat thin – walled tailored blank sections

Fig. 2. Global bending of double hat thin – walled sections

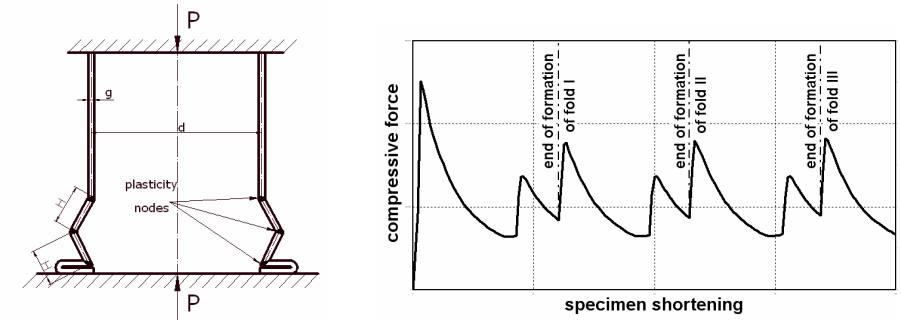

Fig. 3. Formation of folds and corresponding trace of force during compression of thin-walled specimens

The occurrence of a given folding mode can be associated with the values of the specimen geometric parameters: D/t (diameter/thickness), L/D (length/diameter), the yield strength and flange width as well as method of joining.

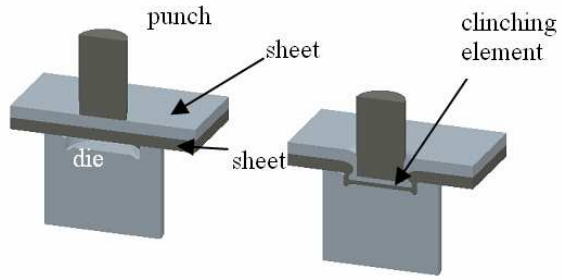

Fig. 4. Idea of clinch joining

The way that the profiles are joined is a highly important parameter affecting their energy consumption. Today car structure components are mostly joined by spot weld-

ing and recently by laser-beam fusing welding. Besides many obvious advantages, the methods have their limitations which are mainly associated with structural changes within the weld, leading to considerable strain hardening of the material in this area and a reduction in its deformability. For this reason new mechanical joining methods are researched [4–7]. The most popular is clinching. It consists in local pressing one metal sheet into another in order to fix the pressed in sheet bottom relative to the pressed out sheet, was used to join energy absorbing profiles. The idea of clinch joining by Eckold GmbH & Co.KG is illustrated in Figure 4.

The method can be used to join elements having the same or different thickness and made from different materials. There may also be an intermediate layer (foil, paint, sealing, etc.), which does not lower the quality of the joint, between the joined elements [5, 6].

The available literature does not provide any information on the dynamic deformation of mechanically joined impact energy absorbing profiles.

In the present paper, the mode of deformation of double-hat thin-walled sections joined by different methods of clinching are presented.

2. Methodology

The geometrics of the researched thin-walled specimens made of steel HSLA 320 are shown in Figure 5. The two kinds of clinching round press joining (RPJ, diameter of bottom bulge – 8 mm, Figure 6a) and square press joining (SPJ, side length – 4 mm, Figure 6b) were applied. In the case of square press joining (SPJ) the material is cut on two edges of punchprint therefore there are two possibilities of their arrangement according to the axis of sample: cut edges are parallel to axis of sample – this kind of clinching is marked by SPJ, and perpendicular to axis of sample – this kind of clinching is marked by qSPJ.

A review of literature showed that pitch of clinching is also very important parameter affecting mode of thin-walled specimens' deformation. The available literature does not provide any information about the pitch of clinching of thin-walled specimens therefore in the presented research the pitch of clinching was chosen on the basis of spot welding pitch. Lee et al. suggested that the optimal weld pitch for the maximum energy absorption was 40–50% of thin-wall specimen width [8].

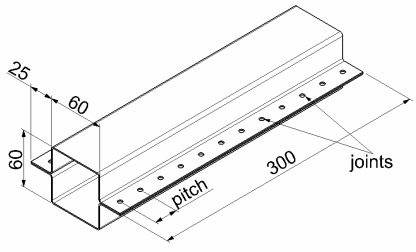

Fig. 5. Dimensions of specimens

In order to check influence of clinching pitch on the mode of deformation the pitch of 25 mm and 20 mm were applied. In this way six kinds thin-walled specimens differ in method of clinching and pitch of clinching were researched. For each kind of joining three specimens were deformed.

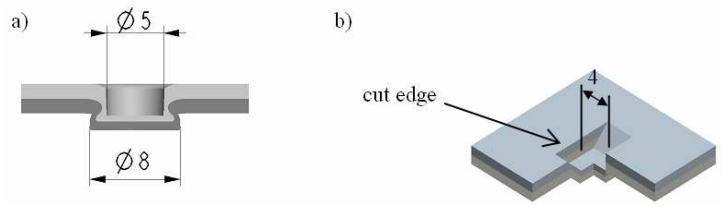

Fig. 6. Idea of clinch joining using: a) round press joining and b) square press joining (Eckold GmbH & Co.KG)

Thin-walled specimens were subjected to quasi-static compression test with constant velocity of 10 mm/min on a TIRA-TEST 2300 tensile machine.

The thin-walled specimens were also subjected to an axial crushing test on a dynamic test stand with a drop crush tower, where thin-walled specimens can be deformed at a very high velocity and data can be registered for very short times. A hammer bob weight of 227 kg and a crush velocity of 7.27 m/s were used in the crushing test [9].

In both dynamic and static experiments the bottom end of sample were fixed in special handle in order to force deformation from top to bottom end (Figure 7).

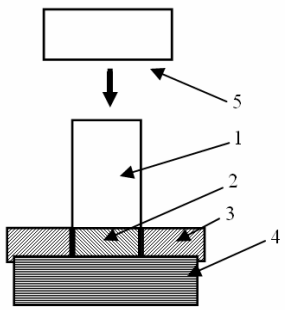

Fig. 7. Arrangement of thin – wall specimen fixed in special handle: 1 – specimen, 2 – internal insert, 3 – external ring, 4 – anvil, 5 – ram

3. Results

The force-displacement curves for the double-hat thin-walled specimens joined by three different methods for pitch of 25 mm in quasi-static compression test are shown in Figure 8.

The first increase in the force is caused by the formation of the first fold. After the formation of plasticity nodes the force decreases. The next folds are formed by a smaller load. Each oscillation of the load curve corresponds to the formation of another fold. The curves as well as modes of deformation for all the specimens are very similar (Figure 9).

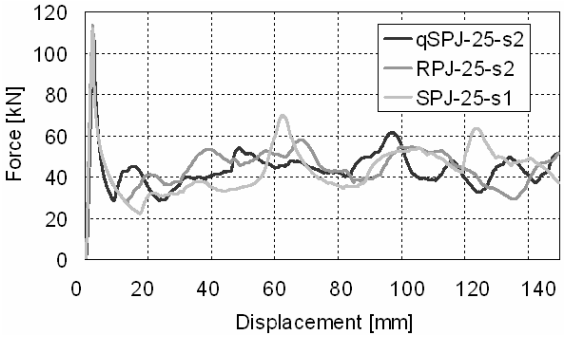

Fig. 8. Load-displacement curve for thin-walled specimens with pitch of 25 mm in quasi-static test

All specimens jointed by round clinching underwent progressive asymmetric folding (regular inward – outward folding). Buckling started from the top end and proceeded towards the centre. Transition from progressive folding to global bending was observed in the some specimens clinched by SPJ, which could have been mainly due to the failure of the joint (Figure 10). The research of many specimens shows that about 25% of samples clinched by SPJ underwent global bending whereas for specimens clinched by RPJ only progressive folding occurs. The global bending of samples causes the instant change of compression force course (pick of the compression force in the Figure 8 at displacement of 60 mm for SPJ clinching).

Fig. 9. Collapse thin-walled specimens with pitch of 25 in quasi-static axial crushing

Fig. 10. Failure characteristic of SPJ clinching

Figure 11 presents the results got from static deformation thin-walled specimens with pitch of 20 mm. The curves for all the specimens are almost the same. The first local force maximum at displacement of 40 mm for all specimens that is much bigger

than further oscillation shows that the deformation was not so uniform as specimens with 25 mm pitch. This observation was confirmed by mode of folds creation visible in the Figure 12 showing collapsed specimens. The mode of deformation thin-walled specimens with pitch of 20 mm is more random. Sometime the deformation started from the centre of samples and progressed towards both ends.

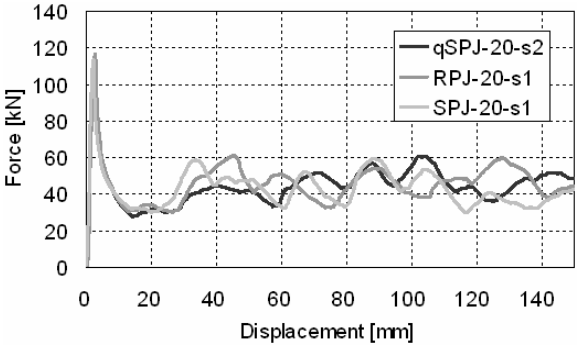

Fig. 11. Load-displacement curve for thin-walled specimens with pitch of 20 mm in quai-static test

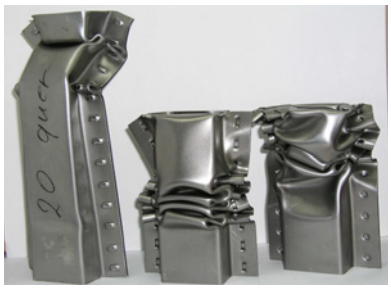

Fig. 12. Collapse thin-walled specimens with pitch of 20 in quasi-static axial crushing

The impact energy in the dynamic crushing test was equal 6 kJ, however about 0.5 J of that is dissipated into the friction of weight bearing and vibration of stand base. The force-displacement curves of the double-hat thin-walled specimens joined by different method of clinching with pitch of 25 mm and 20 mm are shown in Figure 13 and 14 respectively.

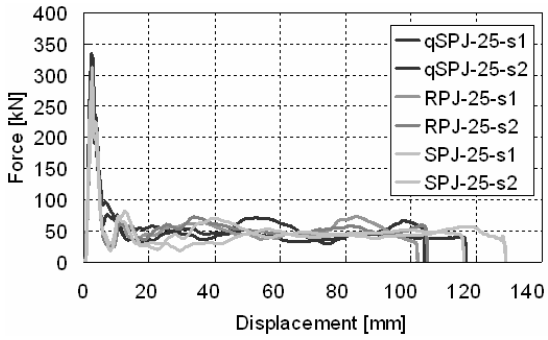

Fig. 13. Load-displacement curve for thin-walled specimens joined by clinching with pitch of 25 in dynamic test

The course of crush force is almost the same for all samples however the maximum force in dynamic test was almost three times larger than in static test. More or less all

specimens jointed by clinching with pitch of 25 mm underwent progressive asymmetric folding (regular inward – outward folding) (Figure 15). In the case of applying pitch of 20 mm only sample clinched by RPJ underwent progressive deformation. Dominant mode of deformation of rest samples was global bending (Figure 16). Then plastic axial displacement of the thin-walled specimens is the largest due to the fact that the mean crushing force is lower and in order to absorb impact energy lager displacement is required.

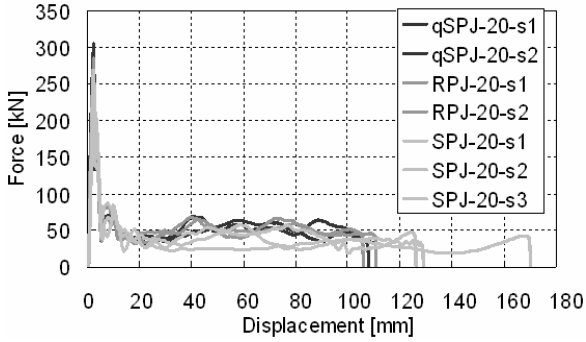

Fig. 14. Load-displacement curve for thin-walled specimens joined by clinching with pitch of 20 in dynamic test

Making general comparison between samples clinched by SPJ and qSPJ, the first are more prone to global bending due to disadvantageous arrangement of clinching according to force acting. The longer cut edges of SPJ clinching are parallel to axis of sample (Figure 16) therefore during folding creation these edges are separated easier then that of qSPJ which is perpendicular to axis of sample. Separation of clinching causes very fast transition from progressive to global bending.

Fig. 15. Collapse thin-walled specimens with pitch of 25 in dynamic axial crushing

Fig. 16. Collapse thin-walled specimens with pitch of 20 in dynamic axial crushing

During dynamic axial crushing test the behaviour of thin – wall samples was better then in static test. It means that more progressive folding occurred when started from top end and progressed downward. In spite of lower maximum crush force in static

test, more often joining separation occurs in this test than in dynamic. In dynamic test failure occurred only for SPJ and in the middle of sample, whereas during static deformation failure very often appeared during formation first folds.

4. Summary

Double-hat thin-walled specimens joined by clinching methods: round press joining (RPJ) and square press joining (SPJ), were investigated. During the dynamic axial crushing test the behaviour of thin – wall samples were better then in static test. There are two the most important parameters of clinching influencing on mode of deformation: technique and pitch of clinching. The experiments show that the RPJ clinching and application of pitch of 25 mm are the best as regards of mode deformation. They are deformed more progressive in both dynamic and quasi-static tests. In spite of lower crush force in static test, more often joining separation occurs in this test than in dynamic. The results show that clinch joining could be applied in controlled body crushing zones.

Acknowledgments

The authors are grateful to Eckold GmbH & Co.KG company for preparing clinched thin-walled specimens and supplying information on clinching technique.

References

[1] Alexander J.M.: *An approximate analysis of the collapse of thin cylindrical shells under axial loading*, Quart. J. Mech. Apply, Math, 13, 1960, pp. 10–15.
[2] Rusiński E. Kopczyński A., Czmochowski J.: *Test of thin-walled beams joined by spot welding*, Journal of Materials Processing Technology, Vol. 1578–158, 2004, pp. 405–409.
[3] Abramowicz W., Wierzbicki T.: *Axial crushing of multicorner sheet metal columns*, Journal of Applied Mechanics, 56, 1989, pp. 113–120.
[4] Neugebauer R., Dietrich S., Kraus C.: *Dieless clinching and dieless rivet-clinching of magnesium*, Key Engineering Materials, 344, 200, pp. 693–698.
[5] Varis J.P., Lepisto J.: *A simple testing-based procedure and simulation of the clinching process using finite element analysis for establishing clinching parameters*, Thin-Walled Structures, 41, 2003, pp. 691–709.
[6] Voelkner W.: *Present and future development of metal forming: selected examples*, Journal of Materials Processing Technology, 106, 2000, pp. 236–242.
[7] Cacko R., Czyżewski P.: *Veryfication of numerical modeling of SPR joint by experimental stack-up*, Computer Methods in Material Science, 7, 2007, pp. 124–129.
[8] Lee H., Kim B., Han B.: *Energy absorbtion characteristics and optimal welding space of square hat type thin-walled tube*, Trans KSME A, 26, 2002, pp. 2703–2714.
[9] Gronostajski J., Gronostajski Z., Niechajowicz A., Polak S., Struś M., Tobota A., Wiewiórski P., Zając P.: *Measurement system of „crash-test" experiments*, Archives of Civil and Mechanical Engineering, 2, 2004, pp. 5–23.

Quasi-statyczne i dynamiczne odkształcanie profili cienkościennych łączonych metodą klinczowania stosowanych w kontrolowanych strefach zgniotu

W ostatnich latach przemysł samochodowy intensywnie rozwija badania nad kontrolowanymi strefami zgniotu. Najbardziej popularną metodą łączenia elementów tworzących te strefy jest zgrzewanie punktowe. Artykuł przedstawia nową metodę łączenia tych elementów za pomocą metody mechanicznej nazywanej klinczowaniem. Dwie metody klinczowania zostały przeanalizowane: klinczowanie okrągłymi i prostokątnymi narzędziami. Badania dynamiczne i quasi-statyczne odkształcania profili cienkościennych łączonych klinczowaniem wykazały, że szczególnie klincze okrągłe mogą znaleźć zastosowanie do łączenia elementów stref zgniotu w samochodach.

ARCHIVES OF CIVIL AND MECHANICAL ENGINEERING

Vol. VIII 2008 No. 2

Numerical and experimental investigations on HYLITE sandwich sheets as an alternative sheet metal

W. HUFENBACH, J. JASCHINSKI, T. WEBER, D. WECK
Technische Universität Dresden, Institut für Leichtbau und Kunststofftechnik, 01062 Dresden, Germany

Current developments show that in the field of sheeting alternative material concepts are successfully applied. In this context metal plastic sandwiches, which are composed of two thin metallic surface layers and a polymer core, represent an interesting group of semi-finished products. Compared to conventional sheet metal materials the structural modification caused by sandwich design provides an increased specific flexural rigidity. Extensive experimental and numerical investigations were carried out for the characterisation of this still young group of semi-finished products. The evaluation of suitable calculation methods represents a crucial step to a broad application of semi-finished metal plastic sandwiches within bulk production processes.

Keywords: *sheet metal, sandwich, Hylite*

1. Introduction

The reduction of mass of motor vehicles is a permanent challenge for the automotive industry in order to improve both, the handling characteristics and the energy efficiency. In a market segment that is strongly affected by bulk production, it is always necessary to consider both, the economical and the technical criteria, when selecting materials and semi-finished products. In order to achieve the objectives mentioned above, in the case of sheet metals the wall thicknesses were constantly reduced in the past years. At the moment a further mass reduction by means of a further thickness decrease is hardly possible taking into account the stability behaviour. Current developments show that in the field of sheeting alternative material concepts are successfully applied. In this context metal plastic sandwiches, which are composed of two thin metallic surface layers and a polymer core, represent an interesting group of semi-finished products.

Compared to conventional sheet metal materials, the structural modification caused by sandwich design provides an increased specific flexural rigidity. Under bending the top layers bear the tension and compression loads, and the core bears the transverse shear loads. Additionally the polymer core provides an additional function integration regarding the dynamic, acoustic and thermal characteristic. Therefore, the application of this sandwich material eliminates the necessity to use additionally damping and insulating materials and to add to weight and costs [1].

At the Institut für Leichtbau und Kunststofftechnik of TU Dresden extensive experimental investigations were carried out for the characterisation of this still young

group of semi-finished products. Beside the determination of the mechanical, thermal and acoustic properties also the joining behaviour of the metal plastic sandwiches is studied. Accompanying these investigations numerical studies were carried out, in which effective and exact modelling strategies are determined. The evaluation of suitable calculation methods represents a crucial step to a broad application of semi-finished metal plastic sandwiches within bulk production processes.

2. Sandwich sheet concepts – market review

In the permanent attempt to increase the flexural rigidity by cross section modification, a vast number of sandwich compounds were developed in the past (Table 1). There are several possible criteria for their classification such as differentiates between continuous and discontinuous core design, for the kind of core material or for the material of the top layers [2, 3].

For the use in automotive applications a contemplation of the workability is useful. One may divide in highly exploded cross sections, which can not be processed in conventional forming techniques, and less exploded cross section compounds, which are suitable for deep drawing. With regard to practical considerations a limitation is made to sandwiches with metallic top layers, which could be designated as sandwich sheet metals even in a closer sense.

Table 1. Classification of sandwich sheet concepts

Cross section	typical sandwich	sandwich sheets
Examples	▪ Joint Composite ▪ Trapezoid sheet ▪ Web sheet ▪ Honeycomb sheet ▪ Sandwich with foamed core	▪ Napped sheet ▪ HYLITE ▪ Twin sheet ▪ Bondal ▪ HSSA [4] ▪ CAMBOSS [4]

A particularly interesting group are the metal/polymer/metal sandwich sheet elements. Due to their continuous structure they are especially useful in the automotive industry. They can be employed in the outer shell because forming processes do not produce marks of the inner structure at the top layers. Therefore the following statements concentrate on this group of sandwich sheet concepts, whereas the investigations especially focus on the product Hylite of the company Corus.

3. Weight saving potential – analytical considerations and numerical approaches

The employment of sandwich sheets is useful for applications in car body sheets, which require a high local or global flexural rigidity. The increasing flexural rigidity directly leads to a higher buckling stiffness, generating advantages regarding touch by persons or piece impact.

An important value is the specific weight, i.e. the mass per unit area. Apart from the comparison of the flexural rigidities it is also necessary to compare the specific weight when comparing different, alternatively employable sheet materials. Alternatively sheets of the same specific weight but different materials could be contrasted with each other as it is done in [1].

During the development and the employment of sandwich sheets not only the technical feasibility but also the classification into the market of car body sheets has to represent an important criterion. In this scope sandwich sheets compete with conventional steel sheets as well as several aluminium alloys. Hence a benchmarking with regard to these types of sheets is necessary.

For the analytical investigations a simplified model of the metal/polymer/metal sandwich sheet is used. A sketch of the model which neglects the adhesive layer between core and top layers is shown in Figure 1. The material properties of the considered materials are summarized in Table 2.

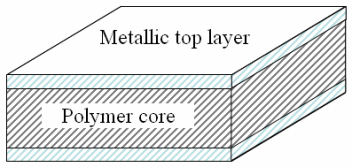

Fig. 1. Sandwich sheet structure (simplified for the analytical investigations)

Table 2. Material properties (assumptions) used in the analytical investigations

		Aluminium	Polymer
Young's modulus	[MPa]	70000	1200
Poisson's ratio		0.3	0.3
Yield stress	[MPa]	190	30
Density	[g/cm³]	2.7	0.9

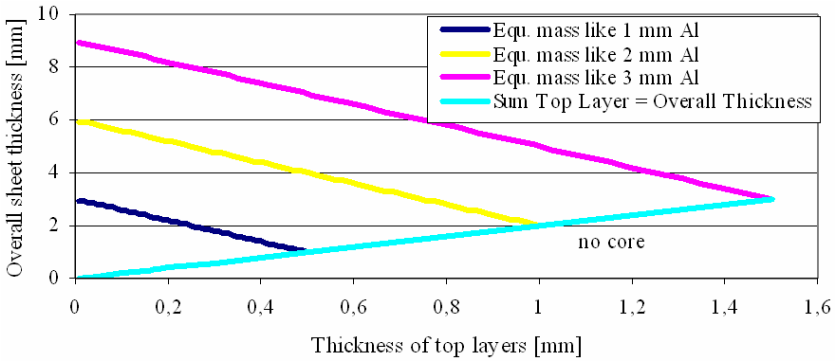

Fig. 2. Possible layer thickness using aluminium top layers

In the first instance it is examined which variations of sandwich sheets arise out of the combination of equal-thick top layers with a polymeric core under the restriction of using the specific weight of aluminium sheets of varying thickness as a reference value.

Figure 2 clearly illustrates, that regarding the overall thickness a lower limit exists at which the two top layers together reach the overall thickness, so that there is no core possible. In reality there is a technological limit at the left margin of the diagram, because the production and processing of arbitrary thin top layer sheets is inefficient.

Favourable to an analytical investigation is at first the calculation of the flexural rigidity using the equations for a conventional sandwich compound. The flexural rigidity per unit width $E \cdot I/b$ of a symmetric sandwich structure can be calculated according to

$$\frac{E \cdot I}{b} = E_{TL}\left[\frac{s_{all}^3}{12} - \frac{\left(s_{all} - 2 \cdot s_{TL}\right)^3}{12}\right] + E_C\left[\frac{\left(s_{all} - 2 \cdot s_{TL}\right)^3}{12}\right] \tag{1}$$

with the Young's modulus of the top layer material E_{TL} and the core material E_C, the overall thickness of the sandwich s_{all} and the thickness of the single top layers s_{TL}. The contribution of the polymer core to load bearing – as well as the influence of the used width – can be neglected for the sandwich thicknesses of technical interest. By the example of metal/polymer/metal sandwich sheets it is demonstrated in Figure 3, which range of top layer thickness are useful in technical applications. With regard to a better comparability, the mass of the sandwich sheet is always equal to the mass of an aluminium sheet with a thickness of 1 mm.

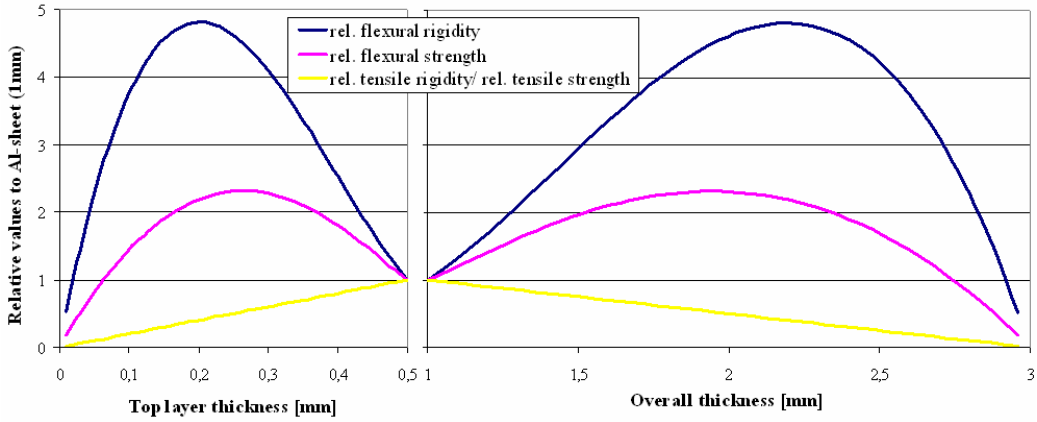

Fig. 3. Sandwich sheet properties based on a monolithic 1 mm thick aluminium sheet versus the overall thickness of the sandwich sheet (a) and versus the top layer thickness of the sandwich sheet (b)

As expected there are high flexural rigidity and strength values for thin top layers and therefore high overall thicknesses of the sandwich sheet. The tensile rigidity and strength grow with increasing top layer thickness, understandably (Figure 3). Therefore it is necessary to find a compromise between the required properties for bending and tension load.

With respect to the previous results it makes sense to examine the weight saving potential of sandwich sheets when employed in car bodies. It can be recognized that with a consequent substitution of steel sheets by sandwich sheets, the weight of the car body of Ford Taurus and Dodge Neon can be reduced by 80 kg (8.7%) and 49 kg (4.8%), respectively. The overall stiffness of the car body is slightly reduced. But for evaluating the vehicle rigidity another value is more important, the so called "Leichtbaugüte" L. As described in [5], L is defined by

$$L = \frac{m_{CB}}{C_T \cdot A} \tag{2}$$

with the mass of the car body m_{CB}, the torsion rigidity of the car body C_T and the footprint of the car body A. Using sandwich sheets this coefficient is even improved due to the reduced mass.

4. Numerical investigations

Numerical simulations are performed using the ANSYS software with parametric model input. To reduce the effort in computing the models, existing symmetries are used to reduce the model size. In all models the elastoplastic material behaviour of aluminium is approximated based on the elastoplastic stress-strain curve according to Gosh.

Several element types are evaluated and validated in terms of accuracy of results as well as modelling and computational effort (see Section 4.2). After that, the numerical results are compared to those of the experiments and different mesh refinements are validated (Section 4.3).

4.1. Experimental determination of the mechanical and structural properties

The following tests were used to investigate the mechanical and structural properties [6]:

- Tensile test on the single material of face and core and the sandwich structure with different temperatures (23 °C, 60 °C and 90 °C) and speed of deformation,
- Three point bending test with different support length,
- Bending test without transverse force (QFB; a modified four point bending test, Figure 4),

- In plane shear test,
- Twisting test to determine the twist stiffness,
- Temperature gradient test,
- Quasistatic and dynamic tensile tests of joined specimens (screw and blind rivet, Figure 4).

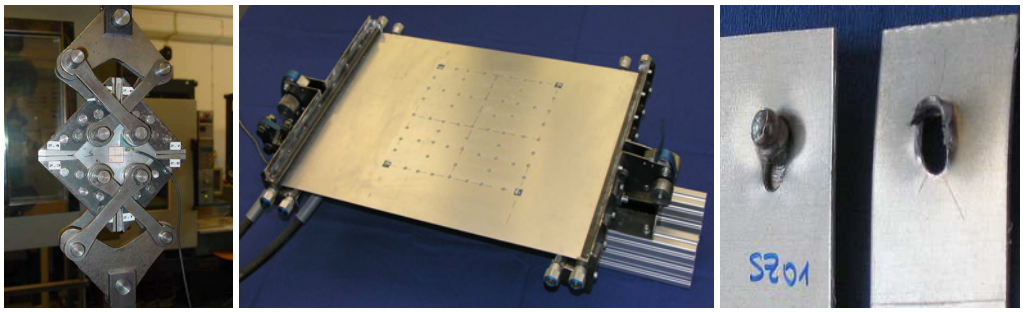

Fig. 4. In plane shear test device, QFB testing device and joined specimens after tensile test

4.2. Potential of solids and shells

The discretization of the sandwich sheet structure with solids following the conventional meshing guidelines for bending dominated problems leads to a huge number of nodes (and degree of freedoms) in the finite element model. Due to the fact that the time of computation increases with the number of degrees of freedom in quadratic way, large structures cannot be simulated with solids in an effective way. Therefore it is fundamental to find alternative possibilities to simulate sandwich sheet structures.

First of all modified solids (Solid46) are evaluated. This solid element type gives the opportunity to implement only one element over the thickness of the sandwich sheet structure because of a modified element definition. The lay-up of the sandwich sheet is stored in the element definition internally. Further several shell element types (Shell91, Shell99 and Shell181) are investigated. These element types assume a very thin structure and therefore neglect the stresses in transverse direction. Comparable to the element Solid46, the structure of the sandwich sheet is stored in the element definition as well. As an extra feature, the element types Shell91 and Shell181 can account for plastic deformations. Finally a combination of solid and shell elements is considered. All simulation results are validated with a finite element model discretized by conventional solid elements (Solid45). Further information concerning the several element types can be obtained in [7].

4.3. Exemplary simulations of simple experiments

As expected, the simulation of a sandwich structure under pure tensile load can performed with very few elements. For all solids as well as for all shell elements even

only one element provides satisfying results. Therefore, tension dominated problems can be solved with every one of the above considered elements at almost the same computional and modelling effort. The simulated results fit well the experimental results (Figure 5).

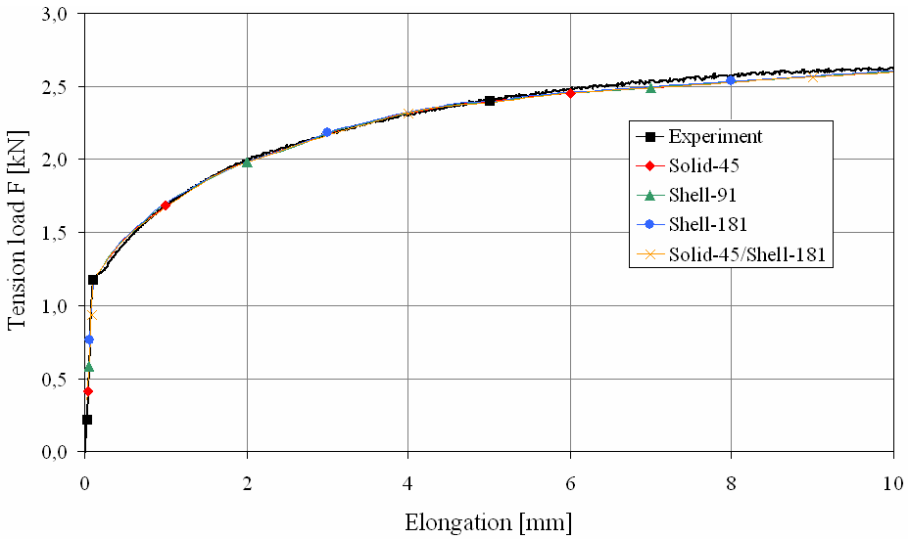

Fig. 5. Tension test with Hylite 1.2 mm

In the following investigated three point bending test with three different support distances (60, 30 and 20 mm) is marked by high plastic deformations. Therefore only element types with nonlinear capabilities are considered in this topic. To be able to simulate also the behaviour of the sandwich sheets after reaching the maximum load, all the simulations are done using displacement boundary conditions. The employment of contact boundary conditions allows a realistic reproduction of the experimental conditions. The discretization of the support and the plunger is carried out using rigid elements.

The stress plots for 60 mm support distance show a good qualitative accordance for all the different element types. The maximum stress in *x*-direction (located directly beneath the plunger) obtained with shell elements are 10% smaller than the stresses obtained with solid elements. This difference, which is only detectable within a small region of 1 mm width in *x*-direction, is probably caused by transverse load effects.

Regarding smaller support distances, it is observed that finite element models containing Shell181-elements deliver results differing increasingly from the Solid45 elements and even experience divergence problems. Therefore, Shell181-elements should not be used in load cases with small flexural radii (respectively with high stress gradients across the element thickness). In contrast, the models using Shell91-elements

achieve results fitting well the ones of the Solid45-model even for small support distances.

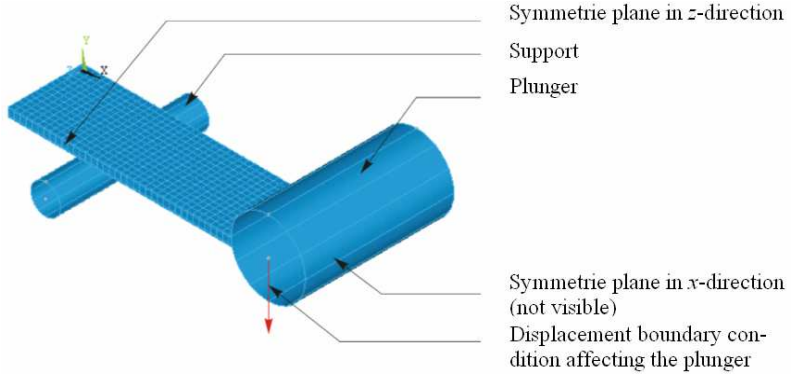

Fig. 6. Finite element model used to simulate the three point bending test

The validation of the simulation is carried out using the results of the three point bending test of Hylite 1.2 mm with a support distance of 60 mm and 20 mm, respectively. In the case of 60 mm support distance the experimental and simulation results fit very well with each other (Figure 7). The simulations hit the end of the elastic range very well and satisfactory portray the trend of the curve of the plastic range. The maximum deviation of the plunger force amounts for less than 5%. The combination of Solid45 and Shell181 elements gets into divergence problems for higher deformations.

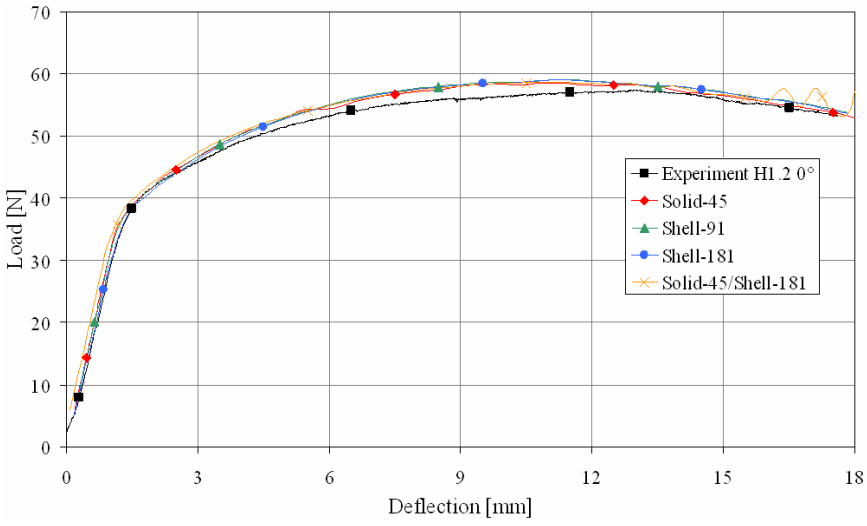

Fig. 7. Load-Deflection-Curves of the three point bending test with a 60 mm support distance

Regarding the experiment with a support distance of 20 mm, one has to state that the virtual elastic module of the Solid45- and the Shell91-model differ from each other. As experienced in the experiment, the virtual elastic modulus determined in the Solid45 model decreases because of the shorter support distance. Additionally, the Shell91 models show a 5% higher plunger force in the plastic range compared to the Solid45 model. The background of this stiffer behaviour of the Shell91 elements has to be the element definition of Shell91, which does not account for the the transverse load shear and the weak-in-shear core influences on the sandwich sheet deflection.

Compared to the experiment, the Solid45 model fits the experimental results very well, especially in the plastic range. The plunger force of the Solid45 and Shell91 model differ from the experimental results by 4% and 9%, respectively. The failure of the real structure cannot be portrayed by the simulation because missing failure definitions in the model.

A universal advice for the best element type cannot be given for this load case. It is necessary to differentiate after the desired results and the grade of deformation. The mesh convergence studies show that a shell element edge length of 1 mm in *x*-direction is sufficient even for high plastic deformations. For moderate plastic deformations Shell181 should be chosen because they provide a faster calculation due to fewer nodes compared to Shell91. If the local stress maxima are of interest, it is necessary to simulate a model discretized with three Solid45 elements across the thickness of each layer. Additionally, the Solid45 elements should have turned on full integration with extra displacement shapes which leads to a higher computation time and disk space. Therefore, it might be advantageous sometimes to use Shell91 instead.

The transverse-load-free bending test gives the possibility to eliminate the influence of the transverse load in the investigated region of the specimen. The flexural moment is applied by means of a clamped support. This clamped support is equipped with flexural pressure tubes; hence it does not inhibit local deformations of the sandwich sheet structure. The deformations of the sandwich sheet remain in the elastic range for this test configuration.

According to Figure 8, the flexural moment is applied by means of pressure loads which follow the structural deformation. The finite element model is supported in *y*-direction in the middle between the loaded element faces. In the case of conventional solid elements, the overall dimensions of the specimen (500 mm × 700 mm) lead to a finite element model which needs a lot of time and disk space for simulation. Therefore, the element type Solid45 is not investigated.

The stress and deformation results of all the finite element models differ only slightly from each other (less than 3.5%), regardless of the used element types. The simulation results are evaluated with the measured flexural radii of the sandwich sheet structure (Figure 9). After adjusting the experimental results by removing the initial curvature of the sandwich sheet, the experimental and simulation results show a good agreement with each other until a flexural moment of approximately 4.5 Nm. Beyond

that border, the motion limit of the testing rig is reached and the radius of the sandwich sheet remains nearly constant.

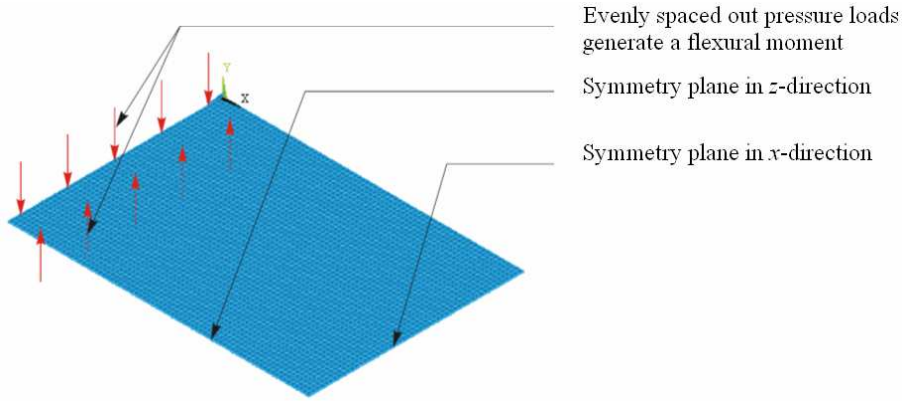

Fig. 8. Finite element model used to simulate the transverse-load-free bending test

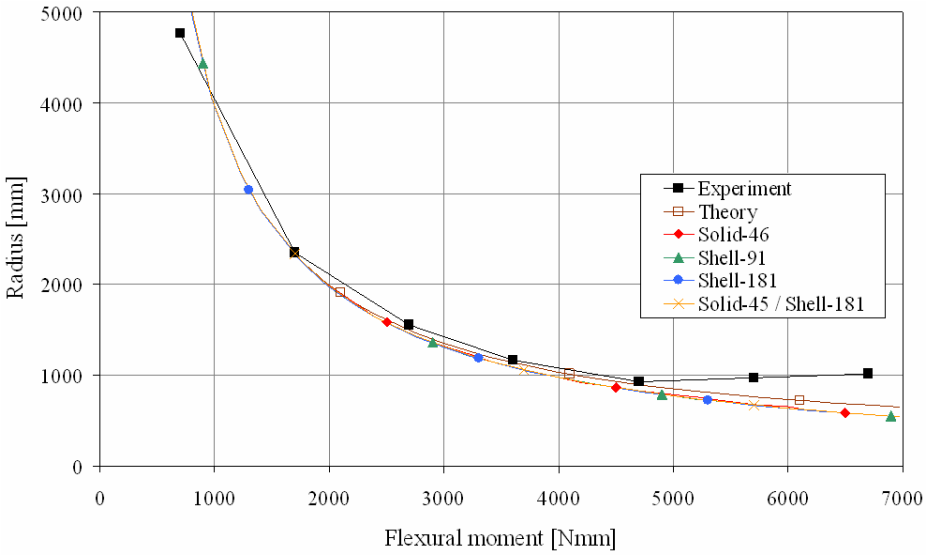

Fig. 9. Bending radius of the sandwich sheet structure versus the flexural moment

Regarding the computational effort, the combination of solids and shells requires the highest time effort to solve the problem and occupies the most disk space. Because of its quadratic element formulation, the Shell91 element does not reach the simulation times of Solid46 (three degrees of freedom per node) and Shell181 (linear element type). These two element types are nearly equivalent in the duration of solution

and the amount of generated data. Altogether, Shell181 are recommended for modelling the sandwich sheet structure under flexural load, if the load remains in the elastic range. It is possible to use relatively large element sizes (edge length of over 14 mm) under the restriction that no local transverse forces are existent.

5. Evaluation of numerical simulation on representative deep drawn specimens

The comparison between simulation and experiment based on real deep drawn structures becomes necessary to evaluate shell elements as the most efficient numerical method for such sandwich sheets.

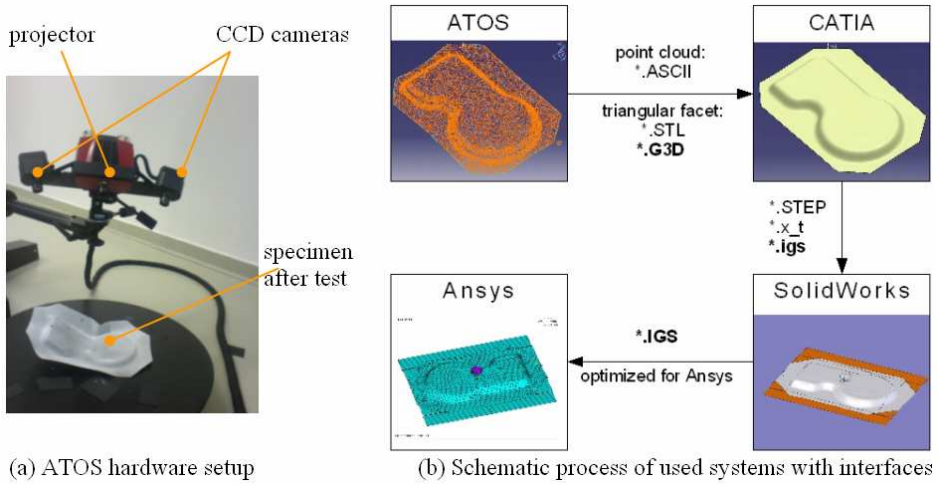

(a) ATOS hardware setup (b) Schematic process of used systems with interfaces

Fig. 10. Setup for the 3D scanning (a) and schematic drawing of the used systems with possible interfaces (used one in bold print)

To get an exact CAD model adapted from the real specimen the method of reverse engineering is used. This work is split into two parts, on the one hand there is the experimental setup for the three-dimensional scanning (Figure 10a; system: ATOS gom mbH) and on the other hand there is the generation of a parametric CAD model based on the measured data, this is done for each specimen. For both parts special systems with special interfaces are necessary (Figure 10b).

To have experiments with practical solution a bending load, induced by a kind of penetration test, is used.

For a good comparison between simulation and experiment the tests were captured by digital image correlation (system: ARAMIS gom mbH) additional to the recorded test machine data.

6. Penetration test

The so called penetration test is done with a Zwick Z250 universal test machine. As shown in Figure 12 the specimen is fixed on a four sided aluminium frame and penetrated with a steel hemisphere. The frame with the specimen moves towards the hemisphere and a bending load is induced into the part. As machine data input the test speed is given by 5 mm/min and as machine output the reaction force dedicated by an additional 10 kN load cell and the traverse path is defined.

In the force-displacement-diagram a good relation between test and simulation (here are two shell elements in use) is shown. The curve describes a process with local peak in the first part and global peak before the part collapses. The collapse can be characterized as a kind of instability. A local instability caused by geometric nonlinearity preceded the global collapse.

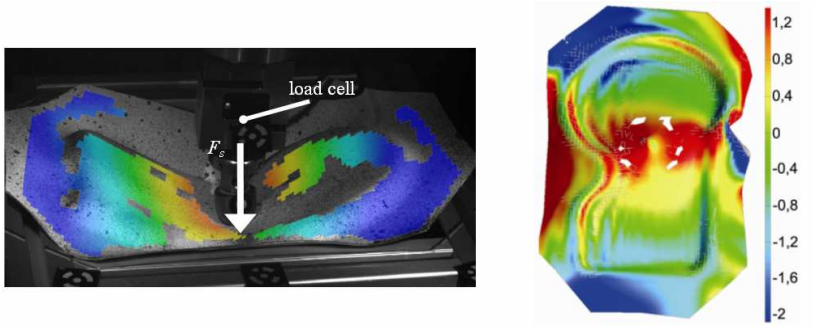

(a) image correlation at highly deformed structure (b) structure comparison of real and FEA part

Fig. 11. Analysis of highly deformed structure

The advantage of the image correlation is to validate the displacement of the whole part in a high quality. Due to this it can be captured, that the FEA is highly accurate particularly with regard to the force-displacement-diagram. Based on an efficient FE model the regions of instability can be located reliably. And the force-displacement diagram can be interpreted in a detailed way.

For highly deformed structures the image correlation is limited by physical restriction due to the test setup like camera position and shade caused by the test rig (Figure 11a). The problem is solved by comparison after collapse, between virtual and real specimen. This was made possible by an export of the deformed FE model surface (Figure 11b). The comparison shows a deviation from maximally 1.2 mm, which is an acceptable quality if one proceeds from a stamp way with 60 mm.

7. Conclusion

At the Institut für Leichtbau und Kunststofftechnik of TU Dresden extensive experimental investigations were carried out to characterize the still young group of

sandwich sheets. Based on different experimental tests, numerical investigations were done, in which effective and exact modelling strategies of load cases with practical impact are determined. The comparison between experiment and FEA validates the capabilities of effective shell elements to abstract different load cases in an acceptable quality and with an acceptable effort, especially for static loads. The evaluation of suitable calculation methods represents a crucial step to a broad application of semi-finished metal plastic sandwiches within bulk production process.

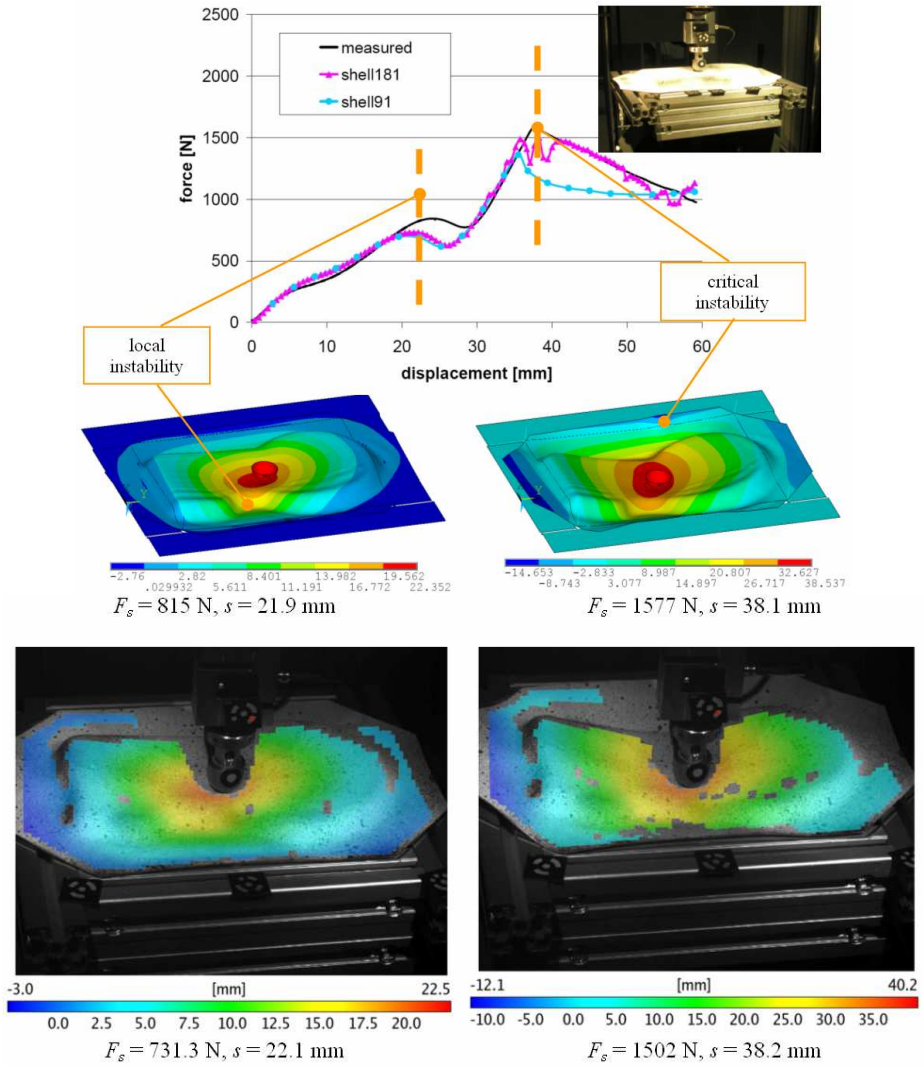

Fig. 12. Comparison of reaction force and displacement topology
at penetration test, especially with Shell181

Investigations related to dynamic loads are in focus of future research. Especially the character of different joining methods is of interest. For this purpose the application of complex test (e.g. dynamic high strain test) and measuring system (e.g. image correlation coupled with high speed cameras) becomes necessary.

References

[1] Burchitz, I., et al.: *Highlights of designing with Hylite – a new material concept*, Materials and Design 26, 2005, pp. 271–279.
[2] Adam, F.: *Zum anisotropen Strukturverhalten mehrschichtiger Leichtbauverbunde als Flächentragwerke*, Dissertation, TU Dresden, 1999.
[3] Hufenbach, W., Ochmann, H., Adam, F.: *Strukturierung und Klassifizierung von Stahlblech-Mehrschichtverbunden*, In: Entwicklungen im Karosseriebau, VDI-Berichte Nr. 1264, Düsseldorf: VDI-Verlag, 1996, pp. 133–147.
[4] Markaki, A.E., Clyne, T.W.: *Mechanics of thin ultra-light stainless steel sandwich sheet material Part I. Stiffness*, Acta Materialia 51, 2003, pp. 1341–1350.
[5] Lüdke, B.: *Anforderungen des PKW-Baues an neuartige Stahlleichtbaustrukturen*, Dresdener Leichtbausymposium, 1997.
[6] Neugebauer, R., Scheffler, S.: *Schaffung umformtechnischer Grundlagen bei der Verarbeitung von Metall-Kunststoff-Verbunden*, EFB-Forschungsbericht, Nr. 248, Hannover: EFB, 2006.
[7] SAS IP, Inc.:ANSYS 10.0, Documentation, 2002.

Numeryczne i doświadczalne badania płyt warstwowych typu HYLITE jako alternatywne materiały dla blach konwencjonalnych

Aktualne kierunki rozwoju pokazują, że w obszarze kształtowania blach są stosowane z powodzeniem alternatywne materiały. W tym kontekście kształtowane plastycznie materiały wielowarstwowe typu „sandwich", które są złożone z dwóch cienkich metalicznych warstw powierzchniowych i rdzenia polimeru, reprezentują interesującą grupę półproduktów. W porównaniu z konwencjonalnym kształtowaniem blach modyfikacje struktury spowodowane przez projektowanie materiału wielowarstwowego prowadzą do wzrostu sztywności materiału. Obszerne badania doświadczalne i numeryczne zostały zrealizowane w celu scharakteryzowania tej nowej grupy półproduktów. Oszacowanie odpowiednich metod obliczeniowych jest decydującym krok do obszernego stosowania półwyrobów z materiałów wielowarstwowych kształtowanych plastycznie typu „sandwicz" w objętościowych procesach produkcyjnych.

ARCHIVES OF CIVIL AND MECHANICAL ENGINEERING

Vol. VIII 2008 No. 2

The effect of abrasive cutting on the temperature of grinding wheel and its relative efficiency

JÓZEF KACZMAREK
Technical University of Łódź
Department of Production Engineering, Stefanowskiego 1/15 90-924 Łódź, Poland

The thermovision method was applied for determination of the temperature of grinding wheel during abrasive cutting. Abrasive cutting of steel workpieces by using grinding wheels purchased from 3 different manufacturers was conducted under different conditions. Temperature distribution along the grinding wheel circumference and along its radial cross-section was determined. The relative efficiency of grinding wheel was estimated.

Keywords: *abrasive cutting, cutting grinding wheels, temperature of grinding wheel, relative efficiency of grinding wheel, thermovision measurement*

1. Introduction

Grinding wheels have been applied for cutting in different branches of industry and by individual users. These cutting tools have been used in steel mills, steelworks, foundries, forges, mechanical and repair departments of factories, in building industry, for repair of roads and railway tracks as well as by individual users. Abrasive cutting is applicable to metal workpieces with different hardness and to very hard non-metal materials (e.g. concrete, silicon tiles). Studies on abrasive cutting have hitherto focused on mechanical durability of grinding wheels [6–13], which is of great importance for their operational safety and reliability [1–3]. Too high temperature of the grinding wheel during the process of cutting can have a negative impact on the bonding agent, which binds abrasive particles. This in turn affects the operational reliability of grinding wheel and can lead to a lower cutting efficiency and an increased emission of environmentally harmful gases. This work presents results of studies on distribution of temperature along the circumference of grinding wheel and along its radial cross section and on the relative efficiency of this process. The temperature of grinding wheel was measured by using the thermovision camera, which facilitated recording temperature in each site of the grinding wheel.

2. Heat emission during abrasive cutting

The source of heat is work used during cutting for elastic and plastic deformations, removal of chips and friction interaction between abrasive particles and the workpiece. An approximate value of heat flux can be calculated from the Equation [17]:

$$\Phi = F_c \cdot v_s \,[W], \tag{1}$$

where:

F_c – cutting force [N],

v_s – cutting speed [m/s].

The heat flux generated during abrasive cutting penetrates the workpiece (Φ_w), chips (Φ_{ch}), grinding wheel (Φ_s) and is dissipated to the atmosphere (Φ_p) in the form of irradiation – (Figure 1). The shares of aforesaid components of the heat flux are as follows [18]: $\Phi_{ch} \approx 60\%$, $\Phi_s \approx 20\%$, $\Phi_w \approx 10\%$, $\Phi_p \approx 10\%$.Temperature of grinding wheel depends on the density of heat flux $\varphi = \mathrm{d}\Phi_s/\mathrm{d}A$, which passes through the grinding wheel-workpiece interface A, and on thermal characteristics of this grinding wheel. Cutting is usually carried out by using narrow grinding wheels. The surface of their interaction with the workpiece is relatively small. Also the thermal conductance of grinding wheels is low. Both these factors cause that an excessive increase in the temperature of the grinding wheel can negatively affect its cutting performance and, probably to a lesser extent, also its operational reliability.

The distribution of the heat flux in the shearing zone can have a strand-like character for cutting with the radial feed [4, 15–16, 19], or a triangle-like character for cutting with the longitudinal feed [20–21]. The abrasive cutting is usually characterized by the radial feed (f_p) which is conducive to the strand-like distribution of the heat flux.

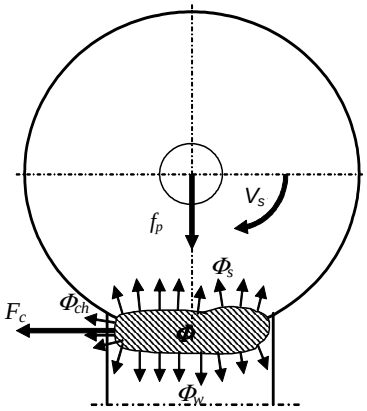

Fig. 1. The heat flux and its distribution in the shearing zone

The quantity of generated heat flux Φ depends mainly on the cutting speed v_s and feed f_p. Because the cutting speed is determined by standards and recommendations [22–26] so the feed value f_p is the most important factor in this respect. Abrasive cutting is usually carried out by using manual grinders which are characterized by the lack of precise control of the feed. Too large feed superimposed by the small area of

the grinding wheel-workpiece interface and poor thermal conductance of the grinding wheel may result in intensive emission of heat. The high heat flux density may lead to grinding wheel melting and in consequence to its increased wear. Additionally, apparent changes of coloration in the shearing zone, structural alterations of the ground material (approaching the depth of 0.2 mm from top surface [3]), thermal flush, etc. can occur.

3. Relative efficiency of grinding wheels

The wear of grinding wheels depends first of all on their technical characteristics, properties of the ground material and grinding conditions. The determination of this wear is usually based on determination of the coefficient of relative efficiency of grinding G [5]. This coefficient equals to the ratio of the volume of chips removed during grinding V_M to the drop in the volume of grinding wheel during this process V_S (2).

$$G = \frac{V_M}{V_S} = \frac{\frac{\pi \cdot d^2}{4} \cdot b}{\frac{\pi}{4} \cdot (D_{S1}^2 - D_{S2}^2) \cdot T} = \frac{d^2 \cdot b}{(D_{S1}^2 - D_{S2}^2) \cdot T}, \tag{2}$$

where:

D_{S1} – grinding wheel diameter before grinding [mm],
D_{S2} – grinding wheel diameter on completion of grinding [mm],
d – the diameter of the rod subjected to grinding [mm],
b – the width of slit on the rod [mm],
T – the width of grinding wheel [mm].

In case of abrasive cutting, the coefficient G equals to the quotient of the cross-section surface area of the workpiece subjected to cutting divided by the loss of the head surface of grinding wheel caused by cutting. In this process, an assumption that $b = T$ leads to conversion of Equation (2) to (3).

$$G = \frac{d^2}{D_{S1}^2 - D_{S2}^2}. \tag{3}$$

Under appropriate cutting conditions the values of coefficient G are large. Small values of this coefficient result from an excessive self-sharpening of the grinding wheel, which in turn increases the costs of machining.

4. Experimental studies

The experiments were carried out by using the workstand schematically presented in Figure 2. The principal tool in this workstand was a grinder BS-300 (no. 1). It was

used to cut-off cylindrical, reinforcing steel rods (no. 3) with two different diameters. The quantity of interaction force between the grinding wheel and the rod was determined by gravity, it means with the aid of the appropriately matched system of pull rod. An object glass of the thermovision camera PN – 290 (no. 4) pointed toward the grinding wheel (no. 2) and the rod subjected to cutting. The camera was coupled to the PC computer (no. 5) equipped with the program Termolab (The thermovision camera and the program Termolab' are the property of the Department of Electronic Systems and Thermography at the Institute of Electronics, Technical University of Lodz. They were made available during presented experiments). It ensured recording of measurements. The detailed description of the workstand was published elsewhere [14].

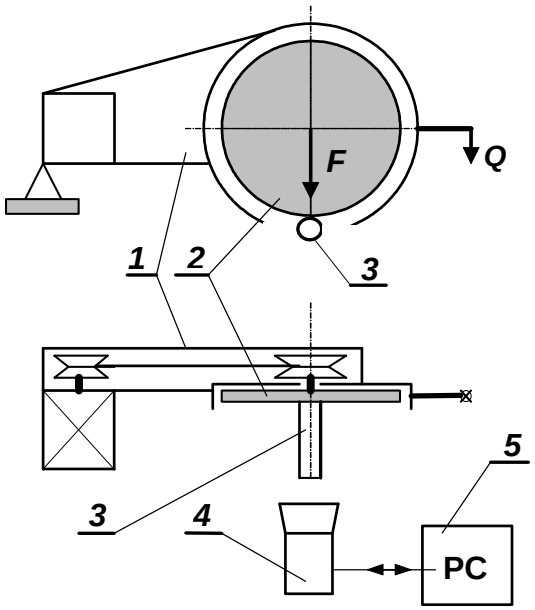

Fig. 2. Schematic diagram of the workstand used for investigation of grinding wheel efficiency during abrasive cutting: 1 – grinder, 2 – grinding wheel, 3 – workpiece, 4 – thermovision camera, 5 – computer, Q – grinding wheel loading, F – interaction force of grinder to cutting bar

The grinding wheels 41 300×3.5×32 A30 R6 BF, which were used in machining trials were purchased from three different manufacturers (further referred to as: no. 1, no. 2, no. 3). This type of grinding wheels is most frequently applied for cutting. The experiments were carried out for three different interaction forces between the grinding wheel and the rod subjected to cutting, which were determined through preliminary trials [14]. Their values ensured smooth cutting. These friction forces were: F_1 = 62 N, F_2 = 72 N, and F_3 = 82 N.

The diameters of cylindrical rods subjected to cutting were: d_1 = 12 mm and d_2 = 20 mm. Each cutting trial under these conditions was repeated twice.

4.1. Results of measurements of temperature distribution

The executed cutting trials were recorded by the camera and the soft-ware as "films", which show the course of each trial. An example of a take (a frame) of such a "film", also termed a thermogram, is shown in Figure 3.

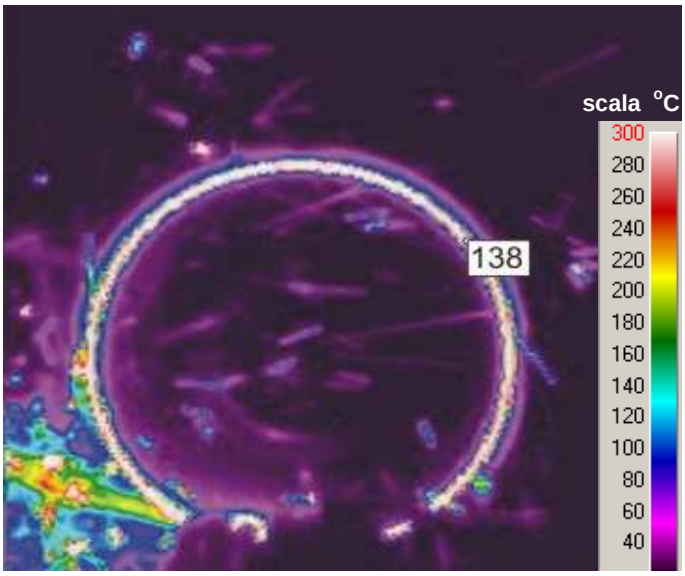

Fig. 3. An example of a grinding wheel thermogram, which was recorded during abrasive cutting trial under the following conditions: grinding wheel no. 3, F = 62 [N], d =12 [mm]

The applied soft-ware ensures, among others: measurement of the temperature of randomly selected point on the grinding wheel (the temperature of one of selected points, equal to 138 °C, is shown in Figure 3), recording changes in this temperature throughout the cutting trial and determination of temperature distribution along any circumference or segment, which were randomly selected against the recorded thermogram. These facilities enabled determination of temperature distribution:

- along the circumference of grinding wheel, as shown in Figure 4 (the plots reflect the true situation),
- along the radius of grinding wheel, as shown in Figure 5.

Distribution of temperature may ensure determination of thermal load of grinding wheel during abrasive cutting.

The maximum temperature at the circumference of the grinding wheel was determined on the basis of the recorded thermograms. The mean values of the maximum temperature of grinding wheel were estimated for the applied grinding conditions. They are shown in Table 1 and Figure 6.

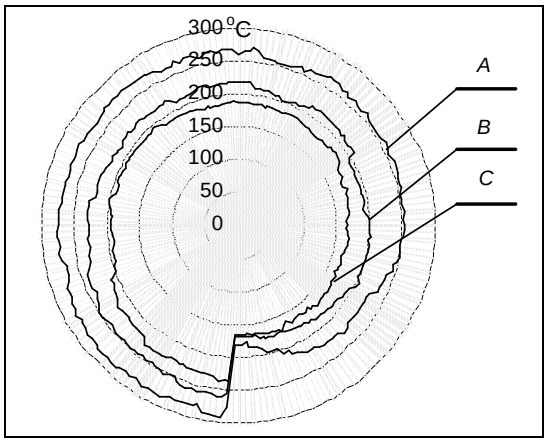

Fig. 4. Distribution of temperature along grinding wheel circumference for 3 different values of the depth of cut, expressed as a ratio of the depth from the rod top surface g to the rod diameter d: A – g/d = 1/3, B – g/d = 1/2, C – g/d = 3/4

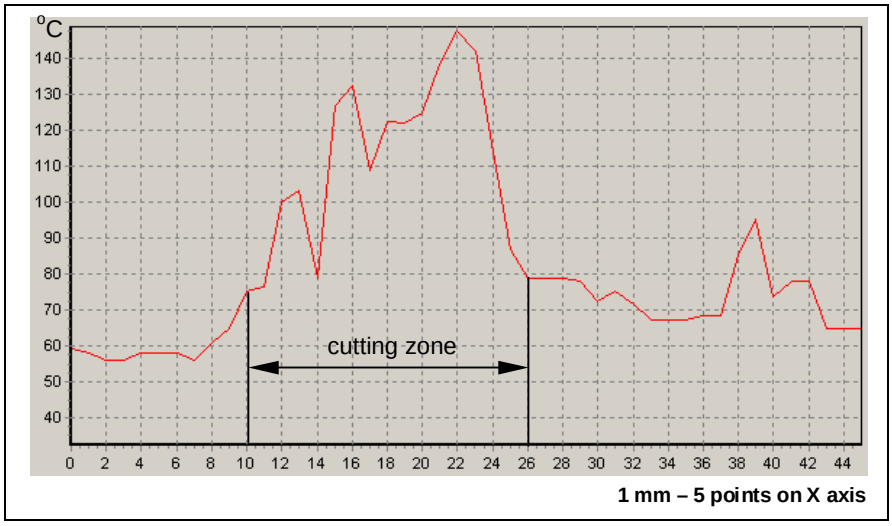

Fig. 5. Distribution of temperature along the radius of grinding wheel for the following cutting conditions: grinding wheel no 3, F = 62 [N], d =12 [mm]

Table 1. Values of the maximum temperature of grinding wheel during the process of cutting

No of wheel		1			2			3		
Interaction force F [N]		62.0	72.0	82.0	62.0	72.0	82.0	62.0	72.0	82.0
		Maximum temperature t [°C]								
Diameter of bar d [mm]	12	170.2	285.4	235.2	187.4	277.8	237.2	150.2	252.9	215.3
	20	246.7	370.5	360.4	296.8	411.6	390.5	305.4	402.5	395.2

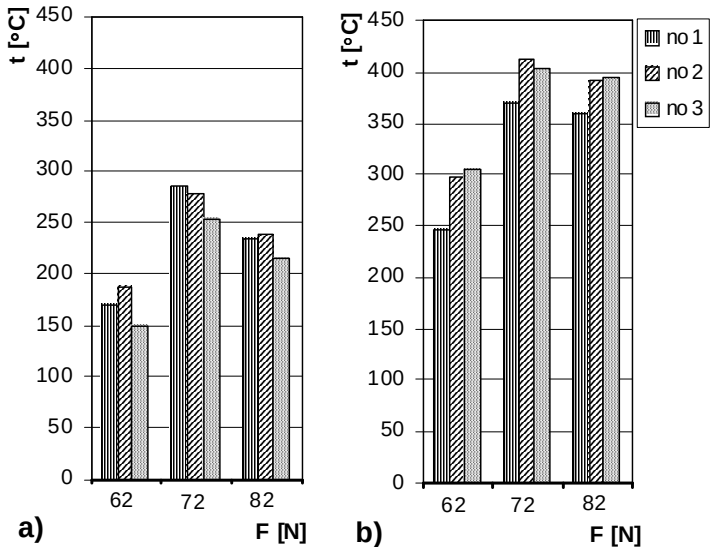

Fig. 6. The effect of interaction force between the grinding wheel and the workpiece on the maximum temperature of grinding wheel during cutting for: a) – the rod with diameter d_1 = 12 mm, b) – the rod with the diameter d_2 = 20 mm; no. 1, no. 2, no. 3 – numbers of grinding wheels purchased from three different manufacturers

The analysis of temperature distribution along the grinding wheel circumference (Figure 4) leads to conclusion that the temperature decreases co-linearly to the direction of the grinding wheel rotation. It is caused by heat dissipation to the surrounding air despite the high circumferential speed (circa 50 m/s) and very short pauses between the contacts of each point on the grinding wheel circumference with the zone in which the heat is generated.

The analysis of temperature distribution along the grinding wheel radius (Figure 5) indicates that the highest temperature occurs along the circumference of the grinding wheel, in the zone of a "ring", which has the width of the depth of cut. A rapid decrease in temperature (in the direction from the grinding wheel circumference to its center), which is collinear to the radius (its gradient ranges from 60 °C/mm to 80 °C/mm) provides evidence of a low heat conductivity of this tool.

The maximum temperatures of grinding wheels with the same technical characteristics but purchased from different manufacturers differ by approximately 30% if the cutting process was conducted under the same conditions. It means that it is very difficult to obtain the same functionability of grinding wheels produced by different manufacturers.

The cutting trials showed that the temperature of cutting increases with the diameter of the ground workpiece (Figure 6). It is caused by the larger area of the interface between the grinding wheel and the workpiece, despite the lower unit pressures.

A rise in the interaction force between the grinding wheel and the workpiece, within the range from 62 N to 72 N results in an increase in the maximum temperature of grinding wheel. The further increase in the interaction force up to 82 N brings about a drop in this temperature (Figure 6), which is most probably caused by self-sharpening of the grinding wheel, which results from high loading of abrasive particles. The self-sharpening is characterized by the occurrence of the larger number of sharp abrasive particles in the shearing zone.

4.2. The relative efficiency of grinding wheel

The relative efficiency of grinding wheels applied for the cutting trials was determined on the basis of Equation (3). The experimental results are shown in Table 2 and Figure 6.

Table 2. Results of measurements of the coefficient of relative efficiency G during abrasive cutting

No of wheel		1			2			3		
Interaction force F [N]		62.0	72.0	82.0	62.0	72.0	82.0	62.0	72.0	72.0
		G ratio								
Diameter of bar d [mm]	12	3.45	1.59	1.26	4.42	1.14	1.11	3.32	1.48	1.15
	20	4.36	7.63	2.26	3.05	6.78	2.18	4.26	7.55	2.12

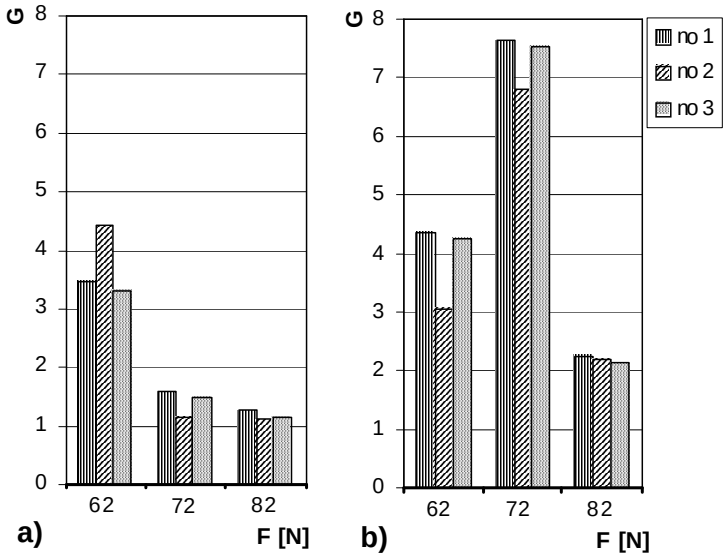

Fig. 7. Values of the coefficient of relative efficiency of grinding wheels G for the cutting trial conducted for: a) the rod with a diameter of d_1 = 12 mm, b) the rod with the diameter of d_2 = 20 mm; no. 1, no. 2, no. 3 – numbers of grinding wheels purchased from different manufacturers

Analysis of these results indicates that in case of cutting grinding wheels of cylindrical rods with lower diameter, the values of coefficient *G* decrease with a rise in the interaction force between these rods and the grinding wheel (Figure 7a). The lower values of coefficient *G* were also observed for cutting of cylindrical rods with larger diameters but only when the interaction force was increased (Figure 7b). The decreased relative efficiency of grinding wheels was most probably caused by intensification of the process of self-sharpening under the latter conditions.

5. Summary

The thermovision camera coupled to the computer soft-ware, which were applied in the abrasive cutting trials ensured the accurate and easy recording of temperature distribution along the circumference and along the radius of each grinding wheel.

The cutting trials proved that utilitarian properties of grinding wheels used for cutting can be accurately determined on the basis of temperature distribution and the coefficient of relative efficiency.

The recorded, different maximum temperatures of grinding wheels purchased from different manufacturers and different coefficients of their relative efficiency can be used for improvement of technological processes of their manufacturing.

Acknowledgments

Research carried out under the Research Project no 4T07 D01029.

References

[1] Biegalski H., Feld M.: *Prognozowanie właściwości użytkowych ściernic do przecinania*, XXIV Naukowa Szkoła Obróbki Ściernej, Kraków-Łopuszna, 2001, pp. 341–348.

[2] Biegalski H., Feld M.: *Możliwość zmniejszenia zanieczyszczeń pyłami i gazami podczas przecinania ściernicowego*, XXV Naukowa Szkoła Obróbki Ściernej, Wrocław-Duszniki Zdrój, 2002, pp. 81–86.

[3] Biegalski H.: *Badania nieniszczące i koncepcja stanowiska do badań eksploatacyjnych ściernic do przecinania*, XXVI Naukowa Szkoła Obróbki Ściernej, Łódź-Spała, 2003, pp. 89–94.

[4] Chanzin N.N. i inni: *Razcziet temperaturnogo polia pri szlifowanii metałow*, Stanki i Insrumient, No. 8, 1981, pp. 27–28.

[5] Kaczmarek J.: *Ocena skrawności ściernicy w wybranych odmianach szlifowania*, Praca doktorska, Łódź, 1985.

[6] *Maszyna do badań wytrzymałości dynamicznej ściernic przy obciążeniach bocznych*, XXII Naukowa Szkoła Obróbki Ściernej, Gdańsk-Jurata, 1999, pp. 163–166.

[7] Kaczmarek J., Fiks W., Dębkowski R.: *Urządzenia do badania wytrzymałości dynamicznej ściernic na rozrywanie*, Magazyn Przemysłowy, Vol. 25, No. 2, 1999, pp. 51.

[8] Gołąbczak A., Kaczmarek J.: *Elektroerozyjne obciąganie ściernic supertwardych elektrodą segmentową*, XXV Naukowa Szkoła Obróbki Ściernej, Wrocław-Duszniki Zdrój, 2002, pp. 143–148.

[9] Kaczmarek J.: *Odkształcenia ściernic do przecinania*, XXVI Naukowa Szkoła Obróbki Ściernej, Łódź-Spała, 2003, pp. 67–72.
[10] Kaczmarek J., Kubiak T.: *Metody określania naprężeń w ściernicy do przecinania obciążonej siłą boczną*, XXVI Naukowa Szkoła Obróbki Ściernej, Łódź-Spała, 2003, pp. 59–66.
[11] Kaczmarek J.: *Wpływ prędkości roboczej i jednopunktowego odciążenia bocznego na wytrzymałość ściernicy*, XXVII Naukowa Szkoła Obróbki Ściernej, Koszalin, 2004, pp. 243–250.
[12] Kaczmarek J., Świniarski J.: *Analiza wytrzymałości ściernicy uwzględniająca ich wymiary geometryczne i sposób zamocowania*, XXVIII Naukowa Szkoła Obróbki Ściernej, Warszawa-Mszczonów, 2005, 32–36.
[13] Kaczmarek J., Świniarski J.: *Analiza wytrzymałości ściernicy do przecinania przy obciążeniu bocznym trójpunktowym*, XIX Naukowa Szkoła Obróbki Ściernej, Gdańsk-Jurata, 2006, pp. 123–126.
[14] Kaczmarek J., Kuliński M., Ostrowski B., Więcek B.: *Zastosowanie termowizyjnego pomiaru temperatury ściernicy podczas przecinania ściernicowego*, Materiały VII Konferencji Krajowej Termografia i Termometria w Podczerwieni pod redakcją Bogusława Więcka, Ustroń-Jaszowiec, 2006, pp. 339–342.
[15] Konig W., Honscheid W., Lowin R.: *Untersuchung der beim Schleifprozess endstchenden Temperaturen und ihre Auswirkungen auf das Arbeitsergebnis*, Forschungsberichte des landes Nordhein-Westfalen Nr 2628, Westdeutscher Verlag.
[16] Marcler R., Malkin S., Molinsdorf J. C.: *Thermal Stresses Form a Moving Band Source of Heat on the Surface of a Semi Infinite*.
[17] Marciniak M., Filipowski R.: *Techniki obróbki mechanicznej i erozyjnej*, Oficyna wydawnicza Politechniki Warszawskiej, Warszawa, 2000.
[18] Oczoś K., Porzycki J.: *Szlifowanie. Podstawy i technika*, WNT Warszawa 1986.
[19] Snoyes R., Maris M., Peters J.: *Thermaly Induced Damage in Grinding*, Annals of the CIRP, Vol. 39, No. 2, 1990, pp. 345–347.
[20] Vensevenant E.: *An Imroved Mathematical Model to Predict Residual Stresses in Sufrace Plunge Grinding*, Annals of the CIRP, Vol. 36, No 1, 1987, pp. 413–416.
[21] Vensevenant E.: *A Subsurface Integrity Model in Grinding*, Praca doktorska, KU Leuven, September 1987.
[22] DSA 102 Badanie narzędzi ściernych na stanowiskach badawczych.
[23] PN-EN 12413, 2001, Warunki bezpieczeństwa dla narzędzi ściernych spojonych.

Wpływ warunków przecinania ściernicowego na temperaturę ściernicy i względną wydajność szlifowania

W artykule przedstawiono zastosowanie termowizyjnego sposobu pomiaru temperatury ściernicy podczas przecinania ściernicowego. Opisano badania przecinania stali ściernicami trzech producentów w różnych warunkach tego procesu. Zaprezentowano wyniki badań dotyczące rozkładu temperatury na obwodzie ściernicy i wzdłuż jej przekroju promieniowego oraz ocenę względnej wydajności ściernicy.

Analiza uzyskanych rozkładów temperatury wzdłuż obwodu ściernicy pokazuje, iż wartość temperatury ma tendencję malejącą w kierunku obrotu ściernicy określającą stopień jej wychłodzenia w powietrzu.

Analiza otrzymanych rozkładów temperatury wzdłuż promienia ściernicy wskazuje na to, iż największa temperatura ściernicy występująca przy jej obwodzie podlega spadkowi wyrażonemu gradientem od 60 °C/mm do 80 °C/mm, co świadczy o niskiej przewodności cieplnej badanego narzędzia. Maksymalne temperatury uzyskane dla ściernic różnych producentów o tej samej charakterystyce technicznej w tych samych warunkach przecinania różnią się o około 30%. Ze wzrostem średnicy przecinanego przedmiotu temperatura przecinania rośnie. Jest to skutkiem zwiększonego kontaktu ściernicy z przedmiotem pomimo mniejszych nacisków jednostkowych. Wzrostowi siły docisku ściernicy w procesie przecinania od 62 N do 72 N towarzyszy wzrost maksymalnej temperatury ściernicy. Dalszy wzrost siły docisku do 82 N powoduje spadek tej temperatury, którego przyczyną może być powstające przy dużych obciążeniach ziaren ściernych zjawisko samoostrzenia ściernicy.

Analiza wyników badań wydajności względnej ściernic wskazuje, iż ze wzrostem siły docisku ściernicy maleją wartości wskaźnika wydajności względnej przy przecinaniu prętów o mniejszej średnicy. Zmniejszone wartości tego wskaźnika zaobserwowano także podczas przecinania prętów o większej średnicy tylko dla większych sił docisku. Wykazane tu pogorszenie wydajności względnej ściernic do przecinania należy wiązać z intensyfikacją w tych warunkach przecinania zjawiska samoostrzenia ściernicy.

ARCHIVES OF CIVIL AND MECHANICAL ENGINEERING

Vol. VIII 2008 No. 2

Magnesium semi-finished products for vehicle construction

R. KAWALLA, G. LEHMANN, M. ULLMANN
Freiberg University of Mining and Technology, Institute for Metal Forming, Bernhard-von-Cotta, 09596 Freiberg, Germany

H.-P. VOGT
MgF Magnesium Flachprodukte GmbH, Agricolastr. 24, 09599 Freiberg, Germany

At the Institute of Metal Forming, basic research-oriented and application oriented, two research foci on magnesium are pursued. One focus is on the production of semi-finished products for magnesium sheets and strip production by twin-roll-casting, the other focus is on the production of long products as wire, intended for the fabrication of joining elements.

Magnesium sheets produced by twin-roll-casting and subsequent rolling offer very good processing properties and are partly superior to conventionally produced sheets. Advantages result from a shortened process chain whose technology leads to a favourable initial condition for strip production. Additionally, economical advantages due to the few process steps clearly exist. Wire production for the production of joining elements is based on a specifically developed calibration which causes advantageous stress and deformation conditions during caliber rolling.

Properties of both product groups of magnesium alloy AZ21, AZ31, AZ91 and WE 43 are described comprehensively. Their application for the production of parts and components is shown on examples.

Keywords: *twin-roll-casting, strip-rolling, magnesium alloys, magnesium wire rod*

1. Introduction

The growing significance of the material magnesium is closely associated with the progressive development in the field of automotive lightweight construction. The announcement of the VW AG of constructing a one-litre-automobile can be deemed to be a proof of the actuality of research and development in the field of magnesium alloy processing. That automobile, whose frame structure is widely made of magnesium, shall be mass-produced before end of 2010 [1]. The material magnesium does not compete only with other metallic materials, also in particular with novel material concepts of the plastics industry. In this connection the better recycle ability and therefore the better environmental compatibility compared to the plastics is an essential advantage of magnesium.

In cooperation with the MgF Magnesium Flachprodukte GmbH the twin-roll-casting technology has been developed to series-production readiness. It enables a continuous production of near-net shape strips compared to the conventional light metal casting. So far the twin-roll-casting technology has successfully been tested on the pilot plant in Freiberg with the alloys AZ21 and AZ31 [2], [3].

With increasing use of magnesium parts, the interest on suitable connection technologies for this material grows. In cooperation with ESKA Automotive GmbH in Chemnitz first trials for the suitability of rolled wire rod made of alloys with higher strength AZ91 and WE43 for the production of screws were carried out [4].

2. Magnesium sheets and strips

The existing twin-roll-caster produces strips with a thickness of 3, 5 to 7 mm and a maximal width of 700 mm (see Figure 1a). With the help of a strip rolling mill the strips were rolled down to final thickness (see Figure 1b). Further details regarding the twin-roll-casting and rolling technology can be found in the literature [2], [5–9].

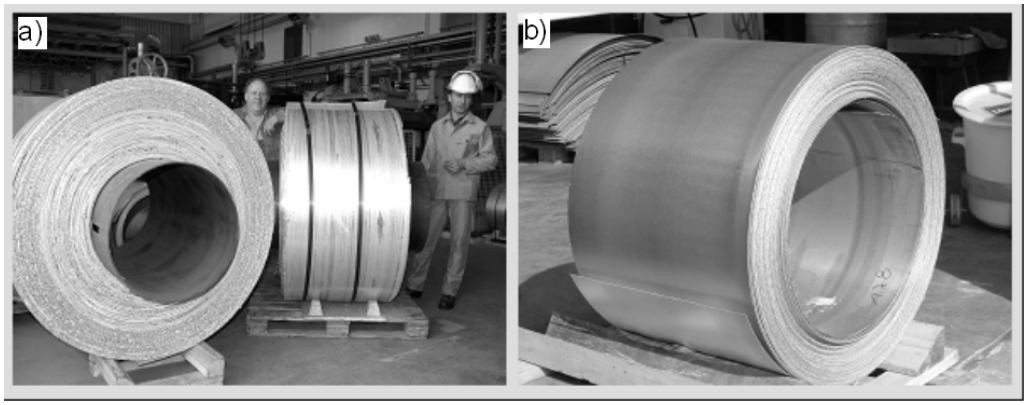

Fig. 1. Twin roll casted and rolled coils made of magnesium alloy AZ21:
a) Twin roll casted strip, b) Rolled strip

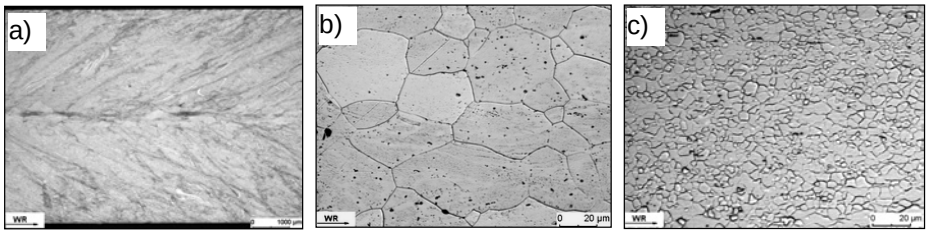

Fig. 2. Microstructure of the twin-roll-casted AZ21 strip after slow cooling down to room temperature (a) and after homogenization at 480 °C, 1h (b), as well as the microstructure of the final strip (c)

By means of this technology, which consists presently of the process steps twin roll casting, homogenization, hot rolling and subsequent annealing, it is possible to produce sheets with favourable mechanical properties and advantageous deep drawing and stretch forming properties. Figure 2a shows the typical microstructure of the strip in twin-roll-casted condition. Due to the high cooling rate and partial forming in the roll

gap of the mill a fine fishbone like solidification structure with a dendrite-grain-meshwork is created. In the following annealing process the microstructure is transformed into a homogeneous globular structure (Figure 2b). After rolling and subsequent annealing a very fine grained homogeneous microstructure is available (Figure 2c).

Figure 3 shows examples of the temperature and deformation degree dependence of the flow stress for the twin-roll-casted and hot rolled (1 pass, 30% reduction) condition of AZ21 alloy at a strain rate of 1 s^{-1}.

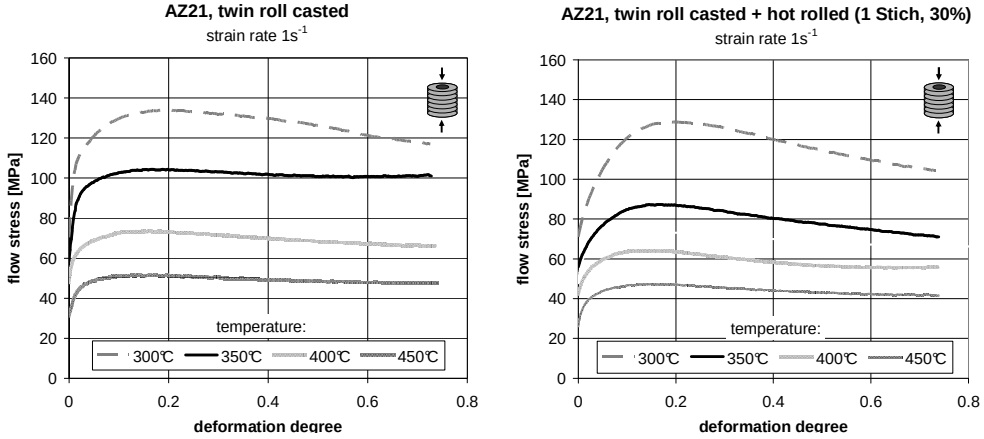

Fig. 3. Flow curves of magnesium sheets at elevated temperatures in the twin-roll-casted (a) and twin-roll-casted + hot rolled (b) condition; strain rate 1 s^{-1}, determined in ferrule compression test

The characteristics of all flow curves reveal a decreasing trait. The decrease of the curves is described by an interaction of hardening and softening mechanism, at which the dynamic recrystallization exerts a stronger influence seen in the decline of the curve. Both conditions have in common that with increasing temperature the flow curves run lower with a less developed maximum, which means that hardening decreases with increasing temperature because of the dominant influence of thermal activated processes. Further on, it is obvious that the rolled samples have a lower flow stress than the twin-rolled-casted and on room temperature cooled samples. The flow stress maxima of all samples appear approximately at the same deformation degrees. Due to a finer grain structure the maximum of the flow stress of rolled samples is pronounced.

In the following the properties of the sheets produced by twin-roll-casting and hot rolling is explained. In all cases the results were achieved on sheets with a thickness of 1.5 to 0.6 mm.

At the room temperature those Mg sheets offer yield points of 140–200 MPa, tensile strengths above 240 MPa and total elongations (A_{80}) above 17%, whereas total elongations of 25% are achievable, too. The level of strength and forming behaviour

depends on the Al-content in the case of AZ-alloys. Thus, AZ-alloys with an Al-content of 2% can achieve yield points of approximately 140 MPa and A_{80}-elongations of 20% for example.

Figure 4 clarifies better forming behaviour in tensile test at elevated temperatures. An increase in temperature from 20 to 100 °C leads to a remarkable increase of total elongation. In the area of 100 to 200 °C there is no nameable improvement in total elongation. Above 200 °C an increase of total elongation with increasing temperature is noticeable again, due to additionally activated slip systems in the hexagonal lattice and the interaction with thermal activated processes in the microstructure. At a deformation temperature of 300 °C total elongations of 80% are achievable. Even in the area of 150 and 200 °C total elongations of 45 to 50% are possible.

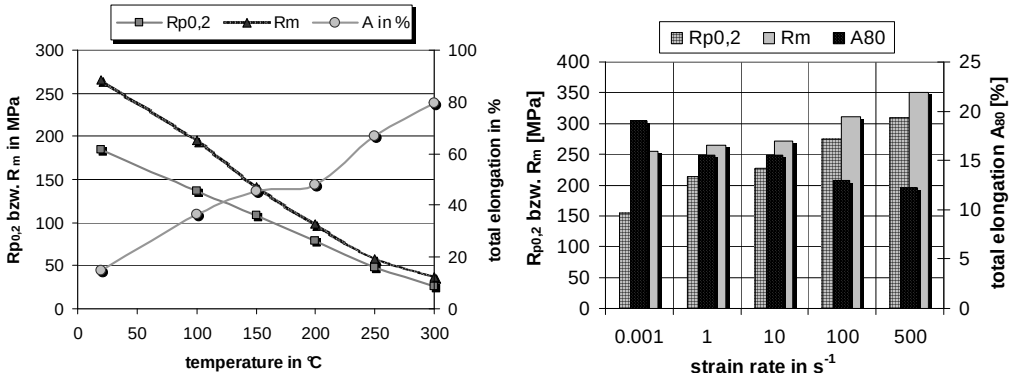

Fig. 4. Influence of temperature (a) and deformation rate (b) on the mechanical properties in tensile test, rolled and annealed twin-roll-casted strip AZ21

Besides temperature the strain rate is an important influencing factor (see Figure 4b). The raise of strain rate from 1 to 500 s^{-1} leads to an increase in strength values of 35–40%. The total elongation decreases by only 2% which complies with a relative reduction of 15%. The increase in strength with increasing strain rate is important for crash-relevant components.

In order to process Mg-sheet by deep drawing and stretch forming, as low as possible dependence of properties on the rolling direction is aimed for. Figure 5a shows the mechanical properties of AZ21 depending on the rolling direction. It is observable that the sheet produced by twin-roll-casting, homogenizing, hot rolling and subsequent annealing feature a lower anisotropy in the sheet plane.

For further evaluation of the forming properties of magnesium sheets, forming limit diagrams are used. These diagrams help to asses the forming behaviour as well as the limit of forming at different stress- and forming states. At elevated temperatures the limit curves are displaced towards higher φ_1 values, which mean that the forming limit ability increases (Figure 5b). Depending on the applied condition the forming limit can be 100% higher at 300 °C compared to 200 °C. The forming limit increases at

all temperatures, when going from uniaxial homogeneous tension ($\varphi_2 = 0$) to uniaxial tension ($\varphi_1 = -\varphi_2$).

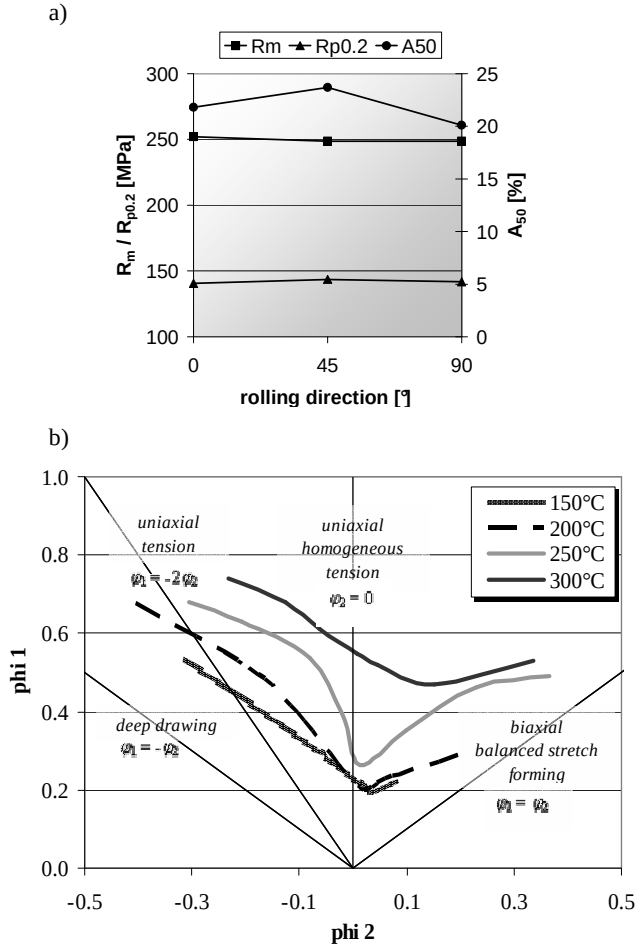

Fig. 5. Influence of rolling direction on mechanical properties (a) and forming limit diagram (b)

Forming tests with different techniques have shown a good workability of the sheets. Figure 6 shows different deep drawn parts made of magnesium alloy AZ31 (produced by twin-roll-casting).

3. Magnesium components for cars

By use of fasteners such as screws, rivets, pins, etc. made of the same base material; corrosion can widely be avoided at the connection points of the magnesium com-

ponents. At least simple components with fewer load dependent connections, easier, safer and finally more cost-efficient constructions are realisable.

The successfully conducted first investigations are part of the actual research and development in the area of the production of magnesium wire rod at the Institute of Metal Forming. Comparable to the production of sheet an economical production of wire is achievable due to the use of effective and continuous rolling and drawing processes. The main focus of the work at the Institute of Metal Forming is on the development and testing of roll pass design and drawing sequence according to the processing of magnesium alloys [4, 10].

Two magnesium alloys with high strength were chosen for investigations, the AZ91 alloy (with reduced Al content) and the cost-intensive WE43 alloy.

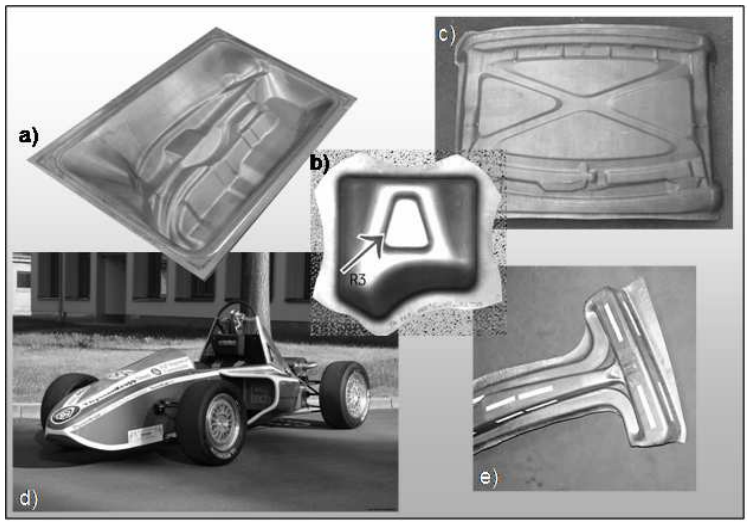

Fig. 6. Examples of use magnesium alloy AZ31 with lowered Al-content, a) door inner reinforcement, b) sample part, c) roof inner reinforcement, d) racing car for „Formula Student Series 2007", the complete body consists of magnesium sheet, e) B-pillar

The flow curves of both wire rods, which are also tend to recrystallization dynamically, are shown in Figure 7. In comparison to the sheets of AZ21 and AZ31 the flow stress are on a higher level. A specific characteristic is the curve development in the area of small deformation degrees, which is caused by the dominant influence of twinning. Both alloys (AZ91 and WE43) show especially at high strain rates or low temperatures considerable signs of twinning.

After rolling, the alloys were solution treated and drawn. The determination of the mechanical properties of the drawn wires takes place in tensile test, whereas the material was differently heat treated in order to investigate the possibilities of the strength improvement (see Table).

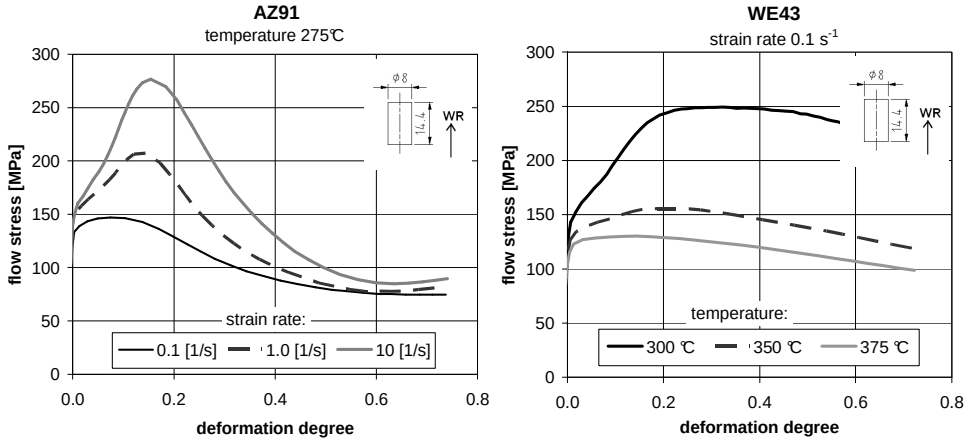

Fig. 7. Flow curves of wire rods (∅ 8.5 mm) made of a) AZ91 at 275 °C depending on the deformation rate and b) WE43 at 0.1 s^{-1} depending on temperature

Table. Parameter of heat treatment on drawn wire

Material	AZ91		WE43	
Drawing	Strain hardening		Strain hardening	
Solution treatment	400 °C / 0.5h	–	525 °C / 0.5h	–
Aging treatment	200 °C / 2h	200 °C / 2h	250 °C / 2h	250 °C / 2h

Figure 8 presents the mechanical properties of the drawn wires after heat treatment in comparison to the rolled condition. For both alloys tensile strengths of 400 MPa are reachable due to strain hardening during drawing and subsequent annealing.

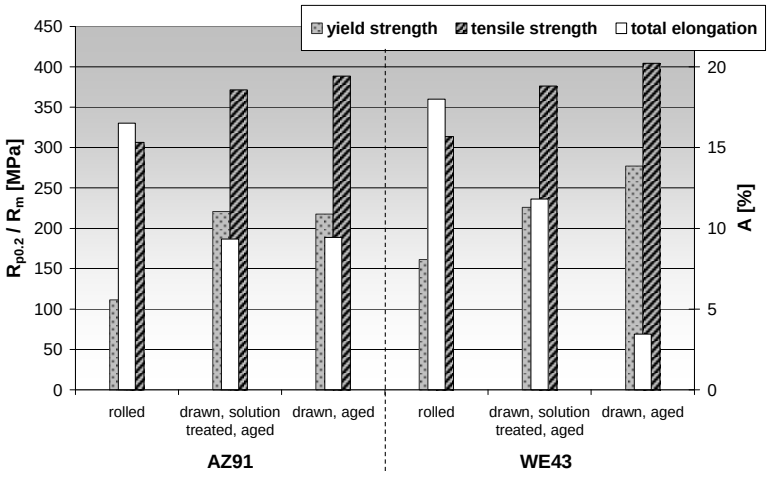

Fig. 8. Mechanical properties of the drawn wires (∅ 8 mm) after heat treatment in comparison to wire rod

The Figure 8 shows that the solution treatment prior to the aging treatment has no significant influence. Only the tensile strength of the samples directly subjected to aging treatment after work hardening was marginally higher. The strain hardened and aged sample of the alloy WE43 offers tensile strengths above 400 MPa, but with extremely low elongations. With the help of a solution treatment in between the forming behaviour can be improved with a low loss in strength (see Figure 9).

Fig. 9. Demonstrator component (AZ91) after thread rolling

Within these investigations the practicability of formed fasteners made of high strength magnesium alloys could be determined. In cooperation with the Saxon company ESKA Automotive GmbH the complete process from the production of the wire rod to the component was carried out. Figure 9 shows a demonstrator component made of the alloy AZ91 after thread rolling.

Acknowledgement

The authors thank the Saxony State Ministry for Economic Affairs and Labor (SMWA) – technology promotion (Development Bank of Saxony, SAB) for the financial support.

References

[1] Reisener T.: *VW baut Ein-Liter-Auto*, Rheinische Post, 09.10.2007.
[2] Engl B., Kawalla R.: *Entwicklung eines neuartigen kostengünstigen Verfahrens zur Herstellung von Magnesiumband*, MEFORM 2006, Freiberg, pp. 96–117.
[3] Kawalla R., Lehmann G., Vogt H.-P.: *Magnesiumhalbzeuge für den Fahrzeugbau*, proceedings 14. Sächsische Fachtagung Umformtechnik, 2007, Freiberg, pp. 1–10.
[4] Brethfeld A., Lehmann G., Wissmeier H.-J.: *Verbindungselemente aus Magnesiumlegierungen*, proceedings MEFORM 2007, Freiberg, pp. 312–325.
[5] Kawalla, R.; Lehmann, G.; Pircher, H.; Weber, M.: *Magnesiumblechherstellung Stand und Perspektiven*, 8. Sächsische Fachtagung Umformtechnik, 2001, Freiberg, pp. 236–246.
[6] Kawalla R., Ullmann M., Oswald M., Schmidt C.: *Properties of Strips and Sheets of Magnesium Alloy Produced by Casting-Rolling Technology*, Dresden: Proceedings of the 7th International Conference on Magnesium Alloys and Their Applications, K. U. Kainer, proceedings Magnesium, pp. 364–369.

[7] Oswald M., Schmidt C., Waengler S., Cuong N.-D.: *Einfluss der Umformbedingungen beim Walzen von Magnesiumgießwalzband aus der Gießhitze auf die Feinblech - und Bandqualität*, MEFORM 2006, Freiberg, pp.128–143.
[8] Ullmann M., Oswald M., Cuong N.-D.: *Werkstoff- und technologische Kennwerte für Feinbleche am Bsp. von Magnesium*, MEFORM 2006, Freiberg, pp. 65–80.
[9] Chabbi L., Lehnert W., Kawalla R.: *Hot and Cold Forming Behaviour of Magnesium Alloys AZ31 and AZ61*, Magnesium Alloys and their Applications, DGM, Wiley-VCH Verlag GmbH 2000, pp. 621–627.
[10] Lehmann G., Brethfeld A., Lange R.: *Untersuchungen zum Umformverhalten von Magnesiumlegierungen der Güten AZ31, AZ91 und WE43*, Proceedings MEFORM 2006, Freiberg, pp. 51–64.

Półwyroby magnezowe stosowane do budowy pojazdów

W Instytucie Przeróbki Plastycznej TU Bergakademie Freiberg, zasadnicze badania i ich zastosowania skupione na magnezie, prowadzone są w dwóch kierunkach. Pierwszy kierunek dotyczy produkcji półwyrobów z blach magnezowych i produkcji taśm przez odlewanie do walców w walcarkach typu duo/kwadro, drugim kierunkiem badań jest produkcja wyrobów długich, takich jak druty, przeznaczonych do wytwarzania elementów łączonych. Blachy magnezowe wytwarzane przez odlewanie do walców i walcowanie na gorąco z wykorzystaniem ciepła odlewania oferują bardzo dobre własności przetwórcze, które są częściowo lepsze od konwencjonalnie produkowanych blach. Korzyścią jest również skrócone procesu, co przynosi duży efekt ekonomiczny. Produkcja drutu do wytwarzania elementów łączonych jest oparta na szczególnie rozwiniętym kalibrowaniu, które powoduje korzystny nacisk i warunki odkształcania podczas walcowania kalibrującego. W pracy opisano obszernie własności obu grup produktów uzyskanych ze stopów magnezu: AZ21, AZ31, AZ91 i WE 43. Ponadto zostało przedstawione na przykładach ich zastosowanie w produkcji części i komponentów.

ARCHIVES OF CIVIL AND MECHANICAL ENGINEERING

Vol. VIII 2008 No. 2

Advanced high strength steels for automotive industry

R. KUZIAK
Instytut Metalurgii Żelaza, ul. Karola Miarki 12-14, 44-100 Gliwice, Poland

R. KAWALLA, S. WAENGLER
Institute for Metal Forming, Bernhard v. Cotta Str. 4, 09596 Freiberg, Germany

The aim of this paper is to present the basic concepts of advanced high strength steels (AHSS) for use in the automobile industry, including chemical composition design, microstructure and mechanical properties development during thermomechanical processing, production technology characterisation, potential applications and performance in service. AHSS steels are considered to be the major materials for future applications in this production sector. As opposed to the cold formable single phase deep-drawable grades, the mechanical properties of AHSS steels are controlled by many factors, including: phase composition and distribution in the overall microstructure, volume fraction, size and morphology of phase constituents, as well as stability of metastable constituents. The main feature of these steels is that they do not permit to rely on the well-established traditional microstructure-properties relationships. Therefore, many different alloy concepts and alternative processing routes are still under development by different steel producers for comparable steel grades.

Keywords: a*dvanced high strength steels, automobile industry, microstructure, mechanical properties, thermomechanical treatment, weldability, crash worthiness*

1. Introduction

Over the last decade, a strong competition between steel and low density metal industries has been observed as a result of increasing requirements of passenger safety, vehicle performance and fuel economy. The response of steel industry to the new challenges is a rapid development of higher strength steels, named Advanced High Strength Steels (AHSS) [1]. These steels area characterised by improved formability and crash worthiness compared to conventional steel grades. The category of AHSS covers the following generic types: dual phase (DP), transformation induced plasticity (TRIP), complex phase (CP) and martensitic steels (MART).

The AHSS may be distinguished based upon the strength properties that roughly can be defined: yield strength > 300 MPa and tensile strength > 600 MPa. As opposed to the conventional high strength steels, in which ductility decreases with strength, modern AHSS steels combine high strength and formability/ductility. General classification of these steels is as follows:

- Highs strength steels with a high energy absorption potential (DP and TRIP steels with UTS < 1000 MPa), for dynamic loading occurring during car crashes or collisions.

• Extremely high strength steels, typically martensitic steels, with a very high UTS (>1200 MPa), providing high stiffness, anti-intrusion, load-transferring barriers for the protection of automotive passengers.

• The rationales for increased use of the AHSS in the automotive industry are as follows:

• The reduction of the car weight resulting from the use of high strength thinner gauge sheet steel, reducing the fuel consumption.

• Increased passenger safety by an improved crash worthiness.

• The strong competition from the light-weight materials, such as Al and Mg alloys and plastics.

AHSS derive their properties from multi-phase complex microstructure. Since these steels are relatively new, their classification differs from conventional high strength steels and was developed by Ultra-Light Steel Automotive Body – Advanced Vehicle Concept (ULSAB-AVC) Consortium [1]. The accepted practice involves specification of both yield strength (YS) and ultimate tensile strength (UTS) in the following way:

XX aaa/*bbb*,

where *XX* is type of steel, *aaa* is minimum YS in MPA and *bbb* is minimum UTS in MPA.

For example DP 280/600 designates dual phase steel with 280 MPa minimum yield strength and 600 MPa minimum ultimate tensile strength.

2. Microstructure – mechanical properties characterisation

2.1. Dual phase steels

Microstructure of dual phase steels is composed of soft ferrite matrix and 10–40% of hard mastensite or matrensite-austenite (M–A) particles (Figure 1). This type of microstructure allows achieving the ultimate tensile strength in the range of 500–1200 MPA. When the volume fraction of martensite exceeds 20%, DP steels are often called partial martensitic. For some applications, also baintic constituent may be desirable in the DP steel microstructure. This dual phase type of microstructure can exhibit the following advantageous features over the conventional high strength steels:

• The strength of the DP steel microstructure is controlled by the amount of martensite and ductility by the size and distribution of this phase,

• DP steels do not exhibit yield point elongation,

• DP steels posses low UTS/YS ratio (around 0.5) and high strain hardening characteristics (high *n* value), especially at the beginning of plastic deformation,

• They can be strengthened by static or dynamic strain ageing (BH effect),

• Grades containing low carbon content have been shown to exhibit excellent resistance to fatigue crack propagation at growth rates close to fatigue threshold intensity range ΔK_{th}.

Very important for the development of DP steel is the effect of carbon and alloying elements, which was summarized in Table 1.

Table 1. Effect of alloying elements in DP steels

Alloying element	Effect and reason of adding
C (0.06–0.15%)	▪ Austenite stabilizer ▪ Strengthens martensite ▪ Determines the phase distribution
Mn (1.5–2.5%)	▪ Austenite stabilizer ▪ Solid solution strengtheners of ferrite ▪ Retards ferrite formation
Si	▪ Promotes ferritic transformation
Cr, Mo (up to 0.4%)	▪ Austenite stabilizers ▪ Retards pearlite and bainite formation
V (up to 0.06%)	▪ Austenite stabilizer ▪ Precipitation strengtheners ▪ Refines microstructure
Nb (up to 0.04%)	▪ Austenite stabiliser ▪ Reduces M_s temperature ▪ Refines microstructure and promotes ferrite transformation from non-recrystallized austenite

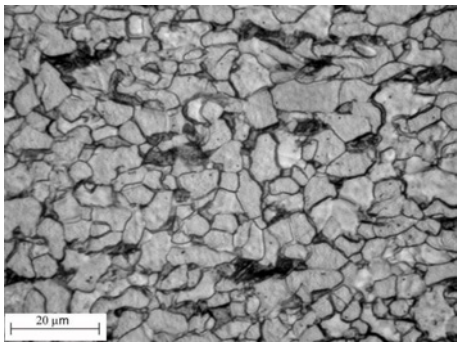

Fig. 1. Photomicrograph of the dual-phase steel microstructure

The microstructure of DP steels do not allow obtaining of high plastic strain ratio value (r_m), which means that these steels are not good candidates for applications that require high drawability. They usually exhibit poor hole expansion ratio values. This drawback, however, can be eliminated by adding Ti with the aim of inducing the precipitation strengthening in ferrite to reduce the differences in hardness between the two phases. Alternatively, M-A constituents may be replaced by bainitic phase. Dual

phase steels can be welded with all conventional welding methods currently used in the automotive industry (resistance spot welding, laser welding, arc welding).

The most important features influencing mechanical properties of the dual-phase microstructure comprise shape, size, amount and distribution of ferrite and martensite, the carbon content of martensite, and the volume fraction of retained austenite.

In DP steels, for a fixed volume fraction of M-A constituents, both applied stress and the work hardening rate at a given true strain can be related to the average size of M-A particles by the Hall-Petch type equation. Frequently cited expressions, for f_{MA} = 0.2, were developed by Lanzilotto and Pickering [2]:

$$\sigma_{f(\varepsilon=0.2)} = 350 + 18.1\lambda^{-0.5}, \tag{1}$$

$$\frac{d\sigma}{d\varepsilon_{(\varepsilon=0.2)}} = 40.1\,\lambda^{-0.5}, \tag{2}$$

where λ is the average size or diameter of M-A particles.

The coefficients of Equations (1) and (2) suggest that $d\sigma/d\varepsilon$ increases more rapidly than σ_f. This suggests that refinement of the M-A constituent in DP steels should result in an increase in uniform elongation. The variation of stress as a function of martensite content in DP steels has been frequently modelled on the basis of the rule of mixtures, applying the continuum mechanics models [3]:

$$\sigma = V_m\,\sigma_m + (1 - V_m)\,\sigma_f, \tag{3}$$

where σ_m, σ_f, σ are the stresses of the martensite, ferrite and composite structure respectively.

The dependence of stress on strain in composite and components is modelled with the following constitutive equation:

$$\sigma = k\,\varepsilon^n. \tag{4}$$

The rule of mixtures can be applied to either isostrain or isostress conditions [4]. Equation (3) is frequently applied with the assumption that σ_m and σ_f are invariant with respect to the volume fraction and morphology of the respective phases. However, most of the experimental results show that this approach is obeyed for martensite volume fraction of up to approximately 0.5. Chang and Preban proposed the model capable of explaining the variation between yield strength and volume fraction of martensite [5]. In their model, yield stress in DP steels is assumed to be influenced by the mean free path in ferrite, λ_f, through a Hall-Petch type relationship:

$$\sigma_y = \sigma_{0y} + K_y \, \lambda_f^{-0.5}, \tag{5}$$

where σ_{0y} is a frictional stress of the matrix, K_y is the dislocation-locking constant. In the model, both σ_{0y} and K_y are functions of V_m.
Bag et al. [6] proposed the new approach that allowed the prediction of yield stress using the following equation:

$$\log(\sigma_y) = 2.8565 - 0.25441 \log(\lambda_f). \tag{6}$$

Equation (6) can be used for the prediction of yield stress over a wide range of V_m parameter and is independent of this parameter. This is connected to the fact that the mean free path in ferrite is dependent on the martensite content.

2.2. TRIP steels

Advanced high-strength transformation-induced plasticity (TRIP) steels are well suited for light-weighing car body construction with added advantage to reduce the safety problems. The possible development of this type of steels was first discovered by Zackay et al. [7]. They proposed that the strain or stress induced transformation of retained austenite present in the microstructure in a sufficient amount can substantially harden the steel during deformation, and therefore results in a higher ductility. The mechanical properties of TRIP steels are derived from their disperse multi-phase microstructure which is composed of ferrite – α (0.50–0.55), bainite (0.30–0.35), retained austenite – γ_R (0.07–0.15), and possibly martensite (0.01–0.05). Retained austenite is the most important phase constituent of TRIP steels. An example of the EBSD map of this phase in TRIP steel is given in Figure 2. During deformation, retained austenite transforms to martensite. The TRIP mechanism in steels with dispersed austenite is shown schematically in Figure 3. The crucial technological challenge concerning TRIP steels lies in the necessity of producing in their structure of sufficiently high content of very stable austenite.

The TRIP steels are characterised by a relatively low content of alloying elements. For example, in current 800 MPa TRIP steels, the total content of alloying elements is about 3.5 wt.%. Thus, the selection of suitable alloying elements and the amount required to produce the intended properties is a critical stage in the alloy design stage. Conventional TRIP steel compositions concept proposed by Matsumura, is based upon the following C, Mn and Si content [8]:

C: 0.12 – 0.55 wt.%; Mn: 0.20 – 2.5 wt.%; Si: 0.40 – 1.8 wt%.

The carbon content plays a fundamental role in TRIP steel composition design, since its distribution among the main microstructural constituents is fundamental to

the material properties. To obtain the best mechanical properties in a product, first of all, carbon should distribute to austenite and enrich this phase as much as possible to preserve the M_s^{σ} of this constituent of 15–25°C below the room temperature. Carbon content in the current TRIP steels is limited to 0.20–0.25 wt.% due to the weldability concerns. For the hardenability reasons, the Mn content in low alloy TRIP steels is around 1.5 wt.%.

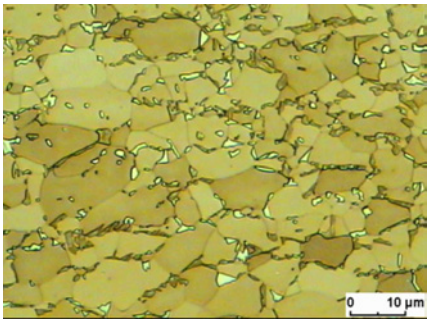

Fig. 2. EBSD map of retained austenite in TRIP steel microstructure

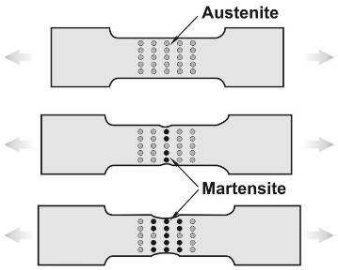

Fig. 3. Illustration of the TRIP effect during tensile test

Manganese is an austenite stabilizer and it lowers the cementite start temperature. It also lowers the carbon activity in austenite and ferrite and increases the carbon solubility in ferrite. Manganese is also soluble in cementite. On the contrary, silicon significantly increases the carbon activity in both ferrite and austenite and decreases its solubility in ferrite. As a result, Si inhibits the formation of cementite during the austempering stage. It has extremely low solubility in cementite, an thus, it affects the nucleation of this carbide. It is believed that the accumulation of Si around a cementite nucleus could considerably increase the C activity which prevents its diffusion to nucleus. The minimum level of Si needed to effective suppress the cementite formation is believed to be around 0.8 wt.%. However, it is important that note that Si slows down the kinetics of bainitic transformation. As a result, cold rolled TRIP steels should be further annealed on a long line with long over-ageing section allowing the

long austempering stage to be conducted. The exploitation of Si to prevent against the carbides formation is currently being limited due to the requirement for continuous galvanizing of AHSS sheet steel. The high silicon content in TRIP steels results in film-forming surface oxides which prevent the formation of the inhibition layer during the hot dip galvanizing which prevents the wetting of the sheet surface by the liquid Zn.

The reasonable solution to handle the model production lines requirement is to limit the silicon content and use increased aluminium content in TRIP steels, preferably, apply the partial replacement of 1 wt.% of Si by 1 wt.% of Al. The CMnAl TRIP steels have received much attention over the last years, because, the high Al content in these steels results in a high C content in retained austenite. Quite similar to silicon, aluminium is insoluble in cementite and, generally, retards its formation, but more importantly, it accelerates the bainite transformation kinetics. This effect of aluminium is very important for the TRIP steel industrialization since it allows the adoption of currently available continuous lines dedicated to IF steels, that does not have long overageing sections. The disadvantages of using of Al are that this element lowers solid solution hardening effect as compared to silicon, and increases the M_s temperature.

The recent developments in the TRIP steel production concept includes only partial replacement of Si by a limited amount of Al and use P in the amount of 0.05–0.10 wt.%. Lower Si content makes the steel galvanizable. The use of P is intended to limit the Al content, since P also suppresses the cementite formation and is a very effective solid solution hardening element. It was shown for TRIP steels low in Si that P increases the amount of retained austenite. P also significantly increases the C activity in ferrite.

2.3. Complex phase steels with bainitic matrix

Complex phase (CP) steels belong to a group of steels with very high ultimate tensile strength of 800 MPa or even greater. The chemical composition of CP steels, and also their microstructure, is very similar to that of TRIP steels, but, additionally it contains some quantities of Nb, Ti and or V to cause the precipitation strengthening effect. Typically, CP steels have no retained austenite in the microstructure, but contain more hard phases like martensite and bainite. The microstructure of CP steels is composed of a very fine ferrite with the high volume fraction of hard phase, For cold shaped structures, a triple phase steel containing ferrite, bainite and martensite can be designed which are obviously more difficult to produce. Their mechanical properties are characterised by continuous yielding and high uniform elongation. CP steels with the bainitic matrix have superior formability because the difference between the hardness of bainite and martensite is relatively small. In bainitic CP steels polygonal ferrite is replaced by bainitic ferrite. The bainitic ferrite is strengthened by a high density of dislocations, i.e., $> 10^{12}/cm^2$, and by a fine dispersion of MA second phase and carbonitrides or carbides.

The bainitc CP microstructure exhibits better strain hardening and strain capacity than that for fully bainitic microstructure. This is illustrated in the schematic stress-strain diagram shown in Figure 4. It involves a strength-graded microstructure where the martensite and bainitic ferrite phases are separated by a third phase of intermediate strength.

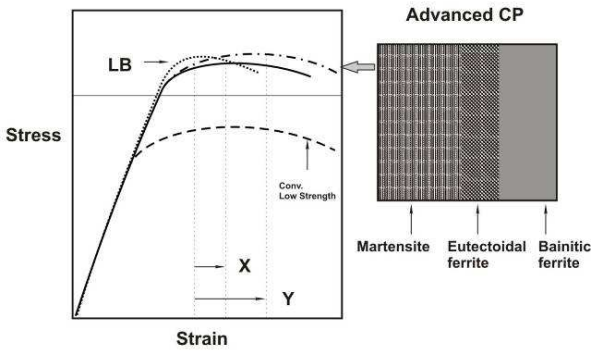

Fig. 4. Stress-strain schematic for advanced CP steels compared with lower bainite (LB) steel and conventional, low strength DP steels

2.4. Martensitic steels

Martensitic steels provide the highest ultimate strength in final products, up to 1500 MPa. Their concept is based upon a well established rules with respect to chemical composition and processing technology design. Microstructure of martensitic steels is mainly composed of lath martensite, which is developed by the transformation of austenite during quenching after hot rolling or annealing. They are often subjected to post-quench tempering with the aim of improving ductility and provide good formability even at very high ultimate strength. The concept of chemical composition of martensitic steels is based upon the proper carbon content adoption, since this element increases hardenability and strength. Manganese, chromium, silicon, molybdenum, boron, nickel and vanadium are also used in various combinations to increase hardenability.

3. Manufacturing technologies of AHSS steel strips

3.1. Dual phase steels

Modern AHSS are produced in complex processes involving thermomechanical processing followed controlled cooling. Alternatively continuous annealing following cold rolling is being used. Both types of processes will be characterised for DP and TRIP steels.

The cooling path in the rolling technology of DP steel strips is schematically shown in Figure 5. The last deformation in the DP strip rolling is conducted at approximately $Ar_3 + 40$ °C.

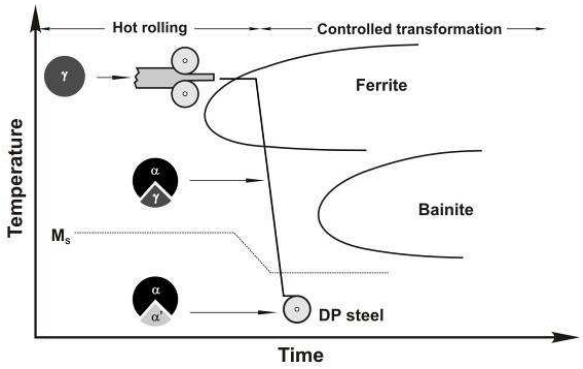

Fig. 5. Cooling schedule in the production of the DP strips

The cooling process after rolling starts with slow cooling stage on the run out table after rolling in which the desirable amount of ferrite is obtained as a result of the austenite transformation. Alternatively, the hot band can be subject to accelerated cooling to the temperature of the lowest austenite stability, followed by a slow cooling to allow the austenite decomposition into ferrite. The ferrite transformation allows the carbon content enrichment in the remaining austenite, which increases its hardenability and reduces M_s temperature. After that, the strip is accelerated cooled to the coiling temperature which must be below M_s. A critical cooling rate to obtain fully martensitic structure of the second phase is given by the following Equation [9]:

$$\log(C_R) > 5.36 - 2.36\,Mn - 1.06\,Si - 2.71\,Cr - 4.72\,P\,, \tag{7}$$

or [10]:

$$\begin{aligned} &\log(C_R) = 5.36 - 2.36\,Mn_{eq} \\ &Mn_{eq} = Mn + 0.45\,Si + 1.15\,Cr + 2\,P. \end{aligned} \tag{8}$$

Dual phase microstructure can also be developed in a cold rolled sheet material by the application of continuous annealing followed by hot dip galvanising. A schematic diagram of temperature changes during the annealing process is given in Figure 6.

During the annealing process, a sheet is heated to a temperature slightly above Ac_1. During this stage, around 15 % of microstructure composed of ferrite an pearlite transforms to austenite. After this, the sheet is quenched causing the austenite transforma-

tion to martensite. As a result, the final strip's microstructure contains predominantly ferrite and martensite in proper proportions.

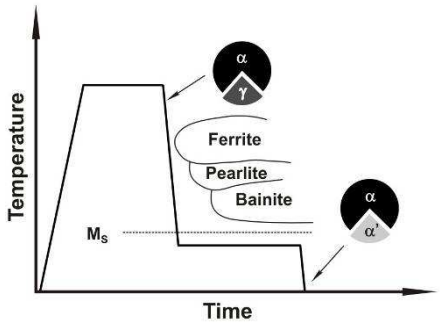

Fig. 6. Temperature changes during continuous annealing of DP steel sheets [11]

3.2. TRIP steels

The optimal combination of strength and ductility of TRIP steels is achieved by decreasing the mean free path in ferrite and by grain refinement and obtaining an uniform distribution of fine second phase particles. The cooling stage in the strip rolling process of TRIP steels, shown in Figure 7, is more complicated than that for DP strips. First, slow cooling is applied in the ferrite transformation temperature range. The transformation causes carbon content to increase in austenite to around 0.4%. After producing 50–60% of ferrite in the microstructure, accelerated cooling with cooling rate greater than 20 °C/s to the coiling temperature which lies in the bainitic transformation temperature range, is realised. During coil cooling, bainitic transformation proceeds, further increasing of carbon content in remaining austenite to around 1.2%. Part of this austenite, in the amount of 10–15%, remains untransformed accounting for the TRIP effect.

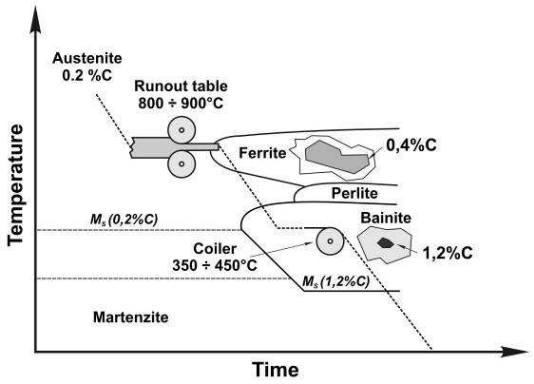

Fig. 7. Cooling schedule in the production of the TRIP strips [11]

TRIP strips can also be cold rolled and annealed. In such a case, a two-stage heat treatment with intercritical annealing in the temperature range 780–880 °C followed by cooling and isothermal annealing in the range 350–450 °C and cooling to ambient temperature is applied (Figure 8).

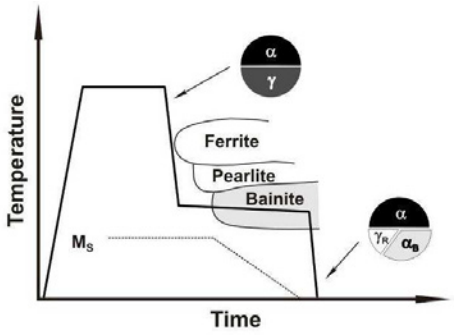

Fig. 8. Temperature changes during continuous annealing of TRIP steel sheets [11]

During the intercritical annealing, the microstructure composed of almost equal portions of ferrite and austenite is formed. However, as opposed to the case of hot rolled strips, during this process, a significant amount of ferrite exists in the initial microstructure prior to annealing. The holding time during the bainitic transformation equals to several minutes. After bainitic transformation, the microstructure contains around 50–60% of ferrite, 25–40% of bainite and 5–15% of retained austenite.

3.3. CP steels

The concept of CP steels is essentially similar to those of TRIP steels, however less stringent cooling practice can be imposed on the hot band during the last stage of processing. This is due to the fact that no presence of retained austenite is required in their microstructure.

3.4. MART steels

Martensitic steels are produced by applying rapid quenching from the austenitic phase to produce the laths martensite microstructure. Tempering after quenching may also be used to improve the strength/ductility relations.

4. Applications aspects of AHSS

The combination of high strength and ductility that provide modern AHSS can allow thinner components to be used in the cars construction and also to improve the safeness due to their high energy-absorption capabilities. The better formability of

AHSS, compared with conventional high strength steels of comparable strength give the automobile designer a high degree of flexibility to optimize the component geometry. Other component performance criteria comprise stiffness, durability, crash energy management. Below, a short characterization of AHSS with respect to these criteria is given.

Stiffness. The stiffness of a component is affected by material module of elasticity (E), as well as, its geometry. The module of elasticity is constant for steel, which means that changing steel grade does not affect the stiffness. Therefore, to improve stiffness, the component geometry must be changed. AHSS offer greater design flexibility to optimize the stiffness due to their enhanced formability. This can be done without increasing mass or decreasing strength. Reduction in gauge can be counterbalanced by changes in geometry or by using continuous joining techniques such as laser welding or adhesive bonding.

Strength. Strength of a component depends on its geometry and yield and/or tensile strength. AHSS provide an advantage in the design flexibility over conventional high strength steels due to their higher formability and work hardening characteristics. These grades also have good bake hardening ability. Therefore, it is important to account for this strength increase during the design process of car components in order to avoid the over design that may occurs when the design process is based upon as rolled mechanical properties specification. Both these features enable achieving high strength of as-manufactured components.

Fatigue. Fatigue properties of structural components depend on geometry, thickness, applied loads and material endurance limit. The endurance limit of a material increases with tensile strength. Thus, high strength combined with superior work hardening and bake hardening, resulting in a significant increase in the as-manufactured strength of AHSS components, also results in a better fatigue resistance.

Crashworthiness. Crashworthiness is an important characteristics that is currently becoming increasingly important. Recent trends require for a material to absorb more energy in crash scenario. The potential absorption energy can be assessed based upon the area under the stress-strain curves. Better performance in crash of AHSS compared to classical high strength steels is associated with higher work hardening rate and high flow stress. This feature account for a more uniform strain distribution in components in the crash event. Both, work hardening and bake hardening significantly improve the energy absorption characteristics due to the flow stress increase.

Formability. AHSS have many advantageous characteristics connected to formability compared to those of HSLA steels with comparable yield strength. AHSS in general have a higher initial work hardening rate, their higher ultimate tensile strength and, especially DP steels, have lower ratio of yield strength to tensile strength. All these advantages combined with an excellent elongation show, that AHSS combine high strength with good formability. High work hardening exponent accounts for the ability of a sheet metal to stretch and the ability of steel to distribute the strain more

uniformly in the presence of a stress gradient. An important advantage of DP steels is very high *n*-value at low strains which restricts the onset of strain localization and development of sharp gradients.

In the past, the selection process of materials for vehicle-body components was based solely upon their mechanical properties measured in the static tests. Members of ULSAB-AVC consortium adopted significantly different approach to the design of the body structure. They decided to use the established dependence of steel strength on strain rate. This is due to the fact that strain rates under crash conditions are much higher than during the static tests. Higher strain rates induce higher strength of the deformed material which, in turn, results in higher energy absorption. It was decided that the engineering experience of the vehicle designers would be supplemented with FEM simulations to assess forming behaviour. The particular attention in the course of the simulation is paid to:

- Assessment of the possibility of forming a car body component in the assumed tooling and making eventual design changes.
- Selection of the proper steel grades for components commonly considered of difficult or even impossible to form.
- Identification of alternatives to expensive materials or processes.

Table 2. Master materials list

Steel grade	YS (MPa)	UTS (MPA)	Total EL (%)	n-value (5–15%)	r-bar	Application code
Mild 140/270	140	270	38–44	0.23	1.8	A, C, F
BH 210/340	210	340	34–39	0.18	1.8	B
BH 260/370	260	370	29–34	0.13	1.6	B
IF 260/410	260	410	34–38	0.20	1.7	C
DP 280/600	280	600	30–34	0.21	1.0	B
IF 300/420	300	420	29–36	0.20	1.6	B
DP 300/500	300	500	30–34	0.16	1.0	B
HSLA 350/450	350	450	23–27	0.22	1.0	A, B, S
DP 350/600	350	600	24–30	0.14	1.1	A, B, C, W, S
DP 400/700	400	700	19–25	0.14	1.0	A, B
TRIP 450/800	450	800	26–32	0.24	0.9	A, B
HSLA 490/600	490	600	21–26	0.13	1.0	W
DP 500/800	500	800	14–20	0.14	1.0	A, B, C, W
SF 570/640	570	640	20–24	0.08	1.0	S
CP 700/800	700	800	10–15	0.13	1.0	B
DP 700/1000	700	1000	12–17	0.09	0.9	B
Mart 950/1200	950	1200	5–7	0.07	0.9	A, B
MnB	1200	1600	4–5	n/a	n/a	S
Mart 1250/1520	1250	1520	4–6	0.07	0.9	A

Application Code: A – Ancillary parts, B – Body structure, C – Closures, F – Fuel Tank, S – suspension/Chasis, W – Wheels

Steel producers, who participated in the ULSAB-AVC, have proposed various steel grades that should be used for manufacturing the vehicle body structure components. In the final concept design, specific steel grades were selected in a manner that best combine their unique mechanical properties, accounting for the structural demands of specific vehicle body component. The selection has been done for two body structure classes, for the C-class size vehicle and the PNGV-type vehicle.

The C-class is often called the VW Golf class while the PNGV (Partnership for a New Generation of Vehicles) class vehicle is defined as 5/6 passenger sedan with the interior volume of 3.115 m3, curb weight of 907 kg and fuel consumption of up to 3 l per 100 km. Table 2 contains the master materials for ULSAB-AVC. This Table gives the static mechanical properties of ULSAB-AVC body structure, closures, ancillary parts, suspension and wheels.

5. Summary

A substantial progress has been achieved during last years in the development of AHSS for applications in the auto body construction. The new strategy for introducing the technological advances into the mass production has been suggested. The most important contribution in this area should be ascribed to ULSAB and ULSAB-AVC research projects.

The approach adopted in these projects takes into account the diversification of material properties with respect to formability and energy absorption. To master the AHSS auto body components production technology, it is necessary to develop modern production lines that assure an accurate processing parameters control in the subsequent production stages. Temperature is the most important process parameter that must be precisely controlled after hot rolling and during continuous annealing of AHSS sheets.

References

[1] ULSAB-AVC *Body Structure Materials*, Technical Transfer Dispatch No. 6, May, 2001.
[2] Lanzillotto C.A.N and Pickering F.B.: *Structure-Property Relationships in Dual-Phase Steels*, Met. Sci., Vol. 16, 1982, pp. 371–382.
[3] Bleck W., Papaefthymiou S., Frehn A.: *Microstructure and Tensile Properties of Dual Phase and TRIP Steels*, Steel Reasearch. int., Vol. 75, No. 11, 2004, pp. 704–710.
[4] Korzekwa D.A., Lawson R.D., Matlock D.K., Krauss G.: *A consideration of Models Describing the Strength and Ductility of Dual-Phase Steels*, Scripta Metallurgica, Vol. 14, 1980, pp. 1023–1027.
[5] Chang P.H., Preban A.G.: *The Effect of Ferrite Grain Size and Martensite Volume Fraction on the Tensile properties of Dual Phase Steel*, Acta Metall., Vol. 33, No. 5, 1985, pp. 897–903.

[6] Bag A., Ray K.K.: *Influence of Martensite Content and Morphology on Tensile and Impact Properties of High-Martensite Dual Phase Steels*, Metall. Mat. Trans., Vol. 30A, 1999, pp. 1193–1202.
[7] Zackay V.F., Parker E.R, Fahr D., Bush R.: *The Enhancement of Ductility in High-Strength Steels*, Trans. Am. Soc. Met., Vol. 60, 1967, pp. 252.
[8] Matsuma O., Sakuma Y., Takechi H., Camp-ISIJ, 1985-S1293, pp. 89.
[9] Abe M., Mater. Sci. Technol.: Vol. 7, No. 7, 1992, pp. 285.
[10] Furukawa T. et al.: Trans. Iron Steel Inst. Jpn., Vol. 21, 1981, pp. 812.
[11] Bleck W., Phiu-On K.: *Microalloying of Cold-Formable Multi Phase Steel Grades*, Mat. Sc. Forum, Vols. 500–501, 2005, pp. 97–112.

Wielofazowe stale wysokowytrzymałe dla przemysłu samochodowego

Celem artykułu jest przedstawienie najważniejszych koncepcji projektowania składu chemicznego oraz technologii obróbki cieplno-plastycznej i właściwości mechanicznych oraz użytkowych nowoczesnych stali wielofazowych dla przemysłu motoryzacyjnego. Stale te, do których zalicza się następujące gatunki; DP, TRIP, CP i MART, uważane są za najważniejsze materiały do zastosowań w konstrukcji samochodów w przyszłości. Ich cechą charakterystyczną są bardzo skomplikowane zależności między strukturą a właściwościami mechanicznymi.

ARCHIVES OF CIVIL AND MECHANICAL ENGINEERING

Vol. VIII 2008 No. 2

Numerical and physical modelling of microstructure evolution – new approach to the development and optimisation of cold rolling and annealing technology of IF steel strips

R. KUZIAK, R. MOLENDA
Institute of Ferrous Metallurgy, ul. K. Miarki 12, 44-100 Gliwice, Poland

M. PIETRZYK
AGH – University of Science and Technology, al. Mickiewicza 30, 30-059 Kraków, Poland

Modelling of cold rolling and continuous annealing of the IF steel is the objective of the paper. Experimental plastometric tests were performed to determine flow stress in the temperature range characteristic for cold rolling. Physical simulations of the annealing were performed at various heating rates to various temperatures. The kinetics of recrystallization model based on the additivity rule was identified on the basis of the experimental results. In connection with the finite element model of cold rolling, the complex model for the whole manufacturing cycle is obtained. This model can be used for optimisation of cold rolling and annealing technology of IF steel strips.

Keywords: *IF steel, cold rolling, annealing, modelling*

1. Introduction

Automotive industry is the most important market for ultra low carbon (ULC) and interstitial free (IF) steel strips. These strips are characterised by exceptional formability, which is achieved trough the application of very complex cold rolling and annealing technologies. Therefore, the development and application of these technologies for automotive steels is the field of research in numerous laboratories. Obtaining of increased and consistent properties of products is the main objective of the research. Proper design of the rolling technology should guarantee not only achieving the dimensional accuracy, but also required microstructure, texture, mechanical properties and performance of sheets in further processing. Control of the process cycle composed of cold deformation, annealing and galvannealing, accounting for microstructure evolution, is an inevitable condition required to reach that goal. Design of the new technologies is currently based on physical and numerical simulations, and it is the objective of this work. The models for cold rolling and annealing only are presented in the paper. IF steel is considered as an example of the capabilities of these models. Adding galvannealing to this complex model will be the objective of further research, which will allow optimization and control of the whole manufacturing chain.

2. Experiment

The first part of the experiments included plastometric tests. The axisymmetrical compression of the IF steel samples was performed on the Gleeble 3800 simulator in the Institute for Ferrous Metallurgy in Gliwice, Poland. The axisymmetrical samples measuring ϕ10×12 mm were deformed at temperatures 20, 100, 200 and 300 °C and at constant strain rates of 1, 20 and 100 s^{-1}. Loads and temperatures were recorded as a function of the die displacement in each test. Shape of the sample was measured after the tests and the friction coefficient was determined on the basis of the observed barreling. Selected results of load measurements are presented in Figure 1. It is seen in this Figure that for low values of the Zenner-Hollomon parameter the material becomes insensitive to the temperature.

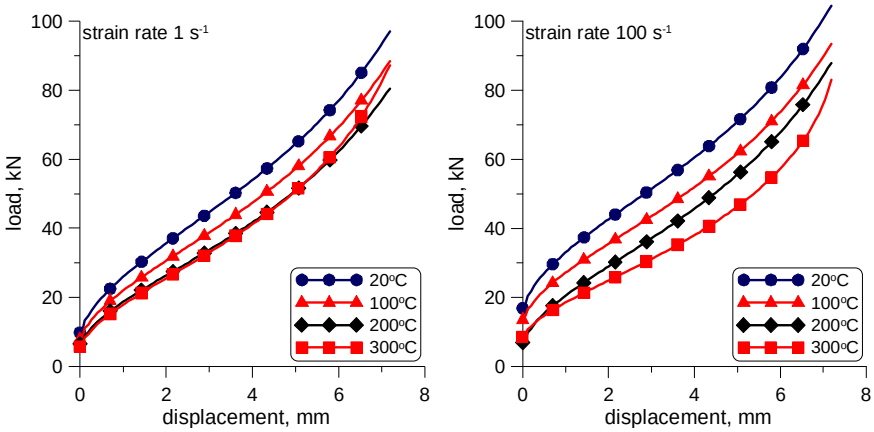

Fig. 1. Loads recorded in the axisymmetrical compression of IF samples

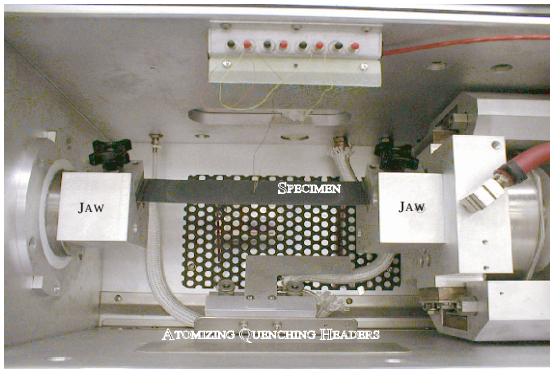

Fig. 2. Equipment for physical simulation of the continuous annealing of strips for the automotive industry

The second part of the physical modelling focused on the annealing. Thermal cycles were reproduced on the Gleeble 3800 simulator, which is shown in Figure 2. The samples measuring 55×250 mm, which were cold rolled with the reduction of 74%, were used. Samples were heated to 600, 650, 700, 750 and 800 °C with the heating rates of 0.5, 4 and 50 °C/s, and then quenched in the water-air mist. Relation between microstructure and time-temperature history was determined for various degrees of softening of the cold deformed material.

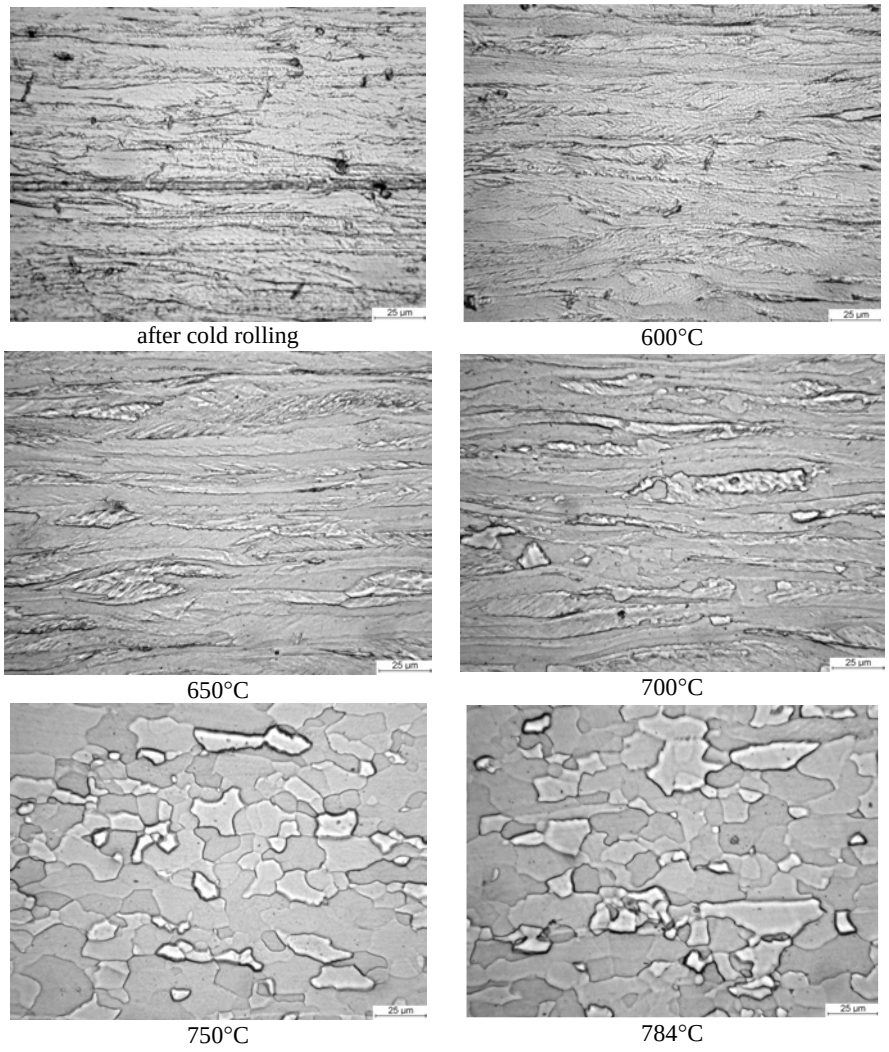

Fig. 3. Microstructures of the IF steel after cold rolling, heating to various temperatures and quenching

Microstructures after cold rolling and annealing with the heating rate of 4 °C/s to various temperatures are shown in Figure 3. Nonuniform microstructure, typical for a cold deformed material, is observed in the sample after rolling. The etching did not reveal plastic strain localization in all grains, but the effect of the micro shear bands is observed in a majority of them. Beginning of recrystallization during heating was noticed at 650 °C. During farther heating small increase of the nuclei is observed at both shear bands and boundaries of previous austenite grains. Fast growth of nuclei is seen at 700–750 °C and recrystallized volume fraction above 0.9 is reached at 750 °C.

Microstructure of the sample after the full cycle of annealing is shown in Figure 4. Hardness of all samples was measured after cooling to the room temperature and the recrystallized volume fraction was evaluated on the basis of these measurements. Relation between the recrystallized volume fraction and the temperature for various heating rates is presented in section 4 together with the results of simulations. Analysis of results has shown that heating rate has significant influence on the kinetics of the recrystallization.

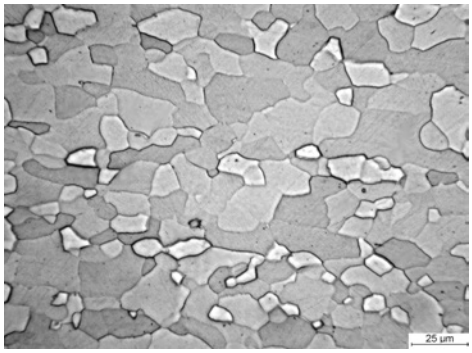

Fig. 4. Microstructure after full cycle of the continuous annealing, heating to 800 °C and quenching

Method of evaluation of the recrystallized volume fraction based on hardness measurements probably overestimates this fraction at low temperatures for samples heated with the low rate of 0.5 °C/s. Analysis of microstructure of that samples allowed to conclude, that decrease of the hardness at the beginning of heating is due to recovery of the dislocation structure, without contribution from recrystallization.

3. Flow stress model

It is well known that accuracy of simulations of rolling depends mainly on the correctness of description o materials flow stress. The objective of this part of the project was determination of the rheological model for the IF steel for the conditions of cold rolling. Inverse algorithm described in [1] was used to determine the real flow stress

insensitive to the effect of friction and deformation heating in the plastometric tests. The simple flow stress function is used:

$$\sigma_p = \sigma_0 + a_1 \varepsilon^n \dot{\varepsilon}^m \exp\left(\frac{Q}{RT}\right), \tag{1}$$

where:

R – gas constant,

T – absolute temperature,

ε – strain,

$\dot{\varepsilon}$ – strain rate.

There are 5 coefficients in Equation (1): σ_0, a_1, n, m and activation energy Q. These coefficients, as well as friction coefficient, were determined using inverse calculations. The quadratic norm of the error between measured and calculated loads and shape of the sample after compression was used as the objective function:

$$\phi = \sqrt{\frac{1}{Nt}\sum_{i=1}^{Nt}\left[\frac{1}{Nr}\sum_{j=1}^{Nr}\left(\frac{R_{ij}^m - R_{ij}^c}{R_{ij}^m}\right)^2 + \frac{1}{Ns}\sum_{j=1}^{Ns}\left(\frac{F_{ij}^m - F_{ij}^c}{F_{ij}^m}\right)^2\right]}, \tag{2}$$

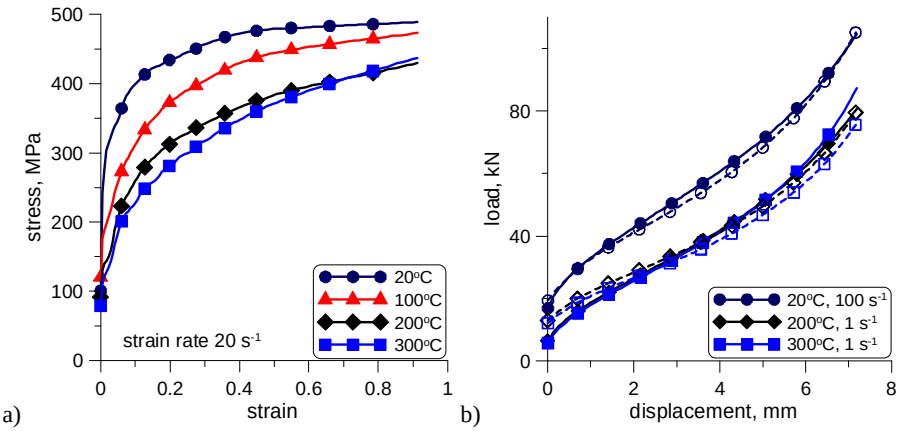

Fig. 5. Example of the flow stress as a function of strain determined using inverse analysis (a) and comparison of measured and calculated loads in the axisymmetric compression (b)

where:

Nt – number of tests,

Nr – number of radius measurements along the sample height,

Ns – number of load measurement sampling points,

F_{ij}^{m}, F_{ij}^{c} – measured and calculated load,

R_{ij}^{m}, R_{ij}^{c} – measured and calculated radius of the sample after the test.

The results obtained for the IF steel are: $\sigma_0 = 0$, $a_1 = 285$, $n = 0.2$, $m = 0.0133$ and $Q = 1532.8$. The friction coefficient of 0.11 was determined. The plots of the flow stress of the IF steel are shown in Figure 5a, b, c. Validation of the flow stress model is made in Figure 5d, where loads calculated using finite element method with the flow stress Equation (1) in the constitutive model are compared with measurements.

4. Model of continuous annealing

Various numerical models have been proposed for the isothermal recrystallization in cold deformed metals. Majority of them are based on the JMAK model:

$$X(t) = 1 - \exp\left[-k(T)t^{n}\right], \tag{3}$$

where:

$X(t)$ – recrystallized volume fraction,

t – time,

k, n – coefficients.

In Equation (3) $k(T)$ is the term, which incorporates both nucleation and growth of grains.

In the continuous annealing of cold rolled strip the recrystallization occurs in non isothermal conditions. In the experiments described in section 2 heating rates between 0.5 and 50 °C/s were applied. Thus, the model of the continuous annealing has to account for changes of the temperature. The additivity rule, proposed by Scheil [2], is applied in this work for prediction of the incubation time. According to this rule the recrystallization begins when the sum of certain fractions reaches unity:

$$\int_0^{\tau} \frac{dt}{\tau_n(T)} = \int_0^{\tau} \frac{1}{\tau_n(T)} \frac{dt}{dT} dT = \int_0^{\tau} \frac{1}{\upsilon \tau_n(T)} dT = 1 \tag{4}$$

where:

$\tau_n(T)$ – incubation time at constant temperature T,

υ – heating rate.

Additivity rule can be applied under certain conditions, which are discussed in [2, 3], and which are fulfilled in the experiment in this project. Briefly, if the progress of the phenomenon at any instant depends only on temperature, the process is additive. Thus, recrystallization during annealing can also be modelled using the additivity rule Since only k in Equation (3) is temperature dependent, Equation (3) can be written as:

$$X = 1 - \exp\left[-\int_{T_0}^{T} \frac{k(T)^{\frac{1}{n}}}{\upsilon} dT \right], \tag{5}$$

where:

T_0 – temperature at the end of the incubation time.

Equation (5) is valid for the heating stage only. Derivation of this equation, as well as its extension to the holding and cooling stages of the annealing process, is described in [4]. Dependence of the coefficient k on the temperature follows the Aarhenius rule:

$$k(T) = A \exp\left(\frac{Q}{RT} \right). \tag{6}$$

Thus, there are 3 coefficients in the model: A, n and Q, which were determined on the basis of experiment as follows: $A = 6 \times 10^9$, $n = 0.46$ and $Q = 190$ kJ/mol.

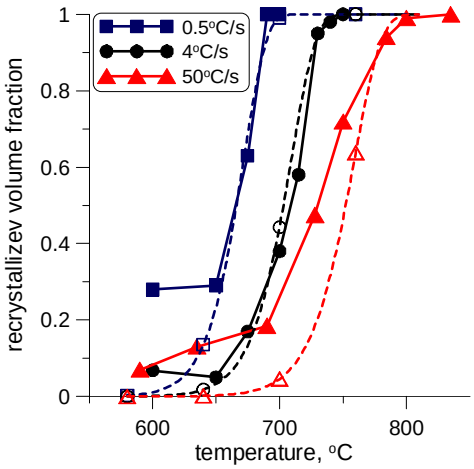

Fig. 6. Measured and predicted recrystallized volume fraction as a function of the temperature

Comparison of the model predictions with the measurements is presented in Figure 6. Analysis of the results in this figure confirms earlier observations. At the beginning of the process the predictions for the heating rate of 0.5 °C/s underestimate the measured softening, what is probably due to the fact that it is rather recovery not recrystallization, which is responsible for the softening at this stage of the process. Beyond this initial stage of the recrystallization, an excellent agreement between predictions and measurements is observed for the heating rates of 0.5 °C/s and 4 °C/s. Slightly worse results were obtained for the heating rate of 50 °C/s.

5. Simulation of cold rolling

Analysis of the cold rolling process in the 4-stand tandem mill in one of the steel plants in Poland was performed. Work roll diameter was 525 mm and the remaining rolling mill parameters are given in [5]. Simulation was performed using the FE program developed by the Authors. The solution uses rigid-plastic flow formulation proposed in [6]. The constitutive model is based on the Levy-Mises flow rule with the flow stress given by Equation (1). Details of the model can be found in [7]. Main parameters of the rolling process and results of simulations are given in Table 2.

Table 2. Rolling parameters and results of modelling for the IF steel (T – temperature, h – thickness of the strip, r – reduction, v – rolling velocity, ω – rotational velocity of rolls, t – interpass time, p_{av} – average roll pressure, F – rolling force, M – roll torque

passno	T, °C	h, mm	r	v, m/s	ω, rpm	t, s	p_{av}, MPa	F, kN	M, kNm
0	–	3.0	–	2.8	–	–	–	–	–
1	1230	2.22	0.26	3.78	128	1.6	626	13819	313
2	1208	1.38	0.378	6.09	206	1.0	669	15597	358
3	1141	0.88	0.362	9.55	323	0.6	638	11665	202
4	1113	0.75	0.148	11.2	379	–	434	4054	30

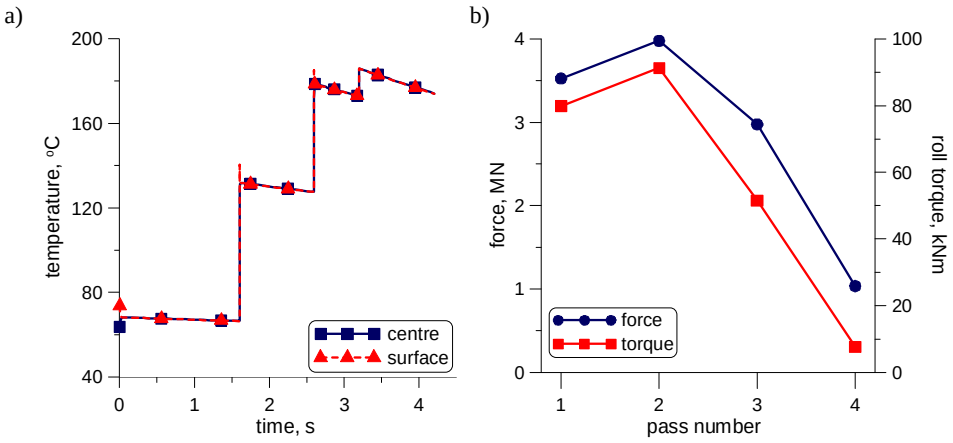

Fig. 7. Time-temperature history at two locations through the strip thickness (a) and loads and torques (b) calculated during rolling of the IF steel strip in the 4-stand tandem mill

Calculated temperatures at two locations, centre and surface, are presented in Figure 7a. Effect of the deformation heating is well seen in this figure. This heating is larger close to the surface, what is due to the effect of friction and additional shear strains. Since the strip is thin, there is no noticeable difference in temperatures between the centre and the surface locations during the interpass times. Loads and torques for the four passes are shown in Figure 7b.

6. Conclusions

The complete model for rolling and annealing of the IF steel is presented in the article. Physical simulations were performed and used to identify the model. Beyond this, the relation between the recrystallized volume fraction and the annealing temperature was determined. It is concluded that continuous annealing at 740 °C is required to obtained complete recrystallization. Numerical tests for the 4-stand tandem mill confirmed qualitatively good predictive capabilities of the model.

Acknowledgement

The work within the project DS/AGH/KISiM/2008.

References

[1] Szeliga D., Gawąd J., Pietrzyk M.: *Inverse Analysis for Identification of Rheological and Friction Models in Metal Forming*, Comp. Meth. Appl. Mech. Engrg., 195, 2006, pp. 6778–6798.
[2] Scheil E.: *Anlaufzeit der Austenitumwandlung*, Arch. Eisenhüttenwesen, Archiv. Für Eissenhuttenwesen, Archiv. Für Eissenhuttenwesen, 12, 1935, pp. 565–567.
[3] Cahn J.W., *Transformation kinetics during continuous cooling*, Acta Metall., 4, 1956, pp. 572–575.
[4] Ferry M., Muljono D., Dunne D.P.: *Recrystallization Kinetics of Low and Ultra Low Carbon Steels during High-rate Annealing*, ISIJ Int., 41, 2001, pp. 1053–1060.
[5] Pietrzyk M., Kusiak J., Głowacki M.: *Some Aspects of Development of Models for Automatic Control of Rolling Mills*, Steel Res., 61, 1990, pp. 359–364.
[6] Kobayashi S., Oh S.I., Altan, T.: *Metal Forming and the Finite Element Method*, Oxford University Press, New York, Oxford, 1989.
[7] Pietrzyk M.: *Finite Element Simulation of Large Plastic Deformation*, J. Mat. Proc. Techn., 106, 2000, pp. 223–229.

Numeryczne i fizyczne modelowanie rozwoju mikrostruktury – nowe podejście do projektowania i optymalizacji technologii walcowania na zimno i wyżarzania stali IF

Modelowanie procesu walcowania na zimno i ciągłego wyżarzania jest podstawowym celem projektu. Wykonano próby plastometryczne dla wyznaczania naprężenia uplastyczniającego w zakresie temperatur odpowiadającym walcowaniu na zimno. Przeprowadzono fizyczne symulacje ciągłego wyżarzania z różnymi prędkościami nagrzewania do różnych temperatur. Opracowano model kinetyki rekrystalizacji wykorzystujący regułę addytywności i równanie typu Avrami'ego, a współczynniki modelu wyznaczono na podstawie wyników badań doświadczalnych. Model ten został połączony z programem MES dla walcowania. Taki kompleksowy model cieplno-mechaniczno-mikrostrukturalny może zostać wykorzystany do optymalizacji procesów walcowania na zimno i ciągłego wyżarzania.

ARCHIVES OF CIVIL AND MECHANICAL ENGINEERING

Vol. VIII 2008 No. 2

Application of flywheel machine for sheet metal dynamic tensile tests

A. NIECHAJOWICZ, A. TOBOTA
Wrocław University of Technology, Wybrzeże Wyspiańskiego 25, 50-370 Wrocław

Modernization and application of flying wheel machine for dynamic testing of sheet metal samples were researched. The machine gives constant velocity of displacement of grips with easy velocity control. The sample shape and dimensions, holders, the measurement system based on single Hopkinson bar were prepared. High kinetic energy of the forcing disk assures almost constant velocity of the test independently of dimensions and properties of samples as well as the stiffness of the measurement bar. The tests show that Young's modulus lower holder should be equal to modulus of sample material, the significant decrease in disturbance of tensile force course was obtained.

Keywords: *dynamic properties, sheet metal, dynamic test, flywheel*

1. Introduction

The development of designing methods of metal forming processes running faster and faster due to improve efficiency of processes causes increasing demands for material testing results in wide range of strain rate [1, 2]. The results concern elastic, plastic and strength properties, micro and sub micro (nano) phenomena of straining and resulting material structure and product properties.

Observed tendencies in the sheet metal forming development can be specified as [1]:

- improvement of drawpieces dimensional and shape accuracy,
- decrease in the waste,
- improvement of productive reliability,
- increase in productivity,
- application of taylored blanks,
- application of laminar sheets,
- application of new, advanced, high strength steels (HSLA, DP, CP, MS, TRIP).

For a significant progress of the process designing and planning, including their optimization, should be very effective and therefore the modern, complex software must be used – knowledge bases, expert systems or mathematical modeling methods. In turn, efficacy of making the most of these depends on availability of the precise and reliable material data. The strength, elastic and plastic properties, stress- strain curves for wide range strain rate and temperature are these main data [3–4].

The second area of engineering activities, where the plastic properties for dynamic deformation are essential is the problem of car body crashworthiness [5]. Optimizing multifunctional, energy-absorbing structures in a vehicle provides a challenge to safety engineers and to automated design techniques. Energy-absorbing structures serve also as typical parts with required load-carrying ability and rigidity. Yet these same structures must collapse in a prescribed manner during a crash to maximize the amount of energy absorbed by the structure and to limit the forces transmitted to passengers [6].

Crashworthiness problems are characterized by a very complex design space with many peaks and valleys due to their highly dynamic nature. These classes of structural design problems have a very multi-modal, non-convex design space and do not lend themselves well to classical gradient techniques. Moreover, objectives and constraints related to crash energy management are joined by additional requirements on mass reduction, stiffness, strength, and manufacturability [7–8]. These objectives compete strongly against one another, making this a very challenging multi-objective optimization problem. Therefore availability the precise and reliable material data for wide range strain rate is very important also. The data and models allow to predict the performance of automotive structures in vehicle crash situations more accurate. On the basis of existing works and solutions one can assume that the most desirable range of strain rate testing should be in range 10^{-3}–10^{3} s^{-1}, covering the most manufacturing and crashworthiness problems.

There are many methods for dynamic testing as well as accessible results but in the most cases they are presented as nominal stress-nominal strain curves. Giving information on the strain rate effects on the strength and plastic properties don't allow using it as true stress-true strain data. It is caused by a complex nature of the dynamic straining and connected interpretation problems. Especially data for initial strain values are burdened with very high uncertainty [3, 9]. These make difficult or even impossible to use the data in mathematical modeling. Therefore dynamic testing problems have still significant share in research and engineering activities.

Typical tensile testing machines allow straining the samples with strain rate less than 1 s^{-1}, modern servo-hydraulic systems up to 100 s^{-1} and greater strain rate require other solution [3].

The most typical testing method is based on impact loading and Hopkinson-Kolsky conception of wave form propagation, measurement and analysis. The developed modern split Hopkinson pressure bar (SHPB) is now main classic method for dynamic compression test.

The idea of the method is shown in Figure 1. The striker bar, accelerated to desired velocity, strikes the incident bar, producing the elastic incident wave. The length of the signal is proportional to striker bar length. The incident wave is partly reflected at the end of incident bar and partly transmitted by sample to the transmitted bar. Energy of the wave should be enough to plastic deform of the sample leaving bars in elastic state. On the base of the displacements measured on both bars, incident and transmitted by strain gages nominal strain, nominal strain rate and nominal stress of sample

are calculated. The process deformation and calculations are made with assumption that transmitted wave is one dimensional and there is not a waves dispersion. The bars dimensions should be so selected that reflected waves do not interfere during sample deformation.

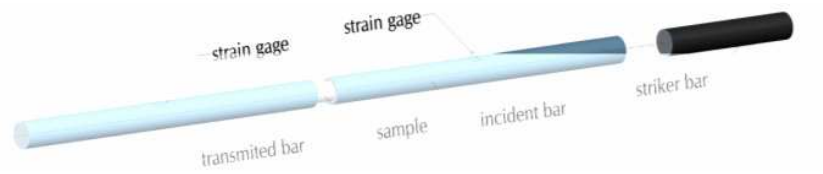

Fig.1. General idea of splitting Hopkinson bar measurement system (SHPB) for compression tests

Dynamic tensile tests were realized by rotating flywheel machines initially. Next, the Hopkinson bar was adapted to a tension test and now is used as main apparatus [10]. Differences between compression and tension test in dynamic conditions are important with respect to the result interpretation. Evaluation of nominal strain and nominal stress for compression tests was prepared with assumption that samples are short. Time of propagation of the elastic wave front from one end of the sample to second one and time for reaching of forces equilibrium is very short thus the only very small initial strain area can be incorrect. The samples for tension test, especially for sheet metal testing must be longer by grip parts and transition areas between grips and a gauge length – the principle of forces equilibrium is violated. Fixation of samples needs holders with different properties than Hopkinson's bars thus additional wave reflections and dispersions can be expected. This problem is common for dynamic tensile test, independently on testing methods [9–10].

The difference between testing by rotating flywheel machines and by split Hopkinson pressure bar (SHPB) technique results from differences in the forcing scheme [11]. The characteristic of SHPB method is energy imposition, neither velocity nor the force. The strain rate is not constant during test and it is hard to control. It distinctly depends on relations between properties and dimensions of sample and a forcing-measurement set. The change of sample properties or dimensions change strain rate also. In spite of undisputed advantages of SHPB methods, other methods, with different forced system are used. For strain rate 100–1000 s^{-1} the rotating flywheel machines seems to be a proper solution. If kinetic energy is properly greater than work done on the sample deformation the constant velocity of deformation can be assumed. In this way the rules of testing by servo-hydraulic systems will be expanded to higher strain rates.

The paper presents the system for dynamic tensile tests of sheet metals with the strain rate range 300–2000 s^{-1}, based on rotating flywheel and a tensile bar measurement system. The aim of the work was preparation of the system and establishing the condition of testing, samples recording data and data interpretation.

2. Description of the experiment

The idea of the rotating flywheel machine and set of stand are shown in Figures 2 and 3 respectively. The basic element, wheel disc with diameter 600 mm and width 100 mm is equipped with a self-aligning, forked hammer. The hammer is normally kept in a wheel pocket and blocked in this position by a slidable pin. The wheel is accelerated by electric motor to selected speed, measured with a rotary encoder. When selected speed is achieved the slidable pin is moved by an electromagnet, unlocking the hammer that rotates to working positions, striking an anvil connected to sample. The hammer velocity range from 5 to 50 m/s giving as a result available, impact energy from 1.4 to 140 kJ. Because the needed work to sample deformation up to fracture is less than 60 J, thus the impact velocity is almost constant during the test.

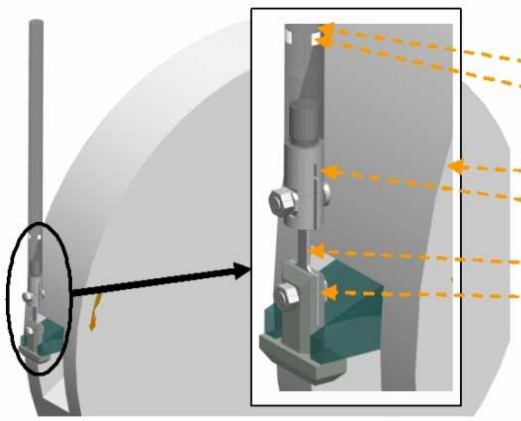

Fig. 2. The idea of dynamic testing on the rotating flywheel machine

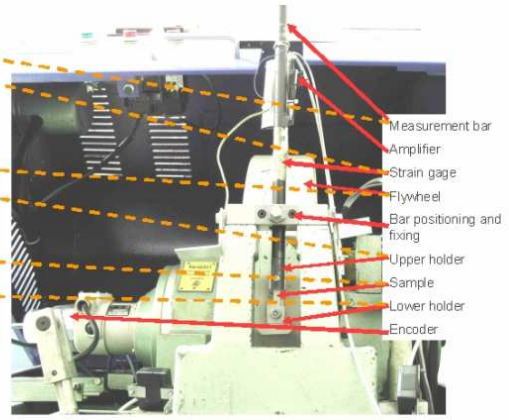

Fig. 3. The flywheel machine and measurement set used for testing

The sample, holders and measurement bar is a most important set of the system, affecting the results quality and accuracy. The basic shape and dimensions of the sheet metal samples are shown in Figure 4. The samples were Wire Electrical Discharge Machined with accuracy ±0.01 mm and high surface quality. The lower sample holder is an anvil concurrently, struck by the hammer and transmitted the loading impulse to the sample. The upper holder is connected to measurement bar. After preliminary testing the upper holder was designed in the fork form that the sample is established by a bolt and fixed axially by friction forces generated by clamping of holder segments with screwed bolt. In this way the main part of loading is carried not by bolt but rather by side sample surfaces. The material of holder is similar to the bar material as well as the diameter (Figure 2).

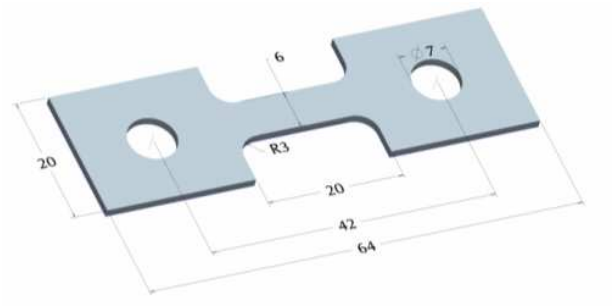

Fig. 4. A sample for dynamic tests

The lower holder, acting at the same time as an anvil, differs from upper one significantly. The arms of the anvil have to be fitted to hammer dimensions, the other dimensions should assure a proper stiffness for the holder as well as samples fitting and fixing. Moreover, the lower holder weight should be as low as possible, according to literature data [3]. By mutually exclusive requests tree holders were made for testing (Figure 5), the more massive, one piece holder (Figure 5a), made from steel (steel long) and titanium alloy (Ti long) and next (Figure 5b), two pieces but more compact, made from titanium alloy (Ti short).

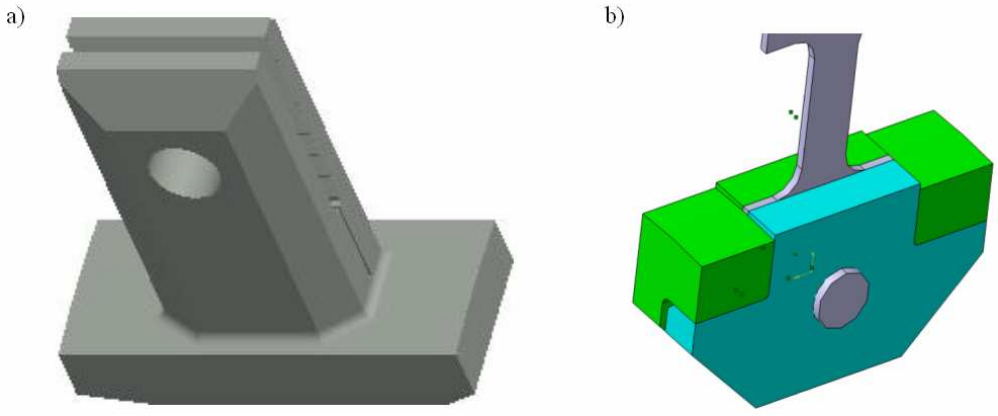

Fig. 5. Lower grips used in tests – a) long holders made from steel and titanium alloy, b) short holder made from titanium alloy

The measurement bar, 6 m long, has strain gages fixed at the distance of 10 bar diameters from the lower end. With the bar length the time of elastic wave propagation by the bar is longer than 2.3 ms that the acquired signal of the sample deformation does not interfere with the wave reflected from upper end of the bar. The strain gage signal is processed by a broad-band amplifier and acquired by an external data acquisition board with sampling rate 1 MHz.

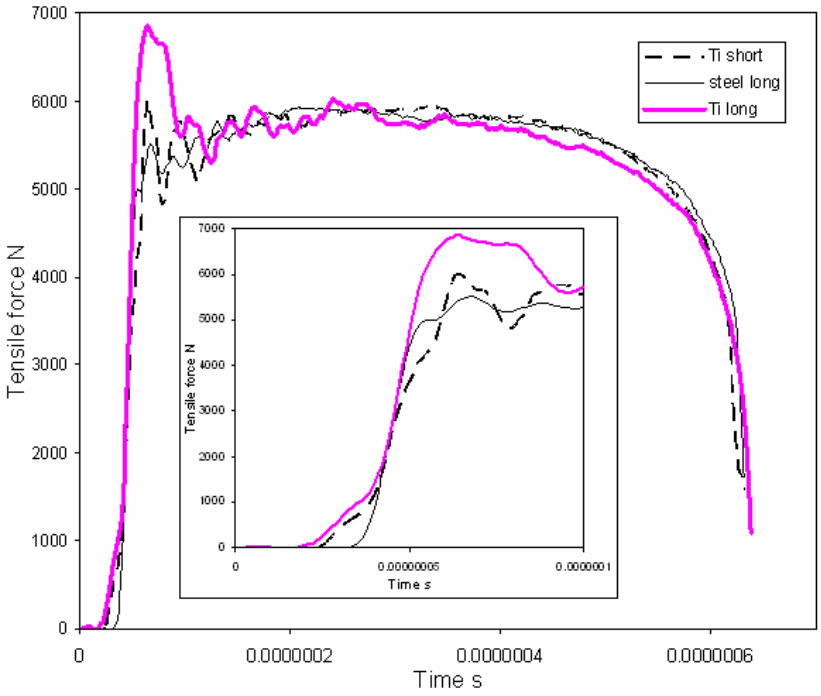

Fig. 6. Tensile curves of samples deformed with strain rate 660 s^{-1} by different holder sets

3. Experimental result

The tensile force courses obtained in tension test with 660 s^{-1} strain rate, for DP600 steel, with three, different, lower grips are shown in the Figure 6, a magnified initial courses of forces are shown also. For bigger elongation, (greater than 3 mm), there are no differences between curves, irrespective of lower holder. The significant differences are seen for initial deformation. The steel, long grip gives, as a result straight, undisturbed line in elastic area and relatively small oscillations in plastic zone. Tests with the titanium alloy, short grip show visibly disturbed course in elastic region and bigger oscillations. Disturbed initial part and a significant peak are typical for the third holder. Results show that for dynamic tension of sheet metal the similarity of elastic properties grips and samples play an important role, especially for small deformations.

The effect of strain rate on tensile force course is shown in Figure 7. Quasi-static tests were made by Instron testing machine, using the same samples and grips. The charts show problems with dynamic stress-strain curves determination for low value of strain. As an independent variable the hammer displacement is taken for dynamic tests and the beam displacement for quasi-static ones. The displacement consists of the plastic elongation of the sample base, transition zones and small, elastic elongation of grips. The individual parts can be easily identified by using an extensometer, grid

analysis or by mathematical modeling. For dynamic condition the nature of displacement is more complex. One can assume constant velocity of hammer and pass over its elastic deformation. On the basis of strain gage signal, the displacement of lower surface of upper grip can be calculated. The elastic deformation of the lower grip for advanced stages of deformation can be calculated also [12–14]. Unfortunately, there are no direct measurements for elastic wave propagation by the lover grip and by sample as well as strain distribution over sample. Because elastic wave front propagation time is long and the wave is reflected inside of sample before plastic strain will be uniform over sample, the elastic properties and displacement of the samples could not be easily determined [15].

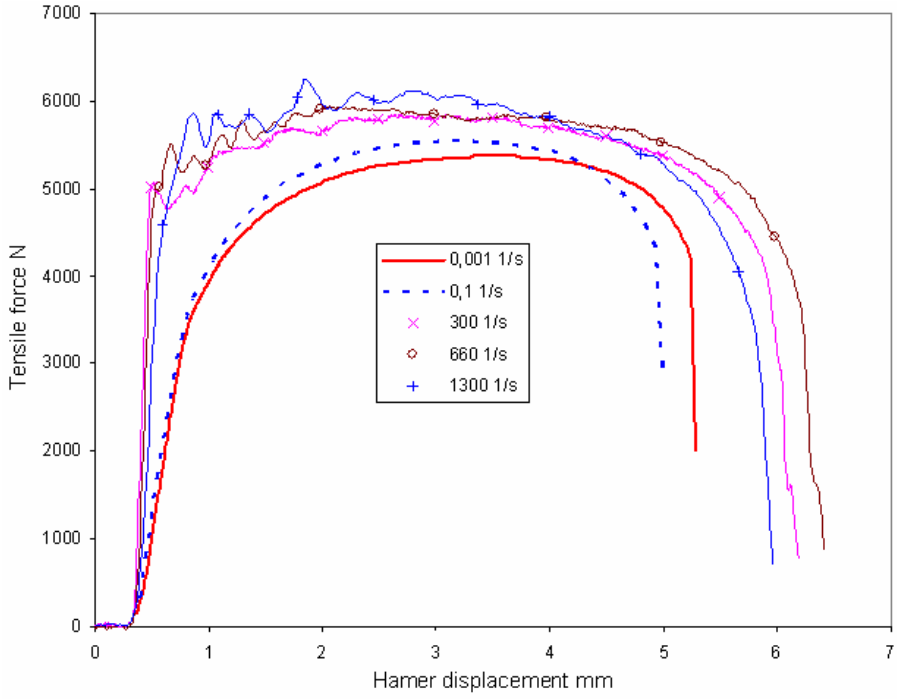

Fig. 7. Quasi-static and dynamic tensile curves

Taking into consideration that the stress-strain curve evaluation is the basic aim, the problem with tension curve interpretation should be resolved. The oscillations of the force can be smoothed by averaging [9]. The results of the using of additional separator from Pb sheet 0.8 mm in thickness between the hammer and anvil are shown in Figure 8. The separator changes the front wave shape and dampens the oscillations. The results are fitted to hypothetical averaged curves, besides initial strain. The problems of yield stress, elastic properties and displacement distribution as well as identification of stress strain curves will be analyzed in the next research.

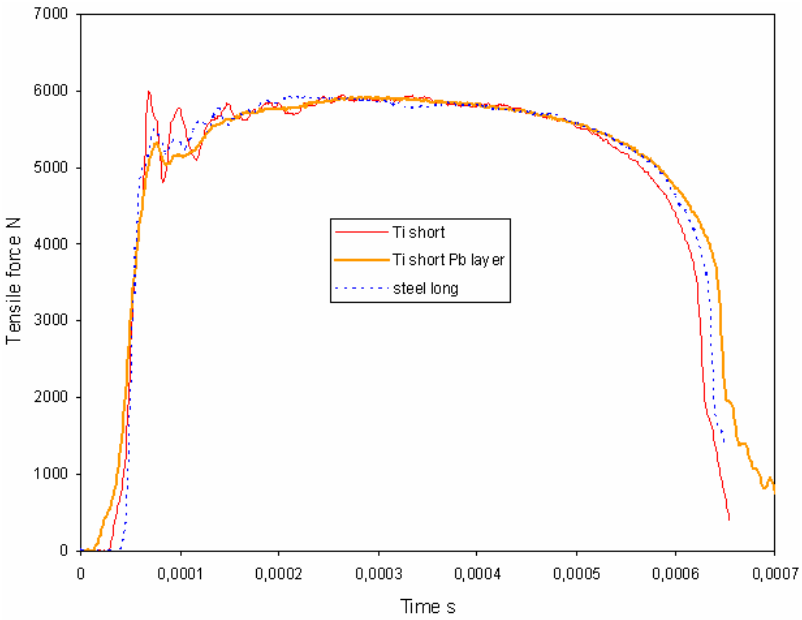

Fig. 8. The effect of Pb separator on tensile curves deformed with strain rate 660 1/s

4. Conclusions

Presented here, the flywheel testing machine can be successfully used for dynamic tensile test with straining velocity 5–50 m/s.

High kinetic energy of the forcing disk assures almost constant velocity of the test independently of dimensions and properties of samples as well as the stiffness of the measurement bar

The structure of the forcing and measurement set minimize elastic wave dispersions and reflections and decrease interferences to applicable level.

A material of a forcing grip should have Young's modulus close to the sample material for decreasing of the tensile force course perturbations.

References

[1] Gronostajski J., Matuszak A., Niechajowicz A., Zimniak Z.: *The system for sheet metal forming design of complex parts*, J. Mater. Process. Technol., Vol. 157–158, 2004, pp. 502.

[2] Gronostajski J., at al.: *The intelligent system for net shape forming of sheet metal product: Third year report*, Raporty Inst. Technol. Masz. Autom. PWr. 2005, Ser. SPR, no. 14.

[3] Rusinek A., Klepaczko J.R.: *Shear testing of a sheet steel at wide range if strain rates and a constitutive relation with strain-rate and temperature dependence of the flow stress*, Int. J Plasticity, Vol. 17, 2001, pp. 87.
[4] Lee O.S., Kim M.S.: *Dynamic material property characterization by using split Hopkinson pressure bar (SHPB) technique*, Nuclear Engineering and Design Vol. 226, 2003, pp. 119.
[5] Campbel J.D., Fergusson W.G.: *The temperature and strain-rate dependence of the shear strength of mild stee*,. Phil. Mag., Vol. 21, 1970, pp. 63.
[6] Tarigopula V., Langseth M., Hopperstad O.S., Clausen A.H.: *Axial crushing of thin-walled hugh-strength steel sections*, Int J. Impact Eng, Vol. 32, 2006, pp. 847.
[7] Peixinho N., Jones N., Pinho A.: *Experimental and numerical study in axial crushing of thin walled sections made of high-strength steels*, J Phys IV, JP, Vol. 110, 2003, pp. 717.
[8] Jones N.: *Structural Impact*, Cambridge University Press, Cambridge, 1989.
[9] Lee W.S., Wang B.K.: *High strain rate mechanical properties of austenitic manganese steel*, Mater. Sci. Technol., Vol. 23, 2007, pp. 151.
[10] Haugou G., Markiewicz E., Fabis J.: *On the use of the non direct tensile loading on a classical split Hopkinson bar apparatus dedicated to sheet metal specimen characterization*, Int. J. Impact Eng., Vol. 32, 2006, pp. 778.
[11] Froustey C., at al.: *Design of an impact loading machine based on flywheel*, Exp. Mech., 2007.
[12] Chen M., Lin D., Xia Y., Liu C.T.: *Strain rate sensitivity of ductility in a Fe-028Al alloy under tensile impact*, Scripta Materials, Vol. 37, 1997, pp. 1243.
[13] Shin H.S, Lee H.M., Kim M.S.: *Impact tensile behaviour of 9% nickel steel at low temperature*, Int. J. Impact Eng., Vol. 24, 2000, pp. 571.
[14] Wang Y., Zhou Y., Xia Y.: *A constitutive description of tensile behaviour for brass over a wide range of strain rates*, Materials Sciences and Engineering, Vol. 372, 2004, pp. 186.
[15] Verleysen P., Degrieck J.: *Experimental investigation of the deformation of Hopkinson bar specimens*, Int. J. Impact Eng., Vol. 30, 2004, pp. 239.

Zastosowanie młota rotacyjnego do dynamicznych prób rozciągania blach

Zaprezentowano zastosowanie zmodernizowanego młota rotacyjnego do dynamicznych prób rozciągania blach. Wymuszanie odkształcania za pomocą koła o bardzo dużej energii kinetycznej, o stałej prędkości jest podstawową zaletą w porównaniu do metod opartych na wymuszaniu odkształcenia impulsem fali sprężystej, np. metody dzielonego pręta Hopkinsona. Zastosowanie do pomiarów długiego pręta pomiarowego (pojedynczy pręt Hopkinsona) wyeliminowało problem interferencji fali sprężystej po stronie utwierdzenia próbki. Na podstawie testów dobrano kształty i wymiary uchwytów minimalizujące zakłócenia od strony wymuszającej. Stwierdzono, że moduł Young'a dolnego uchwytu powinien być równy lub większy od modułu materiału badanego.

ARCHIVES OF CIVIL AND MECHANICAL ENGINEERING

Vol. VIII 2008 No. 2

Cross rolling of parts with non-circular cross section

Z. PATER, A. GONTARZ, W. WEROŃSKI
Lublin University of Technology, Nadbystrzycka 36, 20-618 Lublin

The aim of this paper is to present the possibilities of forming by means of cross rolling method (CR) of the parts with cross section different from circular one. In the paper the methodology of profiled tools forming is provided. These tools application allows for obtaining of parts with cross section in the shape of square, hexagon, oval, etc. The correctness of the worked out forming conception was confirmed by the results of numerical calculations and experimental research. Experiments were made in laboratory rolling mill LUW-2, parts from steel C45 type were rolled in hot forming conditions. Uniquely, it was stated that using profiled tools, parts in the form of stepped axles and shafts which have steps of non – circular cross section can be formed with satisfactory precision. The application in industrial conditions of profiled tools will allow for enlarging scope of CR technological possibilities and decreasing of material consumption.

Keywords: *cross rolling, FEM, physical simulation*

1. Introduction

Cross-wedge rolling (CWR) is a modern technology of stepped shafts and axles manufacturing. Typical parts, fabricated by means of this method, have conical, spherical and cylindrical surfaces [1, 2].

CWR technological possibilities can be increased in the result of such a sizing of tools surfaces that it will be possible to roll parts with cross sections different from circular shape. The way of designing these tools for a typical CWR process was worked out by [3].

Within the frame of this paper the authors present new solutions of tools, which application will allow for cross rolling (CR) of shafts steps with cross sections different from circular shape. A characteristic feature of forming is the lack of cross section reduction.

2. Designing of tool working surface

The idea of the new cross rolling is based on a proper periodical profiling of tools surfaces. The profile is chosen in such a way that it constitutes envelope of the shaft formed step. The methodology of dealing with the tools profile choice allowing for rolling of step of forging with square section is given below.

Figure 1a presents the outline of square step of the part (with the length a = 26.9 mm) formed form cylindrical billet of diameter Ø30 mm. Due to the outline symmetry

in the analyzed case, it is satisfactory to determine the tool profile, which guarantee making by the workpiece 1/8 rotation, that means angle $\varphi = 45°$.

In order to determine the profile, this angle is divided into n different parts, which results in angle splitting $\Delta\varphi$ is equal:

$$\Delta\varphi = \frac{\varphi}{n}, \tag{1}$$

Next, the height h_i of tool profile in plains determined by following lines i = 0, 1, 2… is calculated. In the analyzed case it is:

$$h_i = \frac{a}{2\cos(i \cdot \Delta\varphi)}. \tag{2}$$

Finally, the outline of tool profile is made (as shown in Figure 1b), assuming at the same time that the length Δx_i (determining tool movement while the workpiece rotates by $\Delta\varphi$ angle) can be given basing on the dependency:

$$\Delta x_i = \Delta\varphi \cdot r_0, \tag{3}$$

where r_0 is billet radius and $\Delta\varphi$ is elementary rotation angle given in radians.

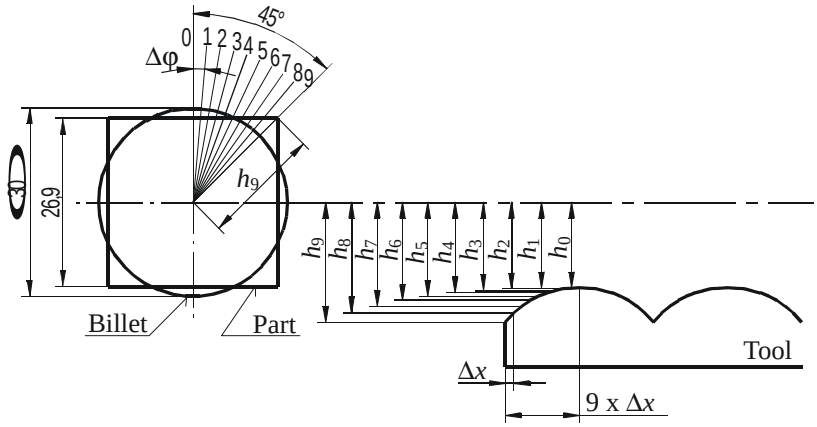

Fig. 1. Scheme illustrating the way of designing of tools for cross rolling of parts with non-circular cross sections

3. Numerical analysis

Numerical modelling based on FEM was used for the initial checking of manufacturing possibilities of CR of parts with steps with non-circular sections. Forming cases

from cylindrical billet of cross section: square, oval and hexagonal were analyzed. These sections dimensions (determined on the basis of the same cross section areas of billet and final part) are shown in Figure 2.

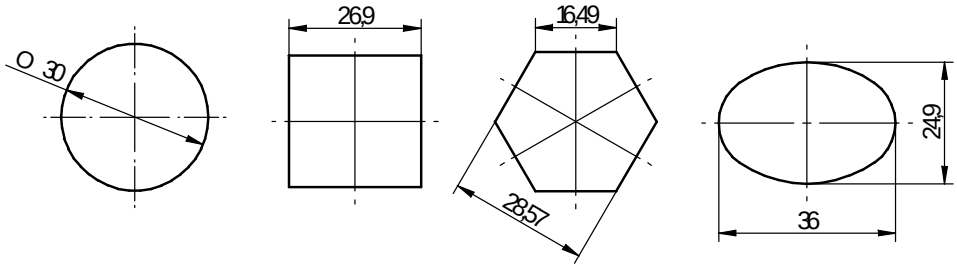

Fig. 2. Analyzed outlines of billet and final parts cross sections

In Figure 3 tools and billet geometrical model is presented. This model was worked out for the cross rolling process of part with central step of square shape. The tool was designed in CAD 3D Solid Edge, next, the 3D model was exported into the software MSC.SuperForm 2005. It was assumed that the section forming would take place during 1 rotation of the rolled billet. In order to guarantee the stability of forming, tools were equipped with guiding paths which should provide conformity of the work-piece rotations during forming with negative rolling depth.

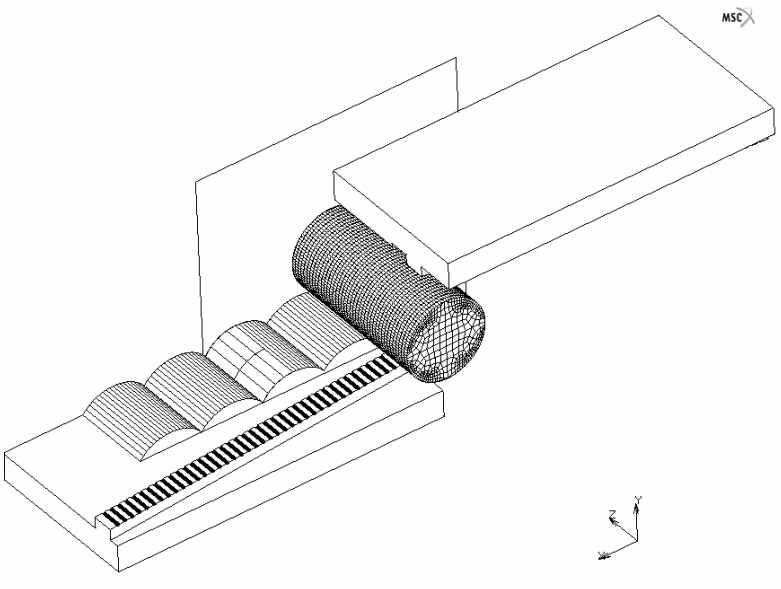

Fig. 3. Geometrical model of cross rolling process of parts with square cross section

In calculations, it was assumed that the material, from which the part was made, was steel of C45 type. The model of this steel was taken from the library of the MSC SuperForm 2005 software. It was assumed that the material was heated to temperature 1150 °C before rolling and that the wedges temperature was the same and equal 30 °C. Other parameters assumed in calculations include: coefficient of heat transfer between material and tools 10 kW/m^{2}K; coefficient of heat transfer between material and air 0.35 kW/m^{2}K; friction factor 1.0; tools velocity 0.125 m/s.

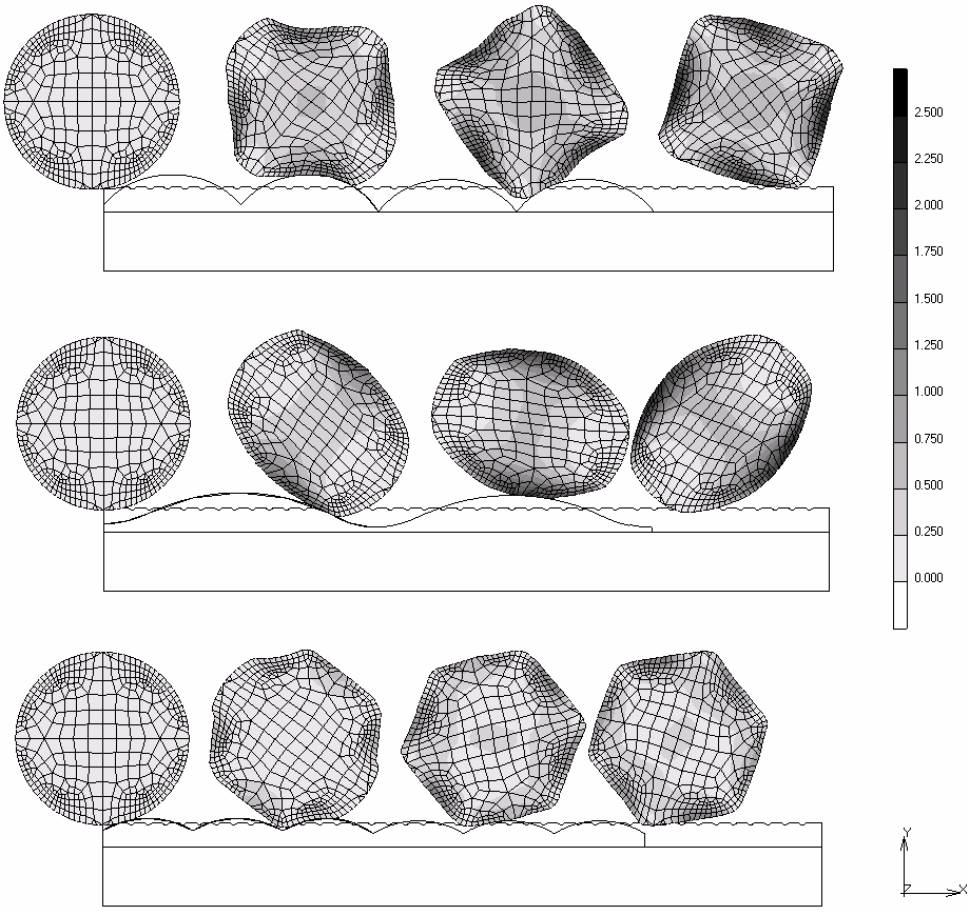

Fig. 4. Calculated by FEM changes of shape of analyzed billets during cross rolling process together with effective strain distribution

On the basis of the calculations the changes of forging shape present during the rolling process were analyzed. In Figure 4 the changes of parts shape depending on the stage of forming process are shown. It was also stated, basing on calculations, that during rolling the material is squeezed into serrations made in tools, which allowed for

forming with negative rolling depth. Because of the part reeling on the tool surface section corners undergo rounding which is especially well visible during rolling of square shaped steps.

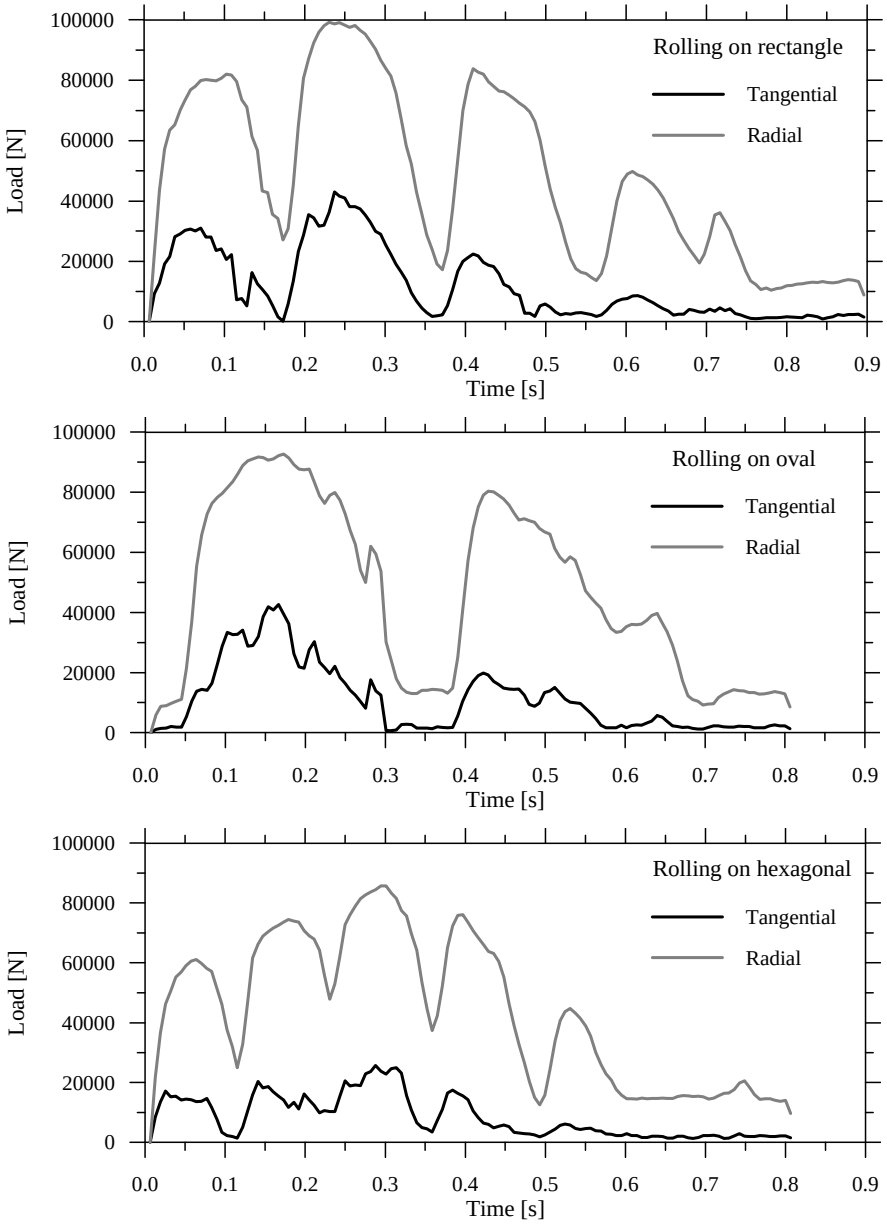

Fig. 5. Calculated by FEM distributions of forces acting on the tool during analyzed cross rolling processes

In Figure 5 the distributions of rolling forces influencing tools during the analyzed cross rolling processes are presented. It is concluded from the date given in this figure that the forces are characterized by large variations (they have oscillating course). The present oscillations of forces are connected with the part cross section shape which causes the change of reduction ratio during rolling.

It should be noticed that the tangent force (pushing tools) is considerably lower (about 3 times) than the radial force (operating in the *y* direction – Figure 3). Hence, the dependency between these forces is similar as in the typical CWR processes.

4. Experimental research

The ultimate verification of the worked out method of forming by means of cross rolling was made in stand tests in laboratory conditions of the Lublin University of Technology. In the research a prototype rolling mill was used, it is shown in Figure 6. This rolling mill consists of body, upper and lower slides and driving unit. In the rolling mill LUW-2 billets from steel with diameter up to Ø35 mm can be formed in hot rolling conditions.

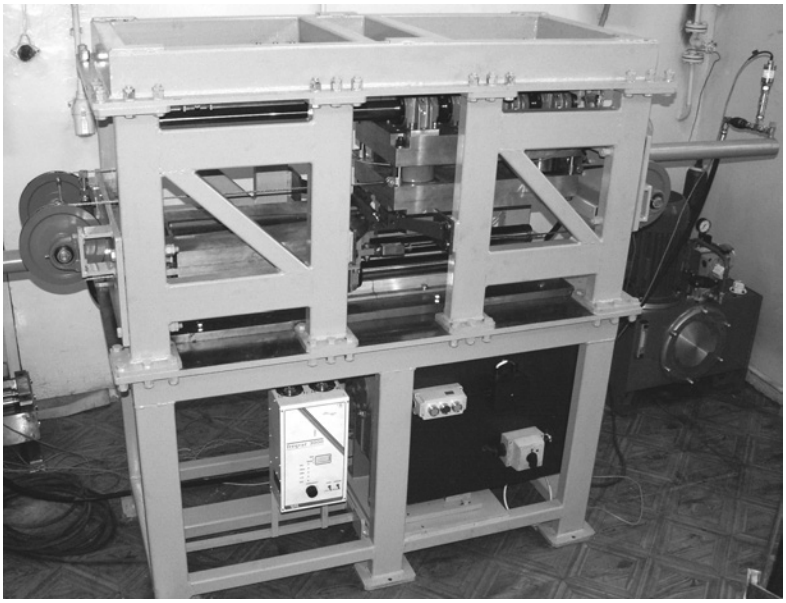

Fig. 6. Prototype rolling mill LUW-2

For the research needs, tools sets shown in Figure 7 were made. They consist of mounting, guiding paths and changeable profiled pads. Tests of parts rolling with cross sections: square, oval and hexagonal (according to Figure 2) were made using these tools.

Fig. 7. Tools sets for cross rolling of parts with non-circular cross sections

Rolling tests took place in hot rolling conditions – Figure 8. Billets with dimensions of Ø30×180 mm (made from steel C45) were heated up to the temperature 1150 °C. The rolling was realized at the wedge velocity of 0.13 m/s.

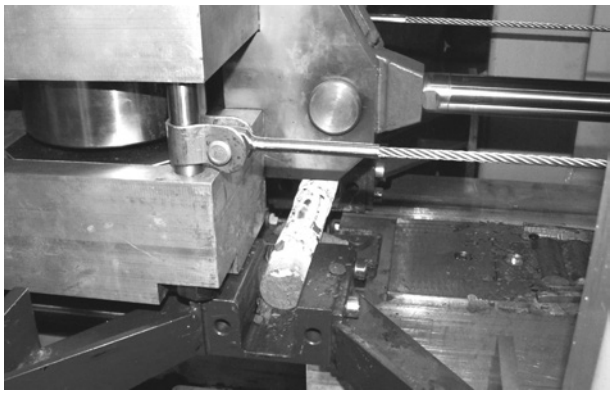

Fig. 8. Specimen after hot cross rolling

The experiment confirmed that it is possible to obtain parts with non-circular sections by means of cross rolling method. In Figure 9 parts obtained in the analyzed cross rolling method, in which profiled tools were used, are shown. Additionally, in Figure 10 cross sections of the obtained parts are presented. The analysis of the precision of particular parts manufacturing showed that nominal dimensions of the obtained

parts were: $26.9^{+0.7}$ mm (side length of square part); $28.57^{+0.8}_{-0.6}$ mm (distance between parallel wall in hexagonal step); $36^{+0.4}$ mm and $24.9^{-0.3}$ mm (length of long and short diagonal of the oval section respectively). Hence, it can be stated that the precision of manufacturing is within the proper scope for metal forming processes in hot conditions.

Fig. 9. Final parts rolled during stand tests

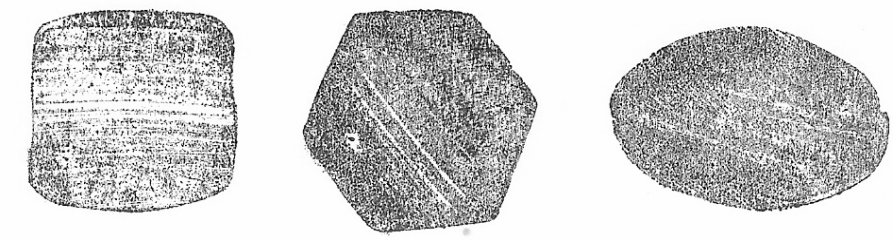

Fig. 10. Outline of cross section of parts obtained in experimental research

5. Summary

As results of the performed research a new way of cross rolling which allows forming the parts with cross section different from circular shape was worked out. Equipping tools segments for CWR with profiled pads will allow for manufacturing of shafts with formed steps. In that way it will be possible to reduce material consumption and to shorten the machining time. On the basis of the research it was also stated that due to the change of reduction ratio during rolling, the forces oscillations were

occurred. Moreover, due to the part reeling on wedge tools surfaces, manufacturing of the sharp corner cross sections by means of cross rolling is impossible.

Acknowledgement

Research work sponsored by The State Committee for Scientific Research in the year 2006–2009 as project no N508 024 31/1444.

References

[1] Fu X.P., Dean T.A.: *Past developments, current applications and trends in the cross wedge rolling process*, International Journal of Machinery Tools Manufacture Design, Research and Application, Vol. 33, 1993, pp. 367–400.
[2] Pater Z., Weroński W.: *Podstawy procesu walcowania poprzeczno-klinowego*, Wyd. Politechniki Lubelskiej, Lublin (in Polish), 1996.
[3] Pater Z., Tomczak J.: *Walcowanie poprzeczno-klinowe odkuwek o przekroju poprzecznym różnym od kołowego*, Obróbka Plastyczna Metali, Nr 2, pp. 31–41 (in Polish), 2005.

Walcowanie poprzeczne części o niekołowym przekroju poprzecznym

Celem opracowania jest przedstawienie możliwości kształtowania metodą walcowania poprzecznego (WP) wyrobów o przekroju poprzecznym różnym od kołowego. W artykule podano metodykę projektowania narzędzi profilowych, których zastosowanie umożliwia uzyskiwanie wyrobów o przekroju poprzecznym w kształcie kwadratu, sześciokąta, owalu i in. Słuszność opracowanej koncepcji kształtowania potwierdziły wyniki obliczeń numerycznych oraz badań doświadczalnych. Próby doświadczalne prowadzono w walcarce laboratoryjnej LUW-2, walcując na gorąco odkuwki ze stali w gatunku C45. Jednoznacznie wykazano, że stosując narzędzia profilowe można z satysfakcjonującą dokładnością kształtować wyroby typu stopniowanych osi i wałów, które posiadają stopnie o niekołowym przekroju poprzecznym. Zastosowanie w warunkach przemysłowych narzędzi profilowych pozwoli na rozszerzenie możliwości technologicznych WP oraz zmniejszy zużycie materiałów.

ARCHIVES OF CIVIL AND MECHANICAL ENGINEERING

Vol. VIII 2008 No. 2

Application of Al alloys, in the form of cast billet, as stock material for the die forging in automotive industry

B. PŁONKA, A. KŁYSZEWSKI, J. SENDERSKI, M. LECH-GREGA
Institute of Non-Ferrous Metals, Light Metal Division, ul. Piłsudskiego 19, 32-050 Skawina, Poland

Recent trends in the application of aluminium alloy stock fabricated by different methods in the process of die forging were presented. Recent trends in the research on application of shaped ingots in die forging have been described as well. The results of the studies on fabrication of die forgings of rocker from billets cast in the horizontal continuous process and compared with the results obtained on extruded rods from the EN AW-6082 alloy were quoted. The fabricated pilot forgings of rocker with cast and extruded material were next examined for their structure and mechanical properties.

Keywords: *aluminium alloys, die forging, structure and mechanical properties*

1. Introduction

The stock used in die forging of Al alloys is commonly composed of the extruded bars, and rolled plates and sheets [1]. However, since some time, at the Institute of Non-Ferrous Metals, Light Metals Division in Skawina, intensive research and developments works have been carried out to replace this stock with billets cast by vertical semi-continuous process and by horizontal continuous process.

Compared to the extruded bars, the use of billets as a stock for die forging reduces the costs of production by 15–20%. The mechanical properties of forgings after heat treatment are similar in both technologies, quite often, due to their low anisotropy, superior even in this novel approach. On the other hand, some differences have been noted to occur in the structure of forgings made from billets in comparison with the extruded bars used as a stock for die forging. Forgings made from the extruded bars may inherit in some sections the fibrous structure of the bar, intersecting the contour of forging (Figure 1), which has an adverse effect on the distribution of mechanical properties in final product. The use of billets as a stock for die forging effectively prevents this, highly disadvantageous, phenomenon (Figure 2).

Nowadays, the use in die forging of billets characterised by a rheocast structure has attracted widespread popularity. Billets of this type are used in thixoforging process [2]. Die forging is a one-stage process, effectively utilising the presence of a liquid phase formed in billet preheated by induction. A billet like this is characterised by a globular structure free from the presence of dendrites. The most popular methods to fabricate by semi-continuous process billets characterised by a dendrite-free structure are the techniques based on stirring of the solidifying metal within the solidification

front. The stirring can use the mechanical or magnetohydrodynamic action (MHD) of the forces of electromagnetic field (Figures 3, 4) [3].

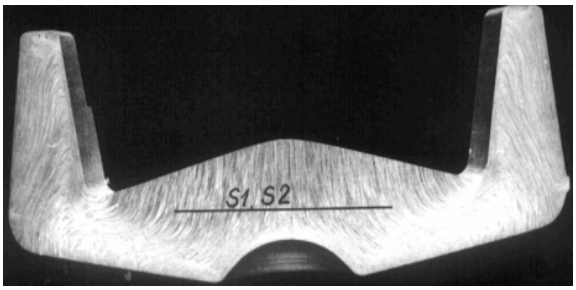

Fig. 1. Macrostructure of forging made from the extruded bar

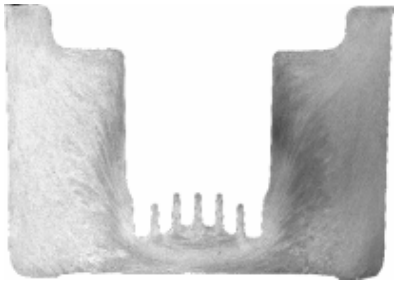

Fig. 2. Macrostructure of forging made from the cast billet

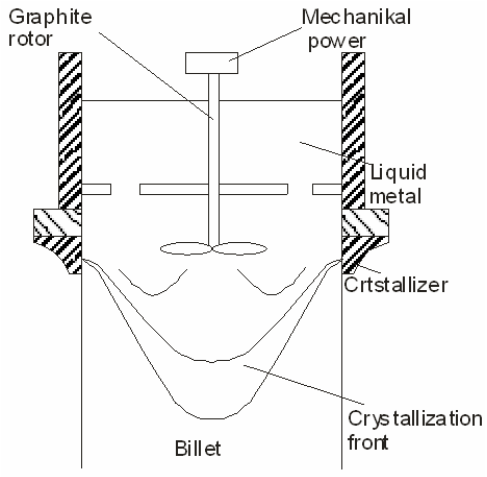

Fig. 3. Schematic representation of a HOT-TOP mould with arm for mechanical stirring

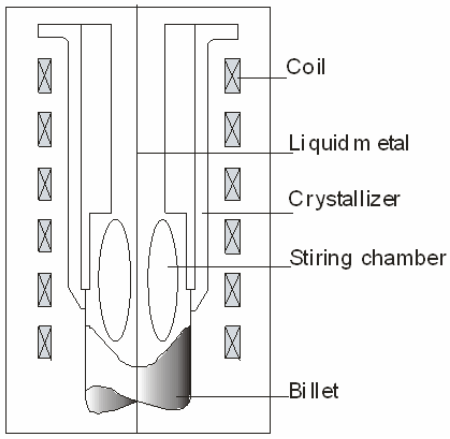

Fig. 4. Schematic representation of electromagnetic stirring

Reduced number of operations, energy savings and the possibility of making complex forgings – all these benefits can be obtained also from casting of shaped billets for die forging (the technology developed by Wagstaff Inc, used by Alcan – casting of billets and Alcoa – die forging) [4]. The schematic representation in Figure 5 shows different stages of the conventional die forging process using the stock after plastic working (e.g. the extruded rods) and shaped billets cast by, e.g., a semi-continuous process.

Figures 6 and 7 show, respectively, examples of shaped billets cast by Alcoa Automotive Castings and a general view of the casting facility [4].

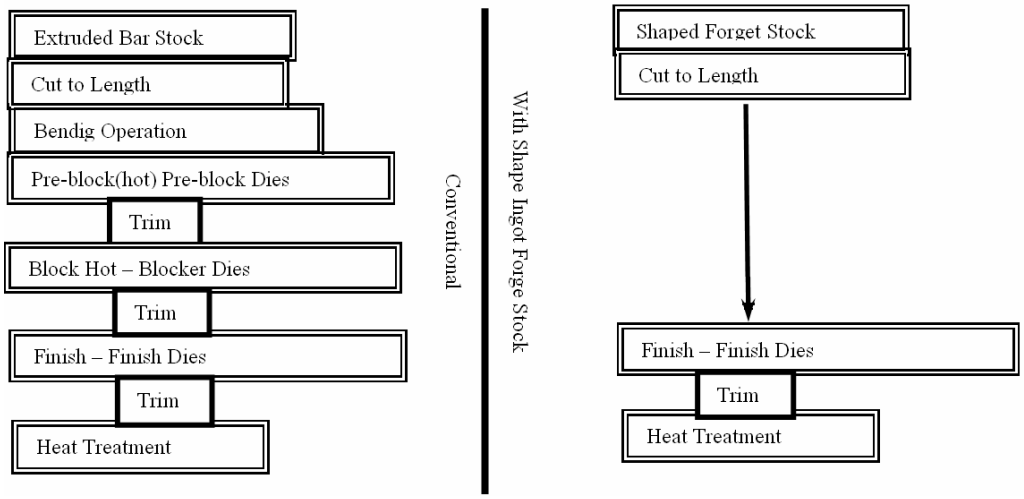

Fig. 5. Stages of die forging using different stock materials [4]

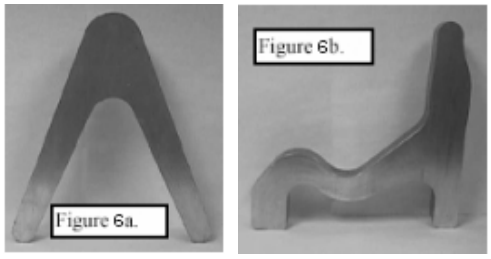

Fig. 6. Examples of cast shapes used as a stock for die forging

Fig. 7. A facility for casting of shaped billets 6 meters long (Wagstaff Inc.)

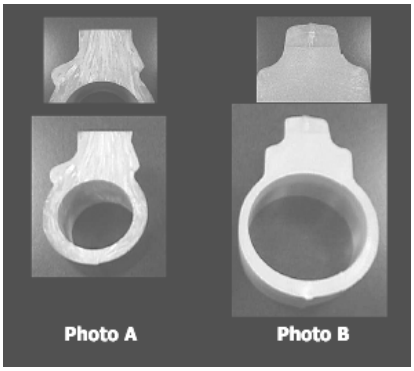

Fig. 8. A comparison of macrostructures obtained in forgings made from: extruded rod and shaped billet. A – forged by conventional technique, B – forged by single operation (single heating) [4]

Table 1. Mechanical properties of elements forged from 6061-T6 alloy [4]

Stock material	Mechanical properties		
	$R_{p0.2}$ [MPa]	R_m [MPa]	A_5 [%]
Extruded rod	277	312	15.5
Shaped billet	316	347	19

2. Experimental

2.1. EN AW-2618A alloys

An example of the application in die forging of billets cast by semi-continuous technique is the developed technology of making die forged pistons from the EN AW-2618A alloy. Figure 9 shows macro and microstructure of a billet assigned for forging, while Figures 10 and 11 show pistons forged from the EN AW-2618A alloy.

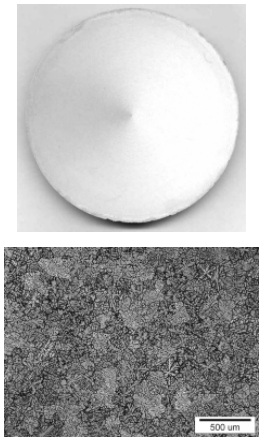

Fig. 9. Macro and microstructure of billet made from the EN AW-2618A alloy

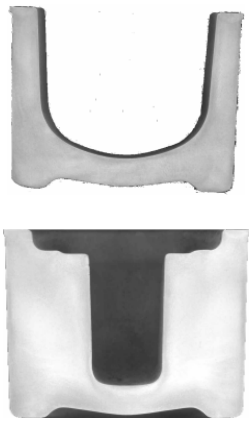

Fig. 10. Macrostructure of piston forged from the EN AW-2618A alloy

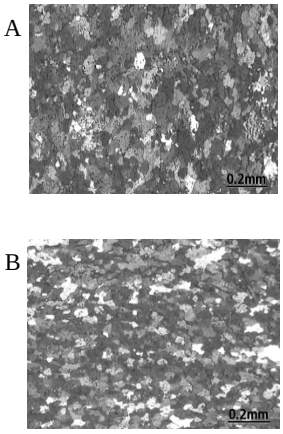

Fig. 11. Microstructure in wall (A) and web (B) of piston made from the EN AW-2618A alloy

In macro- and microstructures obtained for the EN AW-2618A alloy, fine grains evenly distributed on the entire piston cross-section have been observed.

The results of mechanical tests conducted on forgings made from the EN AW-2618A alloy are shown in Table 2.

Table 2. Mechanical properties of pistons made from the EN AW-2618A alloy

Alloy	Place of measurement	Heat treatment parameters	Mechanical properties		
			$R_{p0.2}$ [MPa]	R_m [MPa]	A_5 [%]
EN AW-2618A	wall	solution 530 °C aging 200 °C/20 h	381	430	8.2
	web		365	428	9.7

The results obtained during industrial trials of making die forgings from the EN AW-2618A alloy using stock in the form of billets cast by semi-continuous process revealed very high forgeability of this stock.

The mechanical properties (Table 2) obtained in forgings during all the trials considerably exceeded the required minimum values. Low anisotropy of these properties in the piston wall and web was also observed.

2.2. EN AW-6082 Alloy

Another example of the use of billets as a stock material for forging was a newly developed innovative technology for forging of rockers from aluminium alloys. In this study two stock materials for forging of EN AW-6082 alloy were compared, i.e. the cast stock and extruded rods. The billets from EN AW-6082 alloy were cast by horizontal continuous process on a pilot stand using the technology developed by IMN OML Skawina. Figure 12 shows a photograph of billet cast in a horizontal continuous process with the respective macro- and microstructure.

Fig. 12. Billet cast from EN AW-6082 alloy in a horizontal continuous process and the respective macro- and microstructure (from cross-section)

The rods of 50 mm diameter were extruded from conventional billets cast in a vertical semi-continuous process. Figure 13 shows macro- and microstructure of the extruded ϕ50 mm rod.

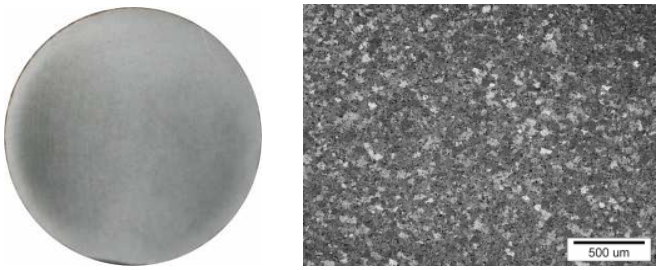

Fig. 13. Macro- and microstructure (from cross-section) in a ϕ50 mm rod extruded from EN AW-6082 alloy

The forging process was two steps. The both stock material was heated up to 510 °C. Figure 14 shows the rocker after heat treatment and its macrostructure obtained for both stock materials on a lengthwise section of the forging.

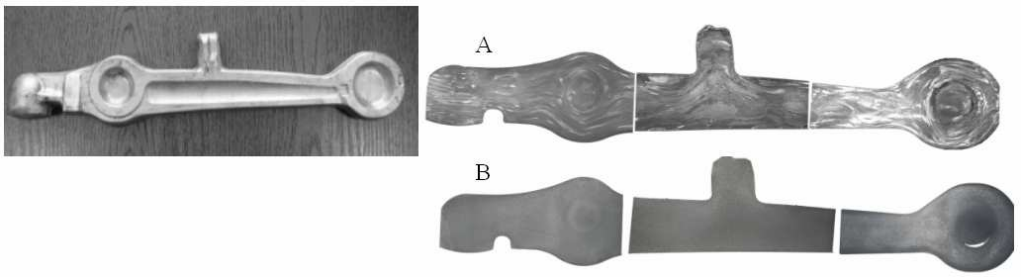

Fig. 14. Forging of a rocker and its macrostructure vs type of stock material:
A – extruded rod, B – cast billet

The macrostructure of a rocker forged from the cast stock is definitely superior to that obtained in a rocker forged from the extruded rod. In forging made from the cast stock the macrostructure is fine-grained and homogeneous, while the use of an extruded stock gives place to large and recrystallised grains (especially after heat treatment), accompanied sometimes by flow lines from the extrusion process intersecting the forging contour, which may result in reduced mechanical properties and variations of these properties along the product length. A comparison of microstructures in rockers forged from the cast billets and extruded rods, shown in Figure 15, also gives results in favour of the cast stock.

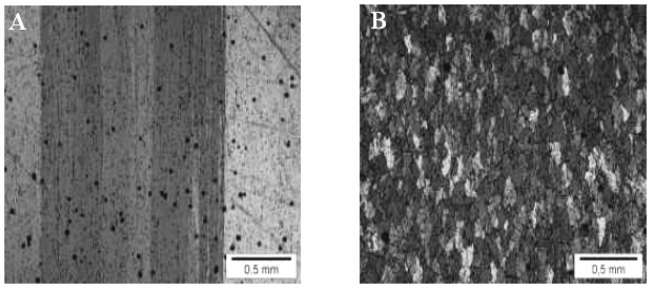

Fig. 15. A comparison of microstructures in rockers forged from:
A – extruded rod, B – cast billet

The industrial trials of die forging of rockers from EN AW-6082 alloy using as a stock material billets cast by continuous horizontal process proved good plastic properties of this forging stock. The examination of structure in forgings made from the cast stock revealed a homogeneous, fine-grained, macro- and microstructure, con-

trary to forgings made from the extruded rods in which the fibrous structure inherited from the extrusion process is very disadvantageous since it causes drop of mechanical properties, and in numerous places after heat treatment a high-rate recrystallisation accompanied by intense grain growth takes place.

In all trials, the mechanical properties (in Table 3 gives results obtained in testing of mechanical properties on rockers from both production lots after heat treatment.) obtained in forgings made from the cast stock considerably exceeded the minimum expected properties.

Table 3. The mechanical properties of rockers made from EN AW-6082 alloy

Alloy	Stock material	Heat treatment parameters	HB	Mechanical properties		
				$R_{p0.2}$ [MPa]	R_m [MPa]	A_5 [%]
EN AW-6082	Extruded rod	solution 530 °C aging 175 °C/8 h	103	295	314	12.3
	Cast stock		110	331	358	10.0

3. Conclusions

1. The results obtained in industrial trials of the die forging of elements from EN AW-2618A alloy using a stock material in the form of billets cast by semi-continuous process revealed good plastic properties of this forging stock and a homogeneous structure characterised by very high and quasi-isotropic mechanical properties.

2. Using billets of EN AW-6082 alloy as a stock material for die forged rockers enables obtaining better macro- and microstructure at a reduced material cost.

3. The rockers forged from billets are characterised by the mechanical properties superior to those obtained in the rockers die forged from the stock subjected to plastic working, i.e. from the extruded rods.

4. The very encouraging results of an investigation on the application of aluminium alloy stock in the form of billets (rods) cast in a horizontal continuous process for die forging give firm economic backgrounds for a wide-scale industrial application.

Acknowledgements

The study was financed from the structural funds assigned for a Target Project WKP_1/ 1.4.1/1/2004/4/4/215/2005/U „Development of an innovative technology for the manufacture of complete rockers from aluminium alloys”.

References

[1] ASM Specialty Handbook, Aluminum and Aluminum Alloys, ASM International 1993 r., pp. 649–690.

[2] Senderski J., Kłyszewski A., Płonka B., Szymański W., Dudek P.: PBZ-15-15, *zadanie 4.3 Opracowanie technologii wytwarzania wyrobów metodą thixoformingu*, pt. *Badania nad technologią wytwarzania wyrobów kutych przy zastosowaniu wlewków ze stopów Al o strukturze rheocast, badania struktury i własności mechanicznych wyrobów kutych*, Gliwice, 1999 (mat. not published).
[3] Stuczyński T., Zamkotowicz Z., Wężyk W., Lech-Grega M.: *Sprawozdanie IMN nr 5697: Nowe materiały i technologie na bazie metali lekkich szczególnie dla przemysłu motoryzacyjnego i transportowego, zadanie 4.2: Opracowanie technologii odlewania wlewków thiksotropowych systemem półciągłym*, (mat. not published).
[4] Anderson M., Bruski R., Groszkiewicz D., Wagstaff B.: *NETCASTTM Shape Casting Technology: Technological breakthrough that enhances the cost effectiveness of aluminium forgings*.
[5] Senderski J., Stuczyński T., Kłyszewski A., Płonka B.: *Influence of manufacturing conditions and of ingot structure on the mechanical properties and structure of die forgings*, International Conference – Aluminium in Transport 2003, Tomaszowice, 22–25. 10.2003, pp. 153–164.
[6] Senderski J., Płonka B., Lech-Grega M., Boczkal S., Kłyszewski A., Stuczyński T., *The die forging of aluminium alloys 2XXX, 4XXX series using different of stock material*, International Conference "Meform 2006", Freiberg, Germany, 29–31.03.2006, pp. 41–50.

Zastosowanie stopów Al w postaci wlewków odlewanych jako materiału wsadowego na odkuwki matrycowe w przemyśle motoryzacyjnym

Osiągnięte wyniki przemysłowych prób kucia matrycowego odkuwek ze stopu EN AW-2618A przy zastosowaniu przygotówek z wlewków odlewanych systemem półciągłym wykazały dobrą podatność plastyczną tego wsadu do kucia oraz jednorodną strukturę o wysokich quasiizotropowych właściwościach mechanicznych. Wykorzystanie jako materiału wsadowego wlewków ze stopu EN AW-6082 do kucia matrycowego wachaczy pozwala na uzyskania korzystniejszej makro i mikrostruktury obniżając zarazem koszty materiałowe. Wachacze kute z wlewków posiadają wyższe właściwości mechaniczne niż kute matrycowo z materiału uprzednio przerobionego plastycznie, czyli prętów wyciskanych. Uzyskane pozytywne wyniki badań nad zastosowaniem przygotówek ze stopów Al w postaci wlewków (prętów odlewanych) w systemie ciągłym poziomym do kucia matrycowego dają podstawę ekonomicznie uzasadnioną dla szerokiej aplikacji przemysłowej.

ARCHIVES OF CIVIL AND MECHANICAL ENGINEERING

Vol. VIII 2008 No. 2

System for design of the manufacturing process of connecting parts for automotive industry

L. RAUCH, L. MADEJ, S. WEGLARCZYK, M. PIETRZYK
AGH – University of Science and Technology, al. Mickiewicza 30, 30-059 Kraków, Poland

R. KUZIAK
Institute of Ferrous Metallurgy, ul. K. Miarki 12, 44-100 Gliwice, Poland

The proposition of complex hybrid system, dedicated to modelling of life cycle of materials and optimization of their in use properties, is presented in the paper. The approach is based on the conventional optimization algorithms, FE simulations of industrial production process and knowledge base, containing both theoretical and practical data in form of rules, facts and equations. Simulation and optimization of the manufacturing of the connecting part used in automotive industry was selected for the purposes of this work. The particular emphasis is put on control of selected in use properties of products by proper design of technological parameters for consecutive stages of the production chain. The concept of the life cycle modelling used in the proposed system, as well as results obtained from simulations, are also presented in the paper.

Keywords: *optimization, life cycle, bainitic steel, modelling*

1. Introduction

Search for new production technologies or modern materials with better in use properties has stimulated materials science research for decades, until late 90-ies of the last century. This traditional approach has changed recently and the customers demands, which beyond mechanical properties take also into account life cycle of products controlled by changes of fashion [1], became the driving force for materials research and development. Increase of expectations of the global market to provide novel solutions is facing manufacturers into a state of continuous adaptation of manufacturing processes to meet these customer demands. In order to meet market pressures, modern manufacturing systems have to be intelligent and adjustable, what can be achieved mainly by the feedback of information from the final product to the stage of manufacturing. Such system has to influence planning and organization of the production line, to create process that is flexible, reconfigurable and cost efficient. These aspects are widely discussed in [1–3]. The basis of those systems is constrained to organization of production without accounting for the technological aspects.

In metal forming oriented towards automotive industry obtaining high exploitation properties of products, such as fatigue resistance or wear resistance, combined with decrease in production costs, is still crucial. Extending the life cycle of products and

fitting in environment protection requirements is another important issue. Combining these tasks with the ever-changing global market is the motivation for development of the hybrid computer systems, which combine simulations with expert systems.

The objective of this work is formulated with the above remark in mind. The first step towards this objective, which is simulation of the entire production chain, is described in the paper. Sensitivity of the product properties with respect to the technological parameters, which is the necessary condition for optimization of the entire production chain, is tested. Creating the system, which allows to account for the product exploitation properties at the stage of the manufacturing technology design is the perspective objective of the whole project. The system proposed in this work is complement to the hybrid system for modelling and optimization described in [4].

2. Life cycle modelling

During last decade, the finite element (FE) method has been widely used in industry to simulate various processes, i.e. cold and hot forging, rolling, extrusion, stamping etc. The FE simulations provide information regarding changes of the product shape and predict distributions of stresses, strains and temperature in one particular deformation process, i.e. forging. Rheological models that were in common use, describe relation between flow stress and external variables like strain ε, strain rate $\dot{\varepsilon}$ and temperature T:

$$\sigma = f(\varepsilon, \dot{\varepsilon}, T). \tag{1}$$

Optimization algorithms had to be applied to obtain numerical results, which are in a closer agreement with material behaviour under industrial conditions. Due to limited power of computers in the early 90-ies of the last century, the number of the optimization variables was limited. Computers capabilities have increased noticeably during the last decade and rheological models could be extended to account for microstructure evolution under loading conditions, i.e. dynamic and static recrystallisation, phase transformation or precipitation. In these approaches, stress becomes a function of time t, again of some external variables and also internal variables, such as density of mobile ρ_m and trapped ρ_t dislocations and grain size of particular phases D:

$$\sigma = f(\varepsilon, \dot{\varepsilon}, T, \rho_m, \rho_t, D, \ldots). \tag{2}$$

In consequence, the number of optimization variables increased, what resulted in much higher accuracy of the numerical results. More information about selection of material models for hybrid simulation-design systems can be found in [4].

Despite the progress in capabilities of rheological models, the FE simulations and optimizations algorithms have been for decades applied mainly to a single deformation process, what prevented possibility of accounting for the influence of other op-

erations in the production chain. Thus, the novel approach to design manufacturing processes has to be developed. This approach should be based on considering not only one stage of manufacturing processes, but it should consider the whole life cycle (LC) of material including manufacturing, processing and exploitation stages. Modelling of the LC, which is in the field of interest of researchers in several laboratories [1–7] provides the possibility to control the final product properties at the stage of manufacturing. It means that required properties and specific behaviour of product under exploitation can be obtained by optimization at the stage of material processing. That would allow to manufacture products with better in use properties.

Proper micro scale material model, which replicates important processes such as microstructure evolution [8], phase transformation [9], failure [10] or strain localization [11], has to be implemented into the FE code. Such model is difficult for engineers, who are inexperienced in the field of numerical simulations. Selection of the proper optimization algorithm, that can be applied to obtain desired material properties in particular manufacturing process, is even more difficult. This is the reason why Authors as continuation of work [4] decided to develop the user-friendly intelligent system, which selects the optimization techniques with the objective function composed of required product properties, as well as selects proper models which predict microstructure evolution and properties during all stages of manufacturing. Main assumptions of the system are presented in the next section.

3. System for optimization

The proposed system is dedicated to support decision making for engineers in industry. The system is designed as the layered software model, where each functional set of components is responsible for the specific activity (Figure 1).

The basic layer consists of knowledge and databases, which are inputs for higher level modules composed of the process design and the Digital Material Representation (DMR) subsystems. The highest layer consists the most important part, which is LC modelling and optimization. All layers are connected to elements of Enterprise Resource Planning (ERP) system, what locates the optimization results inside the enterprise reality. The artificial intelligence optimization methods [13–14] such as genetic algorithms or particle swarm optimization, has recently become popular, but they still require further tests. Thus, conventional methods e.g. Hooke-Jeeves or Rosenbrock, which were tested for metal forming applications and proved its capabilities, are implemented in the system. The basic advantages of the system are as follows:

– *advanced description of processed material* – material data are gathered in data sets specified at different scales (micro, mezo, nano), containing material features, parameters and models. All sets in material database are described using MatML language (www.matml.org), which is built on XML technology and facilitates unified exchange of data in automated way between various components, packages and systems.

The DMR module, which is responsible for preprocessing and analysis of this data, is placed in the second layer of the system;

– *complex modelling of designed forming process* – the data prepared by the DMR module and the Process Design module are used in calculation subsystem called Life Cycle Modelling. Examples of application of this subsystem are presented and analysed in section 3.2 of this paper. This process is performed by the optimization module, which considers final material properties as the objective function and supports selection of dedicated optimization method;

– *accuracy and reliability of results* – the results processed by the optimization module are compared to the data gathered in Technological Knowledge Base, which is stored in the two different sets of static (rules, fact, chapters) and dynamic (equations, simulations) knowledge. The possibility of direct comparison to the model examples from literature and practice offers flexible and powerful tool for industrial users.

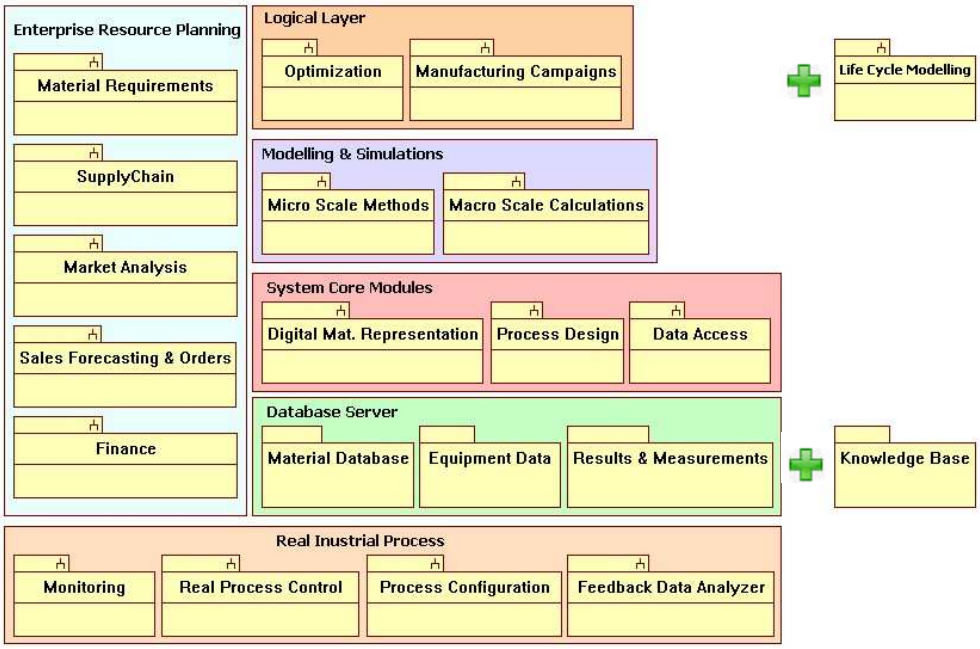

Fig. 1. Diagram of subsystems and packages deployment [4] extended with subsystem of Life Cycle Modelling added in the logical layer of the proposed system and package of Knowledge Base

3.2. Example of system's application

Simulation and optimization of the manufacturing of the connecting part used in automotive industry (Figure 2) was selected as an example. Particular emphasis is put on control of selected in use properties of product at consecutive stages of the production chain. Materials used to manufacture these cold forged components should have

high mechanical properties and fatigue resistance. Low and medium carbon steels are commonly used for bolts manufacturing [7], but heat treatment operations have to be applied to obtain proper ductile properties and high static and dynamic load carrying capacity. Each additional thermomechanical operation leads to increase of production time and, what is even more important, to increase in the production costs. Therefore, researchers look for materials that are characterized by high ductile and strength properties obtained without additional expensive heat treatment. Bainitic steels [12] may be one of possible solutions and this material is used in the simulation in the present paper. The rheological model for this steel was identified in [6].

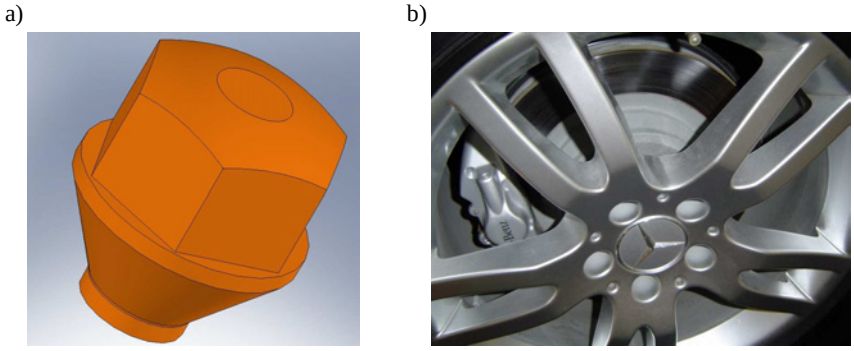

Fig. 2. a) shape of the final product, b) typical application the investigated bolt

The complex modelling of the production chain is the most challenging part of the proposed system for industrial users. It allows to simulate shape of the final product and all important phenomena, which occur in material during forming, and which influence the properties of this product. Each step of the simulation is controlled by the set of production chain parameters, selection of specific material and the initial shape of perform. Selected examples of simulations performed for the entire manufacturing chain for the bainitic steel bolt are presented in Figures 3–5. The two stage forging presented in Figure 3 is flowed by the two stage machining shown in Figure 4. Higher strains causing higher hardness are observed in the area, where thread will appear. Higher hardness in this region is desired, which decreases the probability of material failure under exploitation conditions.

Results obtained from the cold forging are used as the input for the machining, which transfers the final shape of the bolt head to the preform. Machining can be realized as one or two stage process, depending on the shape of the final part. Rolling, which transfers the thread on the bolt, is the final stage of the manufacturing chain. Any subsequent operations like heat treatment are not necessary to obtain desired properties of the final product.

When the numerical model for the entire manufacturing chain is developed, the optimization can be performed. The goal function is the mean square error between

required and obtained properties, e.g. hardness. One or several stages of manufacturing chain can be optimized. Optimization of the entire chain is possible [15], but it requires extreme computation time. Thus, the present paper is constrained only to presentation of the possibility of the optimization of the selected manufacturing operation, to obtain higher strength properties of the bolt. In the modified manufacturing chain a higher reduction of the width was employed in the first and second stages of forging. That resulted in higher strains and hardness in the region of the bolt thread (Figure 5) in comparison with the results in Figure 3.

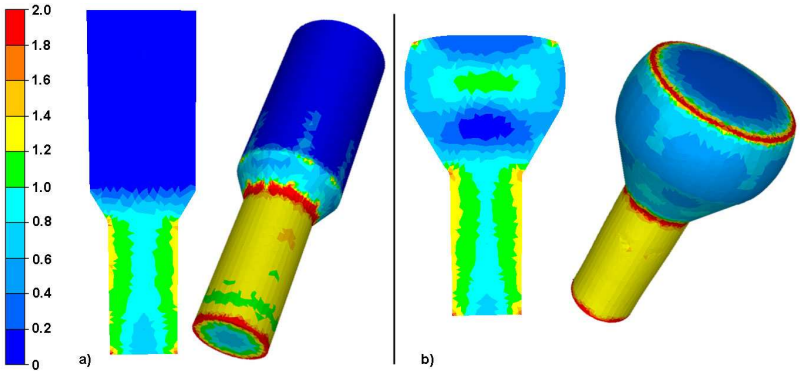

Fig. 3. Strain distribution obtained after: a) first and b) second stage of cold forging

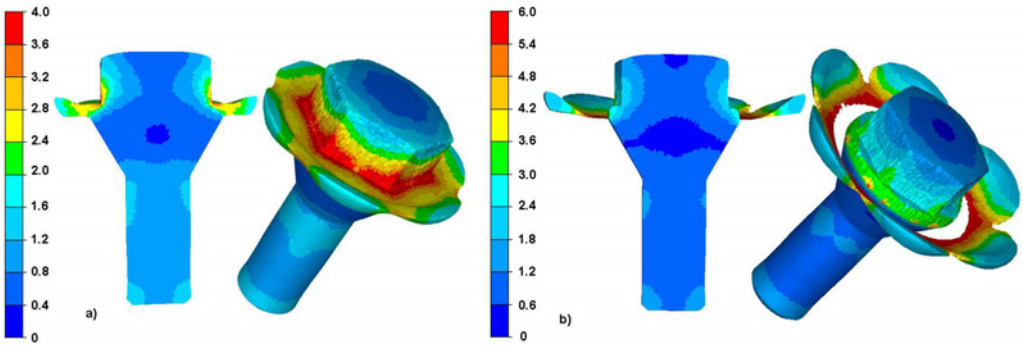

Fig. 4. Strain distribution obtained after: a) first and b) second stage of machining

The strain distribution is not uniform in the entire area of the thread, what results in regions of higher hardness. It influences material behaviour under exploitation. Other steps of optimization process are then performed until the desired properties are obtained. At the last step of simulations the final part is subjected to a series of laboratory tests, which are performed to evaluate its behaviour during exploitation conditions. Example of numerical simulation of the shear test is presented in Figure 6.

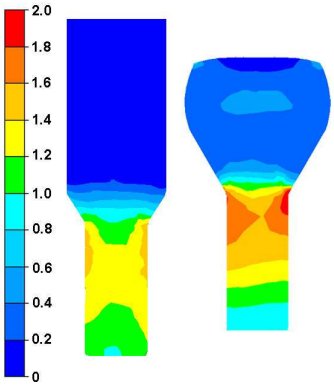

Fig. 5. Strain distribution in the modified manufacturing chain obtained after first and second stage of cold forging

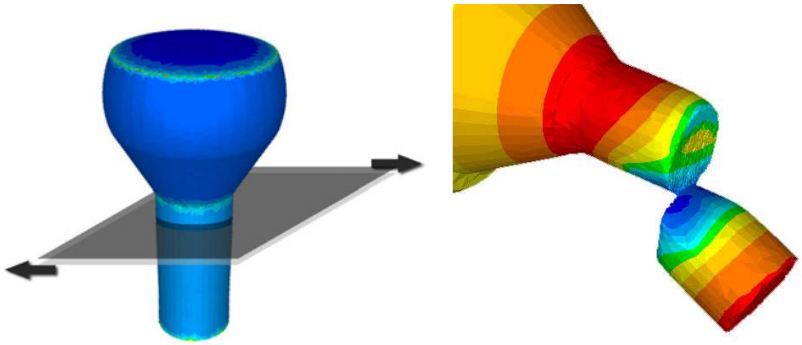

Fig. 6. Simulation of the shearing test

4. Conclusions

The idea of the system dedicated to support decision making for engineers working in industry is presented in the paper. This is an intelligent system, which selects the optimization techniques with the objective function composed of required product properties, as well as helps in selection of proper rheological models for numerical simulations. The system gives a possibility to design the manufacturing process of products with required properties such as strength, crack resistance, fatigue resistance, shear resistance, wear resistance, creep resistance, corrosion resistance, hardness, ductility, porosity, adhesive properties, high temperature resistance, toughness, conductivity, low temperature resistance, etc. Thus, decrease of the number of expensive industrial trials is possible.

Since simulation of the entire manufacturing chain is the core part of the system, the emphasis in this paper was put on development of the FE model for the selected chain of the manufacturing of the bolt for automotive industry. Presented results con-

firm predictive capabilities of the model and show sensitivity of the product properties with respect to the technological parameters of the chain. This is a necessary condition for optimization of the entire production chain.

Acknowledgement

The financial support provided by MNiSzW, project no. R15 012 03, is acknowledged.

References

[1] Hon K.K.B., Xu S.: *Impact of product life cycle on manufacturing systems reconfiguration*, Annals of the CIRP, 2007, 56, pp. 455–458.
[2] Pereira J., Paulre B.: *Flexibility in manufacturing systems: a relational and a dynamic approach*, European J. Operational Research, 2001, 130, pp. 70–82.
[3] Bruccoleri M., Lo Nigro G., Perrone G., Renna P., Noto La Diega S.: *Production planning in reconfigurable enterprises and reconfigurable manufacturing systems*, Annals of the CIRP, 2005, 54, pp. 433–436.
[4] Rauch L., Madej L., Pietrzyk M.: *Hybrid system for modeling and optimization of production chain in metal forming*, J. Machine Eng., 2008, (in press).
[5] Bariani P.F., Bruschi S., Ghiotti A.: *Material testing and physical simulation in modelling process chains based on forging operations*, Computer Methods in Materials Science, 7, 2007, pp. 378–382.
[6] Madej L., Szeliga D., Kuziak R., Pietrzyk M.: *Physical and numerical modelling of forging accounting for exploitation properties of products*, Computer Methods in Material Science, 7, 2007, pp. 397–405.
[7] Madej L., Weglarczyk S., Packo M., Kuziak R., Pietrzyk M.: *Application of the life cycle modeling to forging of connecting parts*, Proc. MS&T 2007, Detroit, USA, 2007, pp. 191–200.
[8] Gawad J., Pietrzyk M.: *Application of CAFE multiscale model to description of microstructure development during dynamic recrystallization*, Arch. Metall. Mater., 52, 2007, pp. 257–266.
[9] Pietrzyk M., Kuziak R.: *Coupling the Thermal-Mechanical Finite-Element Approach with Phase Transformation Model for Low Carbon Steels*, 2nd ESAFORM Conf. on Material Forming, ed., Covas J., Guimaraes, 1999, pp. 525–528.
[10] Allix O.: *Multiscale strategy for solving industrial problems*, Comp. Meth. Appl. Sci., 6, 2006, pp. 107–126.
[11] Madej L., Hodgson P.D., Pietrzyk M.: *Multi-scale rheological model for discontinuous phenomena in materials under deformation conditions*, Computational Materials Science, 2007, 38, pp. 685–691.
[12] Pickering, B.F.: *High-Strength, low–alloy steel – a decade of progress*, in Proc. Symp. Microalloying, ed., Korchynsky, M., Union Carbide Computation, 1996, New York, pp. 9–31.
[13] Wei L., Yuying Y.: *Multi-objective optimization of sheet metal forming process using Pareto based genetic algorithm*, Journal of Materials Processing Technology, Accepted for Publication 11-01-2008.

[14] Kuś W.: *Grid-enabled evolutionary algorithm application in the mechanical optimization problems*, Engineering Applications of Artificial Intelligence, 20, 2007, pp. 629–636.
[15] Stanislawczyk A., Kusiak J., Kuziak R.: *Testowy system optymalizacji cyklu produkcji w przeróbce plastycznej*, Proc. 15th Conf. KomPlasTech, eds, Grosman F., Hyrcza-Michalska M., Korbielow, 2008, pp. 185–192, (in Polish).

System projektowania procesów wytwarzania elementów łącznych dla przemysłu samochodowego

Propozycja kompleksowego systemu hybrydowego, przeznaczonego do modelowania cyklu życia materiałów oraz optymalizacji ich własności użytkowych, została zaprezentowana w niniejszym artykule. Podejście to oparte jest o klasyczne algorytmy optymalizacji, symulacje numeryczne procesów przemysłowych metodą elementów skończonych oraz bazę wiedzy zawierającą zarówno dane teoretyczne jak i praktyczne w formie reguł, faktów i równań. Na potrzeby niniejszej pracy w celu wykonania obliczeń symulacji i optymalizacji wykorzystano procesy wytwarzania elementów łącznych używanych powszechnie w przemyśle samochodowym. Szczególny nacisk został położony na kontrolę wybranych własności produktów poprzez wykonanie odpowiedniego projektu oraz dobór parametrów technologicznych w kolejnych etapach łańcucha produkcji. Koncepcja modelowania cyklu życia materiałów wykorzystana w zaproponowanym rozwiązaniu jak również otrzymane wyniki symulacji również zostały zaprezentowane w artykule.

ARCHIVES OF CIVIL AND MECHANICAL ENGINEERING

Vol. VIII 2008 No. 2

Estimation of hole-flange ability for deep drawing steel sheets

F. STACHOWICZ
Politechnika Rzeszowska, ul. W. Pola 2, 35-959 Rzeszów, Poland

Hole-flanging is a common sheet forming operation to produce structural sheet metal components. Flanges are used for appearance, rigidity, hidden joints, and strengthening of the edge of sheet metal parts. Trial-end-error is the most common approach for tooling and process design in flanging operations. This paper presents some experimental results of hole-flanging process performed on flat deep drawing steel sheets with circular hole drilled in the centre. Three punches of different geometry i.e. cylindrical, hemispherical and conical were used in this experiment. The effect of both the punch geometry and material mechanical parameters (especially strain hardening and plastic anisotropy) on the limit expansion of the hole was determined.

Keywords: *hole flanging, deep drawing steel sheet, forming limit, thickness distribution*

1. Introduction

The modern automobile industry and the household appliance industry have demand precision products for single part or multiple manufacture parts so that the related industrial product precision size of press forming has gradually been required. Collars are used to provide material for thread cutting and to provide additional support for press fits for bolts or for making solder connections with tubes [1, 2].

Hole-flanging is a process in which a sheet blank, with a hole in its center, is rigidly clamped around its periphery by a blank holder, and then a punch is used to force the blank into a die to form a hollow flanged component. During the process, the sheet is bent twice, once around the punch radius and again around die radius. The greatest strains are in the periphery of the expanded hole – the major deformation increases the diameter of the initial hole while thickness is reduced. However, the tensile stress in the circumferential direction at the edge of flanged hole is the main cause of failure due to cracking or tearing [3]. General method to predict the material fracture in the process of forming analysis make use of the fracture strain of the specimen obtained by simple tension test, the limit strain based on plastic instability theory, and the ductile fracture criteria. But the hole-expanding process is different from general forming process because the side face of the hole has no constrains and the fracture propagates trough the side face of a plate during the process [4].

The hole flanging process is limited to a certain limit hole diameter below which material failure could take place. The magnitude of the deformation of flanged parts is usually characterized by the drawing ratio β, which is defined as a ratio of the inside diameter d of the finished collar to the initial hole diameter d_0 (Figure 1). The limit

value of drawing ratio β_{max}, very often is know as Hole Expanding Limit (HEL) [5] and depends on several different parameters [5–8]:

– mechanical properties of sheet material,
– the surface quality of the initial hole edge,
– geometry of forming punch,
– relative hole diameter,
– friction conditions.

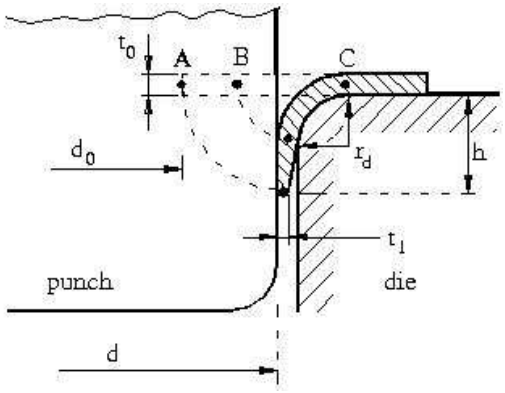

Fig. 1. Schematic diagram of hole flanging

To be able to predict the flange hole formed to a specific geometry with a given material, including diameter of the expanded hole and the flange height, it can save a lot of effort in contrast to the conventional trial-end-error approach. This work aims to investigate the influence of punch geometry: cylindrical (flat-bottomed), hemispherical and conical, as well as mechanical parameters of deep drawing steel sheet metal on the value of hole expanding limit.

2. Material and experimental procedure

The tests were carried out on three different kinds of 1.0 mm thick steel sheet: DQ drawing quality, DDQ deep drawing quality and EDQ extra drawing quality. Tensile specimens of 240 mm gauge length and 20 mm width were prepared from strips cut at 0°, 45° and 90° to the rolling direction of the strip. The experiments were carried out using a special device, which recorded simultaneously the tensile load, the current length and the current width of the specimens. The effective stress – effective strain relationship was described using the Hollomon model in the form of $\sigma = C\varepsilon^n$.

The plastic anisotropy factor r has been determined on the basis of the relationship between the width strain and thickness strain in the whole range of specimen elongation using less square method. The value of the tensile parameters (Table 1) has been

averaged according to: $x_{mean} = (x_0 + 2x_{45} + x_{90})/4$, where the subscripts refer to specimen orientation.

Table 1. Mechanical properties of DQ, DDQ and EDQ steel sheet

Material symbol and specimen orientation	Yield stress	Ultimate strength	Ultimate elongation	Strain hardening parameters		Anisotropy factor
	$R_{0.2}$ [MPa]	R_m [MPa]	ε_u	C [MPa]	n	r
DQ_0	193	351	0.36	554	0.166	1.218
DQ_45	197	372	0.32	591	0.171	0.946
DQ_90	193	353	0.34	563	0.174	1.410
Mean value	196	362	0.34	575	0.171	1.130
DDQ_0	196	336	0.42	557	0.192	1.464
DDQ_45	196	336	0.38	547	0.183	1.180
DDQ_90	198	311	0.41	526	0.177	1.902
Mean value	196	330	0.40	544	0.184	1.432
EDQ_0	151	282	0.44	494	0.221	1.630
EDQ_45	153	293	0.40	497	0.207	1.445
EDQ_90	153	281	0.42	475	0.210	2.031
Mean value	153	287	0.42	487	0.211	1.638

The flanging test was curried out using a special device constructed according to the proposal of standard method [5]. Three punch shapes conical, cylindrical and spherical were prepared for the axisymmetric collar-drawing test. The punch and die geometry was as follow:

- punch diameter – D_p = 30 mm,
- die diameter – D_d = 32 mm,
- die edge radius – r_d = 2 mm,
- conical end angle – α = 60°,
- radius of cylindrical punch edge – r_p = 4 mm.

Sheet specimens 80×80 mm, prepared from the strips with marked orientation according to the rolling direction and with drilled or punched d_0 = 10 mm central hole, were firmly clamped at the periphery and deformed progressively up to visible strain localization at the hole edge. Expansion of the hole was recorded using the digital photo-camera and stored as a *.pws files. Using professional computer code, the *.pws files were elaborated in order to determine changes in a hole diameter in rolling direction and transverse rolling direction.

3. Results and discussion

Maximum diameter of expanded hole (Table 2) visibly depends on both the punch geometry and sheet material type. When the punch geometry is concerned the largest hole expansion was achieved when flanging with the conical punch and the worst in the case of the cylindrical (flat-bottomed) punch. For the conical and spherical

punches, the edges of the hole are in contact with the punch surface so that severe friction in the tangential direction is produced, reduces the thinning of the wall and protects the hole periphery from necking or tearing. Additionally the strain state in flanging with conical punch seemed to be the most beneficial, which resulted also in the lowest collar height in comparison with other punch shapes [9].

Since formability of a sheet metal strongly depends on the plastic properties of the material, e.g. the value of both the strain hardening exponent *n* and plastic anisotropy factor *r*, as well as initial hole performing technology, the effect of these three parameters on sheet flangeability was examined in our investigations. For all three punch geometry the final hole diameter (before strain localization) increases with the *n*-value increase. This relation is more distinct in the case of initial hole punched (Figure 2).

Table 2. Maximum diameter (in mm) of hole expanded using different punch shape and technology of initial hole performing

Material symbol	Punch geometry		
	Cylindrical shape	Conical shape	Spherical shape
Initial hole drilled			
DQ	23.03	26.32	24.12
DDQ	26.80	30.00	28.23
EDQ	30.00	30.00	30.00
Initial hole punched			
DQ	16.34	20.01	18.06
DDQ	20.17	24.22	22.26
EDQ	24.67	30.00	26.76

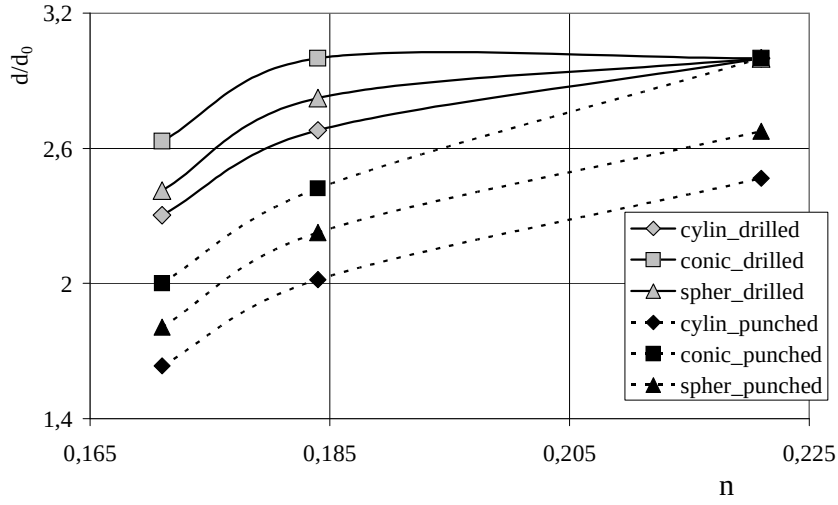

Fig. 2. Hole Expanding Limit (d/d_0) dependence on the value of strain hardening exponent and initial hole performing technology

According to the experimental results we can conclude that the limit value of drawing ratio $\beta_{max} = 3.0$ were achieved in the case of initial hole (Figure 2):

– performed by drilling technology for EDQ steel sheet for all three punch geometry, and for DDQ steel sheet when using conical punch,

– performed by punching technology for EDQ steel sheet when using conical punch.

At the hole edge (point A in Figure 1) material points undergo uniaxial tensile stress and the value of maximum true strain at these points could be calculated as: $\varepsilon = \ln(d/d_0)$. Comparisons between maximum true strains calculated on the basis of the tensile test and hole expanding test demonstrated large differences. The values of maximum strain at the hole edge are nearly to 3 times larger (depending on material and technology of initial hole performing) than the value of maximum strain obtained in uniaxial tensile tests. Larger maximum strains at the hole edge observed in the hole expanding test resulted from interaction between outer and inner material points of flange [1], which delay the moment of strain localization and material failure. Formability of sheet metal could be expressed by the $n \cdot r$ factor, defined as product of strain hardening exponent and plastic anisotropy ratio. The value of strain at the hole edge dependence on the value of $n \cdot r$ factor for all three punches shape is more visible in the case of initial hole performed punching technology (Figure 3).

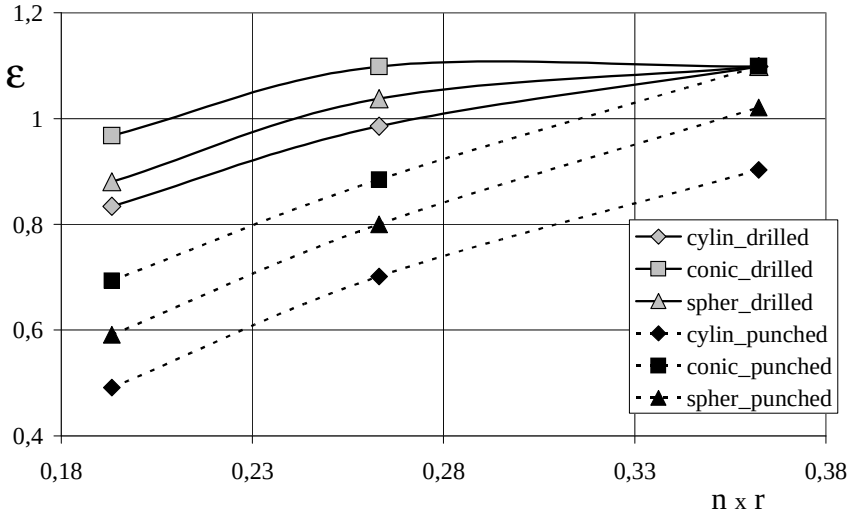

Fig. 3. Strain at hole edge dependence on the value of $n \cdot r$ factor for different initial hole performing technology

4. Conclusions

Hole flangeability of steel sheet is investigated in this study. On the basis of the experimental results the following conclusions could be formulated:

– although a sheet material at the hole periphery undergoes uniaxial tensile stresses the maximum strains at the hole edge are nearly 3 times larger than the value of maximum strain obtained in uniaxial tensile test,

– HEL visibly depends on the punch shape; when using the conical punch, the largest final hole diameter, i.e. hole expanding limit, could be achieved,

– HEL increases with the strain hardening exponent and plastic anisotropy ($n \bullet r$ factor), especially in the case of flanging with cylindrical punch,

– differences in the strain at hole edge are more visible for initial hole performed by punching technology.

References

[1] Erbel S., Kuczyński K., Marciniak Z.: *Obróbka plastyczna*, WNT, Warszawa, 1981.
[2] Lange K.: *Handbook of Metal Forming*, McGraw-Hill Co., New York, 1985.
[3] Huang Y-M.: *An elasto-plastic finite element analysis of the sweet metal stretch flanging process*, Int. J. Adv. Manuf. Technol., Vol. 34, 2007, pp. 641–648.
[4] Ko Y.K., Lee J.S., Huh H., Kim H.K., Park S.H.: *Prediction of fracture in hub-hole expanding process using a new ductile fracture criterion*, J. Mat. Proc. Technol., Vol. 187–188, 2007, pp. 358–362.
[5] Hayashi H., Urabe T., Hisamatsu S., Nagai Y.: *Investigation for standardizing hole-expanding test for evaluating stretch flangeability*, IDDRG WB 1996, Eger, pp. 1–6.
[6] Huang Y-M., Chien K-H.: *The formability limitation of the hole-flanging process*, J. Mat. Proc. Technol., Vol. 117, 2001, pp. 45–51.
[7] Hyun D.I., Oak S.M., Kang S.S., Moon Y.M.: *Estimation of hole flangeability for high strength steel plates*, J. Mat. Proc. Technol., Vol. 130–131, 2002, pp. 9–13.
[8] Thipprakmas S., Jin M., Murakawa M.: *Study of flanged shapes in fine-blanked-hole flanging process (FB-hole flanging process) using finite element method (FEM)*, J. Mat. Proc. Technol., Vol. 192–193, 2007, pp. 128–133.
[9] Sitek M., Stachowicz F.: *Wpływ geometrii stempla na stopień wywinięcia obrzeża otworu*, Rudy Metale, Vol. 49, 2004, pp. 60–64.

Ocena możliwości wywijania otworów w blachach stalowych tłocznych

Proces wywijania krawędzi wokół otworów jest często stosowany w konstrukcjach wykonywanych z blach. Wywinięcia krawędzi obrzeża wykonywane są by umożliwić wykonanie połączenia, bądź też w celu zwiększenia sztywności lub wytrzymałości konstrukcji. Metoda prób i błędów jest częstym sposobem doboru geometrii narzędzi oraz technologii wywijania. Opracowanie to zawiera wyniki badań eksperymentalnych procesu wywijania kołnierza wokół otworów wywierconych lub wykrojonych w próbkach blach stalowych o różnej tłoczności, przy zastosowaniu trzech różnych geometrii stempla – płaskiej stożkowej oraz kulistej. Określono wpływ geometrii stempla oraz właściwości mechanicznych materiału (wykładnik krzywej umocnienia oraz współczynnik anizotropii) na wartość maksymalnego stopnia wywinięcia.

ARCHIVES OF CIVIL AND MECHANICAL ENGINEERING

Vol. VIII 2008 No. 2

The electroplastic effect in the cold-drawing of copper wires for the automotive industry

Z. ZIMNIAK, G. RADKIEWICZ
Wrocław University of Technology, ul. Łukasiewicza 5, 50-371 Wrocław, Poland

The paper presents a comparison between conventional cold wire drawing and wire drawing combined with the application of high-density electric current pulses. The investigations were carried out having in mind the manufacture of copper wire for cables used in the automotive industry. A specially built experimental stand is described. The experiments showed a decrease in the pull force for wire drawing combined with the application of current pulses. The material properties of the drawn wires were tested. It was found that the plastic properties of the wire and its surface quality improved in the case of wire drawing combined with current pulses. The proposed technique of wire drawing is highly promising and potentially can replace the conventional on-line continuous annealing of the material.

Keywords: *electroplastic effect, wire drawing, current pulses*

1. Introduction

Wire drawing is used, among others, in the manufacture of cables for the automotive industry. Such a cable is made up of many twisted copper wires enclosed in plastic insulation. On-line continuous annealing is usually employed in order to ensure that obtained material is homogenous and soft. Since this technique requires direct or alternating current it is highly energy-intensive. Therefore more economical material annealing techniques are sought.

The paper presents the application of high-density electric pulses in the drawing process, aimed at obtaining high quality products. This may result in improved drawing process productivity and reduced production costs. The so-called electroplastic effect (EPE) occurs in metals as they are subjected simultaneously to plastic deformation and a pulsating flow of high-density electric current. As a result, the deformed material's overall properties, particularly its flow stress, internal stresses, defects and microstructure evolution, change.

The effect of a magnetic field on plastic deformation was first investigated by Kravchenko in 1970 [1]. The investigations showed that a strong magnetic field has an effect on dislocation behaviour and results in the deterioration of material plastic properties. The change in the plastic properties of metals under the influence of a magnetic field was called the magnetoplastic effect. The change in the properties of materials under the influence of the pulsating flow of high-density electric current during plastic deformation was discovered by Conrad [2–5] and called the electroplastic effect. The latter can be exploited in forming operations [6].

The electroplastic effect is also used to change the structural phases of a material in order to enhance its fatigue resistance [7]. The lifetime of a part subjected to the pulsating flow of current substantially increases. The observed evolution of a microstructure may lead to the formation of nanostructures in conventional materials after the application of even a single pulse [8].

The electropulsation deformation of metals is used, among others, in the rolling process [10]. Magnesium alloy AZ31 in the form of a 2 mm wide and 0.89 mm thick specimen was used in the investigations. A reduction in the specimen rolling force during electropulsation deformation was observed. The crack resistance increased, which is promising considering the practical applications of this technology.

Also the exploitation of EPE in wire drawing processes, aimed at reducing stresses and increasing the quality of austenitic stainless steel products, was examined [11]. As a result, the drawing stresses for this material were reduced by 10%. Current pulse action also affects the microstructure, resulting in significant grain refinement [12].

2. Experimental procedure

A wire drawing stand, suitable for investigating the process combined with the use of the electropulsation deformation technique, was built (Figure 1). The flow chart of the drawing process employing EPE is shown in Figure 2.

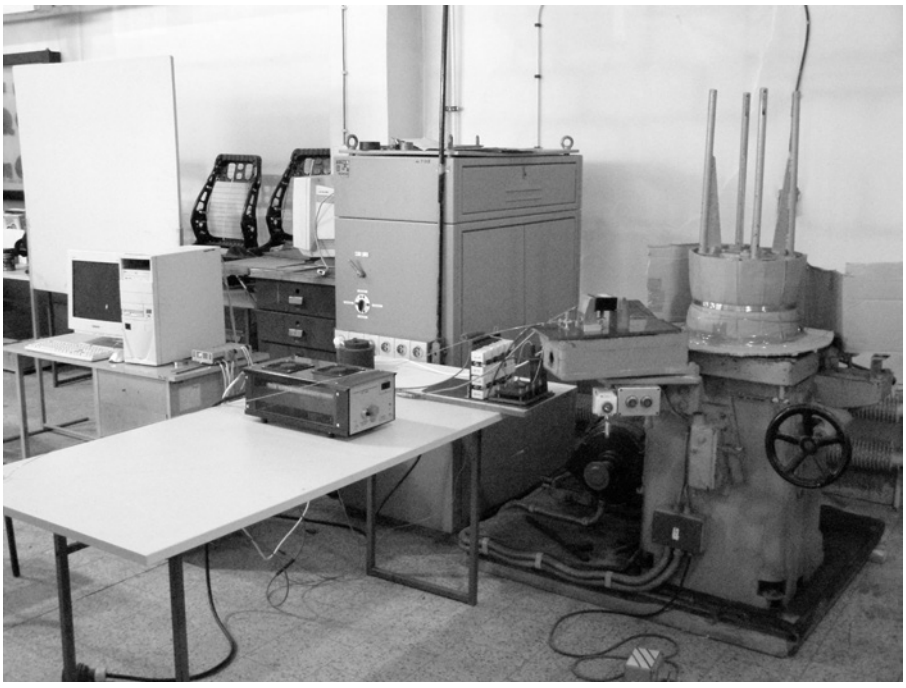

Fig. 1. Photograph of experimental stand for investigating EPE

A fine copper (99.99%) wire with an initial diameter of ϕ1.85 mm was used in the experiments, during which the input material was drawn through two drawing dies respectively ϕ1.68 mm and ϕ1.50 mm in diameter. They were Fortek/Fort Wayne dies with natural diamond inserts.

The wire drawing machine and the drawing dies were the same as the ones used in conventional wire drawing. The stand included an electropulsing generator connected via electrodes to the drawn wire. The drawing process was carried out in two modes:

1) conventional drawing,

2) drawing with the application of set electric current pulses.

Electric pulses were introduced into the system via electric contacts spaced at every 100 mm. A dynamometer, measuring the die pull, was placed after the drawing die. The drum-type wire drawing machine (single-stage) was electrically insulated from the supplied electric current pulses. The pulses were generated by an electropulsing generator with the following specifications: frequency range of 0–10 Hz and voltage regulated up to 3 kV. The generated pulses had a current density of about 10^3 A/mm^2 and a pulse duration of about 8 μs.

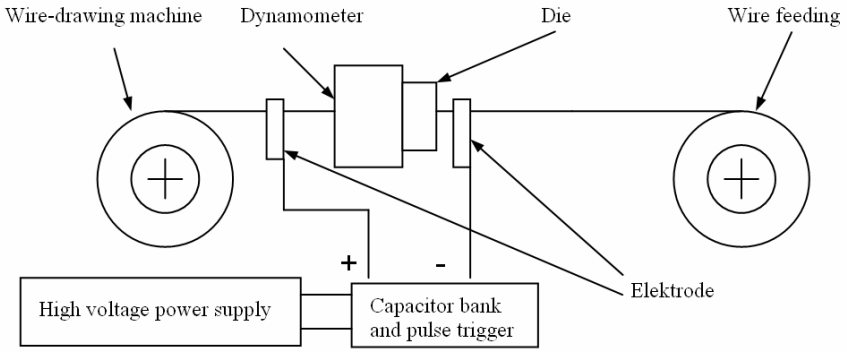

Fig. 2. Diagram of experimental stand for investigating wire drawing process employing EPE

All the drawing process specifications are shown in Table 1.

Table 1. Drawing process specifications

Current frequency	7 Hz
Voltage	2.5 kV
Capacitor bank	5 μF
Drawing velocity	0.7 m/s
Input material	copper ETP-8-CL
Electric conductance	58.58 MS/m
Input material diameter	ϕ1.85 mm
Diameter of die no. 1	ϕ1.68 mm
Diameter of die no. 2	ϕ1.50 mm
Die insert	natural diamond

3. Experimental results

First the wire was drawn through the ϕ1.68 mm die. The experimental results are presented in Figure 3 which shows (superimposed on each other) force diagrams from the two tests: 1) without electric current pulses and 2) with such pulses.

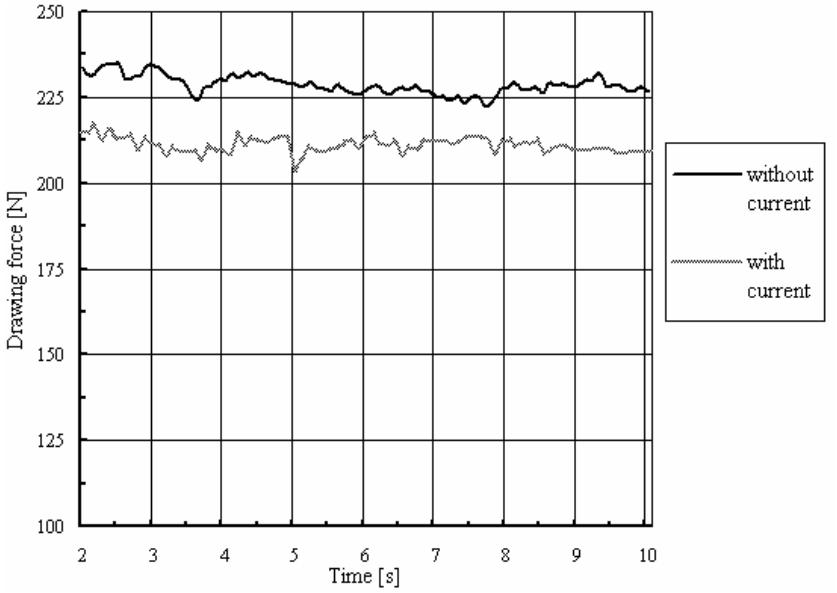

Fig. 3. Comparison of pull forces for ϕ1.68 mm diameter die

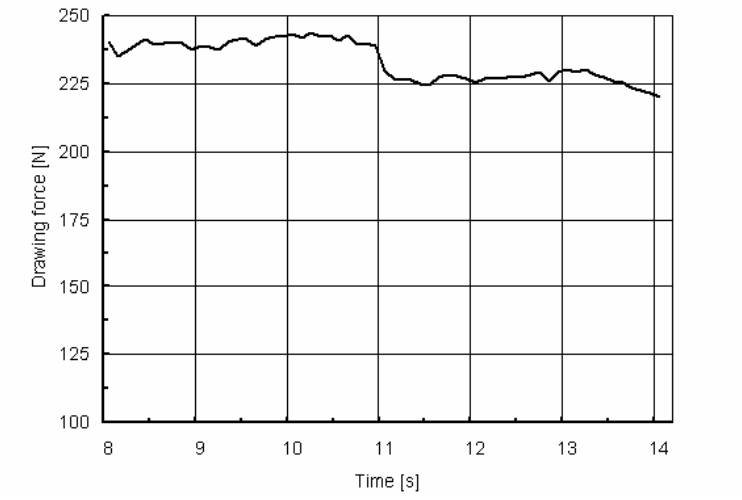

Fig. 4. Pull force for drawing with and without current pulses

It follows from figure 3 that the pull force determined in the test with current pulses is weaker than the one in the test without current pulses. The difference amounts to 10 N.

Then the wire was drawn through the ϕ1.50 mm die. The die pull force is shown in Figure 4. In this test, drawing initially was conducted without electric current pulses and at about the 11th second of the experiment current pulses were applied. As the diagram shows, the pull force instantly decreased by about 15 N.

The experiments have shown that the application of electric current pulses results in a decrease in the pull force, which is due to electroplasticity.

4. Mechanical properties of drawn copper wires

The properties of the drawn ϕ1.68 mm and ϕ1.50 mm copper wire were determined in a static tension test. Two parameters: specimen tensile strength and strain were compared. The specimen's measurement part was 70 mm long. The rate of tension was 3 mm/min.

Six series of specimens were tested. The specimens in series 1–3 were taken from the wire drawn without electric current pulses and the series 4–6 specimens were taken from the wire drawn with the application of electric current pulses.

Figure 5 shows tension diagrams for the particular series. The application of electric current pulses results in a slight increase in the tensile strength and in a significant increase in the elongation of the tested specimens.

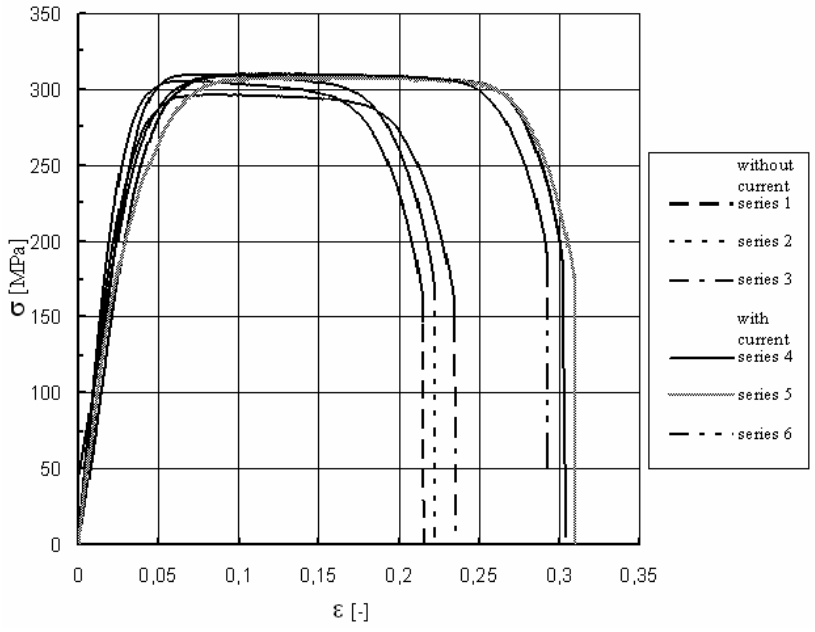

Fig. 5. Stress-strain curves for ϕ1.68 mm wire

The tensile strength and elongation ε for the specimens of each tested series are shown in Table 2. Both tensile strength and elongation increase in comparison with the drawing without current pulses.

Table 2. Specimen tensile strength and elongation for ϕ1.68 mm wire

	Series no.	Tensile strength σ[MPa]	Strain ε[-]
Without current	1	303.0	0.215
	2	305.7	0.223
	3	296.5	0.235
With current	4	309.6	0.305
	5	307.8	0.310
	6	310.0	0.293

5. Conclusions

- The experiments have shown that the pull force decreases when electric current pulses are applied. For the adopted drawing process specifications the pull force was reduced by 15 N, i.e. by about 8 %.
- Therefore drawing combined with the application of electric current pulses can be used to draw hardly deformable materials.
- A similar reduction in the pull force and a similar improvement in the wire surface quality as for stainless steel were obtained [12].
- The use of EPE in wire drawing processes results in a significant reduction in power consumption whereby it contributes to the protection of the natural environment.
- A generally held one is that high-density current pulses are introduced in the form of energy (both thermal and electronic). When the deformation region is activated by the electric pulses, the metal atoms obtain energy to enhance the vibration ability, which changes the activation energy for the motion of dislocations and accelerates their movement. Thus, the internal friction resistance can be reduced in the course of deforming and the plasticity of the metal can be improved.
- On the other hand, worth of notation is the side effect, such as Joule heating with the application of current pulses, which will lead temperature rise during the wire drawing process. During the electropulsing, the rate of the temperature rise can arrive at 10^6 °C s^{-1} order [13]. Such high-rate heating can generate nonsynchronous change of temperature rise and dynamic thermal expansion, that is the thermal expansion lags behind the temperature rise.
- The proposed technique is highly promising and it potentially can replace the conventional on-line continuous annealing methods.
- The technique can be very effective and inexpensive in its technological applications.

References

[1] Kravchenko V.Y.: *JETP*, Lett., Vol. 12, 1970, pp. 381.
[2] Conrad H., Karam N., Mannan S.: *Effect of Electric current pulses in the recrystallization of copper*, Scripta Metall., Vol. 17, 3, 1983, pp. 411.
[3] Di Y., Conrad H.: *Influence of an electric field in the plastic deformation of polycrystalline NaCl at elevated temperature*, Acta Mater., Vol. 46, 6, 1998, pp. 1963.
[4] Wei-di C., Sprecher A.F., Conrad H.: *Effect of strain rate on the electroplastic effect in Nb*, Scripta Metall., Vol. 23, 1, 1989, pp. 151.
[5] Sprecher A.F., Mannan S.L., Conrad H.: *On the temperature rise associated with the electroplastic effect in titanium*, Scripta Metall, Vol. 17, 6, 1983, pp. 769.
[6] Troitskii O.A.: *Pressure shaping by the application of a high energy*, Mater. Sci. Eng., Vol. 75, pp. 37.
[7] Sosnin O.V., Gromova A.V., Yu E., Suchkova, Kozlov E.V., Yu.F. Ivanov, Gromov V.E.: *The structural-phase state changes under the pulse current influence on the fatigue loaded steel*, Int. J. of Fatigue, Vol. 27, 2005, pp. 1221.
[8] Zhang W., Sui M.L, Zhou Y.Z., Li D.X.: *Evolution of microstructures in materials induced by electropulsing*, Micron, Vol. 34, 2003, pp 189.
[9] Yang D., Conrad H.: *Exploratory study into the effect of an electric field and of high current density electropulsing on the plastic deformation of TiAl*, Intermetallics, Vol. 9, 2001, pp. 943.
[10] Xu Z., Tang G., Tian S., Ding F., Tian H.: *Research of electroplastic rolling of AZ31 Mg alloy strip*, J. Mater. Process. Technol., Vol. 182, 2007, pp. 128.
[11] Tang G., Zhang J., Yan Y., Zhou H., Feng W.: *The engineering application of the electroplastic effect in the cold-drawing of stainless steel wire*, J. Mater. Process. Technol., Vol. 137, 2003, pp. 96.
[12] Tang G., Zhang J., Zheng M., Zhang J., Fang W., Li Q.: *Experimental study of electroplastic effect on stainless steel wire 304L*, Mater. Sci. Eng., Vol. A281, 2000, pp. 263.
[13] Zhou Y.Z., Qin R.S., Xiao S.H., He G.H., Zhou B.L.: *Reversing effect of electropulsing on damge of 1045 steel*, J. Mater. Res., Vol. 15, 2000, pp. 1056.

Efekt elektroplastyczny w procesie ciągnienia na zimno miedzianego drutu stosowanego w przemyśle samochodowym

W artykule przedstawiono porównanie konwencjonalnego procesu ciągnienia drutu na zimno oraz ciągnienia z użyciem elektrycznych impulsów prądowych o dużej gęstości. W badaniach wzięto pod uwagę wytwarzanie drutu miedzianego, który później jest wykorzystywany do produkcji kabli dla przemysłu motoryzacyjnego. Opisano budowę specjalnego stanowiska badawczego. Na podstawie przeprowadzonych badań wykazano, że w procesie odkształcania z zastosowaniem impulsów prądowych znacznie obniżyła się wartość siły ciągnienia drutu. Zbadano własności materiałowe przeciągniętych drutów. Dla ciągnienia z impulsami prądowymi wykazano poprawę własności plastycznych badanego materiału oraz wzrost jakości powierzchni drutu. Proponowana metoda ciągnienia drutu jest bardzo obiecująca i może zastąpić w przyszłości konwencjonalne metody ciągłego wyżarzania materiału.

ARCHIVES OF CIVIL AND MECHANICAL ENGINEERING

Vol. VIII 2008 No. 2

Information about PhD thesis at the Civil Engineering Faculty and the Mechanical Engineering Faculty of Wrocław University of Technology

Title: *The outer surface layer constitution of aluminum matrix composites reinforced with saffil fibres using cutting methods* (in Polish) *Konstytuowanie warstwy wierzchniej metodami obróbek ubytkowych aluminiowych materiałów kompozytowych wzmacnianych włóknami saffilowymi*

Author: Paweł Karolczak
Supervisor: dr hab. inż. Piotr Cichosz, Professor of Pwr, Wrocław University of Technology
Promoting Council: Institute of Production Engineering and Automatization of WUT
Reviewers:
Professor Wit Grzesik, Opole University of Technology,
Professor Stanisław Zaborski, Wrocław University of Technology
Date of PhD thesis presentation: September 24th, 2007.
PhD is available in Main Library of Wrocław University of Technology
The monograph contains: 132 pages, 130 figs, bibliography: 145 items
Keywords: *aluminum matrix composites, cutting methods, surface layer*

Abstract: In This work concerned forming methods of machining aluminum matrix composites reinforced with saffil type fibres. It concentrated on decohesion mechanism of composites. This is basic phenomenon due to machining. Mechanisms of composite materials separation were defined and compared with mechanisms of aluminum alloys separation. The quick-stop device has been designed and fixed-up, which has enabled "chilling" of cutting zone. The metallographic specimens of chip roots for research and analyses of materials separating were taken from this zone.

The surface layer of machined composites, quality and rate of structure change in matrix and reinforcement were researched.

Capabilities of aluminum matrix composites forming by electrical-discharge machining were defined. The research was concentrated on surface layer of material after EDM composite, quality and its changes. Influence of current parameters on thickness and quality of surface layer and degree of its destroying, was defined.

Aluminum matrix composites are often used for fabrication parts of braking system. This fact was a contribution to the research presented in last chapter of the work.

Title: *Increase of adhesive and cohesive interaction in adhesive joints of sintered carbides with steel C45* (in Polish)
Zwiększenie oddziaływań adhezyjnych oraz kohezyjnych w połączeniach klejowych węglików spiekanych ze stalą C45

Author: Tomasz Piwowarczyk
Supervisor: Doctor hab. inż. Zbigniew Mirski, Wrocław University of Technology
Promoting Council: Institute of Civil Engineering of Wrocław University of Technology
Reviewers:
Professor Jerzy Nowacki, Professor of Szczecin University of Technology
Professor Andrzej Ambroziak, Professor of Wrocław University of Technology
Date of PhD thesis presentation: March 17th, 2008
PhD is available in Main Library of Wrocław University of Technology
The monograph contains: 169 pages, 129 figs, 31 tables, bibliography: 165 items
Keywords: *gluing, composite adhesive joints, fillers, mechanical strength, thermal conductivity*

Abstract: In this dissertation issue of sintered carbides gluing with steel C45 in aspect of tool fabrication was presented. Gluing has a lot of advantages, so wherever possible, engineers introduce this technology. On the other hand gluing has three main disadvantages, first of all limited strength, secondly poor thermal resistance and last but not least lack of thermal conductivity. This excludes adhesives from many applications, like tool industry, where cutting tools are joined by brazing or high temperature brazing.

Range of PhD research work outcame from two main thesis of dissertation which are following: It is possible to get substantial increase of adhesive interactions by developing technology of preparation of surfaces of sintered carbides and steel, and Cohesive forces in adhesive can be increased by adding different fillers and creating composite joints.

In theoretical part characteristic of adhesive joints were presented - problems occurring in joining processes and its fundamental advantages and disadvantages.

In practical part methods of surface preparing of sintered carbides and steel were selected (mechanical grinding, electrolytical etching and electrolytical etching with additional abrasive blasting).

Results of measurements of surface roughness, metallographic analysis and cobaltic phase content on the surface were demonstrated. Special attention was given to wettability (contact angles and wetting area) of sintered carbides surface and its influence on joint properties.

Final point was thermal conductivity measurements of composite adhesive joints. In this stage the problem of adhesive joints thermal conductivity and attempts of its solving by introduction of metal additive phase to a matrix were presented. Samples preparation process for the measurements and a test stand were specified. Method of thermal conductivity coefficient measurements with use of Poensgen device was described. Examples of thermal conductivity coefficient measurements for glues and plastics were showed. This work includes results of thermal conductivity coefficient measurements of glue based on methacrylate resin and for composite structure adhesive – bonded joints obtained for this glue with iron and aluminum powder additive.

Results of this work have found application in tool industry and machine elements.

Title: *Limit states of rocks and soil materials with layer microstructure* **(in Polish)**
Stany graniczne ośrodków gruntowych i skalnych z mikrostrukturą warstwową

Author: Marek Kawa
Supervisor: Doctor hab. inż. Dariusz Łydżba, Wrocław University of Technology
Promoting Council: Civil Engineering Faculty of Wrocław University of Technology
Reviewers:
Professor Maciej Gryczmański, Professor of Silesian University of Technology
Professor Ryszard J. Izbicki, Professor of Wrocław University of Technology
Date of PhD thesis presentation: February 4th, 2008
PhD is available in Main Library of Wrocław University of Technology
The monograph contains: 193 pages, 177 figs, 2 tables, bibliography: 68 items
Keywords: *strength criterion, layer microstructure, homogenization*

Abstract: In this work multi-scale modeling method of limit states for layered rocks and soils is presented.

In micro modeling domain using homogenization theory, numerical procedures for specifying critical load of layered medium are proposed. Many numerical and analytical solutions for structures with constituents ruled by different strength conditions are also presented.

The micro modeling results are then used in a macroscopic approach. This part of work is focused on identification of macroscopic strength criterion for layer microstructure. The criterion proposed is a conjunction of Pariseau anisotropic failure condition and critical plane equation. The back-analysis procedure for specifying the constituents' properties from experimental data series is also presented.

To grant the possibility of solving boundary-value problems numerical implementation of proposed criterion is performed. The evaluation module written in C++ is intended for using with Flac code as a user-defined constitutive model. In order to present module usefullness two fundamental geotechnical problems are solved: the bearing capacity of strip foundation on layered soil and the plastic zone development during tunnel excavation process in stratified rocks.

The closing paragraph extends former formulation of composite medium strength on masonry and blocky-jointed microstructure

ARCHIVES OF CIVIL AND MECHANICAL ENGINEERING

Vol. VIII 2008 No. 2

Information about PhD thesis at the Civil Engineering Faculty and the Mechanical Engineering Faculty of Wrocław University of Technology

Title: ***The outer surface layer constitution of aluminum matrix composites reinforced with saffil fibres using cutting methods*** **(in Polish)**
Konstytuowanie warstwy wierzchniej metodami obróbek ubytkowych aluminiowych materiałów kompozytowych wzmacnianych włóknami saffilowymi

Author: Paweł Karolczak
Supervisor: Professor Piotr Cichosz, Wrocław University of Technology
Promoting Council: Institute of Production Engineering and Automation, Wrocław University of Technology
Reviewers:
Professor Wit Grzesik, Opole University of Technology,
Professor Stanisław Zaborski, Wrocław University of Technology
Date of PhD thesis presentation: September 24th, 2007.
PhD is available in Main Library of Wrocław University of Technology
The monograph contains: 132 pages, 130 figs, bibliography: 145 items
Keywords: *aluminum matrix composites, cutting methods, surface layer*

Abstract: In This work concerned forming methods of machining aluminum matrix composites reinforced with saffil type fibres. It concentrated on decohesion mechanism of composites. This is basic phenomenon due to machining. Mechanisms of composite materials separation were defined and compared with mechanisms of aluminum alloys separation. The quick-stop device has been designed and fixed-up, which has enabled "chilling" of cutting zone. The metallographic specimens of chip roots for research and analyses of materials separating were taken from this zone.

The surface layer of machined composites, quality and rate of structure change in matrix and reinforcement were researched.

Capabilities of aluminum matrix composites forming by electrical-discharge machining were defined. The research was concentrated on surface layer of material after EDM composite, quality and its changes. Influence of current parameters on thickness and quality of surface layer and degree of its destroying, was defined.

Aluminum matrix composites are often used for fabrication parts of braking system. This fact was a contribution to the research presented in last chapter of the work.

Information for Authors

Send to: *Archives of Civil and Mechanical Engineering*
Polish Academy of Sciences, Wrocław Branch
Podwale 75, 50-449 Wrocław, Poland

Archives of Civil and Mechanical Engineering (ACME) publishes both theoretical and experimental papers which explore or exploit new ideas and techniques in the following areas: structural engineering (structures, machines and mechanical systems), mechanics of materials (elasticity, plasticity, rheology, fatigue, fracture mechanics), materials science (metals, composites, ceramics, plastics, wood, concrete, etc., their structures and properties, methods of evaluation), manufacturing engineering (process design, simulation, diagnostics, maintenance, durability, reliability). In addition to research papers, the Editorial Board welcome: state-of-the-art reviews of specialized topics, letters to the Editor for quick publication, brief work-in-progress reports, brief accounts of completed doctoral thesis (one page is maximum), and bibliographical note on habilitation theses (maximum 250 words). All papers are subject to a referee procedure, except for letters, work-in-progress reports and doctoral and habilitation theses, which are briefly reviewed by the Editorial Board.

The papers submitted have to be unpublished works and should not be considered for publication elsewhere.

The Editorial Board would be grateful for all comments on the idea of the journal.

Detailed information about the Journal on web:
http://www.pan.wroc.pl
www.ib.pwr.wroc.pl/wydzial/czasopismoACME.html
http://www.acme.pwr.wroc.pl
http://www.wmech.pwr.wroc.pl

The papers should be submitted through the webside
http://www.acme.pwr.wroc.pl

Price 15 zł
(0% VAT)

Subscription orders should be addressed to:

Oficyna Wydawnicza Politechniki Wrocławskiej
Wybrzeże Wyspiańskiego 27
50-370 Wrocław